METHODOLOGY FOR THE DESIGN OF GRAVITATIONAL WATER VORTEX TURBINE BY OPTIMIZATION BASED ON SURROGATE MODELS

Laura Isabel Velásquez García

Tesis de grado para optar al título de Doctora en Ingeniería Ambiental

Asesores

Edwin Lenin Chica, Doctor en ingeniería

José Alejandro Posada, Doctor en ingeniería

Universidad de Antioquia

Facultad de Ingeniería

Doctorado en Ingeniería Ambiental

Medellín

2023

Cita	Muñoz Zapata y Martínez Naranjo, 2018 [1]
Referencia Estilo IEEE (2020)	[1] Velásquez, L. "METHODOLOGY FOR THE DESIGN OF GRAVITATIONAL WATER VORTEX TURBINE BY OPTIMIZATION BASED ON SURROGATE MODELS", Seleccione modalidad de grado, Doctorado en Ingeniería Ambiental, Universidad de Antioquia, Medellín, 2023

Doctorado en Ingeniería Ambiental.

Grupo de Energía Alternativa.

I have no special talent.
I am passionately curious.

Albert Einstein

Contents

ABSTRACT

For many years fossil fuels have been considered the main source of energy for electricity, heating and transport applications, but their rapid depletion together with the global warming that their use produces, are significantly affect the way of life of humanity unless the energy takes advantage of renewable sources.

Within renewable energy sources, small-scale hydroelectric power is the main ally in the generation of clean energy, since its developments have a long useful life with more than 100 years demonstrated and even with possibilities of new designs and technological adaptations. Within these new designs, the gravitational water vortex hydraulic turbines (GWVHT) arise. A GWVHT is a run-of-the-river power plant that harnesses the kinetic and potential energy of an artificially induced vortex in a basin with a central outlet. Its main interest is the ability to generate energy in low head and flow ranges, so the turbine allows taking advantage of sites that until now were not possible with conventional hydraulic turbines.

Considering that it is necessary to research and implement generation systems with renewable energies, this doctoral thesis seeks to establish a methodology for the design of the main components of a GWVHT (rotor, basin, inlet channel and discharge), making use of a multi-objective parametric optimization algorithm based on surrogate models, which allow maximizing the conversion efficiency of the system.

A prototype manufactured with the specifications obtained in the optimization was characterized; the characterization allowed validating the obtained equations and plotting the turbine operation curves. The curves allow knowing the operating ranges of the system, that is, the flow and head needs for the system to work, and identify how its efficiency changes in these ranges. The technological product developed could be an alternative for the supply of electrical energy in conditions of environmental sustainability; understanding environmental sustainability as the balance that is generated through the harmonious relationship between society and the nature that surrounds it and of which it is a part. Environmental sustainability implies achieving development results without threatening the sources of natural resources and without compromising those of future generations (Goodland, 1995).

RESEARCH OBJECTIVES

General objetive

Establish a methodology for the design of the main components of a gravitational vortex turbine (rotor, circulation chamber, inlet and discharge channel), using a multi-objective parametric optimization algorithm based on surrogate models, which allow maximizing the conversion efficiency of the system.

Specific objetives

- Apply a design of experiments selecting the geometric parameters (factors) and the levels of these factors, which may be significant in the energy conversion efficiency.
- Evaluate through CFD simulations the conversion efficiency of the different gravitational vortex turbines generated according to the design of experiments.
- Identify the most significant factors in the performance of gravitational vortex turbines through an analysis of variance and obtain a mathematical model that allows predicting the value of the energy conversion efficiency based on the significant factors.
- Determine the best combination of significant design factors that produce maximum energy conversion efficiency using optimization algorithms.
- Propose a set of parametric design equations for the dimensioning of the main components of a gravitational vortex turbine.
- Manufacture a laboratory-scale gravitational vortex turbine considering the geometric parameters established in the proposed design equations, and using materials that exhibit high resistance to corrosion-erosion and that guarantee the structural integrity of the turbine.
- Validate the design equations by experimentally determining the characteristic curves of the manufactured gravitational vortex turbine.
- Evaluate the technical and economical impact of the implementation of gravitational vortex turbines in the Colombian context.

CHAPTER 1

INTRODUCTION AND BACKGROUND

1.1 Introduction

This thesis is written and structured as a compendium of several short scientific or academic pieces of work that are interrelated with each other. In the whole set of works, the candidate is the first author of the publications. Both, the supervisors and the PhD student, chose the format related to a compendium of several academic works because when a compilation thesis is written, the PhD candidate is contributing towards the publication statistics of the University right from the start of her studies. Additionally, by writing the thesis as a compendium of research works, the PhD student is involved in the publishing and the peer review management processes. Below, the integrated nature of the whole research is described to provide a comprehensive overview and coherence of the entire document.

After this first introductory Chapter, a review article, Chapter 2, is opening the compilation of the presented works. The review article is focused on the current state of knowledge concerning GWVHT, including numerical and experimental studies. Chapter 2 concluded with a a brief summary of the results obtained from differents author and a list of challenge for the development of GWVHT. Afterwards, in Chapter 3, a single-objective optimization using the response surface methodology was employed to select the best configuration for the inlet channel, circulation basin, and discharge for a GWVHT with conical basin and spiral inlet channel. The objective in this optimization was to increase the circulation of the vortex. Six geometrical factors were studied simultaneously to evaluate their effect on the circulation of the vortex. The optimization process carried out gives the specific values of the geometric factors that must be used in the design of the turbine to increase the circulation of the vortex. The results obtained in this chapter are additional results to which the authors arrived through their research, originally they were not part of the objectives of the thesis.

Then, for the same geometrical factors using in Chapter 3, a new optimization process was executed. The results are shown in Chapter 4. This time the optimization had two objectives: the minimization of the volume flow rate and the maximization of the circulation. In both optimization processes, the runner was excluded from the analysis. In a optimization with multi-objectives is possible obtain a set of solutions called Pareto optimal front. The final solution is subjective and depends on the need of the designer, who can give more priority to one objective than to other. For this study, a compromise solution within objectives was selected. A compromise solution is a solution just in the middle of the Pareto optimal front.

Usign the solution found in Chapter 4, the response surface methodology was used again, this time to optimize the runner of the turbine. The effect of the relative position of the runner, the number of blades, and the diameter of the blades on the efficiency of the turbine was evaluated. To validate the numerical results, a test

bench with a GWVHT was built. The bench was composed of two water tanks, a centrifugal pump, basin, inlet channel and runner. To observe the vortex inside the turbine, the inlet channel and the basin were made from transparent acrylic. The optimal runner was printed in a 3-D print using polylactic acid (PLA). Since the results obtained in Chapters 4 and 5 were expressed as non-dimensional variables, they can be used to design turbines of multiple sizes.

One of the most important features to perform computational simulations is the correct selection of the turbulence model. As the optimizations carried out in chapters 3, 4, and 5 were done in Ansys Fluent, an additional chapter was written, Chapter 6, only dedicated to the comparison of 4 turbulence models available in the software. A correct selection of the turbulence model allows the numerical results to be much closer to the real phenomenon. The results indicated that the four turbulence models are able to predict a similar behaviour for the mass flow rate but not for the circulation. Without runner, RNG k-ϵ model is a good predictor of the flow behaviour, but in presence of runners, SST k-ω is the model recommended.

Chapter 7 presents a technical, economic, and environmental analysis for the implementation of a GWVHT in the Colombian context. This anaysis started with a description of the renewable energy sources, their current status in the world, followed by a detailed description of the Colombian energy market. Barriers and opportunities in Colombian hydroelectric development were also addressed. Finally, the main conclusions derived from this thesis are covered in Chapter 8.

1.2 Problem statement

The intensive use of energy in the different activities of the economic and social life of man has been transforming traditional work patterns and has allowed the acceleration of the rates of growth and demographic concentration (Aguilera Folgueiras, 2012). By the year 2040, it is expected that the world's energy needs will increase by 30% while the population expands from 7.4 billion to 9 billion inhabitants (Doman, 2017), which is why the world must prepare to meet this energy demand future energy in a sustainable way. World energy consumption increased 2.9% in 2018, reaching the equivalent of 13.8 billion tons of crude oil, with the world's main energy consumers being China, the US, and India. Figure 1.1 shows the evolution of energy consumption by type of source between the years 1992-2017 in millions of tons of crude oil. From Figure 1.1 it is clear the increase in energy consumption for the different types of sources in the last 15 years.

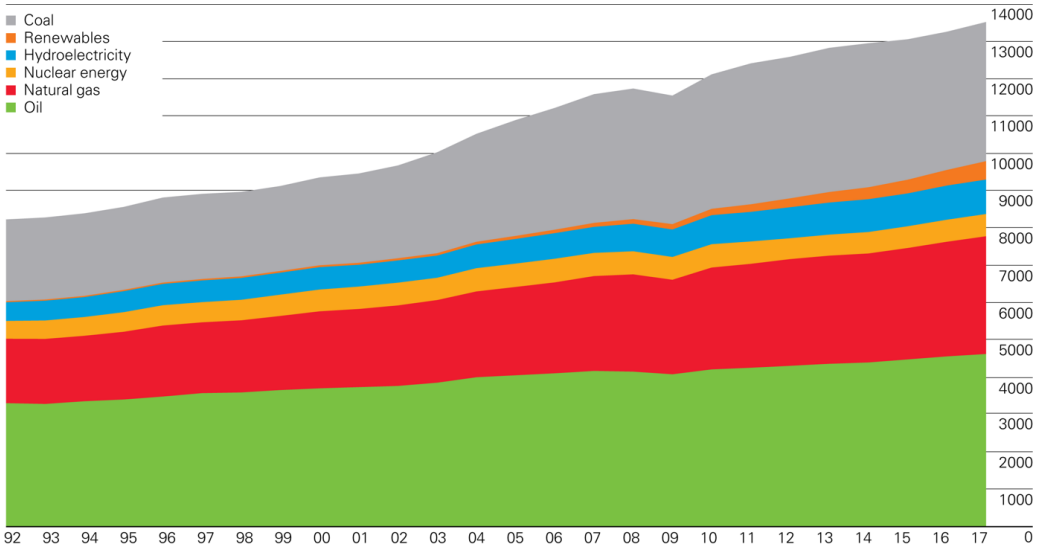

Figure 1.1: Evolution of energy consumption according to type of source between the years 1992-2017. Source: (Dudley et al., 2018).

The energy sector will experience profound changes. There will be a turnaround in the energy sources that

will give electricity to humanity. Future energy options will depend on fossil fuel prices, greenhouse gas emissions, land-use change, forestry and agricultural activities, and your location (FAO, 2018).

Energy sources can be classified using several criteria: according to whether or not they are renewable, according to their degree of availability: conventional or non-conventional, and according to the form of their use: primary or used directly and secondary or final. Renewable energy sources are those whose potential is inexhaustible because they come from the energy that reaches planet earth continuously as a result of solar radiation or the gravitational attraction of other planets and satellites of the solar system. The main sources are solar, wind, hydraulic, tidal, geothermal and biomass energy. This type of sources have a particular characteristic, the variability of their generation. Said variability is a reflection of the behavior of its primary source, such as irradiation and wind, which depend on the climatic, meteorological and hydrological phenomena of the moment. Non-renewable energy sources are those that exist in a limited quantity in nature, such as petroleum derivatives (coal, diesel, natural gas, fuel oil, etc.) and uranium. 70% of global energy demand is currently satisfied by non-renewable sources, while the remaining 30% comes from renewable sources (Dudley et al., 2018). Figure 1.2 shows the regional energy consumption according to the type of source in 2017.

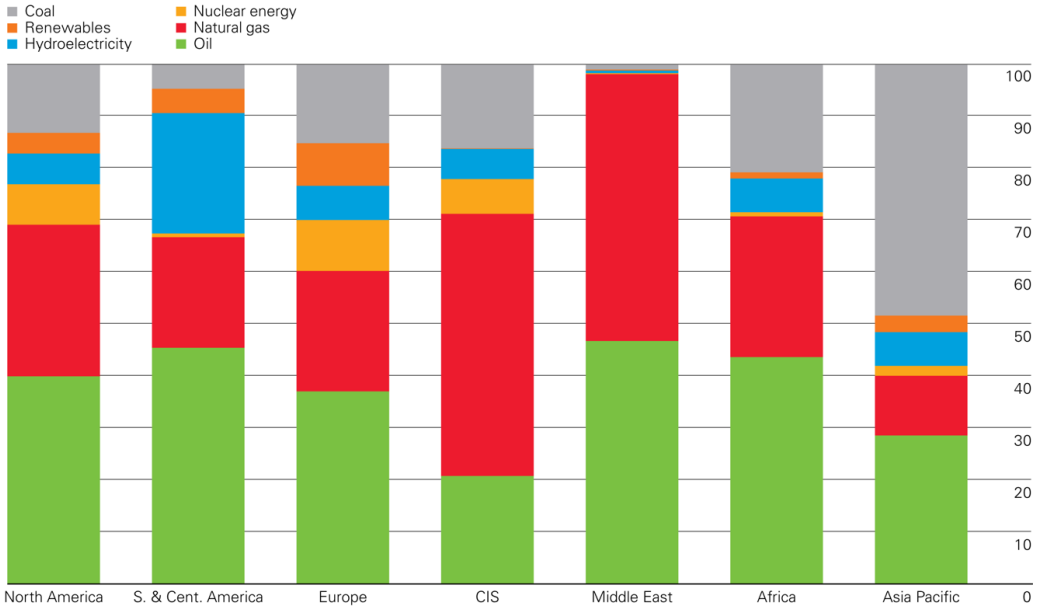

Figure 1.2: Regional energy consumption by type of source in 2017. Source: (Dudley et al., 2018).

According to the second classification criterion, conventional energy sources are those that have an important participation in the energy balances of industrialized countries. This is the case of coal, oil, natural gas, hydraulic and nuclear energy. On the contrary, non-conventional energy sources are those that do not have an appreciable participation in the coverage of energy demand because they are not widely marketed. This is the case of solar, wind, tidal, biomass and small-scale hydropower. Depending on their use, energy sources can be classified into primary and secondary. The primary ones are those obtained directly from nature, such as coal and natural gas. The secondary ones, also called useful or final ones, are obtained from the primary ones through a transformation process by technical means. This is the case of electricity or petroleum-derived fuels.

Figure 1.2 makes it possible to identify that there is a clear global dependence on oil, coal and natural gas, which are fossil resources available in quantities that can be considered relatively abundant but finite. A fundamental characteristic of these non-renewable fuels is that the energy produced is due to the combustion of the carbon present in them, so their use consumes carbon, oxygen from the atmosphere and releases carbon dioxide and energy (exothermic reaction). Because the carbon in these fuels is sequestered in the deposits, the CO_2 released increases its concentration in the atmosphere. Carbon dioxide is a greenhouse gas that allows the passage of shortwave radiation from the sun and retains the infrared radiation emitted by the earth, that is,

it retains the heat that would otherwise escape into space, which which causes an increase in the temperature of the planet. The increase in temperature produces direct effects on ecosystems, constituting a considerable risk for biodiversity, natural resources, human, animal and plant health.

In addition to the effects on the environment, the main deposits of fossil fuels are concentrated in very specific places on the planet, which has given rise to economic and geopolitical situations associated with their geographical distribution and dominance. This scenario has generated in many countries the need to initiate a transition towards the use of non-conventional energy resources. Given the availability of at least one of the non-conventional renewable energy sources in any geographical position on the planet, and the relative abundance of one or more of these sources in some favored regions, the non-conventional renewable energy sources represent immense energy potentials for be exploited as their research, development and commercial deployment of associated technologies continue to advance.

Countries such as China, Germany, Spain, and the United States, are today consolidated as pioneering countries in the development of the largest installed capacities in technologies for the use of hydraulic, wind, solar, and geothermal energy (Lins et al., 2014). Colombia has a national electricity system that is relatively low in carbon emissions (compared to other countries with a greater share of fossil fuels in its energy matrix), is not dependent on imported energy sources, and at the same time has sufficient current generation capacity, with resources abundant fossil fuels and possible gas and oil deposits not yet exploited, does not seem to face the imminent need to resort to non-conventional resources and technologies. However, to date, the trends in cost reduction and risk mitigation associated with non-conventional energy sources added to the successful experiences and technical developments achieved internationally, have already begun to lay the foundations that justify the adoption of a strategy for the development of unconventional sources. This is reflected in current national policies and international agreements and treaties that include sustainable development as a priority objective that does not compromise the natural resources of future generations. An example of this is Law 1715 of 2014 in Colombia, which aims to promote the development and use of non-conventional energy sources, mainly those of renewable nature, in the national energy system, through its integration into the electricity market, its participation in non-interconnected zones (ZNI)[1] and in other energy uses such as necessary means for sustainable economic development, the reduction of greenhouse gas emissions and the security of energy supply.

With demand on the rise, the world will not immediately say goodbye to oil and other non-renewable energy sources; After a transition period, renewable energy production is expected to make up the majority of the world's energy production, although the big challenge is to continue to improve its efficiency and profitability. The increase in the efficiency of devices, systems and processes would reduce the consumption of primary resources while the improvement in profitability would motivate investors, reduce production costs and sales prices.

Of the many alternatives to produce energy from non-conventional renewable sources, the use of energy from water is not new; The novelty is the new turbines that, due to their design characteristics, can be installed in places where conventional turbines (Pelton, Kaplan, and Francis) cannot operate. One of these new turbines is gravitational water vortex hydraulic turbines (GWVHT) that allow the generation of electrical energy in rivers with falls and very low flows, so it can be implemented in streams, ravines, canals, or diverting part of the flow of a river without the need to build dams. Here lies its main advantage: its versatility; but also its main disadvantage: it is low energy density as it cannot accumulate the flow of water. With efficiencies that vary between 17 and 85%, the plants that use GWVHT still have lower efficiencies than those reported by conventional generation systems, with values that sometimes exceed 95% (Goswami and Kreith, 2007).

The question that this research seeks to answer is: **how much would the variation in the efficiency of an electric power generation system with a gravitational vortex turbine for small hydroelectric power plants if for the design of its main components (inlet channel, chamber of circulation, rotor, and discharge) is multi-objective parametric optimization based on surrogate models used?**

[1] Areas that are not integrated into the national electricity interconnected system and supply their energy needs through diesel plants, small hydroelectric plants and, more recently, solar panels.

1.3 Justification

During the last years, the awakening of a sustainable environmental conscience has been observed. New concepts have been borned directed towards the search for the equitable development of technology and science and the balance and preservation of natural resources (Gallego Triana et al., 2015). In this sense, electrical energy plays a fundamental role in the evolution of societies, being the driving force of the economic and industrial development of a country.

The new electricity generation projects must be framed within sustainable development policies and international agreements that involve the use of renewable energy sources; These sources are currently being massively used, seeking to reduce dependence on non-renewable sources of energy generation that are characterized by their lack of self-regenerative capacity and their polluting effects. The hydroelectric power generation process is the most widespread renewable method worldwide, with an installed capacity of more than 21,800 GW, representing close to 20% of the total electrical energy produced or 60% of the installed capacity from renewable sources (IRENA, 2019).

Colombia is positioned as one of the countries with the greatest water reservoirs both globally and in Latin America, with a water supply six times the world average and three times that of Latin America. This water supply added to favorable topographic conditions translates into a hydroelectric potential close to 90,000 MW (UPME, 2018). Currently, with a net installed capacity of 17,000 MW, the country's electricity generation matrix, Figure 1.3, is 68.33% based on water resources.

Figure 1.3: Effective capacity installed in Colombia. Source: (Arango, 2019).

Given the water wealth of Colombia, encouraging and giving more impetus to the development of new electricity generation projects from hydroelectric plants should be the backbone of the Colombian electricity sector. These new projects would not only allow maintaining a clean, renewable, and reliable matrix but would also help meet the growing energy demand.

The country's annual electricity consumption is close to reaching 70,000 GWh/year and for the next 11 years, according to projections made by UPME, an average increase of 2% per year is expected, taking into account dynamic expectations of the industrial sector and the electrification of the economy. To meet this increased consumption projected for the coming years, it is necessary to continue expanding the country's energy infrastructure, both for generation and transmission, distribution, and marketing. With the current installed capacity of the country, the demand will be supplied until 2021 under critical hydrological conditions. Given

a further delay in the start-up of Hidroituango, the country's largest hydroelectric project currently underway with an installed capacity of 2,400 MW, there could be insufficient supply to cover energy needs, and if measures are not taken, it would be possible for new cases of rationing.

Although the generation of electrical energy through hydraulic power plants is already used in the world, on a large scale this energy source has a limited field of expansion, since in the most developed countries most of the important rivers already have a or several plants, and in developing countries large projects can collide with obstacles of a financial, environmental and social nature. As an option, the energy industry has developed medium and small capacity facilities called Small Hydroelectric Power Plants (SHP) which can take advantage of the relatively low flows of rivers with lateral or run-of-the-river catchments without the need to create large reservoirs, conserving the ecological flows and limiting the environmental effects of construction.

The panorama presented for Colombia, which may well be the panorama of other countries, indicates that there is a palpable need to study new versatile and efficient generation technologies, so with this doctoral thesis we seek to establish a methodology for the design of gravitational water vortex hydraulic turbine for the generation of energy through small hydroelectric uses that guarantee maximum conversion efficiency. The development of a high-efficiency gravitational vortex turbine will not only increase energy production, but will also:

- Reduce the use of non-renewable fuels.
- Reduce greenhouse gas emissions.
- Diversify the energy basket.
- Serve as an alternative power supply in non-interconnected areas.
- Facilitate the generation of energy close to consumption sites, creating more autonomous regions with the capacity to supply themselves.
- Ensure adequate energy supply in terms of reliability and cost.

1.4 Hydraulic turbines

Hydraulic turbines are the prime movers that convert the energy of the falling water into a rotational mechanical energy and consequently to an electric energy through the use of the generators that are connected to the turbines. Turbines consist of a row of blades that are fixed on a rotating shaft or a plate. The shaft rotates because of the impact of the difference in velocity and pressure of the water striking the blades (Dincer and Ezzat, 2018).

Hydraulic turbines can be classified based on different categories: the direction of the flow or pressure of water. According with the direction of the flow, the turbines can be axial, radial, crossflow or mixed flow turbines.In axial flow turbines the direction of the water stream is parallel to the axis of rotation of the blades such as Kaplan and propeller turbines. In radial flow turbines, the direction of the water stream is perpendicular to the axis of rotation of the blades such as Pelton turbines. In mixed flow turbines, the direction of the water flow entering the turbine is different from the direction at which the water leaves the turbine such as Francis turbines. In crossflow turbines, the water flow passes through the turbine diagonally or across the turbine blades. In these types of turbines, the water flow passes through the runners two times increasing the efficiency of the turbine; crossflow turbines are utilized at the sites with high water flow and small head.

The hydraulic turbines can also be categorized into two types: impulse and reaction turbines based on the change of the water pressure while passing through the rotor. For impulse turbines, the pressure of the water remains the same when passing through the rotor. However, when the water passes through the nozzle, the energy in the water is transformed into kinetic energy. The high-speed jet then strikes the bucket shaped vanes mounted on a rotating shaft and consequently transforming the kinetic energy of the water to a rotation movement through the runner. Pelton, Turgo and gravitational water vortex turbines are the most common

among the impulse turbines category. For the reaction turbines, water pressure varies depending on the variation of the flow path shape, which comprises fixed guide vanes, adjustable guide vanes, and rotating blades. Francis and Kaplan turbines are the main types of reaction turbines.

The basis of the design of an hydraulic turbine is the velocity diagrams (velocity triangles) at the entry and exit of the turbine rotating element (runner). These lead to the Euler equation for theoretical torque and to the theoretical Euler efficiency of the turbine (Cengel, 2010). Although elemental velocity triangles are employed for preliminary design of the turbine, for large or new turbines, model testing is necessary for verification of performance. Because of the cost and time involved in developmental model testing, more recently, a computerized solution of the inviscid flow equations are employed.In particular, the efficiency of the hydraulic turbine must be optimized. The peak efficiency of a properly designed large hydraulic turbines can be as high as 95%, with typically every point of improved efficiency involving considerable monetary benefits in operation (Gummer, 2011).

To design a turbine, it is necessary to determine the data for the utilizable net head (H_n) and its maximum water flow rate (Q). In some projects, this flow corresponds to the annual minimum that is available, according to the hydrological study; and in other projects, it can be deduced from the brake power that the turbine should deliver to the generator, so that it can, in turn, deliver given amount of power to the electric power system.

The maximum available power of any turbine is given by equation 1.1:

$$P = \rho g Q H_n \tag{1.1}$$

where ρ is the density of the fluid and g the gravity. The output generated power by a turbine is given by equation 1.2:

$$P_{out} = T\omega \tag{1.2}$$

where ω is the angular velocity and T is the torque. The hydraulic efficiency of the turbine (η) is determined by equation 1.3:

$$\eta = \frac{P_{out}}{P} = \frac{T\omega}{\rho g Q H_n} \tag{1.3}$$

1.4.1 Gravitational water vortex turbine

An electric power generation system with a gravitational water vortex turbine is a run-of-the-river plant that takes advantage of the kinetic and potential energy of an artificially induced vortex in a chamber with a central drain. A run-of-the-river or flowing water plant is a plant where the energy of the water must be used at the instant it is available, to drive the turbines. They do not have a water reserve, and the flow supplied varies according to the seasons of the year. The main part of the turbine system consists of a inlet channel, a circulation chamber, a vetical rotor and a discharge.

Operation principle

- The river water is channeled and transported to a circulation chamber. This circulation chamber has a circular hole at its base.
- The combination of localized low pressure in the orifice and induced circulation at the tangential inlet influence the flow into a vortex. A vortex is a region of flow that rotates around an axis, which can be straight or curved. In its most general classification there are two types of vortices: the forced vortex and the free vortex. A forced vortex is called the rotation of a fluid that moves as a rigid solid with respect to an axis. In this case, each fluid particle has the same angular velocity. These vortices are superficial and form concave depressions in the surface of the fluid. In a free vortex each particle moves in a circular

path, at a speed that varies inversely proportional to the distance from the center of rotation. Free vortex typically occurs over a discharge such as in bathtubs or sinks when drained. For a forced vortex to form, an external torque is required to rotate the fluid, while for a free vortex to form, there must be a point of low pressure that sucks the flow towards it. In a GWVHT, both types of vortex coexist, this vortex is called the Rankine vortex. In the Rankine vortex, the inner circular region around the origin is in rotation like a rigid body (forced vortex), while the outer region is free of vorticity (free vortex), the velocity being inversely proportional to the distance from the origin.

- Potential energy is completely converted to rotational kinetic energy in the core of the vortex. Which is extracted using a vertical axis turbine.
- The water is returned to the river through discharge.

For the calculation of the power available and generated by the gravitational water vortex turbine, the same equations are used as for the calculation of the powers of conventional hydraulic turbines. Depending on the use, the amount of water and level difference available, the power of hydraulic turbines can be a few kilowatts up to hundreds of Megawatts. However, regardless of size, the evaluation of models can to predict the performance of large turbines.

1.5 Research results

1.5.1 Published papers

- L. Velasquez, A. Rubio-Clemente, E. Chica, Numerical analysis of the inlet channel and basin geometries for vortex generation in a gravitational water vortex power plant. Renewable Energy and Power Quality Journal. 18, 2020. https://doi.org/10.24084/repqj20.248. ISSN:2172-038X. https://www.icrepq.com/icrepq20/259-20-velasquez.pdf (Velásquez et al., 2020). SJR Q4.
- Velasquez, L., Chica, E., and Posada, J. (2021). Advances in the Development of Gravitational Water Vortex Hydraulic Turbines. Journal of Engineering Science and Technology Review, 14(3) (Velásquez et al., 2021). SJR Q3.
- Velasquez, L., Posada, A., and Chica, E. (2022). Optimization of the basin and inlet channel of a gravitational water vortex hydraulic turbine using the response surface methodology. Renewable Energy, 187, 508-521 (Velásquez et al., 2022). SJR Q1.
- L. Velasquez, A. Rubio-Clemente, E. Chica, Runner optimal position in a gravitational water vortex hydraulic turbine with spiral inlet channel and a conical basin. Renewable Energy and Power Quality Journal. 20, 2022. 143-147. https://doi.org/10.24084/repqj20.248. ISSN:2172-038X. https://www.icrepq.com/icrepq22/248-22-velasquez.pdf. SJR Q4.
- Velasquez, L., Posada, A., and Chica, E. (2023). Surrogate modeling method for multi-objective optimization of the inlet channel and the basin of a gravitational water vortex hydraulic turbine. Applied Energy, 330, 120357. (Velásquez et al., 2023). SJR Q1.

1.5.2 Conferences

- Laura Isabel Velásquez, Edwin Lenin Chica Arrieta, José Alejandro Posada. Evaluación experimental de una turbina hidráulica de vórtice gravitacional con cámara de circulación cónica y canal de entrada envolvente. Segundo congreso internacional Objetivos del desarrollo sostenible: Esfuerzos en America Latina y el Caribe. 2022. Evento que se realizó entre el 19, 20 y 21 de octubre de 2022.
- Laura Velásquez, Edwin Lenin Chica Arrieta and José Alejandro Posada. Determinación del caudal óptimo para la formación de un vórtice fuerte en una turbina de vórtice gravitacional. X Congreso

internacional de Ingeniería Mecánica, Mecatrónica y Automatización. Virtual entre el 05 al 07 de mayo de 2021. Universidad Nacional de Colombia.

- Laura Isabel Velásquez, Edwin Lenin Chica Arrieta, José Alejandro Posada. Avances en el desarrollo de turbinas hidráulicas de vórtice gravitacional para la generación de energía eléctrica a pequeña escala. Congreso internacional: objetivos del desarrollo sostenible. Esfuerzos en América Latina y el Caribe. https://www.ustatunja.edu.co/eventos-usta-tunja/event/94-congreso-internacional-objetivos-del-desarrollo-sostenible-esfuerzos-en-america-latina-y-el-caribe. ISBN 978-958-8628-66-0.
- Laura Isabel Velásquez, Edwin Lenin Chica Arrieta. Efecto de la geometría del canal de entrada en la formación del vórtice para una turbina de vórtice gravitacional. IV Reunión Latinoamericana de Hidropotencia y Sistemas. 16 al 20 de septiembre de 2019. Universidad Eafit. Medellín-Colombia.

CHAPTER 2

LITERATURE REVIEW

Advances in the development of gravitational water vortex hydraulic turbines

Published article

The Journal of Engineering Science and Technology Review (JESTR) is a peer reviewed international journal publishing high quality articles dedicated to all aspects of engineering. The Journal is published by the International Hellenic University, School of Science (Kavala Campus), located in Kavala, Greece.

Highlights

- GWVHT is a turbine suitable to use in low head and small to medium water flow rates.
- The highest power turbine installed until now (20 kW) has an efficiency of 68%.
- The most optimal relationship between the diameter of the conical basin and the diameter of the discharge (d/D) is between 14 and 18%.
- The most common inlet channel used has a rectangular cross-section ($w \times h$)

Advances in the development of gravitational water vortex hydraulic turbines

Laura Velásquez, Edwin Chica and José Posada

ABSTRACT

The availability of energy has been essential for humanity, which increasingly demands more energy resources to cover its consumption and well-being needs. Due to the rapid depletion of fossil fuels, use of alternative energy sources such as non-conventional renewable energy sources is fundamental. Within non-conventional renewable energy sources, small-scale hydroelectric power is an excellent option in the generation of clean energy. Its developments have a long useful life with more than 100 years proven and still with possibilities for new designs and technological adaptations. Among these new designs are the gravitational water vortex hydraulic turbines (GWVHT). A GWVHT is a run-of-river (ROR) hydropower system that harnesses the kinetic and potential energy of an artificially induced vortex. Its main advantage is the ability to generate energy in low ranges of head and flow.

The GWVHT is a new turbine with a wide range of efficiency between 17 and 85% that still needs more research to optimize the geometry of the basin, channel and runner. The aim of this work is to present a comprehensive analysis of various aspect of GWVHT such as modelling, optimum sizing, performance, and challenges for development, and implementation to establish a starting point for further research. Until now, the studies allowed to assert that the conical basins are better than the cylindrical basins but not identify the dimensions of the geometry. About the runner, the shape or number of blades has been varied but the results of the investigations were contradictory.

1. Introduction

The intensive use of energy in different economic and social activities has been transforming the traditional schemes of work and has allowed the acceleration of growth rates and demographic concentration [1]. By 2040, global energy demands are projected to increase by 30%, while the population grows from 7,400 to 9,000 million inhabitants [2]. This is why the world must prepare to supply this demand for future energy.

For many years modern societies have supported their growth in an energy system based mainly on obtaining energy through fossil fuels [3], but their rapid depletion along with the global warming that they produce will affect significantly humanity's lifestyle, unless energy is harnessed from other sources. The increased demands of energy and the decreased of the fossil fuel reserves, have increased the researchers, governmental and non-governmental organization interest to work in the field of renewable energy sources [4].

Energy sources can be classified using several criteria: according to whether they are or not renewable, according to their degree of availability: conventional or non-conventional, and according to the way they are used: primary and secondary. Renewable energy sources are those whose potential is inexhaustible as it comes from the energy that reaches the planet earth continuously as a consequence of solar irradiation or the gravitational attraction of other planets and satellites in the solar system. The main sources are solar, wind, hydraulic, tidal, geothermal, and biomass energy. Some of these sources are not predictable because of their intermittent and stochastic nature of most renewable generation originating from weather conditions. The main common features of renewable generation are variability, uncertainly, and location dependency. This variability is a reflection of the behaviour of its primary source, such as irradiation and wind, which depends on the climatic, meteorological, and hydrological phenomena at the moment. Non-renewable energy sources are those that exist in a limited amount in nature, such as those derived from petroleum (coal, diesel, natural gas, fuel oil, etc.), and uranium. Global energy demand is currently supplied by 70% with non-renewable sources, while the remaining 30% comes from renewable sources [3].

According to the second classification criterion, conventional energy sources are those that have significant participation in the energy balances of industrialized countries. This is the case of coal, oil, natural gas, hydraulic, and nuclear energy. On the contrary, unconventional energy sources are those that do not have appreciable participation

ORCID(s): 0000-0003-1483-0104 (L. Velásquez); 00000-0002-5043-6414 (E. Chica); 0000-0001-5836-0680 (J. Posada)

in the coverage of energy demand because they are not widely marketed. This is the case of small-scale solar, wind, tidal, biomass, and hydraulic energy. Depending on its use, energy sources can be classified as primary, and secondary. Primary sources are those that are obtained directly from nature, such as coal and natural gas. Secondary sources, also called useful or final, are obtained from the primaries sources through a process of transformation by technical means. This is the case of electricity or petroleum-derived fuels.

Given the availability of at least one of the non-conventional renewable energy sources in any geographical position on the planet, non-conventional renewable energy sources represent immense energy potentials. This potential can be supply energy demand growth, to the extent that its research, development and commercial deployment of associated technologies continue to advance.

There are many alternatives to produce energy from non-conventional renewable sources, one of them is the use of water energy. Hydropower is capable of responding to demand of energy rapidly [5], making it the most flexible source of power generation available. Water resource use is not a novelty, the commercial operation of hydropower started in Grand Rapids, Michigan in 1880, where a turbine produced electricity to power 16 brush-arc lamps at the Wolverine Chair Factory [6]. The novelty is the new designs and technological adaptations of turbines that due to their characteristics as small capacities, less time to construct and simple design, can be installed in places where conventional turbines such as Pelton, Kaplan and Francis turbines cannot operate or operate at low efficiency. In 2019, with a global installed capacity of around 1,150 GW, the hydropower contributed 15.9% of the global electricity generation [7].

On a large scale, hydropower has limited scope for expansion. Most of the major rivers, in developed countries, already have one or more hydroelectric power plants, and in developing countries, large projects may run into financial, environmental, and social nature obstacles. On a smaller scale, however, the generation of electricity in small hydroelectric power plants (SHP), projects that generate 10 MW or less of power [8], does offer growth possibilities. SHP can take advantage of the relatively low flow rates of rivers with lateral capture without the need to create large reservoirs, conserving the ecological flows and limiting the environmental effects of civil construction. SHP plants could also supply electricity in remote areas and improve rural people quality of life. The global potential capacity of small scale hydropower is 229 GW, however, it is estimated that only 34% has been utilized [9]. Europe is the continent with the highest percentage of use of its available potential capacity 48% (with a potential of 38.95 GW). Africa, with a potential of 12.2 GW, only uses 5%.

Among the new generation technologies to produce electricity in a SHP are the gravitational water vortex hydraulic turbines (GWVHT). With efficiencies ranging from 17 to 85% [10], plants using GWVHT still have lower efficiencies than those reported by conventional generation systems with values that sometimes exceed 95% [11]. Since its creation in 2006, a large number of research activities have been carried out that seek to understand more deeply how this type of systems operate to improve their efficiency. Through a review of the literature, the frontiers of current knowledge about GWVHT were identified to understand the developments carried out and establish a starting point for future research. This study analysed the strategies involved in developing the GWVHT: modelling approaches, methodologies design optimization and design validations, in numerical and experimental studies.

2. Gravitational water vortex hydraulic turbine

A GWVHT is a run-of-river (ROR) hydropower system that harnesses the kinetic and potential energy of an artificially induced vortex in a basin with a central drain. A ROR hydropower system is a plant where the energy of the water must be used at the moment it is available, to drive the turbine. They do not have a water reservoir, oscillating the flow supplied according to the seasons of the year. In the season of abundant rainfall (high volume flow rate), they develop their maximum power and allow excess water to pass through. During the dry season (low volume flow rate), the power decreases depending on the flow, reaching almost zero in some rivers in the summer season [12]. GWVHT operates at heads between 0.5-2 m and flow rates of 0.05-5 m^3/s, power generation of 0.2-5 kW. Figure 1 shows the GWVHT operation range compared to other hydraulic turbines, like Pelton, Francis, Kaplan, cross flow, Archimedean screw and Turgo turbines. GWVHTs are the turbines that require less volume flow rate and less head to operate.

Considered a new technology, GWVHT was created around 2006 by Austrian engineer Frank Zotlöterer while searching for ways to aerate inactive streams water without external power [14, 15]. In this system, the water is transported through an inlet channel until a basin. The velocity of the water is increased in a convergent section. An artificially induced gravitational water vortex is formed in the basin. Then, using a vertical axis turbine, the energy of the vortex is extracted. Finally, the water return to the river through the discharge orifice [16].

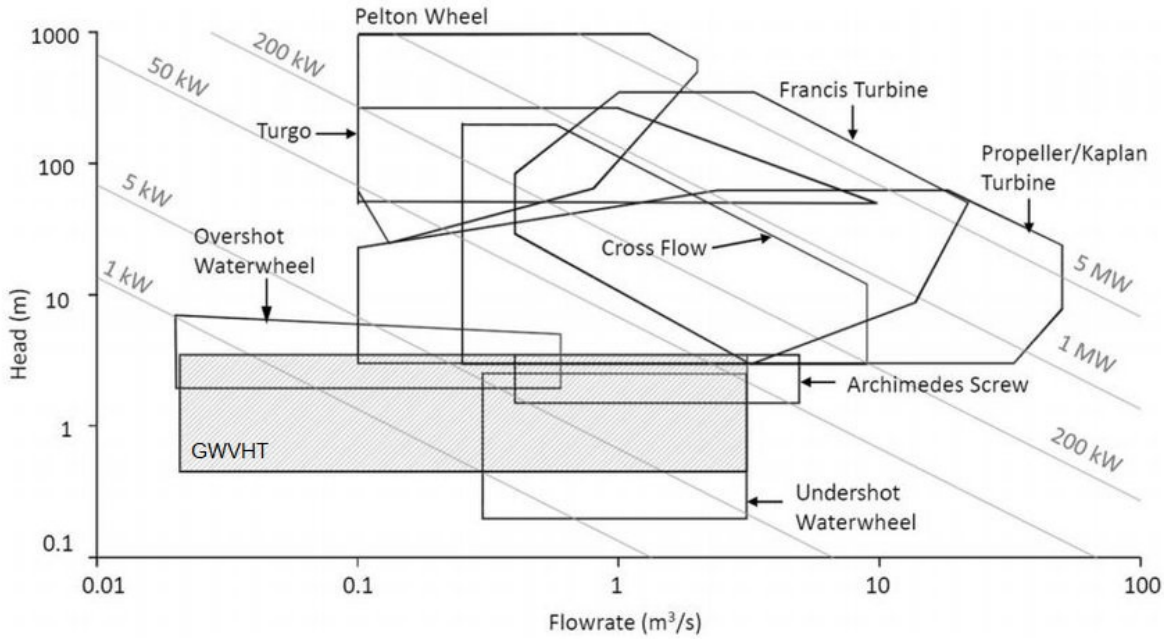

Figure 1: Operating ranges for Pelton, Francis, Kaplan, Cross Flow, Archimedean Screw, Turgo and GWVHT turbines. Modified from: Williamson et al. [13].

Figure 2 shows a general diagram of a hydroelectric power plant with a GWVHT, numbering each of its main elements: catchment, inlet channel, basin, runner, and discharge orifice. The catchment not only allows water to be capture from the river but also controls the flow and the level of suspended sediments to avoid damage to the runner. The inlet channel allows the water to enter the circulation basin in a tangential, controlled way, and without major turbulence, in order to facilitate the correct formation of the vortex.

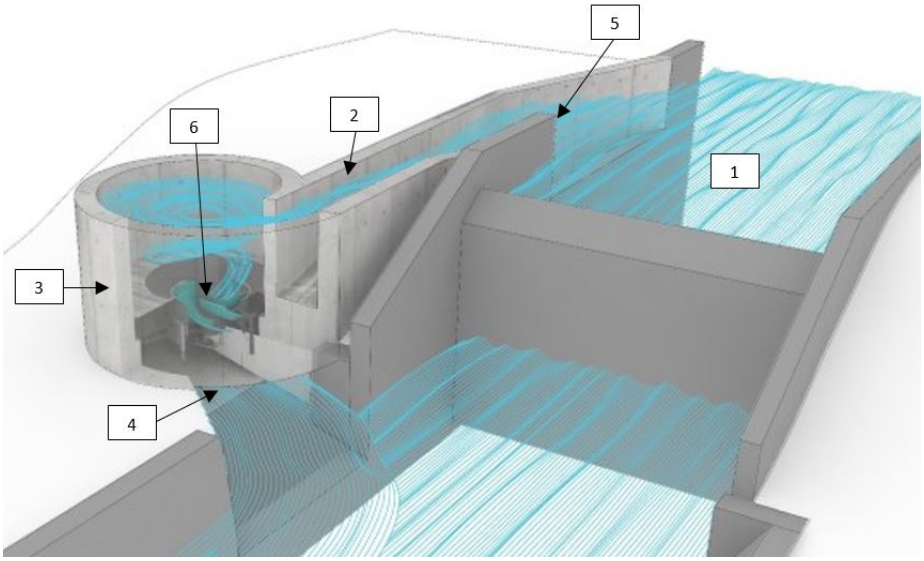

Figure 2: General diagram of a hydroelectric plant with a gravitational water vortex turbine: 1- river, 2- inlet channel, 3- circulation basin, 4- discharge, 5- catchment and 6- runner. Source: Engenhariacivil.com [17]

In the world so far, 20 of such turbines have been installed. Europe is the continent with the most facilities (14), followed by Oceania (3), South America (2) and Asia (1). Table 1 indicates the locations of the GWVHT, their generating power, volume flow rate, head, and efficiency. For the calculation of the available and generated power by the GWVHT systems, the same equations are used as for the calculation of the power of conventional hydraulic

turbines, only a small change is incorporated to calculate the net head H_n. The maximum available power of GWVHT turbine is given by equation 1:

$$P = \rho g Q(H_n - h_1 - h_2 - h_3) \tag{1}$$

where ρ is the density of the fluid, g the gravity, Q the volume flow rate, h_1 is the head loss in the circulation basin, h_2 is the head loss in the inlet channel, and h_3 is the kinetic energy of the outflow [10]. The output generated power by any hydraulic turbine is given by equation 2:

$$P_{out} = T\omega \tag{2}$$

where ω is the angular velocity and T is the torque. The hydraulic efficiency of the vertical axis turbine η is determined by equation 3:

$$\eta = \frac{P_{out}}{P} = \frac{T\omega}{\rho g Q(H - h_1 - h_2 - h_3)} \tag{3}$$

The 20 turbines installed in the world have efficiencies ranging between 17 and 85%, head values between 0.6 and 2.0 m, and output powers between 0.01 and 20 kW [10]. Austria has 10 installations of GWVHT, 4 of these installations have very close generation power, between 4 and 5 kW, with efficiencies of 58% for 4 kW turbines, 60% for the 4.4 kW turbine, and 61% for the 5 kW turbine. These values indicates, at least for this group of turbines, that the greater the power of the system, the greater its efficiency. From the group of 20 installations, the turbine with the highest efficiency (85%) is installed in Indonesia and generates 15 kW. There are two more turbines installed that generate equal power: Switzerland and Chile, they would be expected to have similar efficiencies, but these turbines report efficiencies of only 46 and 57%, respectively. The lowest efficiency turbine (17%) also corresponds to the lowest power turbine 0.01 kW, while the highest power turbine (20 kW) reports an efficiency of 68%. No clear pattern of efficiency behaviour concerning generation capacity is identified.

Table 1
Feature list of GWVHT in the world. Modified from: Timilsina et al. [10].

Location	Head [m]	Flow rate [m^3/s]	Power output [kW]	Efficiency [%]
Austria	1.5	0.9	8.3	63
Austria	0.9	0.7	3.3	53
Austria	1.5	0.5	4.4	60
Austria	1.4	0.5	4.0	58
Austria	1.4	0.5	4.0	58
Austria	1.4	0.6	5.0	61
Austria	1.2	1.2	7.5	53
Austria	1.8	1.0	10.0	57
Austria	1.6	2.0	18.0	57
Austria	1.0	0.9	4.6	52
Germany	1.2	1.5	6.0	51
Switzerland	1.5	1.0	10	68
Switzerland	1.5	2.2	15.0	46
Belgium	2.0	0.25	3.0	61
Australia	0.6	0.11	0.35	54
Australia	0.6	0.01	0.01	17
Australia	0.8	0.05	0.18	49
Perú	1.2	1.02	3.5	29
Chile	1.5	1.8	15.0	57
Indonesia	1.5	1.2	15.0	85

GWVHT has a lower efficiency than conventional turbines. Therefore, research has focused on optimizing the geometry to increase their hydraulic efficiency. Different basins and runners have been used to increase the tangential velocity and form a stable vortex. For the design of the circulation basin and inlet, two geometries are normally used: cylindrical or conical basin both with tangential inlet and with central discharge orifice. These geometries are shown in Figure 3 and 4. For the runner, the original design of Frank Zotlöterer is used: cylindrical runner with a plurality of blades uniformly distributed over the circumference. The studies have been focused on three fields: numerical, numerical-experimental and experimental.

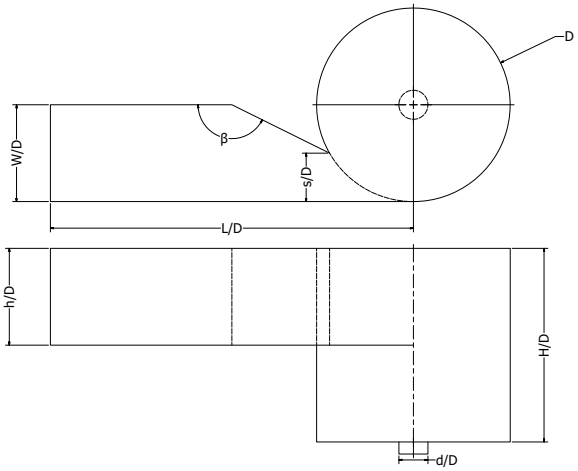

Figure 3: Main dimensions for the cylindrical basin.

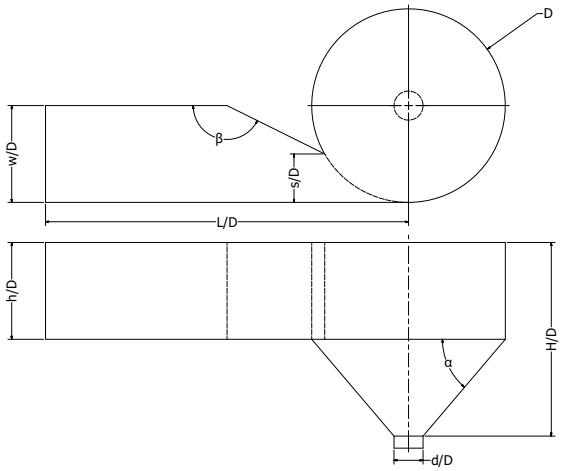

Figure 4: Main dimensions for the conical basin.

2.1. Numerical studies

In 2010, the oldest formal publication on GWVHT was made by Mulligan and Hull [18], who determined the optimal diameter of the discharge orifice for a cylindrical basin. The authors determined that for optimal vortex formation, the diameter of the discharge was between 14 and 18% of the diameter of the basin ($d/D = 0.14 - 0.18$). They also proposed that the vortex height varies linearly with discharge diameter.

Two year later, Marian et al. [19] introduced the use of a conical basin for a GWVHT and determined the effects of basin shape on turbine performance comparing the cylindrical and conical geometries. Marian et al. [19] modelled the

flow of water in the turbine with and without runners. To simulate the flow of water through the basins, they modelled the GWVHT in SolidWorks software. The simulations were developed in Comsol software. For the first case, they did not include the runner; the water flow formed a vortex that extended to the discharge hole. In the second case, the runner was included; in this case, the vortex no longer extended to the discharge because eddies formed near the turbine blades. A helical turbine with multiple stages (installation of two or more runners on the same shaft) was the turbine chosen for this second case of analysis because the authors affirmed that the most indicated turbine to extract the energy of water flow was a helical turbine with hydrofoil profile. Marian et al. [19] concluded that the height of the vortex influences the extraction of the energy from the flow, thus to increase the efficiency in this type of system, it is necessary to maintain the flow regime in which the vortex is extended to the discharge. Figure 5 shows the section through the GWVHT with a helical turbine with multiple stages.

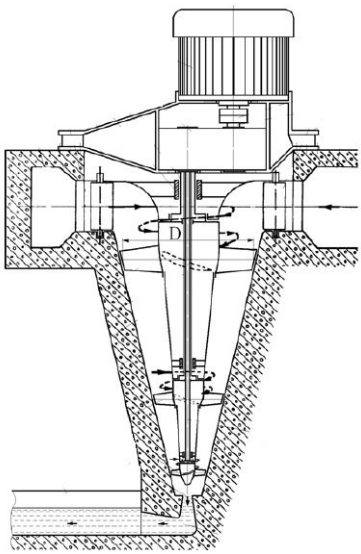

Figure 5: Section through the GWVHT with a helical turbine with multiple stages. Source: Marian et al. [19].

Dhakal et al. [14] studied the effect on conical basin in the vortex formation. They did not include the runner similar to the first study of Marian et al. [19]. For a given volume flow rate and head, the authors changed the diameter (D) and height of the basin (H), and the length (L) and height (h) of the inlet channel. Taking into account the variation in length and height of the channel as study parameters have not been considered until now. Dhakal et al. [14] developed different basin and channel configurations using SolidWorks software and then the models were simulated in ANSYS Fluent. The results showed that there is a dominant effect of basin diameter on the tangential velocity in the vortex, see Figure 6. When the basin diameter increases, the tangential velocity increase until a maximum velocity is reached. The maximum velocity (0.52 m/s) occured when the diameter was 510 cm. After this point, if the basin diameter increases, the velocity decreases. For the channel, they concluded that as its height increases, the tangential velocity also gradually increases until reaching a constant velocity close to 0.5 m/s. The analysis suggests that the diameter of the basin is the most important characteristic that must be taken into account for the design of this type of generation plant since varying the diameter is where the most significant differences in the value of velocity and vortex height are obtained.

Dhakal et al. [20] conducted a study to establish the optimal position of the runner to maximize the output generated power. The study models were designed in SolidWorks software and then exported to ANSYS Fluent, where the computational simulation was performed. The computational models used are shown in Figure 7; the maximum **tangential** velocity was 0.6 m/s for the conical basin and 0.525 m/s for the cylindrical basin. Both velocities were reached at a distance of 0.875 m measured from the surface of the basin, and for the same inlet velocity of 0.1 m/s. The results suggest that conical basin are better than cylindrical ones because higher tangential velocity produces greater output generated power, and that the best position of the runner inside the basin corresponds to a height of between 65-75% of the total height (H) of the basin measured from the top of it.

Sreerag et al. [21] studied the effect of discharge diameter on turbine efficiency as a function of tangential velocity. The computational analysis was executed using ANSYS Fluent 14.5 and allowed to find the tangential and radial

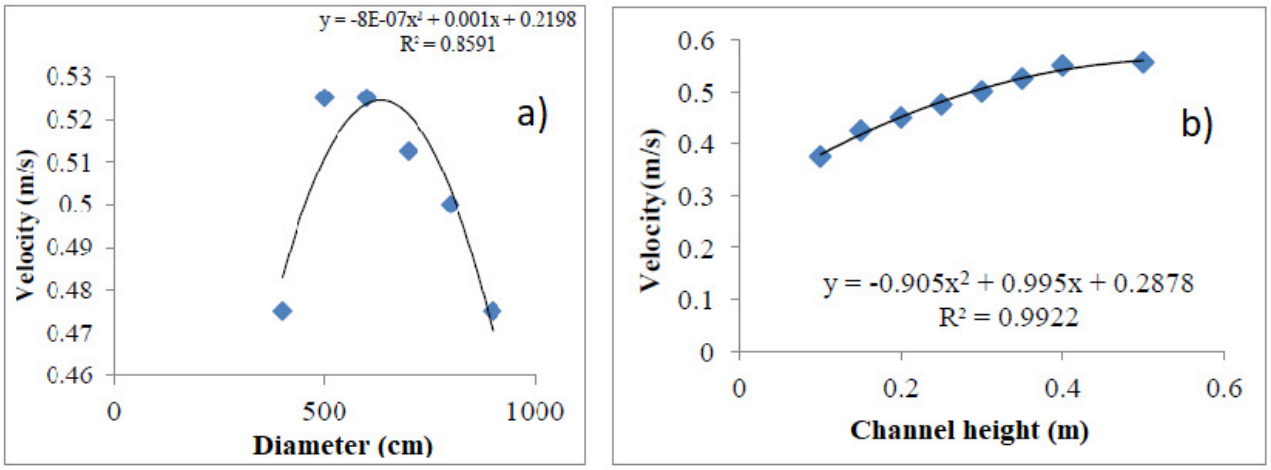

Figure 6: a) Effect of basin diameter vs vortex velocity and b) Effect of channel height vs vortex velocity. Source: Dhakal et al. [14]. Explanatory note: the diameter units in figure a) are cm.

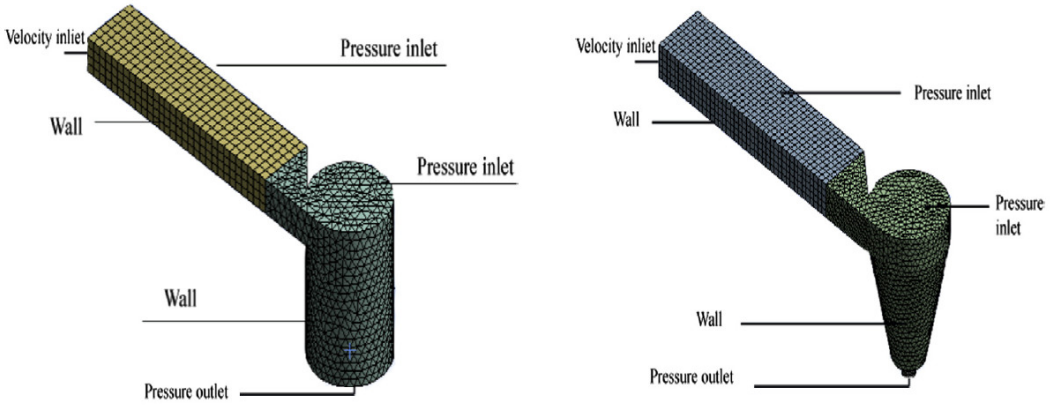

Figure 7: Boundary conditions for cylindrical and conical basins. Source: Dhakal et al. [20].

velocities at different locations within the velocity field. They concluded from the analysis that, for a turbine with a conical basin of 1 m in diameter, 1 m in height and with a cone angle of 14°, a discharge with a diameter of 30% of the diameter of the basin ($d/D = 0.3$) provides the highest tangential velocity and therefore the maximum output power. The ratio between the diameter of the basin and the discharge hole is the double than the ratio proposed by Mulligan and Hull [18].

Chattha et al. [22] investigated different basin design configurations for a GWVHT using CFD with the aim of increasing tangential velocity in the vortex core. For their study, they used a cylindrical basin with a discharge orifice in the centre and varied the diameter of the basin, the diameter of the discharge, and the inlet flow. They found that in order to increase the magnitude of the tangential velocity by up to 15%, it was necessary for a vortex to be generated that went from the free surface of the basin to the discharge orifice. As indicated by Marian et al. [19] in their early investigations. The best way to generate the vortex is to increase the outlet diameter keeping all the other parameters of the basin constant: diameter and height. An increase in the discharge diameter represents an increase in the Froude number, which causes an increase in the value of the critical immersion. When the critical immersion increases, there is a greater tendency towards the formation of the vortex.

Thapa et al. [23] studied the effect of the inlet channel on vortex formation in a GWVHT. ANSYS Fluent was used for numerical analysis. In the experiment, 4 input geometries were taken for the channel: triangular, rectangular, circular, and curved, Figure 9, these figures are viewed from the top. Their study showed that the vortex formed by the use of an entrance channel with triangular geometry is more efficient since it tends to produce a very symmetrical vortex pattern which causes a smaller radial force. Radial steering forces are responsible for creating bending moments

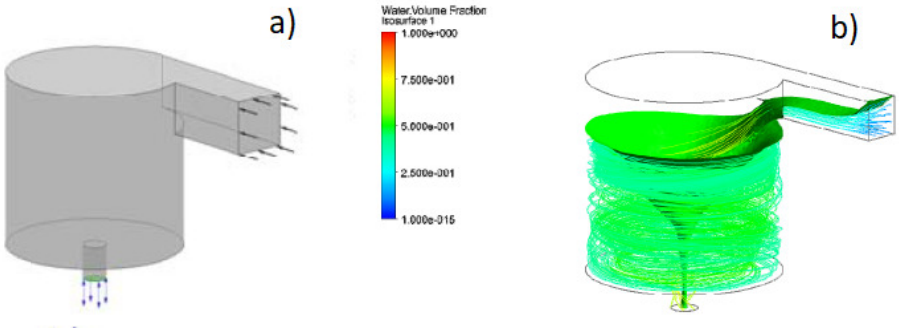

Figure 8: a) Reference geometry initially used for analysis and b) Vortex flow lines formed in the optimized basin. Source: Chattha et al. [22].

on the turbine shaft, reducing the efficiency of the turbine. The study also showed that the rectangular inlet channel produces symmetrical but very high-pressure distribution, implying that the rectangular inlet geometry can be effective on low heads, but can cause turbine shaft failure in heads of magnitude superior due to the generation of unexpected bending moments on the shaft. This was the first investigation to study other geometries for the inlet channel, as previous studies always used rectangular geometries and tried to optimize its dimensions: height (h), width (w), and length (L)).

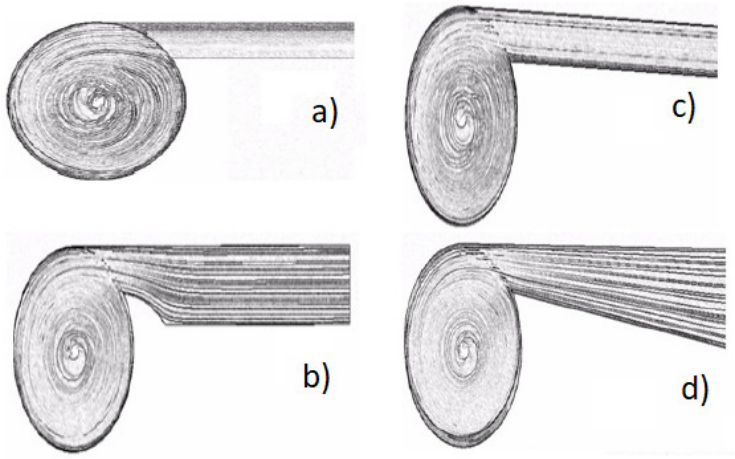

Figure 9: a) Channel with circular geometry, b) Channel with curved geometry, c) Channel with rectangular geometry, and d) Channel with triangular geometry. Source: Thapa et al. [23].

Rehman et al. [24] studied three types of tangential inlet channel: horizontal channel, 30° and 60° inclined channel using a conical basin, see Figure 10. The results show that the highest tangential velocity was achieved when the channel was inclined 60°. That increase in velocity can be attributed to the change of potential head to dynamic head. For the simulations, the ANSYS Fluent software was used, using a constant water entry velocity in each model of 3 m/s. The authors did not elaborate on the simulation settings.

Khan et al. [25] studied the effects of basin diameter (0.4–0.8 m), discharge to basin diameter ratio d/D (0.13–0.17), basin height to diameter ratio H/D (0.5–1.5), inlet channel width ratio w/D (0.1–0.5), inlet channel depth ratio h/D (0.1–0.5), and inlet velocity (0.1–0.6 m/s) on vortex formation and tangential velocities. They used ANSYS CFX to discretize the governing equations using a finite-volume approach. The results show that the configuration with a fully developed air core is the most suitable for increasing the efficiency of the system. When a basin with a large diameter is used, the vortex height decreases. An increase of w/D increases the mass flow, which causes the water height to rise until overflow from the upper walls of the basin occurs. Increasing the ratio d/D allows more water to flow out of the basin; therefore, a reduction in the vortex height in the basin was observed.

Wardhana et al. [26] analysed the behaviour of propeller type impellers when positioned in GWVHT systems.

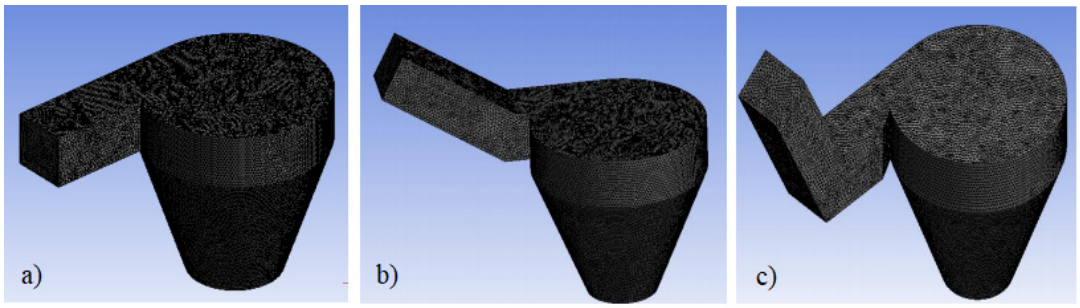

Figure 10: Model with inlet rectangular passage of: a) 0°, b) 30° and c) 60° . Source: Rehman et al. [24].

They made variations in the shape and length of the blade chord, as well as in the number of blades, see Figure 11. The results suggest that the number of blades are inversely proportional to the efficiency; they also concluded that the shape of the blades is more efficient when twisted and they selected the rotors with 3 blades as the most efficients of their study, with an efficiency of 54.4%.

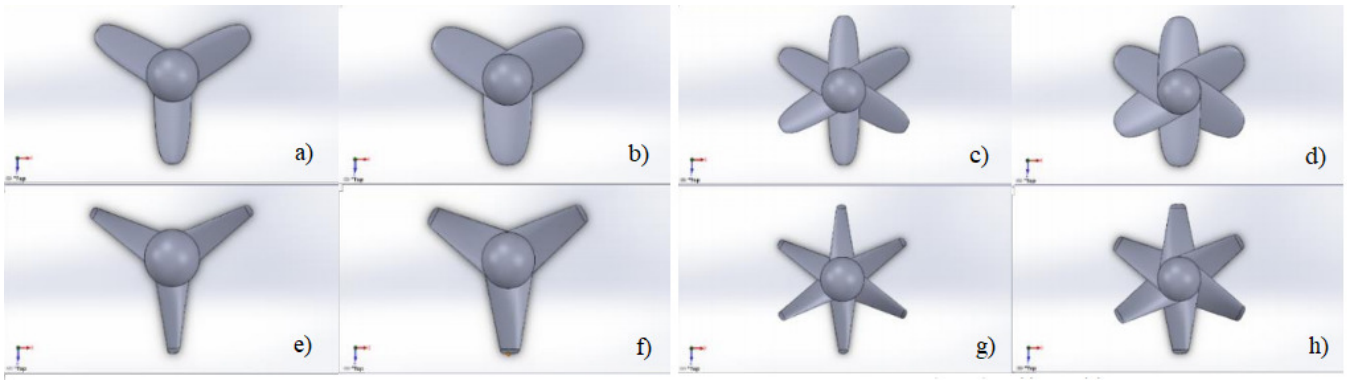

Figure 11: Turbine Models. Source: Wardhana et al. [26].

Havaldar et al. [27] compared two geometries for tangential inlet channel to GWVHT: straight and curve, see figure 12. The models were made in SolidWorks. The meshing and simulations were done in ANSYS Fluent. They found that the average velocity in curve inlet channel was greater than that of the Straight inlet channel. A greater velocity implies that energy extraction could be greater. The authors did not elaborate on the simulation settings.

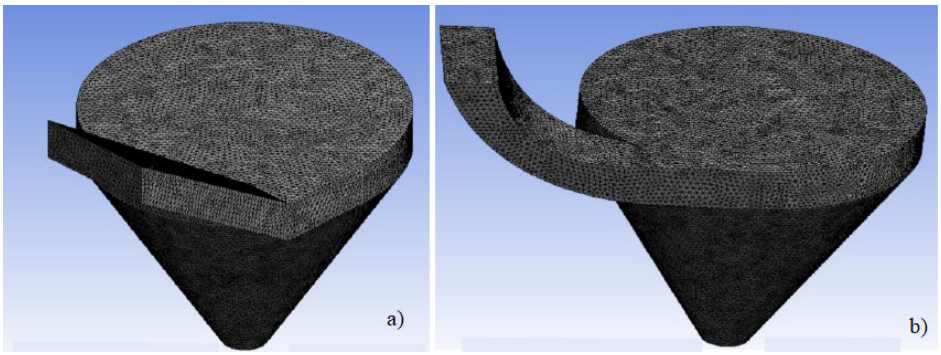

Figure 12: Inlet channel Models. Source: Havaldar et al. [27].

Two inlet channels and two basin geometries of a GVWH were analysed in Ansys Fluent software by Velásquez et al. [28]. The velocity and vortex height were calculated and compared for four geometries: (I) cylindrical basin with

a tangential inlet channel, (II) cylindrical basin with a wrap-around inlet channel, (III) conical basin with a tangential inlet channel and (IV) conical basin with a wrap-around inlet channel. This was the first study where two different geometries connection for the inlet channel were compared: a regular tangential inlet channel and a wrap-around inlet channel, see Fig. 13a). For the simulation, the VOF method was implemented with k-ϵ as a turbulence model. For the whole set of models was used a inlet velocity of 0.1 m/s. The results suggests that the conical basin is better than the cylindrical because conical basin produced more symmetric vortex in comparisons with that generated by the cylindrical geometry. Geometry (d) provided the largest value for tangential velocity (1.55 m/s) when the radius was 0.22 m, see Fig. 13b). Knowing the location of the highest velocity allow identifying the rotor installation point, where a greater extraction of energy from the flow is possible.

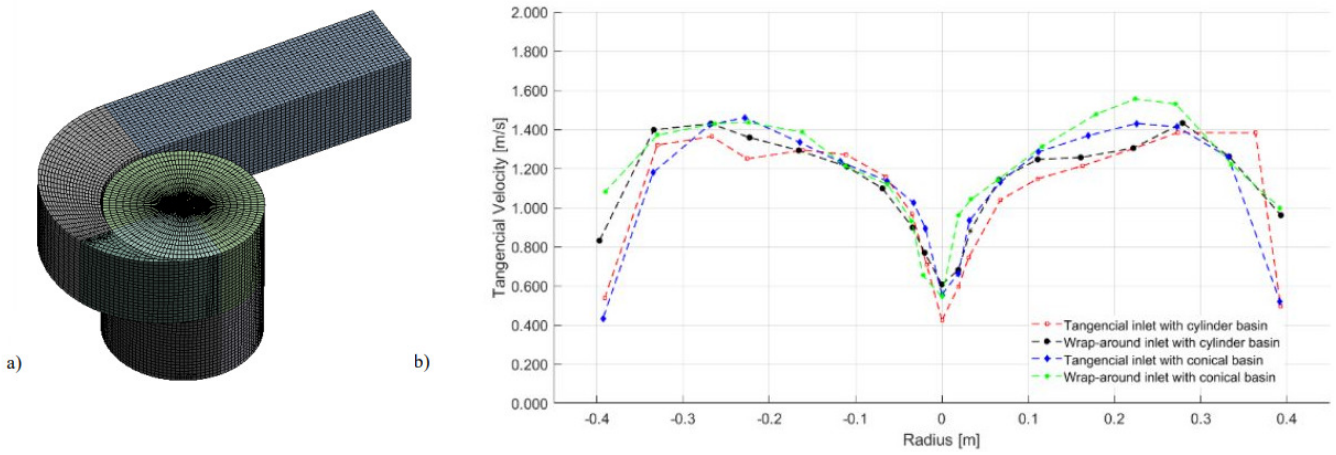

Figure 13: a) Wrap-around inlet with cylindrical basin and b) Tangential velocity distribution Source: Velásquez et al. [28].

2.2. Experimental studies

Dhakal et al. [29] designed, manufactured, and tested 3, 6, and 12 blade runners for a GWVHT. The runners were tested in cylindrical and conical basins to compare the efficiency of the runners in both types of setups. For the cylindrical basin, 12 tests were carried out by changing the runners and their position in the basin. Like the study of Marian et al. [30], Dhakal et al. [29] indicated that the best position for the placement of the turbine is the lowest position, that is, the position closest to the discharge, since it is where the vortex has the highest velocity. They also found that the efficiency values were higher for runners with fewer blades. For the conical basin, with 12 blade runner were carried out. The tests provided a maximum efficiency of 29.63% for the position closest to the discharge, this efficiency was significantly higher than the efficiency obtained by all the cylindrical basin tests, which allows us to infer that conical basins are more efficient than cylindrical, which might be due to higher vortex height. Since the 3 and 6 blade runners were not evaluated in the conical basin, it is not possible to extend the statement made for cylindrical basins that fewer blades provide greater efficiency.

Using two materials for the runner blades: stainless steel and aluminium, Sritram et al. [31] studied the effect on the energy generation efficiency of the GWVHT. Two impellers of 5 curved blades vertically arranged 45 cm wide and 32 cm high were manufactured. These turbines were manufactured and tested in the laboratory with a volume flow rate of 3.63, 2.96, 2.31,1.61,1.33 and 0.68 m^3/min and an electrical load of 100, 80, 60, 40, 20 W, respectively. The electrical load consisted of 5 incandescent light bulbs of 20 W each. The results showed that the maximum efficiency of the aluminium and steel was 34.79% and 33.56%, respectively. Figure 14 shows the efficiency values at different loads for both materials. For the maximum flow rate, it was found that the momentum value and the electricity production of the aluminium turbine were higher than that of the steel turbine. This result showed that the lightweight of the turbine increase the momentum and efficiency. Sritram et al. [31] were the first to evaluate different materials for the construction of the runner.

To determine the best-operating conditions for a GWVHT, Power et al. [32] carried out an experimental investigation. They tested different flow rates, blade sizes, and numbers, and recorded the turbine rotation velocity and the

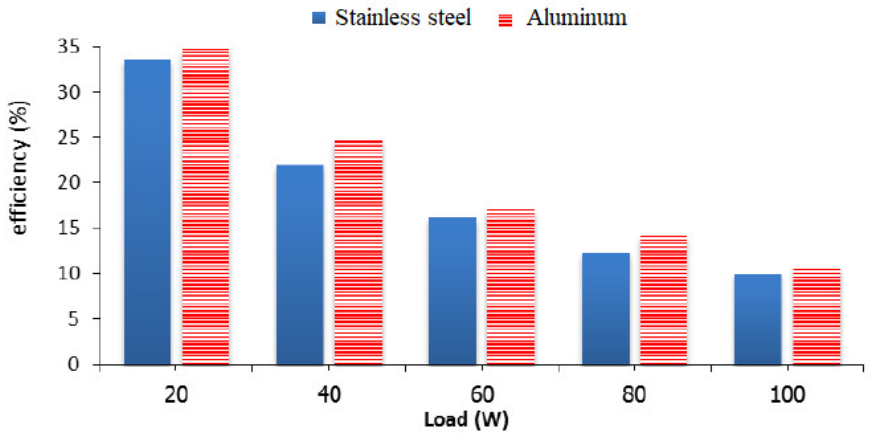

Figure 14: Efficiency of the turbines for a water flow of 3.63 m^3/min. Source: Sritram et al. [31].

vortex height for each configuration. The input and output power, and efficiency were compared for the tests. The turbine used consisted of a cylindrical basin, 0.7 m height, and 0.5 m in diameter, with a central outlet hole of 0.025 m. The model and dimensions of the blades are shown in Figure 15. Turbines with 2 and 4 flat blades with different widths, heights, and thicknesses were tested. Power et al. [32] reported a maximum efficiency of 15.1% for a flow of 0.65 L/s and head of 0.9 m for the configuration of 4 blades with the blade with the largest surface area, this indicates that the efficiency increased with the increasing number of blades from 2 to 4. This conclusion contradicts what was said by Dhakal et al. [29], who indicated that fewer blades in cylindrical basins increase efficiency. The opposing findings indicate that there could be an optimal number of blades for the turbine, and further studies are required to determine it.

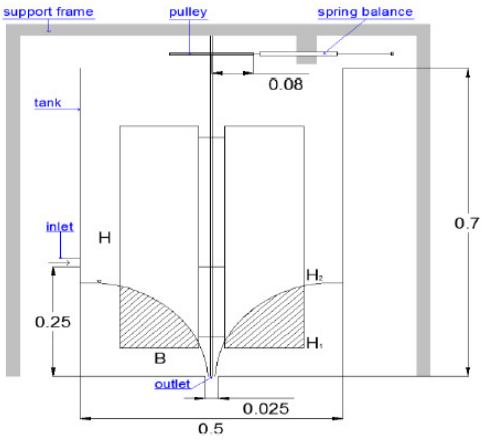

Label	Blade number	H (mm)	B (mm)	W (mm)
I	2	500	150	2
II	4	500	150	2
III	2	500	150	1.5
IV	2	500	75	1.5
V	4	500	75	1.5
VI	2	500	200	1.5
VII	2	250	150	1.5
VIII	4	250	150	1.5
IX	2	250	100	1.5

Figure 15: a) Schematic diagram of the laboratory model and) Configurations of the turbine blades. Source: Power et al. [32].

Ayala et al. [33] designed and implemented an electric power generation system based on a GWVHT with a siphon in Loja-Ecuador. The system works as a flow station and due to its design, it can be installed directly in irrigation channels or rivers, without major civil works. The generation unit called UTG (*Underwater Turbine Generator*) is made up of a Kaplan turbine, a cylindrical basin, and a siphon evacuation to gain potential energy. According to the results of the field measurement, the UTG system with an input flow rate of 0.05 m^3/s and a head of 1.0 m, has a generation capacity of 150 W and can supply electrical energy stable to connected loads with a plant factor of 60%.

The effects of water pressure and the length and number of blades on a runner for a GWVHT were studied experimentally by Rahman et al. [4]. To determine optimal efficiency they designed and tested a cylindrical basin vortex

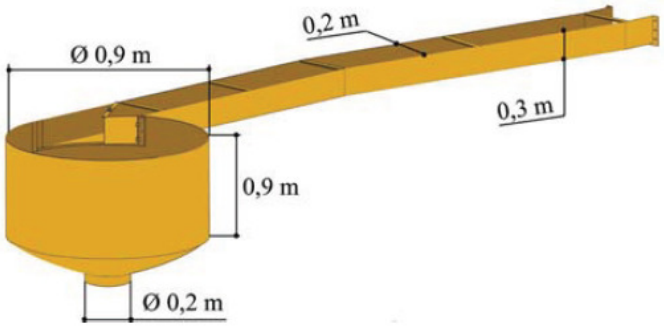

Figure 16: Basic diagram of the UTG generation plant for the province of Loja-Ecuador. Source: Ayala et al. [33].

power generation system with 3 and 6 blade runners, see Figure 17. Experimental results revealed that the tangential velocity of the vortex was highest for a 0.12 m head and the maximum efficiency, achieved with the 3 blade runner and an outlet diameter of 0.027 m, was 43%. They also found that the maximum velocity of rotation does not generate the highest efficiency. This research supports the conclusion of Dhakal et al. [29], a runner with fewer blades is more efficient.

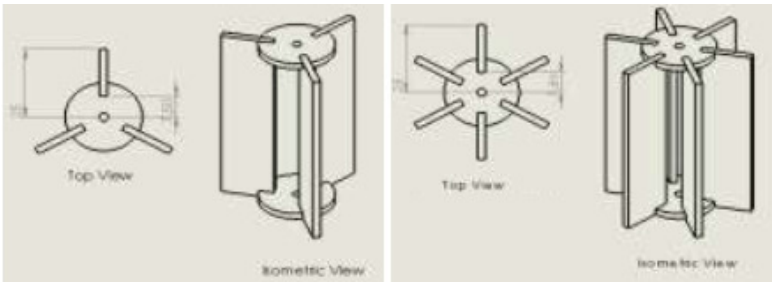

Figure 17: Runners for a gravitational vortex generation system. Source: Rahman et al. [4].

Wichian and Suntivarakorn [34] experimentally analysed the effects on the efficiency of the installation of baffle plates at the bottom and top of the runner blades for a GWVHT. A baffle plate is a metal plate used to direct or restrain the flow of a fluid. For the study, they used a cylindrical basin plant of 1 m in diameter and 1 m high. The flow of water between 0.04-0.06 m^3/s exited through a central hole at the base of the 0.2 m diameter basin. 5 models of 5-blade runners with deflector plates were tested, see Figure 18. The proportion of the plates was 0, 25, 50, 75, and 100%, in relation to the total area of the blades. Model 3, with a ratio of 50 %, was the model that produced the highest torque, increasing efficiency by 4.12% and torque by 10.25%, compared to the model without plates deflectors that generated an average torque of 33.93 Nm and an efficiency of 31.49%. A large baffle plate, 75, and 100% ratio, produces too much inertia and significantly reduces torque and efficiency.

The influences of the rotation velocity and the shape of the blades on the performance of a GWVHT were investigated by Kueh et al. [35]. Two turbines with curved and flat blades were compared. The turbines showed a similar rotation velocity under no-load conditions, suggesting that the circulating force of the vortex has a more dominant effect on the rotation velocity of the turbine, compared to the geometry of the turbine. The turbine with flat blade had a maximum efficiency of 21.63% at 3.27 rad/s, while the turbine with curved blade showed 22.24% at 3.56 rad/s. Both test used a head of 5 m and a mass flow of 15 kg/s. When the load is applied, the curved shape of the blades helps to reduce disturbance in the vortex and therefore provides better performance. The runners used in the study had 4 blades, see Figure 19.

Rahman et al. [36] used a laboratory scale GWVHT to estimate the effect of the inlet flow rates and inlet channel geometry (penstock) in the efficiency. With flow rates increased from 5.6 m^3/h to 8.8 m^3/h, and changing the values of L and S of the inlet channel, they found that the efficiency increased polynomial, see Figure 20, in each case of study. The performance of turbine with Penstock D, E and F was similar. This means that the length of channel, L, have no effects on the efficiency. S have significant effects on the performance of GWVHT especially when it increases.

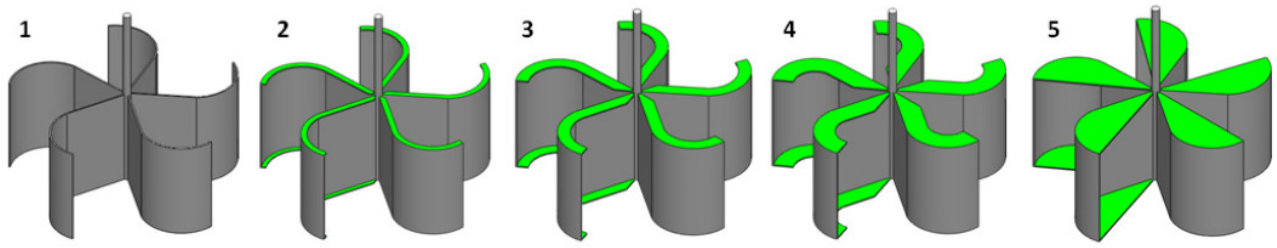

Figure 18: Runners with deflector plates. Source: Wichian and Suntivarakorn [34].

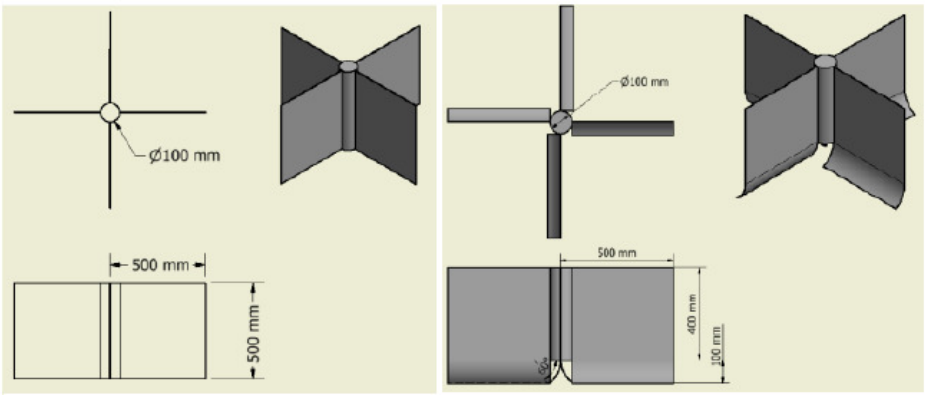

Figure 19: Runner dimensions. Source: Kueh et al. [35].

Penstock B and C with 0.065 m and 0.090 m, respectively, reported lowest efficiency. Reducing the value of S will increase the tangential velocity, hence increasing the power output and improving the efficiency.

a)

Inlet channel	L (m)	S (m)
A	0.513	0.040
B	0.513	0.065
C	0.513	0.090
D	0.385	0.040
E	0.257	0.040
F	0.128	0.040

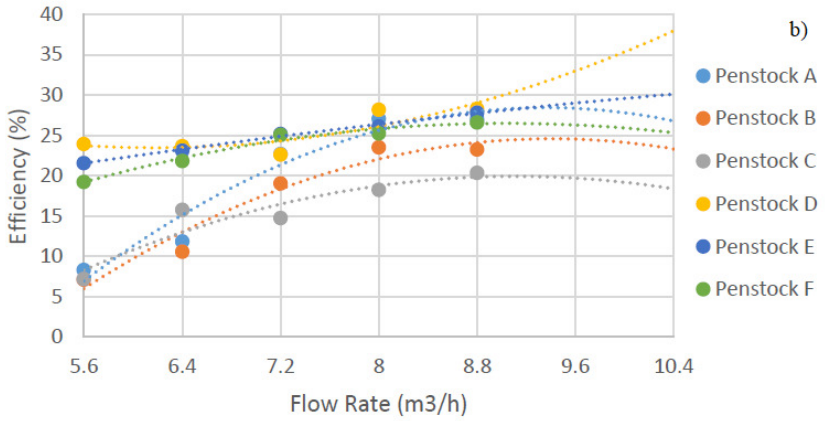

Figure 20: a) Inlet channel dimensions and b) Efficiency with different inlet channel geometries. Source: Rahman et al. [36].

Srihari et al. [37] studied 5 types of conical basins with vortex intensifying nozzles. These nozzles are highlighted in a red box in Figure 21a). The results indicated that the turbine with 6 vortex intensifiers of 50 mm diameter separated 150 mm from the upper surface of the basin presented an increase in output power of 54.42 %, which represents an increase in efficiency 54.41%, with respect to the turbine studied by Dhakal et al. [20]. The intensifier nozzles strengthen the formation of the vortex and therefore increase the efficiency of the turbine.

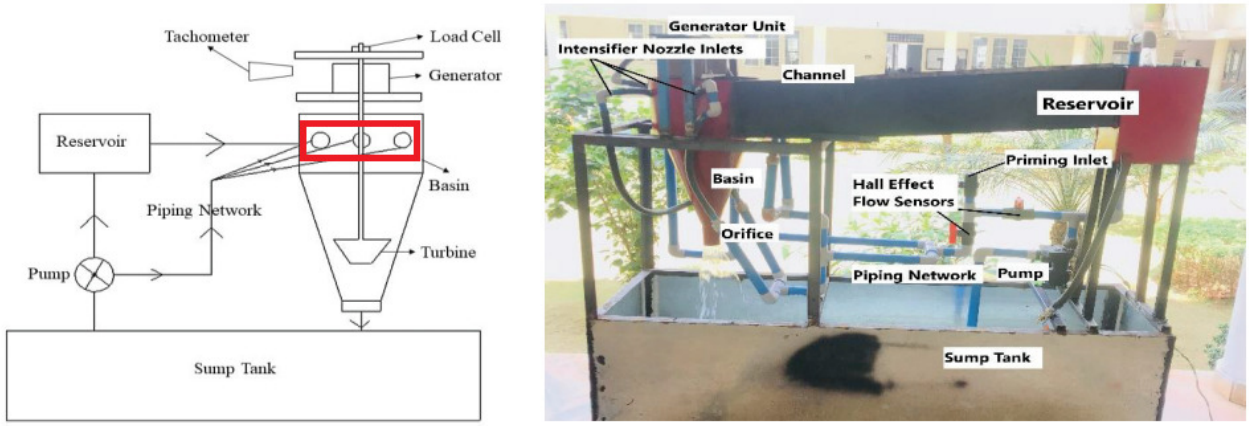

Figure 21: Gravitational water vortex turbine: a) Schematic of experimental setup and b) Fabricated experimental setup. Source: Srihari et al. [37].

Ullah et al. [38] studied the performance of a multi-stage GWVHT with conical basin. Each stages are show in Figure 22. Rotational velocity, momentum, and efficiency were evaluated under different load conditions. The authors found that runners with tilted blades are best suited for the position near the bottom of the discharge, while cross-flow blades are recommended in the top position.

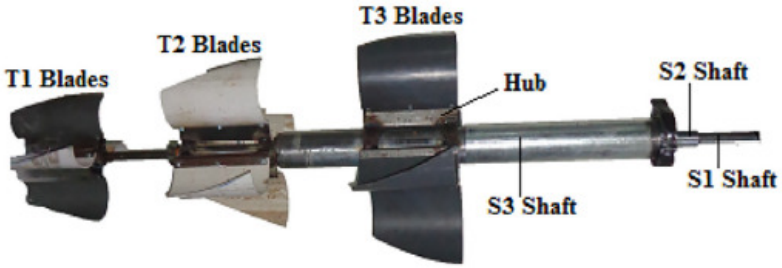

Figure 22: Experimental setup. Source: Ullah et al. [38].

2.3. Numerical and experimental studies

Continuing the numerical study of Marian et al. [19], Marian et al. [30] experimentally investigated the characteristics of the vortex in the presence of runners through a conical basin. The experimental set-up was carried out using two tanks that were connected through a closed circuit of pipes provided with a pump. Four basins with differents height (H = 0.1, 0.15, 0.2 and 0.25 m) were tested with cone angles (α) of 54.04°, 37.56 °, 28.61° and 23.06°, respectively, all with a basin diameter D of 0.12 m and an discharge diameter d of 0.018 m. In these basins and at different depths, 3 turbines with 4 flat blades were installed, see Figure 23. The highest recorded efficiency was obtained when the turbine was located as close as possible to the basin drain hole. Changes in the cone angle α of the basin allowed to identify that an increase in the angle decreases the outflow, which could generate a fluid overflow through the basin if the flow that enters through the channel is higher than the flow that comes out.

In turn, Wanchat et al. [39] performed a numerical and experimental study to find out how the diameter of the discharge, the inlet flow, and the height of the vortex affected the velocity field inside the basin. Flow behaviour was simulated using ANSYS software. The SIMPLE method for the pressure and velocity coupling was adopted to discretize and solve the Navier-Stokes equations. The model used for the simulation was a cylindrical basin with 1 m in diameter and a 1 m in height, with a discharge of variable diameter ($0.1 < d < 0.4$ m). A velocity of 0.1 m/s was imposed as a condition of entry into the system. Experimental and theoretical models showed that for outlet diameters less than 0.2 m, the angular momentum of the vortex was not enough to generate rotation in the turbine because the

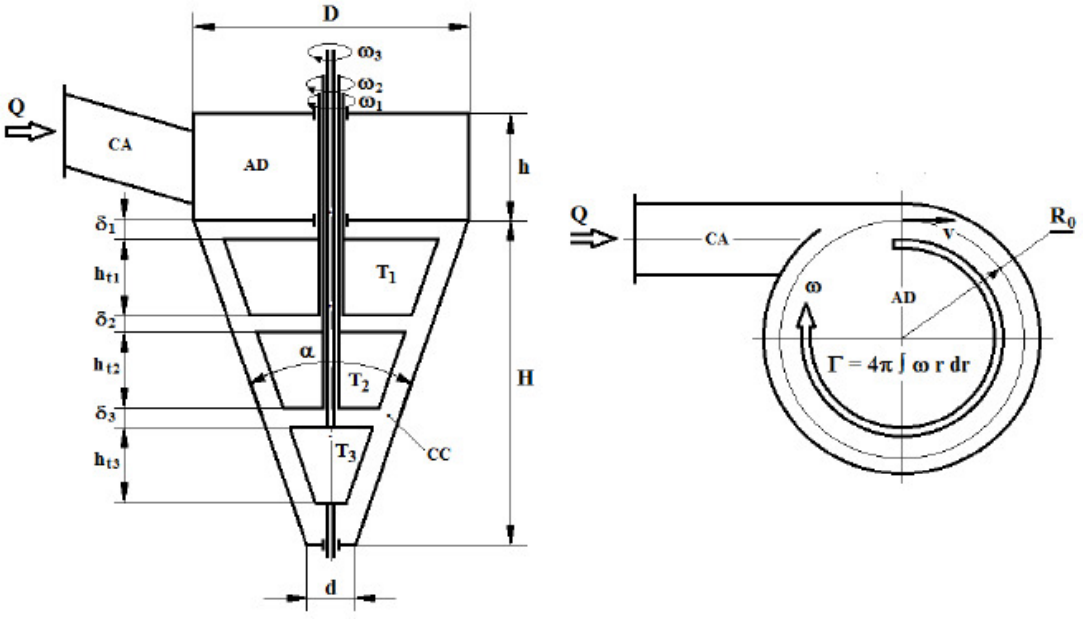

Figure 23: Schematic diagram of a gravitational water vortex generation plant. Source: Marian et al. [30].

water entering the system was greater than the water leaving. On the other hand, when the outlet diameter was equal to or greater than 0.4 m, the vortex height was very low and it also failed to generate enough torque to move the runner. The maximum output power was 60 W for a model with an output diameter of 0.2 m that reached an efficiency of 30%. This diameter corresponds to 20% of the basin diameter. This value of 20% for the relationship between the outlet diameter and the basin diameter is outside the range suggested by Mulligan and Hull [18]. Unlike the study by Marian et al. [19], this research did not include the effects of the runner in the velocity field, but despite this, they also concluded that the vortex height is a determining parameter for power generation.

Two configurations with different discharge diameters were studied numerically and experimentally by Kueh et al. [40]. The basin used for both configurations was a cylindrical basin with a tangential inlet channel. The XFlow 2013 Build 90 software that uses a Lagrangian approach to solve the Navier-Stokes equations was used for the numerical study. It was found that for the smallest diameter configuration ($d = 0.02$ m), the height of the generated vortex was the same in the experimental and numerical model; while for the larger diameter model ($d = 0.025$ m), there were significant differences in vortex height between both models. Having a very large outlet diameter implies greater turbulence, which generates greater errors in the computational solution. The adequate selection of the turbulence models would allow finding a numerical solution that reliably reflects the behaviour of the phenomenon.

Using computational fluid dynamics (CFD), Shabara et al. [41] optimized a system with a GWVHTS. ANSYS Fluent 14.0 was used to simulate the flow in the turbine. The designed cylindrical basin had a heigth of 100 cm, a diameter of 100 cm and a discharge orifice of 20 cm. The runner effect was included in the analysis, and for this purpose, an 8 curved blade runner was designed. Additionally, an experimental test platform was established to carry out the validation of the computational results. The results showed that the maximum efficiency of approximately 40% occurs when the turbine rotates with a velocity between 28 and 38 rpm. The numerical results were similar to the experimental results, which validates the computational model. The position of the runner within the basin is not specified in this study.

Gautam et al. [43] numerically and experimentally studied the effect on generation efficiency of the addition of a second runner (multiple stages) in a GWVHT with conical basin, just as Marian et al. [19] did in their research. For this study, 3- and 6-blade runners were designed. For numerical analysis, the flow domain was modelled in CATIA software followed by domain and solution discretization in ANSYS Fluent 16.2. The solution procedure was based on three-dimensional steady state simulations. During the analysis process, the dimensions of the basin, the channel, the main runner and the location of the secondary runners were the same for the three case studies. Gautam et al. [43] reported an efficiency of 78.65% for a turbine with Type III secondary runner, see Figure 25, representing an increase

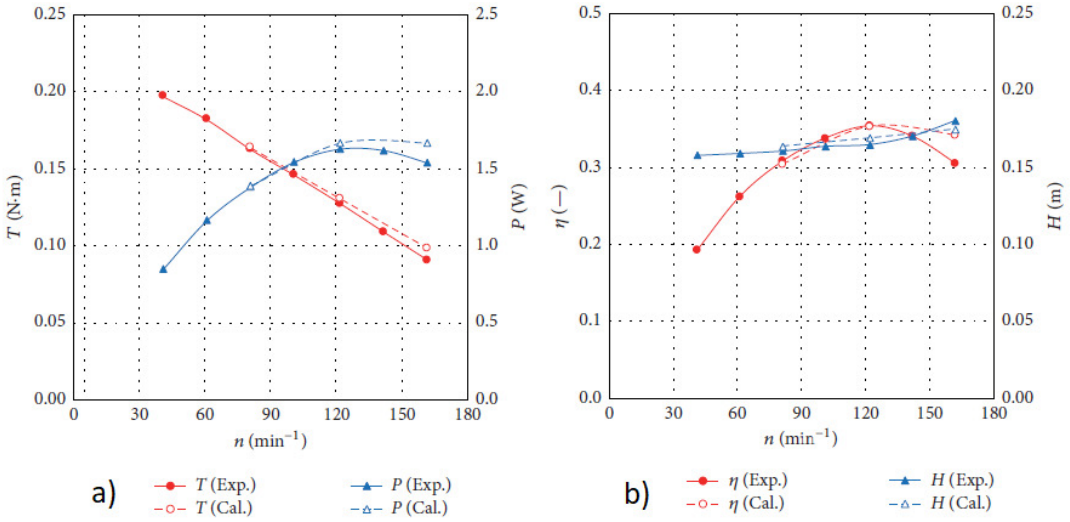

Figure 24: Turbine performance: a) Torque and power vs rotation velocity and b) Efficiency and effective head vs rotation velocity. Source: Nishi and Inagaki [42].

in efficiency of approximately 6% compared to a single runner turbine. To calculate the efficiency of the system, the authors used a brake drum dynamo-meter, a digital tachometer and a current meter is for measuring the flow velocity of water in inlet channel, which was in turn used for the calculation of flow rate. The results of this investigation do not specify the shape or number of blades of the main runner.

Figure 25: Runners. Source: Gautam et al. [43].

Nishi and Inagaki [42] predicted the efficiency of a GWVHT considering the turbulence models, the number of mesh elements, the governing equations, the type of analysis, and the boundary conditions. The authors established that a transient analysis is required. The governing equations (mass and momentum conservation equations) are discretized by the finite volume method (FVM) using ANSYS CFX 15.0. They used the volume of fluid method (VOF), which is a method that allows simulating the behaviour of a flow that has a clear interface between two phases. Water and air were the working fluids. Regarding the turbulence model, the shear stress transport model (SST) was selected, since they considered that it can model the real performance of the turbine using the VOF method. Its final mesh had 2.2×10^6 elements. The boundary conditions stablished were: mass flow at the inlet, relative static pressure of 0 Pa on the upper surfaces of the basin and the inlet channel, non-slip condition for the walls, and outlet pressure at the discharge hole. They made experiments in a test bench using a cylindrical basin with a 490 mm of diameter, a discharge of 100 mm of diameter and a turbine with 20 blade. The runner geometry resembles the runner geometry of a cross-flow turbine. Their numerical and computational results showed that the methodology selected for the simulation was correct, since the experimental and computational values of momentum and efficiency coincided with each other, see Figure 24.

Dhakal et al. [44] carried out an experimental and computational investigation of a runner for a GWVHT using a conical basin. This study focused on optimizing the runner to improve system efficiency. CFD analysis was executed on 3 runner with curved, twisted, and straight blade profiles, all with 6 blades, see Figure 26. ANSYS CFX was used to analyze fluid flow through the turbine. Numerical analysis showed that the curved blade profile, obtained the

maximum efficiency (82%), is the most efficient profile, follow by the twisted blade, 63%, and the runner with straight blades with 46%. The experimental analysis was carried out with the best of the runners found in the numerical study. Using a volume flow rate of 0.004 m^3/s and 0.5 m of head, the maximum efficiency was 71%, 9% less that the predicted by the numerical analysis. The difference between the experimental tests and the computational analysis was mainly attributed to mechanical losses and leakages, the non-ideal construction of the channel, the friction of the basin surface with the fluid, and the increase in the rotation velocity of the turbine. This research is the one that reports the highest efficiency value so far reached.

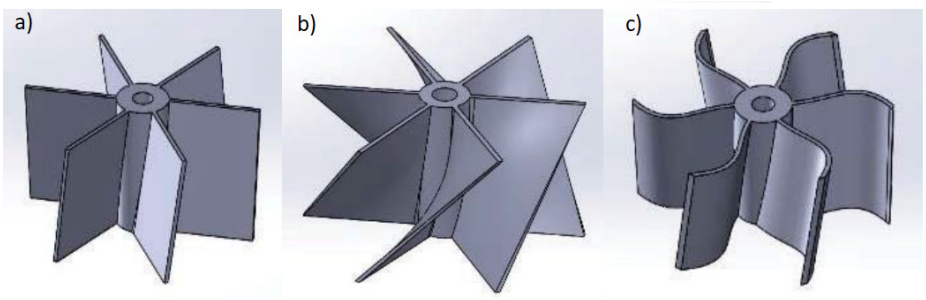

Figure 26: Runners: a) straight blades, b) twisted blades and c) curved blades. Source: Dhakal et al. [44].

The most recent numerical and experimental investigation about GWVHT was made by Nishi et al. [45]. The authors conducted a numerical and experimental study using a cylindrical basin with a diameter of 490 mm and a discharge orifice with a diameter of 100 mm. For numerical analysis, they used ANSYS CFX15.0 and implemented the VOF method. The authors executed a 3D unsteady flow analysis. They found that the net head and the turbine efficiency increased as the volume flow rate increased. Figure 27a shows the experimental apparatus and Figure 27b shows the comparison between numerical and experimental values of the efficiency. The highest efficiency was 55% when the volume flow rate and net head were 0.00379 m^3/s and 0.16 m, respectively. The highest efficiency represented an increase of 5.3%. Although the authors concluded that increasing the volume flow rate increases the efficiency. There must be a limit to the increase in volume flow rate. An excess flow could prevent proper vortex formation or cause flow spillage.

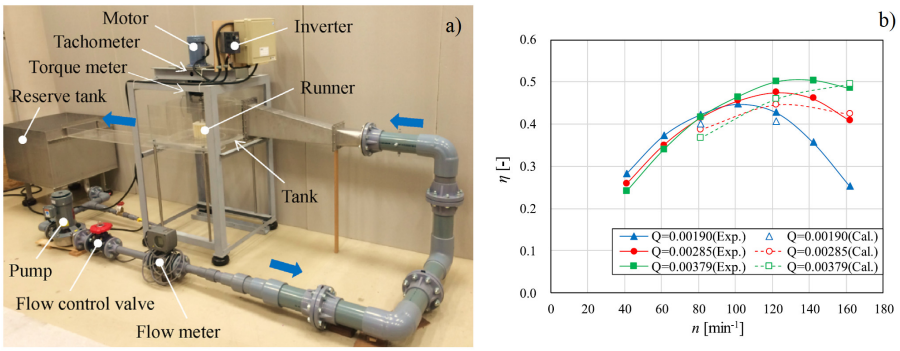

Figure 27: a) Experimental apparatus and b) Turbine efficiency. Volume flow rate Q are expressed in m^3/s. Source: Nishi et al. [45].

2.4. Summary of researches done

Tables 2, 3 and 4 show the summary of the numerical and experimental studies around the GWVHT carried out to date. The tables highlight the type of investigation, whether or not a runner is used, the type of basin and the main findings. Table 5 shows only the numerical studies and they make a brief count of the parameters used to carry out the simulations such as the computational models used, the turbulence model, and the solution schemes.

Table 2
Numerical and experimental investigations and their main findings.

Author(s)	Method	With or without runner / Type of basin	Results
Mulligan and Hull [18]	Numerical	With runner / Cylindrical basin	Optimal vortex formation when outlet diameter is 14-18% of the basin diameter
Wanchat et al. [39]	Numerical and experimental	Without runner/ Cylindrical basin	Maximum efficiency of 30% when outlet diameter is 20% of basin diameter
Marian et al. [19]	Numerical	With and without runner / Conical basin	To increase efficiency is necesary to keep the flow regime in which the vortex extending up to the output section
Marian et al. [30]	Experimental	With runner/ Conical basin	The turbine draws more energy near the outlet where the higher tangential velocities are
Dhakal et al. [29]	Experimental	With runner/ Cylindrical and Conical basin	Efficiency increases with decreasing number of blades. The turbine draws more energy near the outlet
Sreerag et al. [21]	Numerical	without runner / Conical basin	As the basin diameter increases, the velocity of the vortex decreases
Dhakal et al. [14]	Numerical	without runner / Conical basin	The maximum velocity (0.52 m/s) occured when D was 0.51 m. Outlet diameter was within the range of 14% to 18% of D.
Kueh et al. [40]	Numerical and experimental	without runner / Conical basin	As the discharge hole is getting larger, flow is more turbulent and causes more errors in the CFD model
Dhakal et al. [20]	Numerical	With runner / Cylindrical and Conical basin	The optimum position of the turbine is 65% to 75% of the height of the chamber (from the top). The Conical basin has a higher power output than the Cylindrical basin
Shabara et al. [41]	Numerical	With runner / Cylindrical basin	Maximum efficiency 40% when d/D was 0.2. Ideal rotation velocity 28-38 rpm.
Power et al. [32]	Experimental	With runner / Cylindrical basin	Efficiency increases with increasing number of blades. Turbines with 2 and 4 flat blades were tested.
Sritram et al. [31]	Experimental	With runner / Cylindrical basin	Maximum efficiency 35%. Aluminium runner
Ayala et al. [33]	Experimental	With runner / Cylindrical basin	Generation power 60 W with a plant factor of 60%

Table 3
Numerical and experimental investigations and their main findings.

Author(s)	Method	With or without runner / Type of basin	Results
Gautam et al. [43]	Numerical and experimental	With runner / Conical basin	Maximum efficiency 78.65% for 6-blade secondary runners. They do not specify the shape or number of blades of the main runner
Rahman et al. [4]	Experimental	With runner / Cylindrical basin	Maximum efficiency 43%. Efficiency increases with decreasing number of blades
Wichian and Suntivarakorn [34]	Experimental	With runner / Cylindrical basin	Maximum efficiency 32.5% with deflector plate of 50% of the total area of the blades
Chattha et al. [22]	Numerical	without runner / Cylindrical basin	Efficiency increases when the vortex originates from the conical surface to the exit hole
Nishi and Inagaki [42]	Numerical and experimental	With runner / Cylindrical basin	The shear stress transport model (SST) is the turbulence model that best predicts the real performance of the turbine using the VOF method
Kueh et al. [35]	Experimental	With runner/ Cylindrical basin	Maximum efficiency 22.24% with curved blades
Thapa et al. [23]	Numerical	without runner / Cylindrical basin	Triangular inlet channel (viewed from the top) is the most efficient because it tends to produce very symmetric vortex which causes less imbalance radial force that are responsible for the bending for turbine shaft
Dhakal et al. [44]	Numerical	With runner / Conical basin	Maximum efficiency 82% for curved blade runner
Rehman et al. [24]	Numerical	Without runner / Conical basin	The highest velocity was achieved when the channel was inclined 60° downward
Srihari et al. [37]	Numerical	With runner / Conical basin	Intensifier nozzles were found to strengthen vortex formation in the conical basin and thus increase turbine efficiency.
Ullah et al. [38]	Numerical	With runner / Conical basin	Runners with tilted blades are best suited for the position near the bottom of the basin, while cross-flow blades are recommended in the top position
Nishi et al. [45]	Numerical and experimental	With runner / Cylindrical basin	The net head and the turbine efficiency increased as the volume flow rate increased

Table 4
Numerical and experimental investigations and their main findings.

Author(s)	Method	With or without runner / Type of basin	Results
Velásquez et al. [28]	Numerical	Without runner / Cylindrical and conical basin	The largest value for tangential velocity (1.55 m/s) when the radius was 0.22 m using wrap-around inlet channel with conical basin
Rahman et al. [36]	Experimental	Without runner / Cylindrical basin	The efficiency increased polynomial when inlet flow rates increased. Reducing the value of S will improve the efficiency.
Havaldar et al. [27]	Numerical	Without runner / Conical basin	The average velocity in curve inlet channel was greater than that of the Straight inlet channel
Khan et al. [25]	Numerical and experimental	With and Without runner / Cylindrical basin	An increase of w/D increases the mass flow, which causes the water height to rise until overflow from the upper walls of the basin occurs

Table 5
Numerical investigations and simulation parameters used.

Author(s)	Computational method	Turbulence model	Solution scheme	N° of elements	Element sizes [mm]
Wanchat et al. [39]	FVM		Simple scheme		
Sreerag et al. [21]	FVM	$k-\epsilon$	Simple scheme	53,788	
Dhakal et al. [14]	FVM	RNG $k-\epsilon$	Simple scheme	308,851	60
Dhakal et al. [20]	FVM	RNG $k-\epsilon$	Simple scheme	308,851	60
Gautam et al. [43]	FVM	Reynolds Stress	Simple scheme	300,000	
Chattha et al. [22]	FVM	RND $k-\epsilon$			
Nishi and Inagaki [42]	FVM	SST		2,201,000	
Dhakal et al. [44]	FVM	$k-\epsilon$			
Havaldar et al. [27]	FVM	SST	Simple Scheme	391,104	
Velásquez et al. [28]	FVM	$k-\epsilon$	Simple Scheme	901,779	
Khan et al. [25]	FVM	SST		4,816,342	1

Tables 6 and 7 show the main dimensions, efficiency (η) and outlet generated power for the cylindrical and conical basin, used in some investigations. The length dimensions were divided by the diameter basin D to use dimensionless parameters. The empty spaces in the tables indicate that the authors do not report these values in the results of their researches. Tables 6 and 7 have some repeated authors because they used various models.

From Tables 6 and 7, the studied turbines have efficiencies ranging between 17.5 and 78.65% and output powers between 0.0028 and 3.3 kW. The ratio d/D changes between 0.05 and 0.6, the most using values is 0.15. The maximum and minimum value of H/D are 1.00 and 0.23, respectively. The ratio w/D changes between 0.2 and 0.5. The maximum and minimum value of h/D are 0.63 and 0.20, respectively. The ratio L/D changes between 0.57 and 3.9. The ratio s/D is the half of the relation w/D.

Table 6
Main dimensions for the cylindrical basin. Note: The authors do not report the value of β.

Author(s)	d/D	H/D	w/D	h/D	L/D	s/D	η (%)	Outlet power (kW)
Guzmán et al. [16]	0.19	0.23	0.31			0.16	17.50	3.300
Wanchat et al. [39]	0.20	1.00					30.00	0.060
	0.25	1.00					30.00	0.050
	0.30	1.00					30.00	0.045
	0.35	1.00					16.00	0.020
Peña [46]	0.28	1.38	0.28	0.43	3.90	0.14		
Peña Salazar [47]	0.20	1.00					37.41	
Kueh et al. [40]	0.05	1.88						
Dhakal et al. [20]		1.42					27.75	0.028
Shabara et al. [41]	0.20	0.30	0.40	0.30	1.00	0.20	30.00	
Power et al. [32]	0.05	1.40					15.10	
Ayala et al. [33]	0.06	1.88	0.23	0.63		0.11		
Nishi and Inagaki [42]	0.20		0.20	0.20		0.10	35.40	
Chattha et al. [22]	0.14	1.00	0.30	0.30		0.15		
Kueh et al. [35]		0.40					22.24	0.014
Rehman et al. [24]	0.40	0.90	0.25	0.25	0.57	0.13		
	0.50	0.90	0.25	0.25	0.57	0.13		
	0.60	0.90	0.25	0.25	0.57	0.13		
Sritram and Suntivarakorn [48]	0.20	1.00					35.92	0.014
Nishi et al. [45]	0.20		0.20			0.10	50.00	0.003
Rahman et al. [36]	0.18	1.25			1.28	0.10	26.00	
	0.18	1.25			1.28	0.16	22.00	
	0.18	1.25			1.28	0.22	18.00	
	0.18	1.25			0.96	0.10	28.00	
	0.18	1.25			0.64	0.10	26.00	
	0.18	1.25			0.32	0.10	25.00	
Khan et al. [25]	0.16	1.00	0.2	0.2			10.46	

3. Challenges for development of GWVHT

As a new turbine, the challenges of development of GWVHT are immense. There are technical, environmental, economic and policy challenges facing its implementation. The main challenges of development of GWVHT technology observed by the authors are:

- Water resource assessment.Small streams and rivers can safely provide energy to run a SHP as GWVHT; nonetheless, there are commonly no flow gauges in these sites. This problem requires an investigation of streams and rivers characteristics: annual flow, depth and cross section but global databases are not readily usable to analyse the available energy of the flow [54]. Selecting rivers or streams where the volume flow rate is relatively steady throughout the year is ideal to install a GWVHT.
- System design. The optimum design of GWVHT is an important technical challenge. GWVHT requires a variety of components such as runner, inlet channel, basin, power converter, control system and, protection devices, nevertheless, there is insufficient information for the design of each of these components. More studies are required to determine the optimal design of this type of turbine.
- Environmental impacts. GWVHT is known for low carbon energy production [25], however, they can produce downstream flow alterations. These alterations from flow reduction can include reduced aquatic biodiversity and barriers to fish migration [55]. To reveal their effect on natural flow of the river, ecosystem, and wildlife is necessary an investigation on turbine usage for each installation.
- Economic feasibility. The cost of installation of GWVHT is comparable to other different low head micro power plant like Francis, Propeller and cross flow turbine [56]. However, the installed cost depends of the final location.

Table 7
Main dimensions for the conical basin.

Author(s)	d/D	H/D	w/D	h/D	L/D	s/D	β (Deg)	α (Deg)	η (%)	Outlet power (kW)
Marian et al. [30]	0.15	0.83						62.98		
	0.15	1.25						71.22		
	0.15	1.67						75.69		
	0.15	2.08						78.47		
Dhakal et al. [29]	0.17	1.42						73.61	29.60	
Loaiza [49]	0.15	0.27	0.27	0.27	1.82	0.14		32.55		
Dhakal et al. [50]	0.15	1.44	0.50	0.50	2.81	0.25		73.53	74.35	0.157
Ayala et al. [33]	0.22	1.00	0.22	0.33		0.11		68.75		0.150
Gautam et al. [43]		1.50	0.50			0.25	170.00		78.65	
Dhakal et al. [51]	0.23	0.75	0.50	0.40		0.25	170.00	62.68		1.600
Sreerag et al. [21]	0.30	1.00	0.30	0.30	1.80	0.15		70.71		
Dhakal et al. [44]		2.50	0.50	0.50	2.20	0.25	170.00		71.00	0.014
Srihari et al. [37]	0.05	1.42	0.50	0.50	2.83	0.25		71.46	42.47	0.033
	0.50	0.90	0.25	0.25	0.57	0.13		74.48		
	0.60	0.90	0.25	0.25	0.57	0.13		77.47		
Ullah et al. [52]	0.34	2.50	0.42	0.54	2.08	0.21		82.45		
Sedai et al. [53]	0.22	1.22	0.32	0.45				67.00	12.10	

There are some factors that affect the cost: civil work, the complexity of the turbine design, the distance to the distribution area and the system capacity [51]. Civil work represents about 40% of the total cost, turbine and generator set (30%), control equipment(22%) and management cost (8%) [57].

- Policy/regulatory framework. The rapidly growing demand for electricity, together with the increase in the world population, presents an ideal environment for the development of renewable energies, in particular small hydropower plant. However, this type of technology to produce energy is more expensive than conventional power plant with fossil fuels [58]. In order to promote the development of renewable energy sources, the governments of the world have financed investigations and developments of renewable energy technologies to make this kind of energy a competitive one, establishing regulatory frameworks and policies to renewable energy sector.

4. Conclusions

In modern societies, electricity is a basic need, and renewable resources, especially hydraulic resources, have a key role to play in supporting electricity increased demand. Hydropower is the primary source of renewable energy; it contribute almost 60% of the global renewable supply and nearly 20% of all electricity production. Small hydropower plants constitute a feasible and attractive solution to cover the increasing demand and to produce electricity in isolate regions, this facilities can produce electricity operating in small rivers.

Among the different type of turbine, GWVHT allows to take advantage of locations that until now were impossible with conventional generation systems because is a low hydraulic head hydropower plant. The GWVHT is very promising for application in developing countries where the large hydroelectric power plants can be run into financial, environmental, and social nature obstacles. Compared to existing hydropower technologies, the GWVHT is still premature and more research is required to optimize the basin, channel and runner geometry in order to increase the efficiency. The main findings of the numerical and experimental studies are:

- The most optimal relationship between the diameter of the circulation basin and the diameter of the discharge has been studied in numerical and experimental studies, but the authors have not reached the same conclusion. The most using values was 0.15 but the ratio d/D changed between 0.05 and 0.6.

- Some studies investigated the effect of different forms of the inlet channel but made no changes to its dimensions, so the conclusion they reached may be specific to the type of circulation basin used. The studies showed that

the vortex formed by the use of an entrance channel with triangular geometry is more efficient since it tends to produce a very symmetrical vortex pattern which causes a smaller radial force. The most common channel used have a rectangular cross-section ($w \times h$); the maximum and minimum value to h/D are 0.63 and 0.20 and the ratio w/D changes between 0.2 and 0.5. About the long of the channel, the ratio L/D changes between 0.57 and 3.9.

- Regarding the runner, the shape or number of blades has been varied but the results of the investigations were contradictory, therefore, it was not possible to obtain a generalized conclusion. In only one of the reported studies, the authors related the diameter and height of the circulation basin with the height and length of the inlet channel but did not use any runner, so their conclusions could vary depending on the type runner installed in the system.
- With reference to the position of the runner concerning the height of the basin, it was possible to identify that for maximum energy extraction, the runner should be installed as close as possible to the discharge.
- The studies allowed asserting that the conical basins are better than the cylindrical basins because in the conical basins the velocities reached in the vortex are higher. Additionally, there are no recirculation regions in the conical basin as compared to cylindrical basins. These conclusions allows us to identify the best geometry but not the dimensions of this geometry.
- The vortex height influences the efficiency of the turbine, thus to increase the efficiency, it is necessary to maintain the flow regime in which the vortex is extended to the discharge.
- Increasing the volume flow rate in the turbine, increases the efficiency, however, there must be a limit to the increase the volume flow rate, an excess flow could prevent proper vortex formation or cause flow spillage. It is necessary a detail study about incoming flow and how this affect the extraction of energy.
- In GWVHT, two of the main components: inlet channel and circulation basin can be constructed on-site using concrete or other construction materials. Although it is possible to build transportable systems using aluminium or steel. These designs allow the requirements for the implementation of a GWVHT to be less than the requirements for conventional systems, facilitating the construction of many of these plants along the path of a river. A GWVHT can also be integrated in a back flow canal of a water treatment station for self-supply.
- Materials such as plastic, aluminium or composite materials can be used for fabrication of turbine components because they are lightweight materials; changing the material will increase the power/weight ratio, its useful life and the modularity of the system. With a modular and lightweight turbine, the system can be transported and installed in remote areas with significant hydraulic potentials. It is important to develop simple design geometries with reduced civil works that employs basic workshop facilities and local manufacturing to produce these systems possible at a lower cost.
- Several important simulations parameters such as mesh quality, convergence criteria, simulation type, element size, and number of elements are not shown in some of the papers what makes difficult to compare the numerical results. Most of the numerical studies used ANSYS as simulation software. The simple scheme to solve the governing equations was implemented in all studies. The most widely used turbulence model was the $k - \epsilon$ model.
- The GWVHT has efficiency ranging between 17 and 85%, this substantial range can be attributed to the different geometries, different methodologies used to measure the outlet power and the equation used to calculate the available power. This information is not available in all investigations, it is necessary to establish a methodology to carry out an adequate characterization.

The design of GWVHT still has many geometric configurations that have not yet been examined; so many ways are open for further exploration. Today, to develop better and lower-cost products, professionals are opting for optimization methodologies, which are used to carry out a more precise search for improvements. Optimization process employs a mathematical algorithm to select new designs iteratively in search of the optimal point. Using these optimization techniques, the designs of GWVHT could be improved while comparing different configurations, also allowing us to analyse which design factors are the most important and how their interactions affect the efficiency of the system allowing determining the optimum design of this type of turbine.

References

[1] J. A. Aguilera Folgueiras, Fuentes de energía y protocolo de kioto en la evolución del sistema eléctrico español (2012).

[2] L. Doman, Eia projects 28% increase in world energy use by 2040, EIA Report Today in Energy (2017).

[3] B. Dudley, et al., Bp statistical review of world energy 2018, London, UK (2018).

[4] M. M. Rahman, T. J. Hong, R. Tang, L. L. Sung, F. B. M. Tamiri, Experimental study the effects of water pressure and turbine blade lengths & numbers on the model free vortex power generation system, Int J Curr Trends Eng Res (IJCTER) 2 (2016) 13–17.

[5] I. Irena, Renewable energy technologies: Cost analysis series, Concentrating solar power (2012).

[6] C. D. Howard, J. R. Stedinger, Hydroelectric power and the future, in: Toward a Sustainable Water Future: Visions for 2050, 2012, pp. 234–242.

[7] IHA, 2020 hydropower status report, Int Hydropower Association (2020).

[8] T. B. Couto, J. D. Olden, Global proliferation of small hydropower plants–science and policy, Frontiers in Ecology and the Environment 16 (2018) 91–100.

[9] UNIDO, World small hydropower development report 2019, 2019.

[10] A. B. Timilsina, S. Mulligan, T. R. Bajracharya, Water vortex hydropower technology: a state-of-the-art review of developmental trends, Clean Technologies and Environmental Policy (2018) 1–24.

[11] D. Y. Goswami, F. Kreith, Energy conversion, CRC press, 2007.

[12] J. Z. Valencia Balanta, et al., Revisión del potencial para aprovechamiento hidroeléctrico en el municipio de Timbiquí, Cauca, Ph.D. thesis, Universidad Santiago de Cali, 2019.

[13] S. Williamson, B. Stark, J. Booker, Low head pico hydro turbine selection using a multi-criteria analysis, Renew Energy 61 (2014) 43–50.

[14] S. Dhakal, A. B. Timilsina, R. Dhakal, D. Fuyal, T. R. Bajracharya, H. P. Pandit, Effect of dominant parameters for conical basin: Gravitational water vortex power plant, in: Proceedings of IOE graduate conference, 2014, p. 381.

[15] A. M. Mohanan, Power generation with simultaneous aeration using a gravity vortex turbine, Int J Scientific & Engeenering Res 7 (2016).

[16] V. J. A. Guzmán, J. A. Glasscock, F. Whitehouse, Design and construction of an off-grid gravitational vortex hydropower plant: A case study in rural peru, Sustainable Energy Technologies and Assessments 35 (2019) 131–138.

[17] Engenhariacivil.com, Imagem do dia: Engenheiros belgas desenvolvem inovadora turbina de vórtice gravitacional capaz de fornecer energia a 60 habitações, Engenhariacivil.com (2018).

[18] S. Mulligan, P. Hull, Design and optimisation of a water vortex hydropower plant, Undergraduate thesis, Inst. of Tech. Sligo, Sligo, Ireland (2010).

[19] G. Marian, T. Sajin, I. Florescu, D. Nedelcu, C. Ostahie, C. Bîrsan, The concept and theoretical study of micro hydropower plant with gravitational vortex and turbine with rapidity steps, Buletinul AGIR 3 (2012) 219–226.

[20] S. Dhakal, A. B. Timilsina, R. Dhakal, D. Fuyal, T. R. Bajracharya, H. P. Pandit, N. Amatya, A. M. Nakarmi, Comparison of cylindrical and conical basins with optimum position of runner: Gravitational water vortex power plant, Renew Sustain Energy Rev 48 (2015) 662–669.

[21] S. Sreerag, C. Raveendran, B. Jinshah, Effect of outlet diameter on the performance of gravitational vortex turbine with conical basin, J. Scientific & Engineering Res 7 (2016) 457–463.

[22] J. A. Chattha, T. A. Cheema, N. H. Khan, Numerical investigation of basin geometries for vortex generation in a gravitational water vortex power plant, in: 2017 8th Int Renew Energy Congress (IREC), IEEE, 2017, pp. 1–5.

[23] D. Thapa, A. Mishra, K. Sarath, Effect of inlet geometry in the quality of vortex formed using vortex flow channel, Int J Mechanical Engineering and Technology 8 (2017).

[24] W. Rehman, M. Ijaz, A. Munir, Designing of micro gravitational vortex turbine?s vortex pool, in: ASME Power Conference, volume 57618, American Society of Mechanical Engineers, 2017, p. V002T12A002.

[25] N. H. Khan, T. A. Cheema, J. A. Chattha, C. W. Park, Effective basin–blade configurations of a gravitational water vortex turbine for micro-hydropower generation, Journal of Energy Engineering 144 (2018) 04018042.

[26] E. M. Wardhana, A. Santoso, A. R. Ramdani, Analysis of gottingen 428 airfoil turbine propeller design with computational fluid dynamics method on gravitational water vortex power plant, Int J Marine Engineering Innovation and Res 3 (2019).

[27] S. Havaldar, P. Gadekar, S. Baviskar, N. Jadhav, S. Inamdar, Analyzing geometries for inlet flow channels to gravitational water vortex chamber, Int J Res in Engineering Application and Manag (IJREAM) (2019).

[28] L. Velásquez, A. Rubio-Clemente, E. Chica, Numerical analysis of the inlet channel and basin geometries for vortex generation in a gravitational water vortex power plant, in: 18th Inter Conference on Renew Energies and Power Quality, 2020.

[29] S. Dhakal, S. Nakarmi, P. Pun, A. B. Thapa, T. R. Bajracharya, Development and testing of runner and conical basin for gravitational water vortex power plant, J of the inst of Engineering 10 (2014) 140–148.

[30] M. G. Marian, T. Sajin, A. Azzouz, Study of micro hydropower plant operating in gravitational vortex flow mode, in: Applied Mechanics and Mater., volume 371, Trans Tech Publ, 2013, pp. 601–605.

[31] P. Sritram, W. Treedet, R. Suntivarakorn, Effect of turbine materials on power generation efficiency from free water vortex hydro power plant, in: IOP Conference Series: Materials Science and Engineering, volume 103, IOP Publishing, 2015, p. 012018.

[32] C. Power, A. McNabola, P. Coughlan, A parametric experimental investigation of the operating conditions of gravitational vortex hydropower (gvhp), J of Clean Energy Technologies 4 (2016) 112–119.

[33] M. Ayala, H. Benavides, C. Riba, Sistema de generación energía sumergible basado en un vórtice gravitacional con sifón para comunidades aisladas., Revista Técnica Energía (2016).

[34] P. Wichian, R. Suntivarakorn, The effects of turbine baffle plates on the efficiency of water free vortex turbines, Energy Procedia 100 (2016) 198–202.

[35] T. Kueh, S. Beh, Y. Ooi, D. Rilling, Experimental study to the influences of rotational speed and blade shape on water vortex turbine performance, in: J Physics: Conference Series, volume 822, IOP Publishing, 2017, p. 012066.

[36] M. M. Rahman, T. J. Hong, F. M. Tamiri, Effects of inlet flow rate and penstocks geometry on the performance of gravitational water vortex

power plant, in: 8th inter conference on industrial engineering and operations manag, Bandung, Indonesia, 2018, pp. 2968–2976.
[37] P. Srihari, P. Narayana, K. S. Kumar, G. J. Raju, K. Naveen, P. Anand, Experimental study on vortex intensification of gravitational water vortex turbine with novel conical basin, in: AIP Conference Proceedings, volume 2200, AIP Publishing LLC, 2019, p. 020082.
[38] R. Ullah, T. A. Cheema, A. S. Saleem, S. M. Ahmad, J. A. Chattha, C. W. Park, Performance analysis of multi-stage gravitational water vortex turbine, Energy Conver Manag 198 (2019) 111788.
[39] S. Wanchat, R. Suntivarakorn, S. Wanchat, K. Tonmit, P. Kayanyiem, A parametric study of a gravitation vortex power plant, in: Advanced Mater res, volume 805, Trans Tech Publ, 2013, pp. 811–817.
[40] T. C. Kueh, S. L. Beh, D. Rilling, Y. Ooi, Numerical analysis of water vortex formation for the water vortex power plant, Int J Innovation, Manag and Technology 5 (2014) 111.
[41] H. Shabara, O. Yaakob, Y. M. Ahmed, A. Elbatran, M. S. Faddir, Cfd validation for efficient gravitational vortex pool system, Jurnal Teknologi 74 (2015).
[42] Y. Nishi, T. Inagaki, Performance and flow field of a gravitation vortex type water turbine, Int J Rotating Machinery 2017 (2017).
[43] A. Gautam, A. Sapkota, S. Neupane, J. Dhakal, A. B. Timilsina, S. Shakya, Study on effect of adding booster runner in conical basin: Gravitational water vortex power plant: A numerical and experimental approach, in: Proceedings of IOE Graduate Conference, 2016, pp. 107–113.
[44] R. Dhakal, T. Bajracharya, S. Shakya, B. Kumal, K. Khanal, S. Williamson, S. Gautam, D. Ghale, Computational and experimental investigation of runner for gravitational water vortex power plant, in: Renew Energy res and Applications (ICRERA), 2017 IEEE 6th Int Conference on, IEEE, 2017, pp. 365–373.
[45] Y. Nishi, R. Suzuo, D. Sukemori, T. Inagaki, Loss analysis of gravitation vortex type water turbine and influence of flow rate on the turbine's performance, Renew Energy (2020).
[46] J. Peña, Ingeniería de detalle y construcción de un sistema de hidrogeneración basado en vórtice gravitacional, Ingenieria Civil, Geologia y Minas (2013) 184.
[47] J. C. Peña Salazar, Ingeniería de detalle y construcción de un sistema de hidrogeneración basado en vórtice gravitacional, B.S. thesis, 2013.
[48] P. Sritram, R. Suntivarakorn, Comparative study of small hydropower turbine efficiency at low head water, Energy Procedia 138 (2017) 646–650.
[49] P. Loaiza, Generación eléctrica basada en vórtice gravitacional, una opción para la provisión sustentable de energía eléctrica en la zona rural del cantón loja, Ingenieria Civil, Geologia y Minas (2015) 75.
[50] S. Dhakal, A. B. Timilsina, R. Dhakal, D. Fuyal, T. R. Bajracharya, H. P. Pandit, N. Amatya, Mathematical modeling, design optimization and experimental verification of conical basin: Gravitational water vortex power plant, in: dalam World Largest Hydro Conference, 2015.
[51] R. Dhakal, A. Nepal, A. Acharya, B. Kumal, T. Aryal, S. Williamson, K. Khanal, L. Devkota, Technical and economic prospects for the site implementation of a gravitational water vortex power plant in nepal, in: 2016 IEEE Int Conference on Renew Energy Res and Applications (ICRERA), IEEE, 2016, pp. 1001–1006.
[52] R. Ullah, T. A. Cheema, A. S. Saleem, S. M. Ahmad, J. A. Chattha, C. W. Park, Preliminary experimental study on multi-stage gravitational water vortex turbine in a conical basin, Renew Energy 145 (2020) 2516–2529.
[53] A. Sedai, B. K. Yadav, B. B. Kumal, A. Khatiwada, R. Dhakal, Performance analysis of gravitational water vortex power plant using scale-down model (2020).
[54] M. Khan, M. Iqbal, J. Quaicoe, River current energy conversion systems: Progress, prospects and challenges, Renew and Sustain Energy Rev 12 (2008) 2177–2193.
[55] T. Hennig, T. Harlan, Shades of green energy: geographies of small hydropower in yunnan, china and the challenges of over-development, Global Environmental Change 49 (2018) 116–128.
[56] R. Dhakal, R. K. Chaulagain, T. Bajracharya, S. Shrestha, Economic feasibility study of gravitational water vortex power plant for the rural electrification of low head region of nepal and its comparative study with other low head power plant, in: J of 11 th Int conference ASIAN community knowledge networks for the economy, society, culture and environmental stability, volume 3, 2015, pp. 127–135.
[57] A. Elbatran, O. Yaakob, Y. M. Ahmed, H. Shabara, Operation, performance and economic analysis of low head micro-hydropower turbines for rural and remote areas: a review, Renew Sustain Energy Rev 43 (2015) 40–50.
[58] M. A. Schilling, M. Esmundo, Technology s-curves in renewable energy alternatives: Analysis and implications for industry and government, Energy policy 37 (2009) 1767–1781.

CHAPTER 3

SINGLE-OBJECTIVE OPTIMIZATION USING THE RESPONSE SURFACE METHODOLOGY I

Optimization of the basin and inlet channel of a gravitational water vortex hydraulic turbine using the response surface methodology

Published article

The journal, Renewable Energy, seeks to promote and disseminate knowledge on the various topics and technologies of renewable energy systems and components. The journal aims to serve researchers, engineers, economists, manufacturers, NGOs, associations and societies to help them keep abreast of new developments in their specialist fields and to apply alternative energy solutions to current practices. Renewable Energy covers research in the following areas: Biomass Conversion, Photovoltaic Technology Conversion, Solar Thermal Applications, Wind Energy Technology, Solar and Low Energy Architecture, Climatology and Meteorology, Geothermal Technology, Wave, Tide and Ocean Thermal Energies, and Hydropower.

Highlights

- GWVHT is a turbine suitable to use in low head and small to medium water flow rates.
- GWVHT is optimized through the response surface methodology.
- Transition-state, VoF, and k-ϵ RNG model were chosen to perform the CFD analyses.
- The highest circulation obtained was 2.089 m^2/s.

Optimization of the basin and inlet channel of a gravitational water vortex hydraulic turbine using the response surface methodology

Laura Velásquez, Alejandro Posada and Edwin Chica

ABSTRACT

The gravitational water vortex hydraulic turbine is an appropriate turbine to be used under from a small to medium water flow rate and at a low head. This turbine extracts energy from an induced vortex in a basin, using a coaxial rotor with a vertical axis. The gravitational turbine has efficiencies that vary between 17 and 85%. Increasing the circulation was required in order to achieve the highest efficiency. The circulation is a function of some geometric parameters of the turbine, such as the ratios between the basin diameter (D) and the outlet diameter (d), d/D; the basin height (H) and D, H/D; the inlet channel width (w) and D, w/D; the inlet channel height (h) and D, h/D; the inlet channel long (L) and D, L/D; and the wrap-around angle (γ). Response surface methodology was utilized to determine the optimal geometry that results in the highest circulation. The values of the six variables that give the highest circulation of 2.089 m^2/s were d/D=0.167, H/D=1.840, w/D=0.2, h/D=0.599, L/D=0.500 and γ=179.976°. In addition, an exponential equation was proposed for calculating the inlet velocity for each treatment. This equation is a function of d/D and the coefficient of discharge, C_d. The results of the exponential function were compared with experimental data from other investigations.

1. Introduction

Societies use energy to satisfy basic human necessities (e.g., cooking, communication, lighting, mobility, and comfort) and to attend productive processes. The energy demand is increasing quickly because of the economic and population growth, especially in emerging markets [1, 2]. In this regard, the energy of the future requires new horizonts. It is essential to renovate the way how the energy is produced and consumed. To offer access to efficient energy services, renewable energy (RE) will be the main source of long-term energy supply [3].

There are multiple options for producing energy employing RE. One of these possible options is hydroelectric power generation [4]. Hydropower takes advantage of the water moving from higher to lower elevations. The electrical energy generated depends on the amount of water flow rate and the head condition. Hydropower projects include run-of-river and dam installations with storage [5]. These projects give hydropower the capacity to satisfy decentralized rural requirements as well as large centralized urban needs. Hydropower plants can be classified in terms of their generated power in: large (>10 MW), small (<10 MW), mini (<1 MW), micro (<0.1 MW), and pico (<0.005 MW) hydropower plants [6]. Countries around the world follow several guidelines for this classification [5].

The gravitational water vortex hydraulic turbine (GWVHT) is a turbine that is appropriate to be used with a water flow rate from small to medium and a low head. GWVHT is a micro hydropower plant. In the literature, the maximum reported power is less than 0.1 MW [7]. The main advantages of GWVHT are the high power density generated compared to conventional technologies and the production of a higher power output than other types of micro hydropower plants under the same conditions. Additionally, GWVHT are safe for the environment, aquatic life, and water quality; they are easy to be installed; and, their operating and manufacturing costs are low [8].

The rapidly growing demand for electricity and the negative environmental impacts associated with the use of large hydropower plants presents an ideal environment for developing renewable energies, in particular small, mini, micro, and pico hydropower plants [9] as GWVHT. Governments of many countries are providing subsidies to promote the development of this type of technology [10] due to the capacity of GWVHT to take advantage of the relatively low flow rates of rivers with lateral capture without the need to create large damns, conserving the ecological flows and limit the environmental effects of civil constructions. This hydropower plants also can supply electricity to remote areas and improve the quality of life of rural people.

GWVHT consists of channeled water inlet into a cylindrical or conical basin. In order to facilite the vortex formation, the inlet channel allows the water to enter the basin in a tangential and controlled way. The transfer of energy

ORCID(s): 0000-0003-1483-0104 (L. Velásquez); 0000-0001-5836-0680 (A. Posada); 00000-0002-5043-6414 (E. Chica)

from water to the runner is due to the vortex of the free surface created on the open surface of the basin. Recently, the free-surface vortex has been found an unusual application in hydroelectric power generation through GWVHT. Other devices that have incorporated free-surface vortex flows are vortex chambers for particle separation and fluidic throttling devices for controlling tge discharge [11].

Nowadays, 21 GWVHTs have been installed in the world. Europe is the continent with the highest number of installations (12), followed by Asia (4), Oceania (3), and South America (2). The installed turbines have efficiencies, head values and power output, that vary between 17 and 85%, between 0.6 and 2.0 m, and between 0.01 and 20 kW [7]. Among the 21 installations, the turbine reporting the highest efficiency (85%) hsd been installed in Indonesia and generates 15 kW. In turn, the turbine with the lowest efficiency (17%) corresponds to the turbine with the lowest power (0.01 kW), while the one with the highest power (20 kW) reports an efficiency of 68%. Therefor, the efficiency of the GWVHT appears to be independent on the capacity.

In spite of the advantages, the investigations and developments regarding GWVHTs are limited. The literature review shows that researchers have been focused on increasing the efficiency of the power plant. To achieve the highest efficiency, the researchers have changed some geometric parameters of the basin, the inlet channel, as well as the runner types and their positions in the basin, by including or excluding the rotor. When the rotor is included, the objective was obtained using the highest output power [12, 13, 14, 15, 16, 17]. In tunr, when the rotor is excluded the rotor, the way to measure the improvement in the efficiency was by means of the increase in the circulation or tangential velocity [11, 18, 19, 20, 21].

For a solid body, such as the turbine rotor, to be moved by a fluid, surface forces ($\vec{F}$), also called aerodynamic or hydrodynamic forces, must exist. These forced are generated by the fluid in which the body is immersed. Vortex circulation (Γ) and tangential velocity are directly related to the hydrodynamic forces [22]. The hydrodynamic forces generate a moment ($\vec{M}$) about a specific point or axis O ($\vec{M} = \vec{r} \times \vec{F}$). $\vec{r}$ is the position vector from O point to any point on the line of action of $\vec{F}$. The generated power (P) by the moment is proportional to the angular velocity (ω) of the body in rotation ($P = \vec{M} \times \omega$) [23]. A greater hydrodynamic force on the rotating body generates a greater moment, which in turn produces a greater power.

Until now, to increase Γ, the geometric factors of the basin and inlet channel were separately varied from reference values. The tangential velocities in the vortex, the vortex height, the vortex circulation, and the quality of air-core were analyzed [11, 18, 19, 20, 21]. The geometrical parameters that can be varied in the inlet channel and the basin are the basin diameter (D), the outlet diameter (d), the basin height (H), the inlet channel width (w), the inlet channel height (h), the inlet channel length (L) and the wrap-around angle (γ). As a run-of-river turbine, the inlet water flow into a GWVHT is susceptible to changes in the water level in the river therefore in this study the inlet water flow rate was also varied to study their influence on the vortex formation.

The objective of the current work is the optimization of the basin and the inlet channel of a GWVHT to select the configuration with the highest circulation using computational fluid dynamics (CFD) simulations and the response surface methodology (RSM). Six geometric factors were used simultaneously to evaluate their effect on the vortex circulation. According to the authors´ knowledge, it is the first time that optimization with six factors is employed to improve this kind of turbine. Although the optimization of several parameters influencing the turbine performance has been previously conducted, the procedures used in this work have been mainly based on one-factor-at-a-time (OFAT) techniques, which have ascribed several limitations in comparison with the use of the response surface methodology.

2. Methods and materials

2.1. Gravitational water vortex hydraulic turbine (GWVHT)

A GWVHT consists of a channeled water inlet into a cylindrical or conical basin. Fig. 1 shows a model of a GWVHT with the main elements, including the inlet channel, the basin, the runner, the generator, and the discharge.

The selected baseline geometry for the optimization task is shown in Fig. 2. The geometry employed was a turbine with a conical basin and wrap-around inlet channel. The runner was excluded. Six input variables (or factors) were used to define it. These variables are dimensionless since each of them was divided by D. According to the literature, the factors previously reported and used by other authors are listed in Table 1.

2.2. Response surface methodology analysis with Latin hypercube sampling [LHS]

Response surface methodology (RSM) is a method for process optimization that allows to explore the relationship between the independent factors and their combined effect on the studied response [37]. The main disadvantage of this

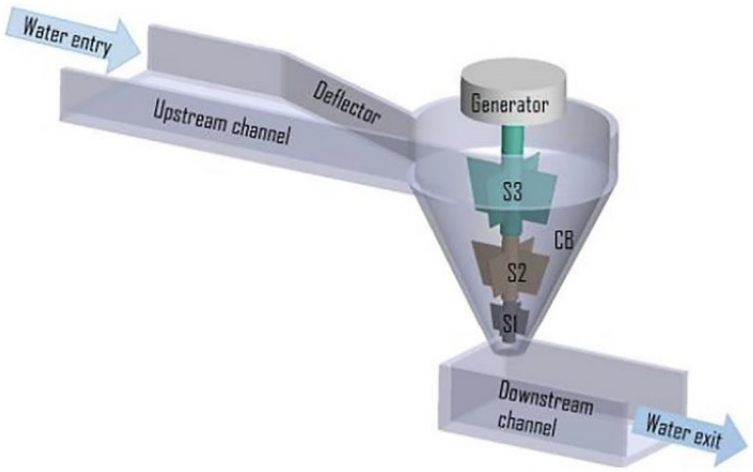

Fig. 1: Model of a GWVHT. Adapted from: [24]

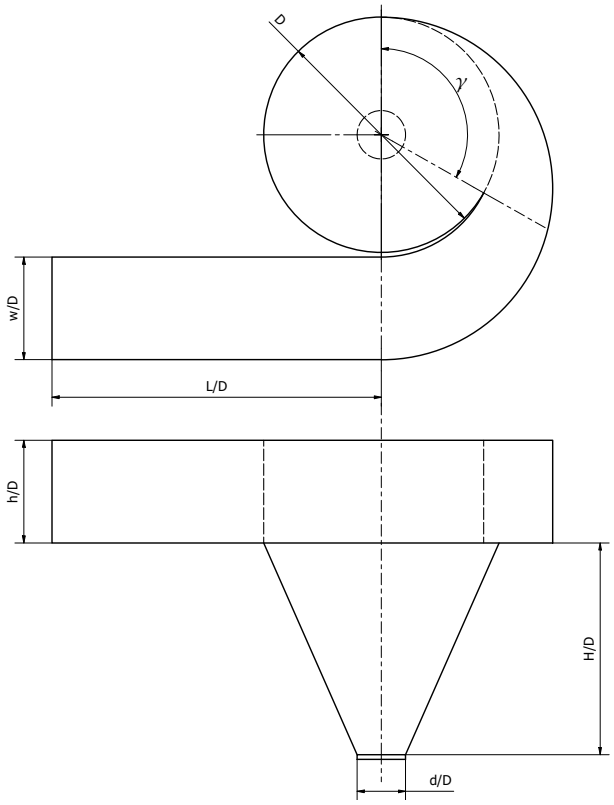

Fig. 2: The selected baseline geometry and geometric factors.

method is that the experimental data are fitted to a second-order polynomial model [38, 39]. In this regard, when the problem cannot be explained by a second-order polynomial model, the reduction of the range of independent factors under consideration is requiered. In addition, RSM is able to make a local analysis. Therefore, the response surface models obtained are valid only in the selected ranges of the independent factors considered [40].

RSM was employed to know how the independent factors (d/D, H/D, h/D, w/D, L/d, and γ) and their interactions affect Γ. To understand the relation between the independent factors and response, numerical or experimental

Table 1
Values of the geometric factors reported in the literature.

Reference	d/D	H/D	w/D	h/D	L/D
[25]	0.17	1.42	–	–	–
[26]	0.15	0.83-2.08	–	–	–
[13]	0.16	1.42	–	–	–
[27]	0.15	1.44	0.50	0.50	2.81
[28]	0.23	0.75	0.50	0.40	–
[29]	0.22	1.00	0.22	0.33	–
[30]	0.30	1.00	0.30	0.30	1.80
[31]	0.15	0.27	0.27	0.27	1.82
[32]	0.15	1.50	0.50	–	–
[33]	0.14	1.53	0.50	0.50	–
[34]	0.10	1.03	0.50	0.50	–
[35]	0.18	0.50	0.63	0.40	–
[36]	0.22	1.06	0.32	0.16	2.08
[24]	0.13	1.96	0.42	0.42	0.45

results for different conditions are required. The different conditions are a combination of geometrical factors. Each combination is called treatments [41]. There are different methods such as factorial, Latin hypercube sampling (LHS), and one factor at a time (OFAT) methods to obtain the treatments [42, 41].

On the other hand, OFAT is a good method for understanding the relationship between the response(s) and the independent factors when there is no interaction between the independent factors. This technique allows to vary only one factor at a time while keeping the others fixed. OFAT needs a higher number of treatments to achieve the same precision in the effect estimation and the optimal setting of factors can be missed [43]. A Factorial design of experiments (DOE) is a method that considers the interactions between the independent factors. A factorial DOE can be a fractional or full factorial design. A full factorial design is a grid of m^{d_i} points where d_i is the number of factors and m is the number of levels of each factor. In turn, full factor sampling calculates all possible combinations of these levels in all input factors [44]. However, it has a disadvantage that limits its practical use, i.e., if one of the independent factors is not important, every single point is evaluated m times. When the number of the selected factors and their levels are large, the full factorial DOE requires many a large number of treatments to be obtained from experiments or simulations. In this regard, fractional factorial designs remove some of the grid points conidered by the full factorial in order, to limit the number of treatments, making them realizable in high-dimensional problems where a full factorial DOEn would take long simulations or experimental time to evaluate each considered run.

A Latin hypercube sampling (LHS) is the most popular sampling technique in computer experiments, thanks to its simplicity [45]. A LHS is created by dividing each dimension in the design space into j equally sized intervals, and assigning only one point at each interval for each dimension [46, 47]. In a LHS design, the number of treatments must be determined in advance so thath the desing space is subdivide into intervals of equal size. As the Factorial design, LHS considers the interactions between the independent factors but requires a smaller size of data [41]. For these reasons, LHS was employed as the experimental design in this work. As mentioned previously, it is necessary to determine previously the number of treatments for the LHS design. Since the relation between the factors and the response variable is not known *a priori*. The equation of the full factorial method was applied to define the possible number of treatments (2^6=64 at 2 levels). The ranges of the six variables used to generate the LHS are given in Table 2. Low and high levels of each variable were determined by employing the values reported in Table 1. The number of final treatments or runs was 60. Fig. 3 shows the LHS distribution. All variables were normalized in the interval (0, 1). In this study, the diameter of the basin (D) was fixed at 0.5 m. As mentioned above, the response variable chosen was the vortex circulation, which was planned to be maximized.

It is important to note that, Γ is a macroscopic measurement of rotation for a finite area of the fluid. The circulation around a closed curve (C) is defined as the integral line evaluated along the curve of the velocity vector component

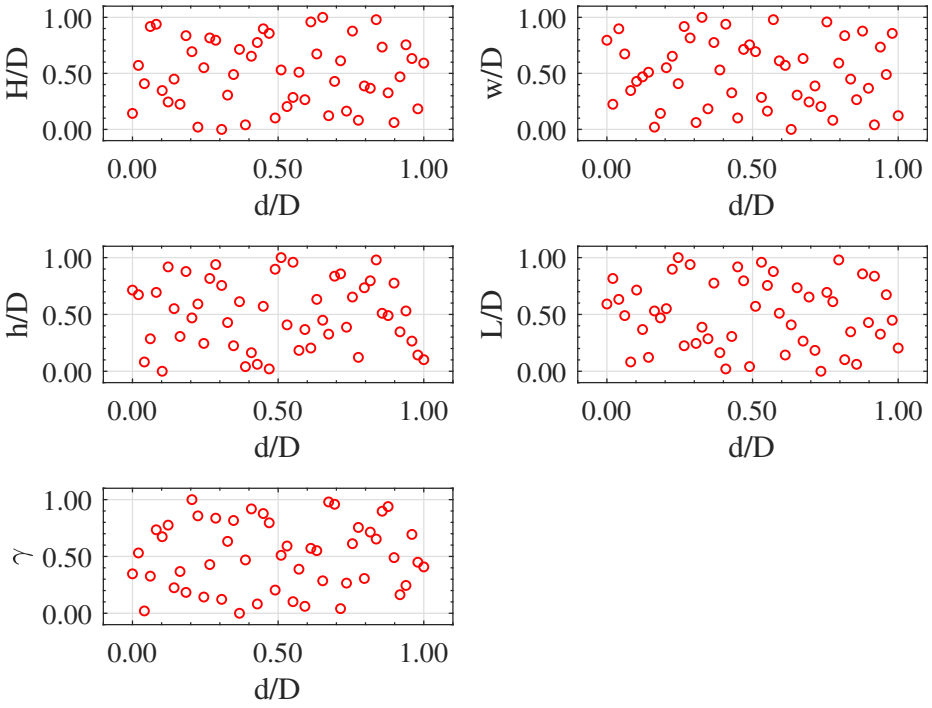

Fig. 3: The Latin hypercube sampling (LHS) distribution.

that is locally tangent to the curve [48]. Thus, for a curve in the horizontal plane the circulation is given by Eq. 1.

$$\Gamma = \oint_C \vec{v} \cdot d\vec{l} \tag{1}$$

where $\vec{v}$ corresponds to the velocity around C and $d\vec{l}$ is a vector representing the differential length of C. By using Stokes' theorem, circulation can be written like a surface integral curve [49], as expressed in Eq. 2.

$$\Gamma = \int_S \vec{\omega} \cdot dS \tag{2}$$

where the vorticity ($\vec{\omega}$) of the fluid is defined as expressed in Eq. 3: [23]. Being ∇ the *nabla* operator.

$$\vec{\omega} = \nabla \times \vec{v} \tag{3}$$

By convention, the circulation is considered positive if Γ>0 for counter-clockwise integration around C.

Table 2
Ranges used for the independent factors.

Independent factor	Low level	High level
d/D	0.10	0.30
H/D	0.50	2.00
w/D	0.20	0.50
h/D	0.20	0.60
L/D	0.25	3.00
γ [°]	90	180

As stated above, a regression model determines the relationship between the response and the independent factors. It can be cubic, quadratic, and linear, or contain some special functions. Thee response variable can be transformed or non-transformed. Whether the response variable is transformed or not will depend on whether the regression model is adequate. In this study, a second-order polynomial model was used to represent the effects of independent factors, and their interactions on the response variable. A regression model with six independent factors and without transformation takes the form described by Eq. 4.

$$\begin{aligned}\Gamma = \beta_0 + \beta_1(d/D) + \beta_2(H/D) + \beta_3(w/D) + \beta_4(h/D) + \beta_5(L/D) + \beta_6(\gamma) + \beta_{11}(d/D)^2 + \beta_{22}(H/D)^2 \\ +\beta_{33}(w/D)^2 + \beta_{44}(h/D)^2 + \beta_{55}(L/D)^2 + \beta_{66}(\gamma)^2 + \beta_{12}(d/D)(H/D) + \beta_{13}(d/D)(W/D) \\ +\beta_{14}(d/D)(h/D) + \beta_{15}(d/D)(L/D) + \beta_{16}(d/D)(\gamma) + \beta_{23}(H/D)(w/D) \\ +\beta_{24}(H/D)(h/D) + \beta_{25}(H/D)(L/D) + \beta_{26}(H/D)(\gamma) \\ +\beta_{34}(w/D)(h/D) + \beta_{35}(w/D)(L/D) + \beta_{36}(w/D)(\gamma) \\ +\beta_{45}(h/D)(L/D) + \beta_{46}(h/D)(\gamma) + \beta_{56}(L/D)(\gamma)\end{aligned} \tag{4}$$

The coefficients of the polynomial model were denoted β_0 (constant term); β_1, β_2, β_3, β_4, β_5 and β_6 (linear effects); β_{11}, β_{22}, β_{33}, β_{44}, β_{55} and β_{66} (quadratic effects); and β_{12}, β_{13}, β_{14}, β_{15}, β_{16}, β_{23}, β_{24}, β_{25}, β_{26}, β_{34}, β_{35}, β_{36}, β_{45}, β_{46} and β_{56} (interaction effects).

Once the 60 treatments were run, the regression model was established from the numerical simulation data. A fourth-power transformation of the Γ values was applied for constituting the regression model. The transformation of the response variable was necessary to satisfy the assumptions of normality, homoscedasticity, and residual independence of the regression model. Statistical significance of each term in the regression model was tested using analysis of variance (ANOVA). Additionally to the tests of independence, normality, and homoscedasticity of the residuals, the adequacy of the regression model was tested to calculate the coefficients of determination R^2 and adjusted-R^2.

2.3. Numerical simulation

2.3.1. Computational domain and meshing

Numerical simulation of the free-surface vortex was performed using ANSYS Fluent. The 60 geometries were modeled in ANSYS Design Modeler. After the geometry preparation, the meshes were created in Fluent meshing solver. The domains were composed of two parts: the basin and the inlet channel. Both parts were meshed using poly-hex core mesh elements. This type of element allows a reduction of 20 to 50% in the total element compared to the conventional Hexcore mesh [50]. A mesh used in the simulations is presented in Fig. 4

The Transition-state, the volume of fluid (VoF), and the $k-\epsilon$ (RNG Renormalization Group) turbulence model were chosen to perform the simulations. The VoF method was employed to capture the interface between two fluids that cohabit in the computational domain: air and water. The $k-\epsilon$ turbulence model is a two-equation model that solves the turbulent kinetic energy (k) and dissipation (ϵ). It is a suitable model only for turbulent flows. It is a model widely used in the study of GWVHT, since it is a model for general purposes allowing the first approach to the phenomenon of a vortex [51]. Futhermore. it is easy to be implemented, enable a fast convergence and has low memory requirements [52].

The coupled scheme and the second-order upwind and body forced weighted pressure were used in these simulations. As boundary conditions, an inlet velocity was established at the inlet channel with a turbulence intensity of 10%; and a relative pressure of 0 Pa was used at the discharge. Furthermore, the upper surfaces of the channel and basin were set to open boundaries (relative static pressure of 0 Pa), so that air could enter and exit freely. To estimate the inlet velocity to each geometry, the coefficient of discharge (C_d) was determined.

This coefficient relates the flow discharge (Q) and its corresponding water head (H^*) [53, 11], as described by Eq. 5.

$$C_d = \frac{4Q}{\pi d^2\sqrt{2gH^*}} \tag{5}$$

where g is the gravitational acceleration and H^* corresponds to the basin height. In turn, Q depends on the area of the discharge section of the conical basin [11]. To establish the value of Q, five geometries with different d/D were

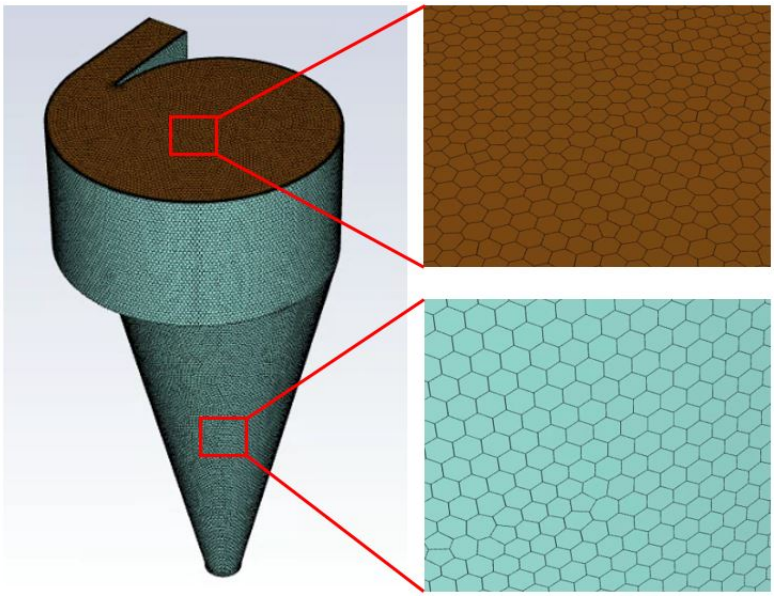

Fig. 4: Hexcore mesh.

considered. The inlet velocity changed between 0.05 and 0.5 m/s, and the circulation was calculated in each selected geometry. Then, the maximum circulation determined the value of Q to each value of d/D. The relationship between C_d and d/D for the results of this study is presented in Fig. 5.

The relation between the coefficient of discharge and d/D is described by Eq. 6.

$$C_d = [0.7721e^{-6.4409\frac{d}{D}}] - 0.0464 \tag{6}$$

The adequacy of Eq. 6 was checked accounting for the root-mean-square error (RMSE) and R^2. The value obtained for these parameters were 0.0048 and, 99.77%, respectively. By using Eq. 6, it was possible to calculate the inlet velocity for the 60 study geometries. The numerical coefficient of discharge was compared with the experimental data found in the literature. Both results indicated that the coefficient of discharge decreases when d/D increases. All the experimental data shown in Fig. 5 correspond to GWVHT a with conical basin but with a tangential inlet channel. The experimental studies reported in the literature implemented the wrap-around inlet channel. The differences between the numerical and experimental results were then attributed to the differences between the inlet channel geometry, particularly its shape and dimensions.

A mesh independence test was performed to ensure that the results with different meshes do not deviate between them. The optimum number of mesh was determined by employing the Grid convergence index (GCI) method. GCI method is based on the Richardson extrapolation, in which an estimation of the exact solution can be provided [54]. The element numbers used for the mesh independence were 211158, 330238, and 435116. In addition, a time-step independence study was conducted to determine the most convenient time-step for the simulations. Time-step used for this test were 0.05, 0.1, and 0.2 s. Figure Fig. 6 represents the results obtained for the independence tests and the Richardson extrapolation solutions. After the Richardson Extrapolation analysis, a time-step of 0.1 s and the mesh number 2 was chosen. The mesh and time-step selected have small deviations to the Richardson extrapolation solution, and reduce the computational time.

3. Results and discussion

3.1. Numerical results

The maximum circulation of the initial treatments was achieved through treatment 43, resulting in a circulation of 1.945 m^2/s with an inlet velocity of 0.224 m/s. The minimum circulation corresponded to treatment 23, leading to a circulation of 0.1 m^2/s with an inlet velocity of 0.170 m/s. The results of the 60 treatments are listed in Table 3. Figure Fig. 7 ilustrates the volume fraction of water to the treatment 43 and 23. The red zone corresponds to the water.

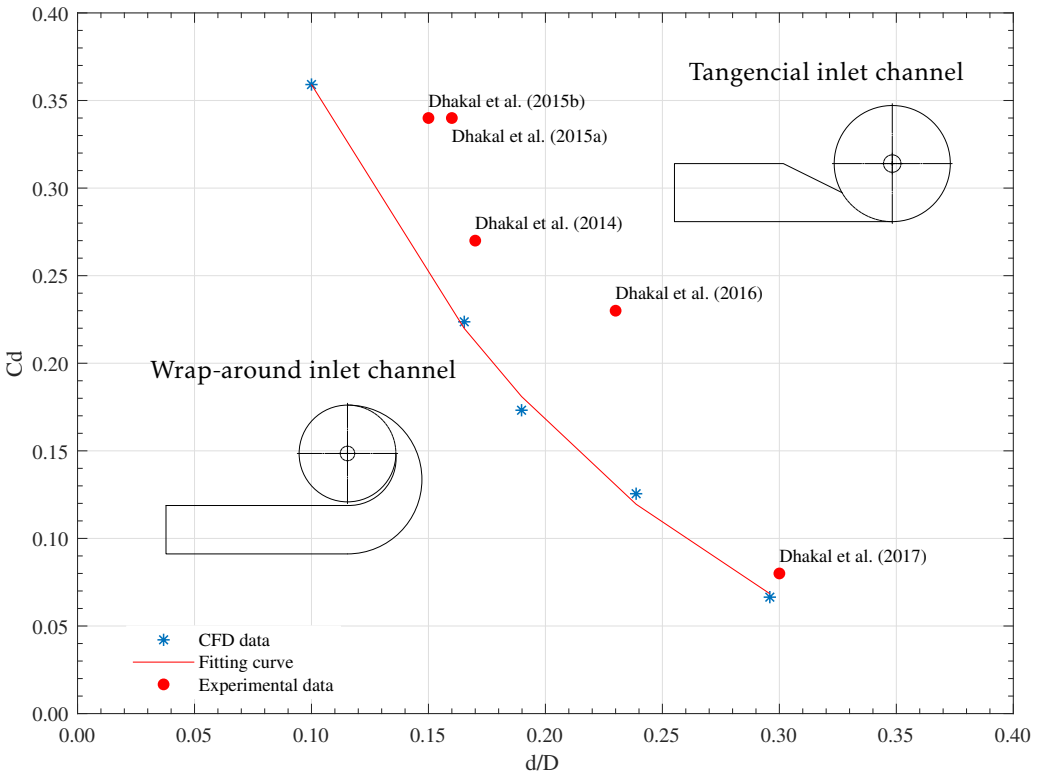

Fig. 5: Dimensionless coefficient of discharge (C_d) as a function of ratio between the basin diameter (D) and the outler diameter (d).

In treatment 43, a stable full air-core vortex extending deep into the basin is formed. This core formation is characteristic of a strong vortex as a result of an induced circulation [11]. In treatment 23, there is not a vortex as the water passes through the basin very close to the walls. The main differences between both treatments are the values of d/D, H/D and γ. These parameters appear to affect the circulation. To prove or reject this statement, a statistical analysis of the numerical results was carried out.

3.2. Statistical analysis

The results of the numerical simulations were analyzed and interpreted employing R statistical software at a confidence interval of 95%. ANOVA and regression analysis were used to examine the statistical significance of the terms and to fit the model. The p-value is the indicator of the significance of the terms considered in the regression model, whose value below 0.05 indicates that the independent factor is significant at a 5% level of significance [55, 56]. In general, the smaller the p-value is, the more significant is the term [57]. This conclusion is also valid to analyze the significance of the whole regression model built. A proper regression model can describe the behavior of the response variable. The p-values for all the terms of the regression model (linear, quadratic, and interaction effects of the independent factors) are compiled in Table 4. The terms with p-values higher than 0.8 were removed from the regression model to minimize the number of terms in the equation. The main factors cannot be removed. It can be observed that the terms H/D, w/D, h/D, $(d/D)^2$, $(H/D)^2$, $(\gamma)^2$, $(d/D)(H/D)$, and $(H/D)(w/D)$ have the smallest p-value, which means that these factors have the highest influence on the circulation. The linear parameter d/D and γ identified as significant terms from a statistical point of view in the previous analysis, are not significant according to the ANOVA results. Nevertheless, the quadratic term d/D^2 and γ^2 are significant. The p-value of the model was 2.40 $\times 10^{-14}$, which means that the model is significant to represent the studied response variable, i.e., the circulation.

In addition, R^2 and adjusted-R^2 were calculated to check the model adequacy. These coefficient represent the deviation in the response ascribed to the model. For a well-fitted model, R^2 and adjusted-R^2 should not be less than 80% (or 0.8) [58]. On the other hand, adjusted-R^2 will always be less than or equal to R^2 [59].

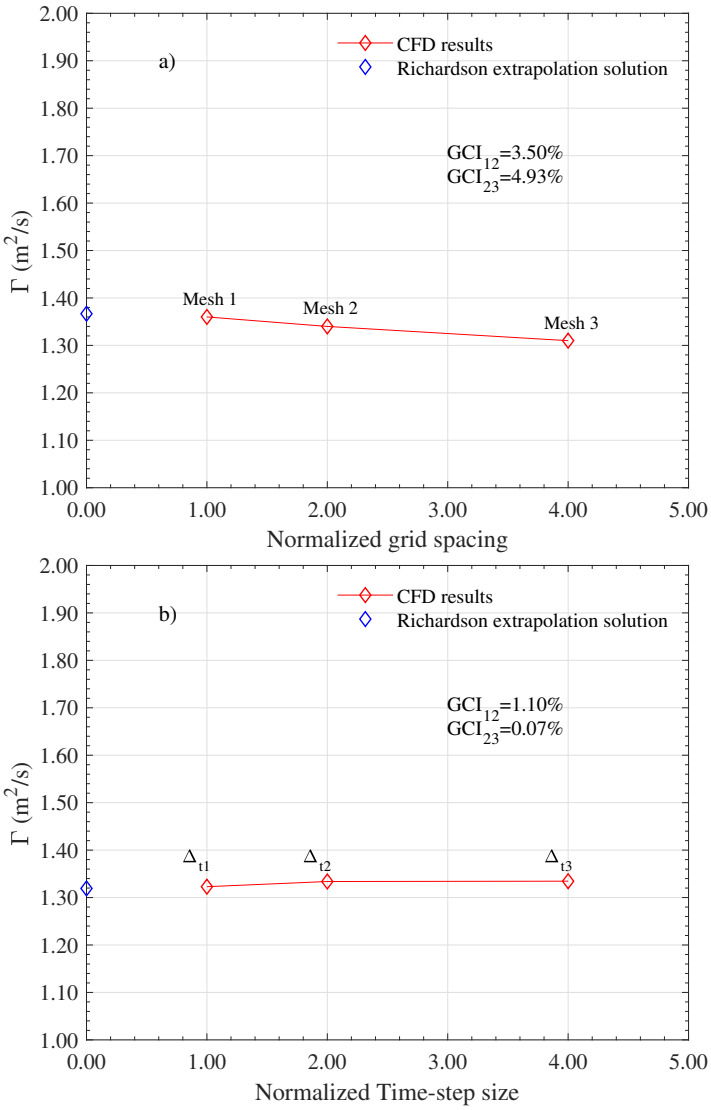

Fig. 6: a) Mesh independence test and b) time-step independence test.

R^2 and adjusted-R^2 were higher than 0.80, indicating that the regression model bulit was appropriate to describe the behavior of the evaluated variable response. The regression model equation that describes the circulation is expressed by Eq. 7:

$$\begin{aligned}\Gamma = -7.127 + 179.9(d/D) + 23.66(H/D) + 18.76(w/D) - 22.46(h/D) + 0.761(L/D) - 0.183(\gamma) - 496.7(d/D)^2 \\ -2.982(H/D)^2 - 10.64(w/D)^2 + 8.328(h/D)^2 + 0.00056(\gamma)^2 - 32.37(d/D)(H/D) + 26.24(d/D)(W/D) \\ +29.20(d/D)(h/D) + 0.13(d/D)(\gamma) - 19.14(H/D)(w/D) - 6.55(H/D)(h/D) + \\ 1.097(H/D)(L/D) + 4.517(w/D)(L/D) - 0.129(w/D)(\gamma) \\ -1.138(h/D)(L/D) + 0.161(h/D)(\gamma) - 0.0208(L/D)(\gamma)\end{aligned} \tag{7}$$

Once the regression model is constructed, its adequacy for representing the response variable must be checked. For this purpose, several tests of hypotheses such as the normality, homoscedasticity and residual independence are used. To check the normality of the residuals assumption, frequency distribution and normal probability were plotted. Normality assumption is satisfied when data are adjusted to the lines represented in Fig. 8. According to these plots, the

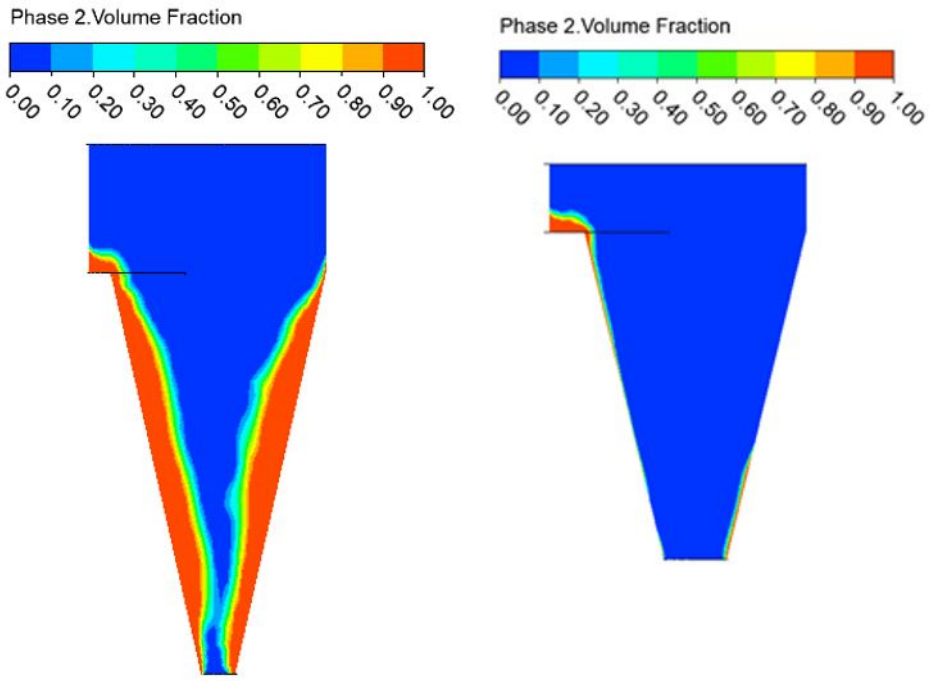

Fig. 7: Volume fraction of water of for: a) treatment 43 and b) treatment 23.

normality assumption is satisfied. The normal probability plot and frequency distribution for the residuals regarding the circulation are illustrated in Fig. 8. In addition to the graphical tests, numerical tests were performed, since they are a more reliable way to check the normality assumption [60]. The results of the normality tests for the circulation residuals are listed in Table 5.

The results indicate that the circulation residuals follow a normal distribution since the set of tests had a p-value higher than 0.05. To check homoscedasticity and residual independence, the studentized Breusch-Pagan, and the Durbin-Watson test, respectively, were used, and the p-values obtained were of 0.4176 and 0.9266, respectively. With a p-value greater than the considered significance level (0.05), it can be concluded that the residuals from the regression model are not autocorrelated and there is not a dependence of the error variance.

As a result, the regression model can be used for predicting the response at any combination of six variables investigated in the experimental domain. Furthermore, the regression model can be used to obtain the highest circulation only valid in the experimental range ; the value of the highest circulation obtained does not necessarily coincide with the value of the maximum circulation of the initial treatments. The highest circulation; was calculated as 2.089 m^2/s when the values of the six variables studied were d/D=0.167, H/D=1.840, w/D=0.2, h/D=0.599, L/D=0.500, and γ=179.976°. The difference between the circulation of treatment 43 and the new treatment (optimal geometry) is 6.85%. The response surface obtained using the regression model can be found in Figs. 9-12. The plots display the behavior of the transformed response concerning simultaneous changes in two independent factors. The optimal value for w/D and L/D corresponded with the minimum value of their respective range shown in Table 2. The opposite behavior occurs with H/D, h/D, and γ, whose optimal values are close to the maximum values of the high level. The optimal value of d/D (0.167) was within the range proposed by multiple researchers ($0.14<d/D<0.18$) who studied the effect of the diameter of the exit hole on the efficiency of the system and the optimal formation of the vortex [61, 12]. The most used value for d/D is 0.15. This value is close to the low level within the domain studied for this paremeter. The most common inlet channel used has a rectangular cross-section ($w \times h$) [9]; the result of the optimization process for the variables h and w coincides with this information since the values for h/D and w/D of 0.599 and 0.2, respectively, were obtained. Therefore, for a given$D$ value, the rectangular section channel dimensions can be determined.

In addition to the results obtained from the response surfaces, an equation was proposed to estimate the coefficient of discharge C_d to each geometry. The value of this coefficient is a function of d/D. C_d allows to estimate the value of the inlet velocity to maximize the value of the vortex circulation. It is highlighted that the coefficient C_d had not

Table 3
Latin hypercube sampling (LHS) distribution and numerical results

Run	d/D	H/D	w/D	h/D	L/D	γ [Deg]	Γ [m^2/s]
1	0.239	1.143	0.273	0.535	2.133	176.327	1.772
2	0.214	1.265	0.494	0.273	2.694	124.898	1.621
3	0.120	1.020	0.329	0.200	2.286	150.612	1.567
4	0.251	1.816	0.488	0.461	2.235	145.102	0.849
5	0.137	1.755	0.243	0.551	1.673	106.531	1.826
6	0.300	1.388	0.237	0.241	1.010	126.735	1.149
7	0.186	1.663	0.298	0.224	1.265	97.347	1.880
8	0.198	0.653	0.427	0.559	0.602	108.367	1.509
9	0.161	0.500	0.218	0.502	1.112	101.020	1.394
10	0.149	1.327	0.322	0.298	3.000	102.857	1.869
11	0.227	1.510	0.200	0.453	1.520	139.592	1.892
12	0.206	0.806	0.286	0.363	2.898	143.265	1.553
13	0.280	0.592	0.310	0.510	1.571	134.082	1.476
14	0.145	0.531	0.396	0.437	2.745	167.143	1.245
15	0.231	2.000	0.292	0.380	2.337	115.714	1.767
16	0.157	1.694	0.445	0.576	2.847	165.306	1.698
17	0.210	0.929	0.249	0.584	2.388	99.184	1.694
18	0.222	1.939	0.371	0.282	0.857	141.429	1.605
19	0.124	0.867	0.341	0.567	1.418	159.796	1.489
20	0.108	1.112	0.469	0.233	2.082	91.837	1.629
21	0.218	0.898	0.384	0.347	1.776	95.510	1.705
22	0.165	0.959	0.500	0.371	1.469	146.939	1.522
23	0.292	1.449	0.347	0.306	2.184	152.449	0.100
24	0.169	1.235	0.255	0.290	1.214	163.469	1.801
25	0.288	1.633	0.420	0.412	1.316	112.041	0.844
26	0.247	0.745	0.261	0.355	0.500	113.878	1.612
27	0.263	1.051	0.451	0.518	0.755	154.286	1.508
28	0.190	1.847	0.231	0.429	2.796	168.980	1.892
29	0.259	1.082	0.378	0.494	2.949	117.551	1.599
30	0.178	0.561	0.359	0.216	0.908	132.245	1.422
31	0.284	1.204	0.212	0.339	2.592	104.694	1.584
32	0.173	1.571	0.433	0.445	2.439	90.000	1.891
33	0.202	1.296	0.408	0.600	1.929	135.918	1.760
34	0.194	1.786	0.414	0.208	2.490	161.633	1.718
35	0.129	1.173	0.353	0.420	0.806	110.204	1.674
36	0.296	0.776	0.457	0.257	1.622	130.408	1.076
37	0.271	1.602	0.280	0.404	0.653	170.816	1.473
38	0.141	1.541	0.365	0.388	1.878	180.000	1.729
39	0.104	1.357	0.267	0.469	2.541	137.755	1.609
40	0.112	1.878	0.402	0.314	1.724	119.388	1.673
41	0.235	0.684	0.390	0.331	1.163	178.163	1.459
42	0.133	0.837	0.206	0.322	1.827	123.061	1.566
43	0.183	1.752	0.307	0.303	2.155	106.740	1.946
44	0.100	0.501	0.213	0.239	2.325	91.737	1.380
45	0.103	0.601	0.251	0.250	2.313	95.015	1.398
46	0.100	0.500	0.429	0.201	0.623	90.000	1.296
47	0.200	1.500	0.200	0.519	1.905	167.583	1.922
48	0.101	0.827	0.407	0.304	0.820	95.060	1.462
49	0.206	1.700	0.201	0.436	2.038	119.574	1.861
50	0.100	0.545	0.232	0.412	2.753	90.343	1.401
51	0.103	0.672	0.260	0.442	2.715	92.009	1.457
52	0.228	1.131	0.202	0.548	0.506	144.912	1.869
53	0.100	0.501	0.221	0.201	1.585	90.733	1.354
54	0.101	0.671	0.225	0.217	1.599	90.977	1.463
55	0.100	0.504	0.295	0.468	1.625	92.859	1.317
56	0.101	0.667	0.275	0.472	1.617	92.906	1.439
57	0.224	1.187	0.204	0.558	0.508	147.385	1.881
58	0.238	0.974	0.201	0.583	0.506	136.883	1.760
59	0.102	0.506	0.213	0.561	1.368	118.823	1.303
60	0.269	0.504	0.223	0.530	0.999	129.168	1.472

been reported before for any GWVHT. The experimental values reported in Fig. 5 were calculated from data reported in the literature [12, 27, 13, 28, 15].

Table 4
ANOVA results for the regression model.

Term	Effect	Degrees of freedom	Sum of squares	Mean squares	p-value	F-ratio
d/D (f_1)	179.9	1	3.40	3.40	0.13344	2.360
H/D (f_2)	23.66	1	246.82	246.82	4.82×10^{-15}	171.279
w/D (f_3)	18.76	1	83.72	83.72	6.12×10^{-9}	58.099
h/D (f_4)	-22.46	1	17.05	17.05	0.00152	11.832
L/D (f_5)	0.761	1	0.06	0.06	0.84303	0.040
γ (f_6)	-0.183	1	0.22	0.22	0.69931	0.152
f_1 f_1	-496.7	1	192.59	192.59	1.67×10^{-13}	133.645
f_2 f_2	-2.982	1	55.35	55.35	4.25×10^{-7}	38.407
f_3 f_3	-10.64	1	1.75	1.75	0.27744	1.217
f_4 f_4	8.328	1	1.35	1.35	0.33945	0.938
f_6 f_6	0.00056	1	7.75	7.75	0.02662	5.358
f_1 f_2	-32.37	1	41.28	41.28	5.53×10^{-6}	28.643
f_1 f_3	26.24	1	2.76	2.76	0.17524	1.914
f_1 f_4	29.20	1	3.71	3.71	0.11764	2.574
f_1 f_6	0.130	1	4.98	4.98	0.07147	3.455
f_2 f_3	-19.14	1	14.50	14.50	0.00314	10.062
f_2 f_4	-6.55	1	2.28	2.28	0.21711	1.580
f_2 f_5	1.097	1	2.42	2.42	0.20379	1.677
f_3 f_5	4.517	1	4.98	4.98	0.07146	3.456
f_3 f_6	-0.129	1	2.60	2.60	0.18796	1.803
f_4 f_5	-1.138	1	1.20	1.20	0.36786	0.832
f_4 f_6	0.161	1	7.24	7.24	0.03149	5.021
f_5 f_6	-0.0208	1	5.34	5.34	0.06234	3.707
Residuals	–	35	50.44	1.44	–	–
R^2	0.9331					
Adjusted-R^2	0.8891					

Table 5
Results of normality tests for the circulation residuals.

Test	P-value
Shapiro-Wilk test	0.2769
Cramer- von Mises test	0.2344
KS Limiting form	0.5341
Shapiro-Francia test	0.3890
Jarque-Bera test	0.3911
Anderson-Darling test	0.2500
D'Agostino & Pearson test	0.3389
KS Lilliefors modification	0.1663

4. Conclusions

The GWVHT efficiencies that vary between 17 and 85%. To achieve the highest efficiency values, it was necessary to begin by analyzing the physics of the problem, i.e., the free-surface vortex. Before increasing the conversion efficiency of the turbine, increasing the circulation by changing some geometric parameters of the basin and the inlet channel was required.

RSM was used to define the optimal geometry that gives the highest circulation. RSM also provides a prediction model representing this responsable variable. A second-order polynomial prediction model was developed using linear regression analysis. The circulation was transformed, using a fourth-power transformation in oder to obtain a suitable

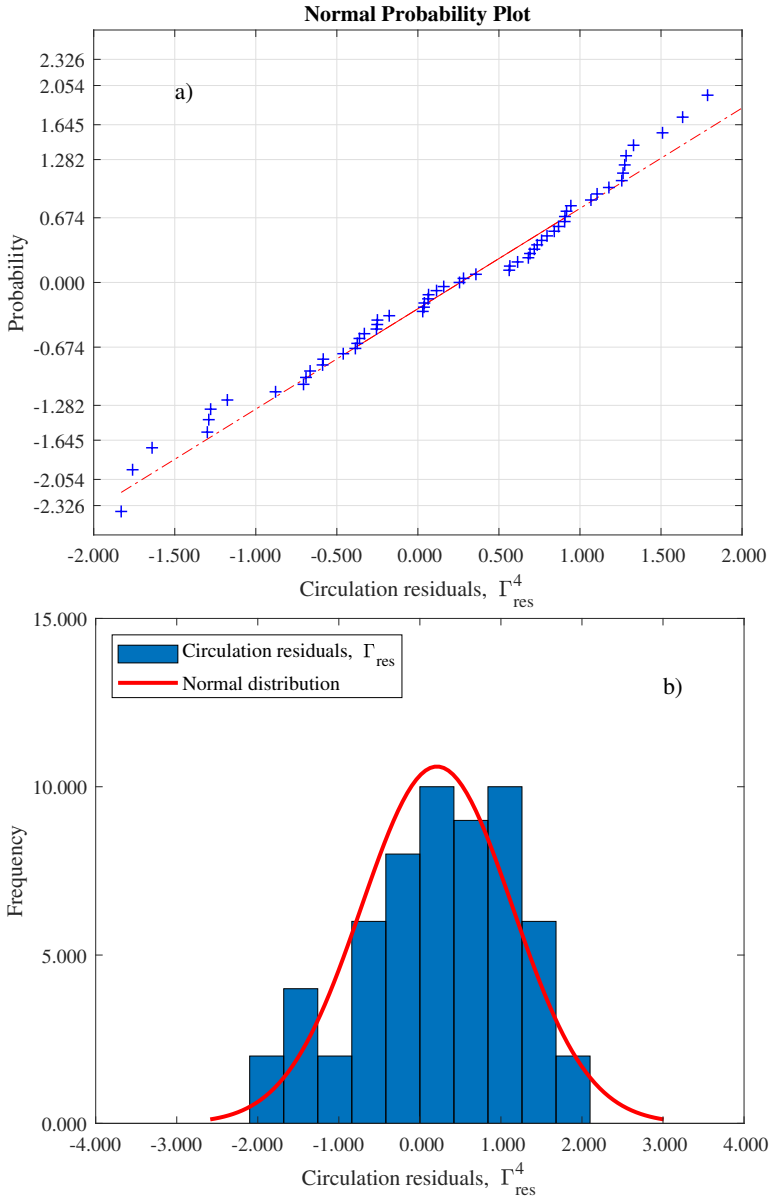

Fig. 8: a) Normal probability plot and b) frequency distribution for the circulation residuals.

estimated regression model. LHS was used to generate the 60 study geometries. The values of the six variables prvoing the maximum circulation of 2.089 m^2/s were d/D=0.167, H/D=1.840, w/D=0.2, h/D=0.599, L/D=0.500 and γ=179.976°. From the second-order regression model, the terms h/D, w/D, H/D, $(d/D)^2$, $(H/D)^2$, $(\gamma)^2$, $(d/D)(H/D)$, and $(H/D)(w/D)$ had the highest influence on the circulation. The difference between the circulation of treatment 43 and the treatment giving the optimal geometry was 6.85%. The increased circulation represents a hogh amount of energy available in the flow to be used for producing electricity. Since the geometric factors are dimensionless due to they were divided by the diameter of the basin, new geometries are feasible to be generated.

Moreover, an equation for the calculation of the discharge coefficient was proposed. This equation is a function of the d/D ratio. C_d allows the calculation of the inlet velocity that maximizes the value of the circulation, and it is suitable to be used when the d/D ratio varies between 0.1 and 0.3.

The design of GWVHT still has many geometric configurations that have not yet been examined. Therefore, there are many options to be explored for future geometric designs. Optimization methodologies, such as RSM, are demonstrated to be efficient alternatives for conducting a more precise search in the improvement of the selected response variable.The priorities for further work are the selection of the runner that allows to extract the greatest

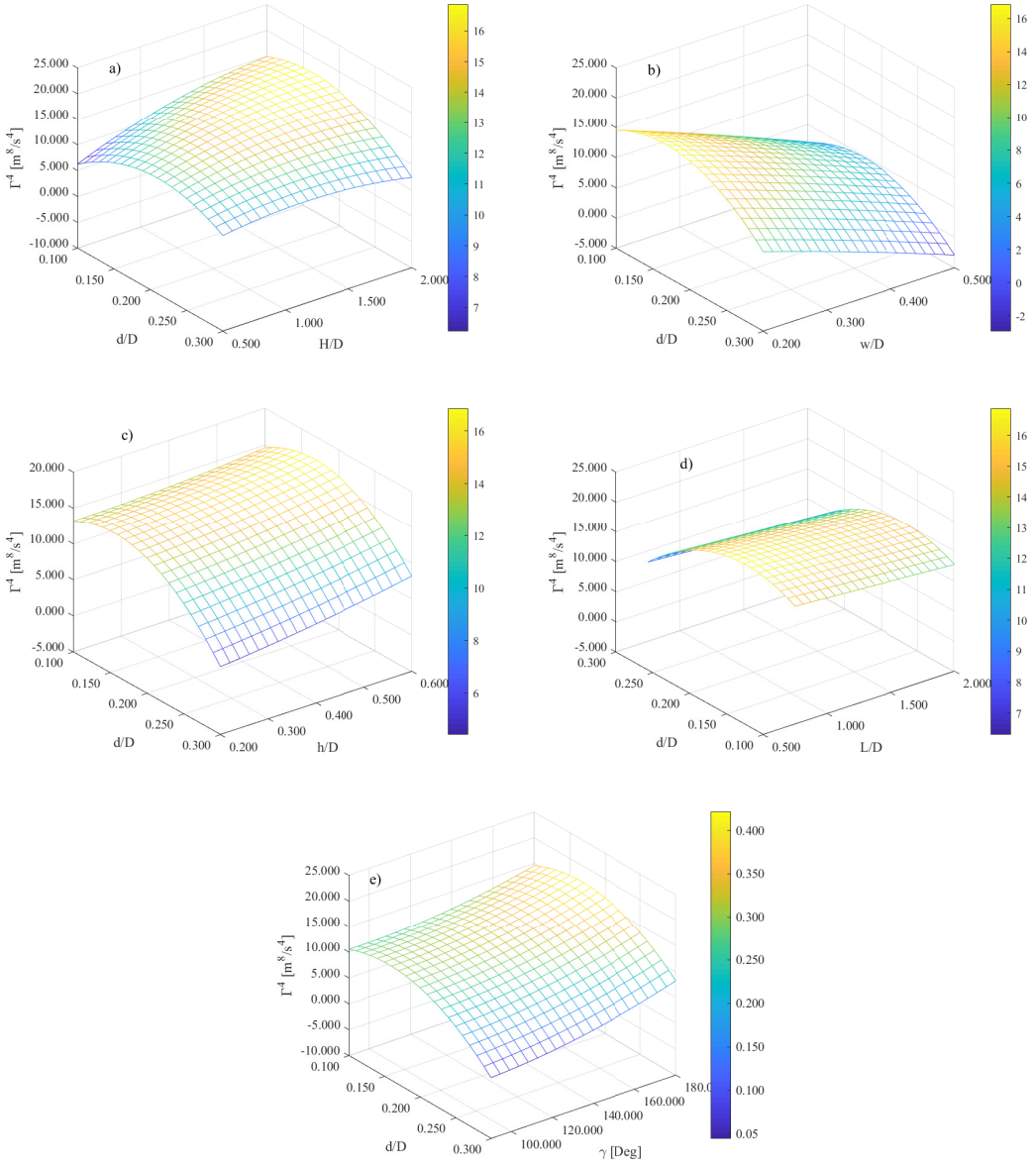

Fig. 9: Response surface plots for the vortex circulation (Γ^4) by using the ansformed regression model. a) Interaction of factors f1 and f2, b) Interaction of factors f1 and f3, c) Interaction of factors f1 and f4, d) Interaction of factors f1 and f5, and e) Interaction of factors f1 and f6. The factors that were not considered in the axis defining the surface plots were set at their optimal values.

energy available in the flow, by using the optimized geometry in this study, and the execution of experimental tests that enable to validate the proposed design geometry.

References

[1] S. Sorrell, Reducing energy demand: A review of issues, challenges and approaches, Renewable and Sustainable Energy Reviews 47 (2015) 74–82.

[2] M. Majid, et al., Renewable energy for sustainable development in india: current status, future prospects, challenges, employment, and investment opportunities, Energy, Sustainability and Society 10 (2020) 1–36.

[3] R. Ploetz, R. Rusdianasari, E. Eviliana, Renewable energy: Advantages and disadvantages, in: Proceeding Forum in Research, Science, and Technology (FIRST) 2016, Politeknik Negeri Sriwijaya, 2016.

[4] G. Boyle, Renewable energy, 2004.

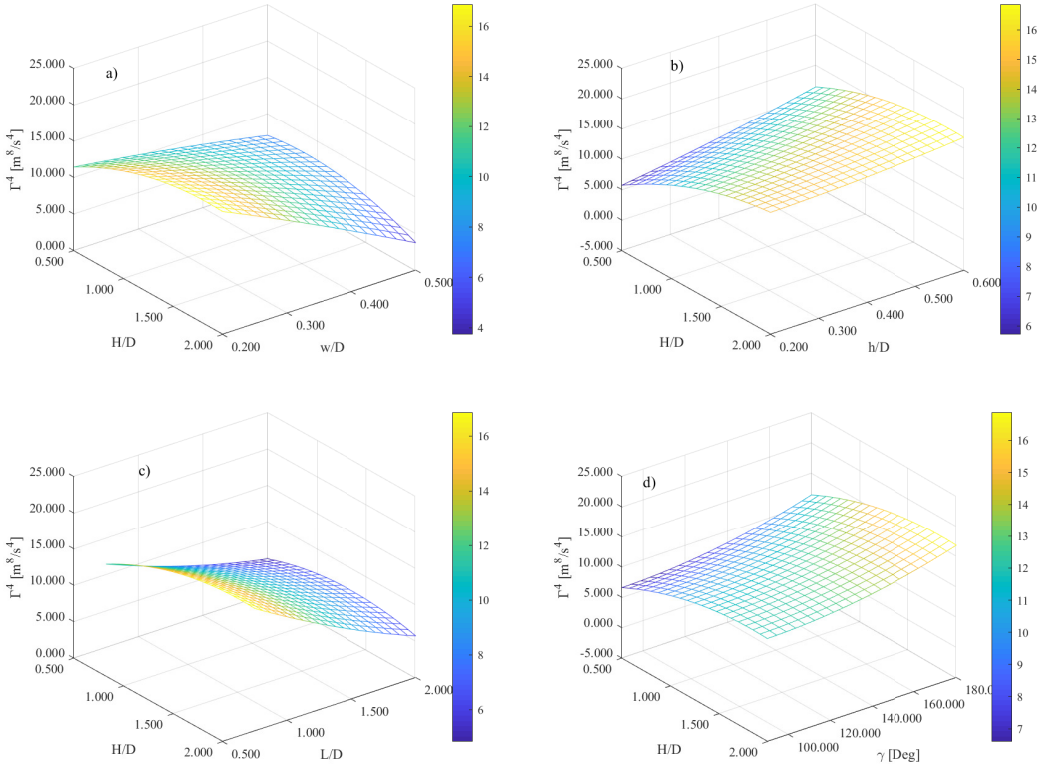

Fig. 10: Response surface plots for the vortex circulation (Γ^4) by using the transformed regression model. a) Interaction of factors f2 and f3, b) Interaction of factors f2 and f4, c) Interaction of factors f2 and f5, and d) Interaction of factors f2 and f6. The factors that were not considered in the axis defining the surface plots were set at their optimal values.

[5] V. K. Singh, S. Singal, Operation of hydro power plants-a review, Renewable and Sustainable Energy Reviews 69 (2017) 610–619.

[6] O. A. Hoes, L. J. Meijer, R. J. Van Der Ent, N. C. Van De Giesen, Systematic high-resolution assessment of global hydropower potential, PLoS One 12 (2017) e0171844.

[7] A. B. Timilsina, S. Mulligan, T. R. Bajracharya, Water vortex hydropower technology: a state-of-the-art review of developmental trends, Clean Technologies and Environmental Policy 20 (2018) 1737–1760.

[8] V. J. A. Guzmán, J. A. Glasscock, F. Whitehouse, Design and construction of an off-grid gravitational vortex hydropower plant: A case study in rural peru, Sustainable Energy Technologies and Assessments 35 (2019) 131–138.

[9] L. Velásquez, E. Chica, J. Posada, Advances in the development of gravitational water vortex hydraulic turbines., Journal of Engineering Science & Technology Review 14 (2021).

[10] A. Kuriqi, A. N. Pinheiro, A. Sordo-Ward, L. Garrote, Influence of hydrologically based environmental flow methods on flow alteration and energy production in a run-of-river hydropower plant, Journal of Cleaner Production 232 (2019) 1028–1042.

[11] S. Mulligan, Experimental and numerical analysis of three-dimensional free-surface turbulent vortex flows with strong circulation, Ireland: Institute of Technology Sligo (2015).

[12] S. Dhakal, S. Nakarmi, P. Pun, A. B. Thapa, T. R. Bajracharya, Development and testing of runner and conical basin for gravitational water vortex power plant, Journal of the Institute of Engineering 10 (2014) 140–148.

[13] S. Dhakal, A. B. Timilsina, R. Dhakal, D. Fuyal, T. R. Bajracharya, H. P. Pandit, N. Amatya, Mathematical modeling, design optimization and experimental verification of conical basin: Gravitational water vortex power plant, in: dalam World Largest Hydro Conference, 2015.

[14] A. Gautam, A. Sapkota, S. Neupane, J. Dhakal, A. B. Timilsina, S. Shakya, Study on effect of adding booster runner in conical basin: gravitational water vortex power plant: a numerical and experimental approach, in: Proceedings of IOE Graduate Conference, 2016, pp. 107–113.

[15] R. Dhakal, T. Bajracharya, S. Shakya, B. Kumal, N. Kathmandu, K. Khanal, N. Kavre, S. Williamson, S. Gautam, D. Ghale, Computational and experimental investigation of runner for gravitational water vortex power plant, in: Proceedings of a meeting held, volume 5, 2017, p. 8.

[16] R. Ullah, T. A. Cheema, A. S. Saleem, S. M. Ahmad, J. A. Chattha, C. W. Park, Performance analysis of multi-stage gravitational water vortex turbine, Energy Conversion and Management 198 (2019) 111788.

[17] T. R. Bajracharya, S. R. Shakya, A. B. Timilsina, J. Dhakal, S. Neupane, A. Gautam, A. Sapkota, Effects of geometrical parameters in gravitational water vortex turbines with conical basin, Journal of Renewable Energy 2020 (2020).

[18] J. A. Chattha, T. A. Cheema, N. H. Khan, Numerical investigation of basin geometries for vortex generation in a gravitational water vortex power plant, in: 2017 8th International Renewable Energy Congress (IREC), IEEE, 2017, pp. 1–5.

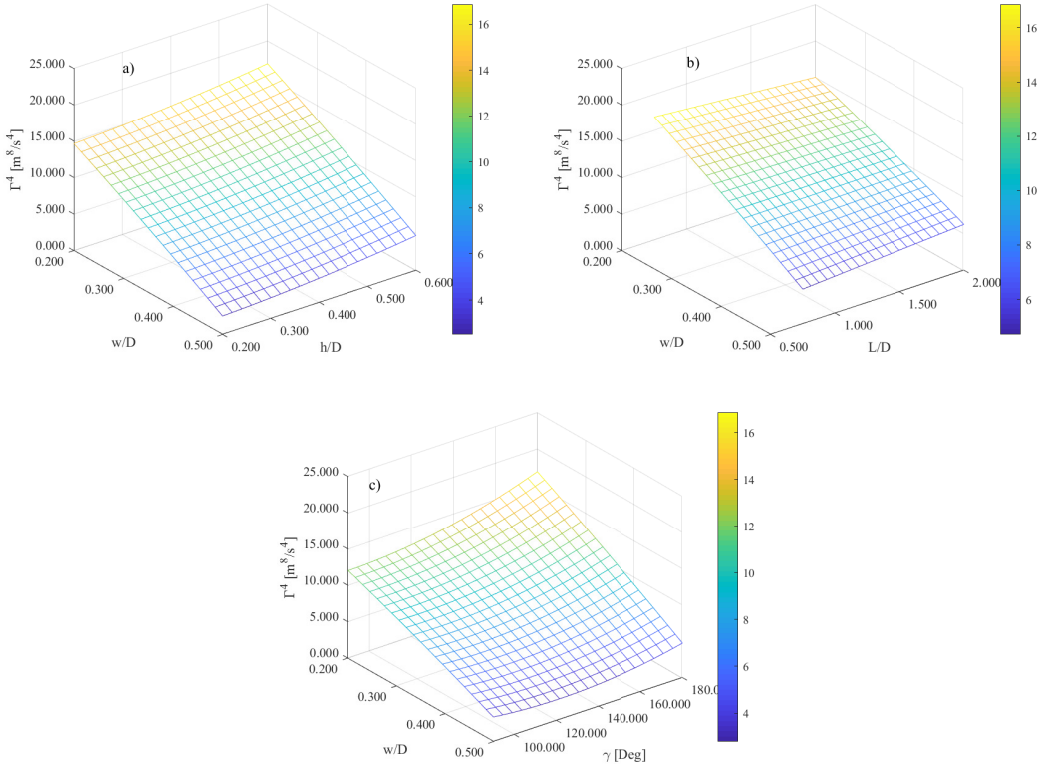

Fig. 11: Response surface plots for the vortex circulation (Γ^4) by using the transformed regression model. a) Interaction of factors f3 and f4, b) Interaction of factors f3 and f5, and c) Interaction of factors f3 and f6. The factors that were not considered in the axis defining the surface plots were set at their optimal values.

[19] L. Velásquez, A. Rubio-Clemente, E. Chica, Numerical analysis of the inlet channel and basin geometries for vortex generation in a gravitational water vortex power plant, in: 18th Inter Conference on Renew Energies and Power Quality, 2020.

[20] C. Christopher, D. Adanta, et al., The effect of basin geometry on gravitational vortex hydropower, in: IOP Conference Series: Materials Science and Engineering, volume 788, IOP Publishing, 2020, p. 012081.

[21] V. J. A. Guzmán, J. A. Glasscock, Analytical solution for a strong free-surface water vortex describing flow in a full-scale gravitational vortex hydropower system, Water Science and Engineering 14 (2021) 72–79.

[22] J. D. Anderson Jr, Fundamentals of aerodynamics, Tata McGraw-Hill Education, 2010.

[23] Y. A. Cengel, Fluid mechanics, Tata McGraw-Hill Education, 2010.

[24] R. Ullah, T. A. Cheema, A. S. Saleem, S. M. Ahmad, J. A. Chattha, C. W. Park, Preliminary experimental study on multi-stage gravitational water vortex turbine in a conical basin, Renewable Energy 145 (2020) 2516–2529.

[25] S. Dhakal, A. B. Timilsina, R. Dhakal, D. Fuyal, T. R. Bajracharya, H. P. Pandit, Effect of dominant parameters for conical basin: Gravitational water vortex power plant, in: Proceedings of IOE graduate conference, 2014, p. 381.

[26] P. Sritram, W. Treedet, R. Suntivarakorn, Effect of turbine materials on power generation efficiency from free water vortex hydro power plant, in: IOP Conference Series: Materials Science and Engineering, volume 103, IOP Publishing, 2015, p. 012018.

[27] S. Dhakal, A. B. Timilsina, R. Dhakal, D. Fuyal, T. R. Bajracharya, H. P. Pandit, N. Amatya, A. M. Nakarmi, Comparison of cylindrical and conical basins with optimum position of runner: Gravitational water vortex power plant, Renewable and Sustainable Energy Reviews 48 (2015) 662–669.

[28] R. Dhakal, A. Nepal, A. Acharya, B. Kumal, T. Aryal, S. Williamson, K. Khanal, L. Devkota, Technical and economic prospects for the site implementation of a gravitational water vortex power plant in nepal, in: 2016 IEEE International Conference on Renewable Energy Research and Applications (ICRERA), IEEE, 2016, pp. 1001–1006.

[29] M. Rahman, T. J. Hong, R. Tang, L. L. Sung, F. B. M. Tamiri, Experimental study the effects of water pressure and turbine blade lengths & numbers on the model free vortex power generation system, International Journal of Current Trends in Engineering & Research (IJCTER) 2 (2016) 13–17.

[30] S. Sreerag, C. Raveendran, B. Jinshah, Effect of outlet diameter on the performance of gravitational vortex turbine with conical basin, International Journal of Scientific & Engineering Research 7 (2016) 457–463.

[31] P. Loaiza, J. Jaramillo, Generación eléctrica basada en vórtice gravitacional, una opción para la provisión sustentable de energía eléctrica en la zona rural del cantón loja, línea]. Available: https://es. scribd. com/document/291952945/Generacion-electrica-basada-envortice-gravitacional-una-opcion-para-la-provision-sustentable-de-energia-electrica-en-lazona-rural-del-canton-Loja.[Último acceso: 8

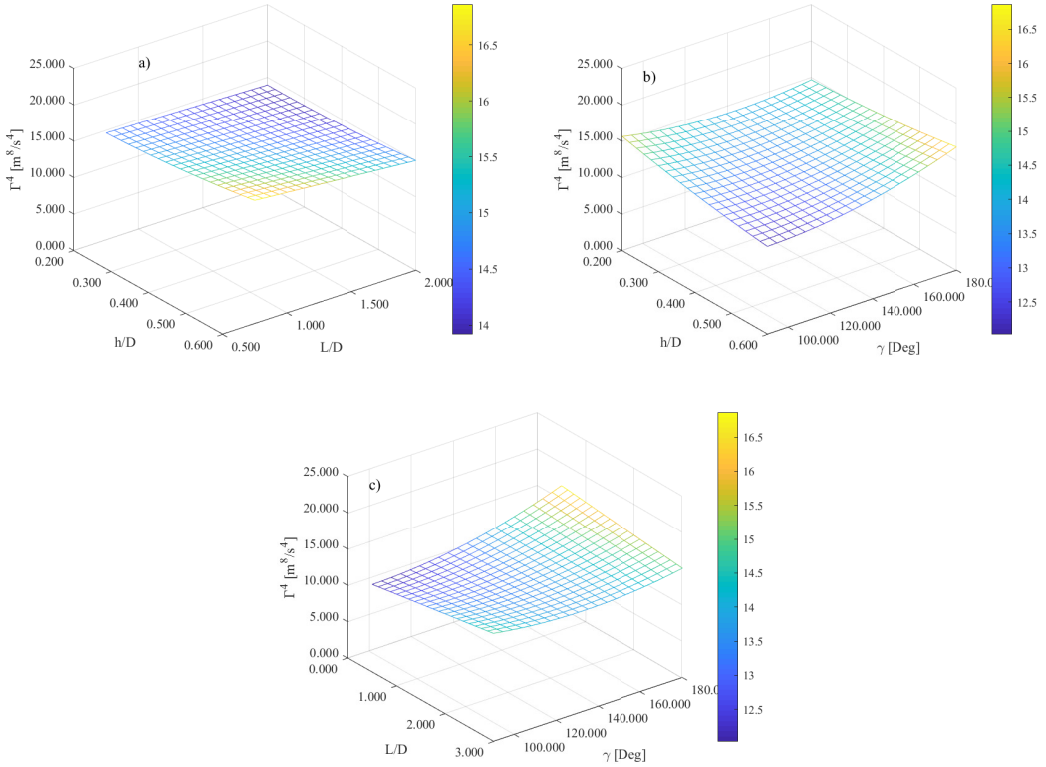

Fig. 12: Response surface plots for the vortex circulation (Γ^4) by using the transformed regression model. a) Interaction of factors f4 and f5, b) Interaction of factors f4 and f6, and c) Interaction of factors f5 and f6. The factors that were not considered in the axis defining the surface plots were set at their optimal values.

2020] (2016).
[32] Y. Nishi, T. Inagaki, Performance and flow field of a gravitation vortex type water turbine, International Journal of Rotating Machinery 2017 (2017).
[33] T. Bajracharya, R. Ghimire, A. Timilsina, Design and performance analysis of water vortex powerplant in context of nepal, in: 20th International Seminar on Hydropower Plants, 2018, pp. 14–16.
[34] S. Acharya, S. K. Ghimire, H. B. Dura, Design study of runner for gravitational water vortex power plant with conical basin, in: Proceedings of IOE Graduate Conference, 2019.
[35] A. Poudel, A. K. Jha, Techno-economic assessment of gravitational water vortex power plant: A case study of sunsari-morang irrigation project, Artech J. Eff. Res. Eng. Technol 1 (2020) 34–41.
[36] A. Sedai, B. K. Yadav, B. B. Kumal, A. Khatiwada, R. Dhakal, Performance analysis of gravitational water vortex power plant using scale-down model (2020).
[37] A. E. Şenaras, Parameter optimization using the surface response technique in automated guided vehicles, in: Sustainable Engineering Products and Manufacturing Technologies, Elsevier, 2019, pp. 187–197.
[38] A. Y. Aydar, Utilization of response surface methodology in optimization of extraction of plant materials, Statistical approaches with emphasis on design of experiments applied to chemical processes (2018) 157–169.
[39] D. Baş, I. H. Boyacı, Modeling and optimization i: Usability of response surface methodology, Journal of food engineering 78 (2007) 836–845.
[40] A. Witek-Krowiak, K. Chojnacka, D. Podstawczyk, A. Dawiec, K. Pokomeda, Application of response surface methodology and artificial neural network methods in modelling and optimization of biosorption process, Bioresource technology 160 (2014) 150–160.
[41] Y. Choi, D. Song, S. Yoon, J. Koo, Comparison of factorial and latin hypercube sampling designs for meta-models of building heating and cooling loads, Energies 14 (2021) 512.
[42] T. Keskin Gündoğdu, I. Deniz, G. Çalışkan, E. S. Şahin, N. Azbar, Experimental design methods for bioengineering applications, Critical reviews in biotechnology 36 (2016) 368–388.
[43] V. Czitrom, One-factor-at-a-time versus designed experiments, The American Statistician 53 (1999) 126–131.
[44] D. C. Montgomery, Design and analysis of experiments, John wiley & sons, 2017.
[45] J. Menčík, Latin hypercube sampling, Concise Reliability for Engineers 1 (2016) 118–119.
[46] A. Forrester, A. Sobester, A. Keane, Engineering design via surrogate modelling: a practical guide, John Wiley & Sons, 2008.
[47] S. Koziel, L. Leifsson, Surrogate-based modeling and optimization, Springer, 2013.

[48] J. R. Holton, An introduction to dynamic meteorology, American Journal of Physics 41 (1973) 752–754.
[49] M. Antuono, A. Colagrossi, D. Le Touzé, J. J. Monaghan, Conservation of circulation in sph for 2d free-surface flows, International Journal for Numerical Methods in Fluids 72 (2013) 583–606.
[50] K. Zore, G. Parkhi, B. Sasanapuri, A. Varghese, Ansys mosaic poly-hexcore mesh for high-lift aircraft configuration, in: 21th Annual CFD Symposium, 2019.
[51] P. Maruzewski, H. Hayashi, C. Munch, K. Yamaishi, T. Hashii, H. Mombelli, Y. Sugow, F. Avellan, Turbulence modeling for francis turbine water passages simulation, in: IOP Conference Series: Earth and Environmental Science, volume 12, IOP Publishing, 2010, p. 012070.
[52] L. F. Toapanta-Ramos, J. A. Zapata-Cautillo, A. I. Cholango-Gavilanes, W. Quitiaquez, C. Nieto-Londoño, Z. Zapata-Benabithe, Estudio numérico y comparativo del efecto de turbulencia en codos y dobleces para distribución de agua sanitaria, Revista Facultad de Ingeniería 28 (2019) 101–118.
[53] M. G. Marian, T. Sajin, A. Azzouz, Study of micro hydropower plant operating in gravitational vortex flow mode, in: Applied Mechanics and Materials, volume 371, Trans Tech Publ, 2013, pp. 601–605.
[54] M. Rakowitz, Grid refinement study with a uhca wing-body configuration using richardson extrapolation and grid convergence index gci, in: New results in numerical and experimental fluid mechanics III, Springer, 2002, pp. 297–303.
[55] A. Cuevas, M. Febrero, R. Fraiman, An anova test for functional data, Computational statistics & data analysis 47 (2004) 111–122.
[56] J. Pietraszek, M. Kołomycki, A. Szczotok, R. Dwornicka, The fuzzy approach to assessment of anova results, in: International Conference on Computational Collective Intelligence, Springer, 2016, pp. 260–268.
[57] S. McLeod, What a p-value tells you about statistical significance, Simply psychology (2019) 1–4.
[58] E. Ostertagová, Modelling using polynomial regression, Procedia Engineering 48 (2012) 500–506.
[59] J. Frost, D. D. Says, J. F. Says, How to interpret r-squared in regression analysis, Statistics By Jim (2017).
[60] M. Bouvant, J. Betancour, L. Velásquez, A. Rubio-Clemente, E. Chica, Design optimization of an archimedes screw turbine for hydrokinetic applications using the response surface methodology, Renewable Energy 172 (2021) 941–954.
[61] S. Mulligan, P. Hull, Design and optimisation of a water vortex hydropower plant", undergraduate thesis, inst. of tech, Sligo, Sligo, Ireland (2010).

CHAPTER 4

MULTI-OBJECTIVE OPTIMIZATION USING SURROGATE MODELING

Surrogate modeling method for multi-objective optimization of the inlet channel and the basin of a gravitational water vortex hydraulic turbine

Published article

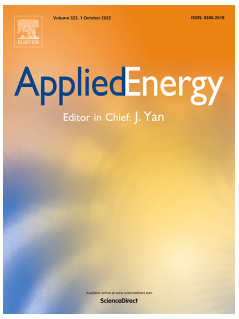

Applied Energy provides a forum for information on innovation, research, development and demonstration in the areas of energy conversion and conservation, the optimal use of energy resources, analysis and optimization of energy processes, mitigation of environmental pollutants, and sustainable energy systems. The journal publishes original papers, review articles, technical notes, and letters to the editor. The breadth of coverage ranges from innovative technologies and systems of both fossil and renewable energy to the economic industrial and domestic use of energy with no or minor impact on the environment.

Highlights

- The gravitational water vortex hydraulic turbine (GWVHT) takes advantage of the potential and kinetic energy of an artificial vortex in a circulation chamber.
- GWVHT was optimized through a multi-objective genetic algorithm.
- Transition-state, volume of fluid (VoF), and $k-\epsilon$ RNG turbulence model were chosen to perform the simulations in CFD.
- The circulation and the volume flow rate for the compromise solution were 1.699 m^2/s and 0.00305 m^3/s, respectively.

Surrogate modeling method for multi-objective optimization of the inlet channel and the basin of a gravitational water vortex hydraulic turbine

Laura Velásquez, Alejandro Posada and Edwin Chica

ABSTRACT

This work presents a high-fidelity surrogate model for generating a multi-objective genetic algorithm to allow the search for the optimal geometry of the inlet channel and the basin of a gravitational water vortex hydraulic turbine. Six parameters were considered for the optimization: the relations between the basin diameter (D) and the basin height (H), H/D; the wrap-around angle (γ), the outlet diameter (d) and D, d/D; the inlet channel width (w) and D, w/D; the inlet channel height (h) and D, h/D; and the inlet channel length (L) and D, L/D. Two conflicting objectives were studied: maximizing the vortex strength (Γ) and minimizing the volume flow rate (Q). The multi-objective optimization problem was resolved by applying the *gamultiobj* function in Matlab R2018b software. The optimization combines the genetic algorithm with Kriging interpolation to obtain the Pareto front. To train the *gamultiobj* function, an initial population of 40 individuals was used. As a stopping criterion, themaximum generation of 500 individuals was established. To improve the Pareto front, 20 optimization cycles (60 new samples) were required, reaching a final population of 100 individuals. It was found from the Pareto front that the values of the six variables providing the compromise solution, between Γ and Q, were H/D =1.572, L/D =1.518, h/D =0.565, w/D =0.361, d/D =0.108, and γ=92.141°. This solution reaches a Q of 0.00305 m^3/s and a Γ of 1.699 m^2/s. The results of this study were compared with the results reported by other authors, who optimized this type of turbine by applying the response surface methodology. The difference between these results was less than 9.61%.

1. Introduction

A hydraulic turbine is a turbomachine, which converts the energy of a fluid to produce a rotational movement that moves a machine (primary energy) or an electrical generator that produces electrical energy (secondary energy). According to their degree of reaction, turbines are classified into action or reaction turbines, differing from each other in the way of transforming water energy [1, 2]. In action turbines, the pressure remains constant throughout the rotor (atmospheric pressure); therefore, the height of the pressure absorbed by the rotor is zero [3, 4]. Action turbines are used with relatively high hydraulic loads, but with relatively low flow rates [5]. The Pelton, Turgo, cross flow and gravitational water vortex hydraulic turbines (GWVHTs) are within this classification [6]. In turn, in reaction turbines, the pressure at the entrance of the rotor is greater than the pressure at the outlet; therefore, the pressure head is different from zero. Reaction turbines are used with relatively low hydraulic loads, but with high flow rates [3, 5]. Francis, Archimedes screw and Deriaz turbines belong to this group of turbines [4]. GWVHTs take advantage of the potential and kinetic energy of an artificial vortex in a circulation chamber (or basin) with an outlet hole in the bottom [7]. A vortex is a region in a fluid in which the flow rotates around an axis [8]. There are two types of vortexes: strong and weak vortexes. In a weak vortex flow, the axial flow dominates, meanwhile in a strong vortex flow, the circulation dominates [9]. A strong vortex is formed because of induced circulation. The vortex has a stable full air core. Contrary to the strong vortex, a weak vortex is formed when the flow depth approaches the critical submergence and air is drawn into the intake [9]. A power generation system with a GWVHT is a run-of-river power plant with a strong vortex. In this type of power plant, water must be used as soon as it is available to drive the turbine. GWVHTs do not have a reservoir; therefore, the flow supplied oscillates according to the season of the year. These turbines develop their maximum power in the season of abundant rainfall, while the generated power is reduced, becoming almost zero in some rivers, during the dry season. By their characteristics, GWVHTs are adequate for distributed energy systems [7]. The 21 installed GWVHTs in the world have efficiencies that vary between 17 and 85% [10]. The number of studies on

ORCID(s): 0000-0003-1483-0104 (L. Velásquez); 0000-0001-5836-0680 (A. Posada); 00000-0002-5043-6414 (E. Chica)

GWVHTs reported in the literature is scarce. Some of them focus on the effects on the efficiency of some parameters of the basins, runner forms and their positions in the basins [10, 11, 12, 13, 14, 9, 15, 16]. Others are focused on the optimization of the inlet channel and the circulation chamber for the formation of the vortex [17, 18, 19]. It is important to note that the optimization procedures used in the field have been mainly based on one-factor-at-a-time techniques (OFATs). OFATs are based on fixing all parameters except one independent variable with an individual effect. These techniques have several limitations, since they require more runs for the same precision in the effect estimation, they cannot estimate interactions between independent variables, missing the optimal setting of the independent variables evaluated [20, 21, 22]. he classic configuration of an optimization process involves the definition of a single objective function to be improved, which depends on several variables. This single-objective formulation aims to obtain the best possible solution available, defined as the global optimum of the problem of interest [23, 24]. However, due to the heavy reliance of real-world problems on different, often conflicting goals, the single-goal formulation has proven to be inadequate for realistic solutions. That is why multi-objective approaches should be considered whether a reliable computational design is to be performed, as it provides rich information for designers to make better compromised decisions [25, 24]. Multi-objective optimization of energy systems has been converted, recently, in a vital optimization strategy. A multi-objective optimization is a methodology to optimize several objectives at the same time [26]. In a multi-objective optimization, the objectives are usually conflicting [27] and, therefore, there is no a single solution (global optimum); in contrast, there is a set of solutions (non-dominated), known as Pareto optimal solutions [28]. Due to its wide efficiency range, the optimization of GWVHTs attracts many researches, especially in recent years [12, 13, 14, 15, 16]. Intuitive or trial and error techniques have been used to design gravitational vortex turbines; in this regard, an appropriate method is sought to optimize this kind of systems. Among the optimization methods the multi-objective genetic algorithm stands out. It is a self-adaptive global searching algorithm. A genetic algorithm is an interactive process based on a population, in which everyone is evolved. The evolution of a population depends on the genetic operators. The genetic operators are selection, mutation, and crossover [29]. For the genetic algorithm to evolve, it does not only require the operators, but also mathematical models are necessary to help predict the behavior of the population. These mathematical models are known as surrogate models or metamodel. Surrogate models are equations that imitate the behavior of the population [30, 31, 32]. Surrogate models were built with training data [33]. These data are obtained from simulations or experiments carried out on the population. Many surrogate models have been developed to optimize systems in various fields, including engineering design problems as environmental modeling, energy systems, and civil and aerospace structures. Aguilar et al. [34] optimized a multi-element hydrofoil to be used in a horizontal-axis hydrokinetic turbine using a surrogate model. The objectives in the optimization process was to maximize the lift coefficient (C_L) and minimize the drag coefficient (C_D) to increase the ratio between C_L/C_D. The results indicated an increase of 9.5% in the value of C_L/C_D. Ghorani et al. [35] used Kriging (KRG) surrogate model to estimate the optimal combination of the blade inlet and the outlet angles, the blade wrap angle, the runner inlet width and the number of blades in a pump as turbine (PAT) to decrease the irreversible hydraulic losses and to increase the hydraulic efficiency of the PAT. The results of the surrogate model allowed a reduction of 3.8% in the irreversible hydraulic losses and an increase of 5.72% in the efficiency. Do Nascimento et al. [36]conducted an optimization process to find the optimal design of a counter-flow plate-fin compact heat exchanger (PFHE). The surrogate model was designed to achieve the maximum effectiveness, the minimum volume and the pressure drop at the hot and cold sides in the PFHE design. The optimized results showed that the volume and effectiveness values are in agreement with the literature, decreasing approximately 55.4% and 72.3% of the pressure drop at the hot and cold sides, respectively, which showed that the convective heat transfer was enhanced, and the flow resistance was also significantly reduced. In turn, Zhang et al. [37] employed the subrogate model to design a bistable laminates. Bistable laminates have wide application prospects as deployable structures of aerospace structures and wind turbines. The trigger forces of bistable laminates during snapping to another stable configuration were the mechanical objective functions, while the curvatures of their different stable configurations were used as the conflicting objective functions. The bistable laminate initial design was compared with the optimal design in experiments, and the ability of the optimization method was verified. Under this scenario, this study is focused on the numerical optimization of the inlet channel and the circulation chamber of a GWVHT using surrogate model. The objectives of the optimization process were to increase the vortex strength and minimize the volume flow rate. The vortex strength and the volume flow rate are directly related to the power generation. The power generation increases when the volume flow rate and the vortex strength increase; therefore, to maximize the vortex strength, increasing the volume flow rate would be required, which was stated in the proposed objective. The minimization of the volume flow rate was an objective of the study due to the need to optimize the turbine for the dry season; i.e., the optimization of a turbine for the minimum critical volume flow rate conditions. In

this regard, multi-objective genetic algorithm and computational fluid dynamics (CFD) simulations were used. This optimization problem involves six factors or geometrical parameters. The geometrical parameters considered in the optimization were the basin height (H), the basin diameter (D), the inlet channel length (L), the inlet channel height (h), the inlet channel width (w), the outlet diameter (d) and the wrap-around angle (γ). The study excluded the runner. The six geometric factors were used simultaneously to evaluate their combined effect on the two conflicting objectives: the vortex strength (Γ) and the volume flow rate (Q). The results allowed the identification of a Pareto optimal solution set to select a compromise solution between the conflicting objectives.

2. Methods and materials

2.1. Gravitational water vortex hydraulic turbine

GWVHT is a low hydraulic head hydropower plant. The main components of this turbine are the inlet channel, the circulation chamber or the basin, and the runner. In a GWVHT, a vortex is induced in the circulation basin when water exits through a hole at its base. The generated mechanical energy of the vortex is converted to electrical energy using a generator [38]. An overview of a GWVHT is shown in Figure 1 [39]. For the circulation chamber, cylindrical and conical chambers with tangential inlet channel are normally used [7]. Conical basins are preferred since they produce higher tangential velocity, which represents a higher output-generated power [11, 40]. In this study, the turbine to be optimized has a wrap-around inlet channel and a conical chamber. A wrap-around inlet or spiral inlet channel is normally utilized as a cyclone separator [41, 42, 43, 44]. A cyclone is a mechanism for separating solid particles from a flow. This mechanism uses the centrifugal force produced by the spiraling flow to separate the solid particles [45]. A vortex is created inside of the cyclone. This vortex is like a vortex in a GWVHT. Six variables were used to define the geometry of the turbine.

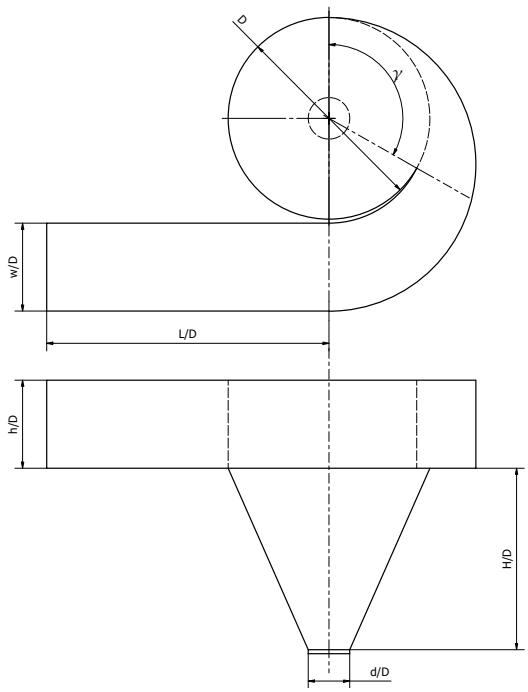

Fig. 1: Gravitational water vortex hydraulic turbine without runner: a) top view and b) front view [39].

The low and high levels of the variables used to define the geometry are reported in Table 1. These ranges were determined according to the research carried out by Velásquez et al. [7]. Velásquez et al. [7] tabulated the values of the variables D, d, w, h, L and H used in previous studies by several authors. These variables were non-dimensionalized by dividing by D. The same range of values for the variables of interest was used by Velásquez et al. [39], for the

optimization using response surface methodology. Only one study has been found where spiral inlet channels have been used for the GWVHT. Velasquez et al. (2022) [39] established a range between 90 and 180° for the wrap-around angle (γ), which was the same range used in this research. γ has significant effects on the vortex strength since this angle increases or decreases the inflow area of the flow toward the basin. When the volume flow rate is constant, a decrease in the inflow area means an increase in the flow velocity.

Table 1
Ranges for design variables

Independent factor	Low level	High level
d/D	0.1	0.3
w/D	0.2	0.5
h/D	0.2	0.6
L/D	0.2	3.0
H/D	0.5	2.0
γ [Deg]	90	180

The vortex strength in a GWVHT is regulated by the circulation parameter (Γ) given by Eq. 1 [10].

$$\Gamma = 2\pi r v_\theta \tag{1}$$

where v_θ is the tangential velocity, and r describes a radial position from the center of rotation. The volume flow rate (Q) is given by Eq. 2 [46].

$$Q = Av \tag{2}$$

where A is the cross-section area of a section of the inlet channel and v refers to the velocity of the fluid in that section of the inlet channel. The volume flow rate controls the circulation. An increase in the flow results in an increase in the circulation [47]. In some events, such as the change of the season, a decrease in the volume flow rate is caused, which would affect the circulation and the outlet power generated. Therefore, it is necessary to find a geometry so that, in spite of a decrease in the volume flow rate, the circulation is not affected to the same extent.

2.2. Multi-objective optimization problem using Evolutionary Algorithms

A multi-objective optimization is a problem with two or more objective functions f_m, which are required to be maximized or minimized. The problem has several restrictions or constrains that any solution must satisfy [48]. This type of problem has a set of optimal solutions [49]. Each solution found is called the optimal Pareto, and the representation in the space of these solutions forms the Pareto front. The multi-objective optimization problem with constraints is defined by Eq. 3.

$$\begin{aligned}
&\text{Minimize/Maximize} = f_m(\vec{x}),\ m = 1, 2, \ldots, \mathrm{M};\\
&\qquad \text{Subject to:}\\
&\qquad\qquad h_k(\vec{x}) = 0,\ k = 1, 2, \ldots, \mathrm{K};\\
&\qquad\qquad g_j(\vec{x}) \geq 0,\ j = 1, 2, \ldots, \mathrm{J};\\
&\qquad\qquad x_i^L \leq x_i \leq x_i^U,\ i = 1, 2, \ldots, \mathrm{n};
\end{aligned} \tag{3}$$

where $\vec{x}$ is the vector with the variables to be optimized $x_i^L \leq x_i \leq x_i^U$ is called variable bound or variable range and restring each variable to take a value within a lower x_i^L and an upper x_i^U bound. This bound constitutes a decision or design space [50]. $g_j(\vec{x} \geq 0)$ and $h_k(\vec{x} = 0)$ are called constraint functions and they can be inequal or equality constraints. A solution that does not satisfy all constraints and all variable bounds is called an infeasible solution [51].

The multi-objective optimization problem is classified into three categories: deterministic, stochastic and enumerative. The genetic algorithm (GA), on which this work is focused, is framed within the stochastic techniques [51].

Evolutionary algorithms try to solve optimization problems based on the principle postulated by Darwin: *the survival of the fittest* [52, 53]. From the current population (called parents), new individuals (called children) are produced by the genetic operators. The best suited children survive, and the rest are extinguished [54]. Some of the most used evolutionary computing techniques are evolutionary strategies, genetic programming, genetic algorithms and differential evolution [55]. The genetic algorithm is preferred in energy system optimization [56, 57, 58].

2.2.1. Surrogate models

Many optimization problems in engineering and applied sciences are defined by expensive and complex models; i.e., a set of functions expressed by many variables, which is reflected in a longer processing time (computational cost). Evaluating a solution in one of these models takes several minutes, hours or even days [47]. An alternative to reduce the time needed to evaluate a solution is the use of surrogate models. Surrogate models are an approximate function representing the original system behavior using models less expensive than the original. These functions are assembled by performing multiple experiments or simulations (called samples), examining the results, and choosing a model that estimates the entire system behavior [59]. There are three main steps that are required to be conducted to develop a surrogate model. First, it is necessary to produce a set of training points (also called initial population) from the design space. To produce the set of training points, sampling techniques (SMTs) can be used. The original population must be large enough to ensure the coverage of the design space [59]. Second, the surrogate model is trained on those points, and it predicts the output values. The quality of the model is estimated using the error metrics as cross-validation (CV) and hypervolume indicator (HV) [60]. CV splits the data once or several times. One part of the data is used for training the algorithm and the remaining one, called the validation sample, is used for calculating the risk of the algorithm to estimate the value of the validation samples [61]. HV measures the quality of non-dominated solutions by calculating the area of the region faced by the non-dominated solutions and enclosed above by a reference point [62, 27]. Based on the quality of the model, the designer decides if further samples are needed. Lastly, using all the data collected so far, a new meta-model is created, and the model quality is calculated once again. When the model is assembled, it can be used to execute the optimization process. The multi-objective optimization problem using evolutionary algorithms and surrogate models is shown in Figure 2.

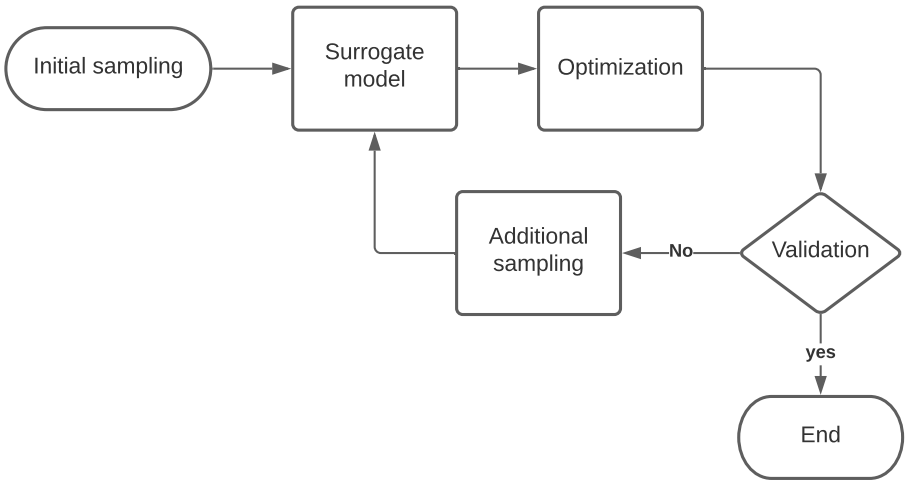

Fig. 2: Optimization process.

There are several types of surrogate models; their selection depends on the system to be represented. Linear and polynomial functions, radial basis function (RBF) and Kriging models are popular choices [63, 64]. RBF and Kriging stand out, among the aforementioned models, as the error is minimal near the sample points, they require few samples and work adequately in problems with dimensions greater than 25 [65]. A linear model is a combination of linear prediction functions from the inputs to model the output. The advantage of a linear model is that the user can perceive how the inputs relate to each other. Additionally, the linear models are simple to be analyzed and interpreted. An expansion of these models is the addition of the interaction between inputs in the form of quadratic terms [66]. The

radial basis function is a nonparametric regression modeling technique. The method uses linear combinations functions based on the Euclidean distance [67]. Gaussian process regression, also known as Kriging, can predict the response value $\widehat{y}$ at a sample point located within a design space based on the observed data available at other sample points within the same design space [68]. Kriging was initially employed in the field of gold mining and geology. This method does not model linear coefficients, like linear models, but models the error term of the model. Its simplest form can be expressed by Eq. 4.

$$\widehat{f}(\vec{x}) = \widehat{y} = \beta_0 + Z(\vec{x}) \tag{4}$$

where β_0 is the mean of the observed values and Z is a Gaussian function [59]. The Gaussian function has a zero mean and a covariance different from zero. The covariance of $Z(\vec{x})$ is expressed by Eq. 5.

$$cov(Z(\vec{x}_j), Z(\vec{x}_k)) = \sigma^2 \mathbf{R}[R(\vec{x}_j, \vec{x}_k)],\ \text{j, k=1, …, N} \tag{5}$$

where σ^2 is the standard deviation of the response variable of the sample points, $\mathbf{R}$ is the symmetric correlation matrix of dimension $N \times N$ with the number one on the diagonal, and R is the correlation function between $\vec{x}_j$ and $\vec{x}_k$ (solutions sample). The correlation function is a function of the distance between points $\vec{x}_j$ and $\vec{x}_k$ in the design space [63]. The Gaussian exponential function is the most applied correlation, and it is shown in Eq. 6.

$$R(\vec{x}_j, \vec{x}_k) = EXP\Big[-\sum_{k=1}^{n} \phi_k (\vec{x}_{j,i} - \vec{x}_{k,i})^2\Big] \tag{6}$$

where ϕ_k refers to the unknown correlation parameters or hyperparameters. The number of correlation parameters is equal to the number of variables N [69]. Hyperparameters are estimated by maximizing the likelihood function using the method of maximum likelihood or the method of least squares [70]. Therefore, the prediction $\widehat{y}$ of a solution $\vec{x}$ is shown in Eq. 7.

$$\widehat{y} = \beta_0 + \widehat{r}^T(\vec{x}) R^{-1}(\vec{y} - \mathbf{1}\beta_0) \tag{7}$$

where $\widehat{r}$ is the vector between the prediction points and the points used to create the model, $\vec{y}$ is the vector of the response values, and $\mathbf{1}$ denotes a N-vector of ones.

An advantage of using the Kriging model is that it provides information on the confidence intervals for the estimated values, which can be obtained at no additional cost. Another advantage is its suitability for complex functions. In this work, Kriging method was selected as the surrogate model due to its previous successful use in aerodynamic design optimization [71, 72, 73, 34, 74], and accessibility in several software packages.

2.2.2. Sampling for surrogate training

The surrogate model must be trained by employing several initial simulations. The initial simulations are defined by SMT [75]. Different methods are used for sampling. Typical sampling methods are central composite design , Box-Behnken design, Latin hypercube sampling (LHS) and orthogonal array [76, 77, 78]. Because of its simplicity, Latin hypercube sampling is a popular SMT [76]. To generate an LHS, each dimension in the design space is divided into m (total samples) equally sized intervals. One point (one sample) is inserted in each interval for each dimension [68]. The number of samples is established previously to divide the space into intervals of equal size. For six factors, at least 28-sample (simulations) are necessary to develop a full quadratic polynomial regression model [79]. With an oversampling of 1.4 (the typical oversampling factor is around 1.5), 40 simulations were generated using LHS [80]. To determine the 40 elements of the initial sample, an algorithm was implemented in Matlab R2018b software. This algorithm was based on the Morris-Mitchell criterion. This criterion allows to generate an optimized Latin hypercube where a certain degree of dispersion is guaranteed in the design. The algorithm is available at Keane et al. [79]. The complete design matrix of the simulations carried out, with the results obtained, are shown in Figure 3 and Table 2. The results in Table 2 were obtained from numerical simulations. It is important to note that numerical simulation

section will explain in a more detailed way how these simulations were implemented. Mathematically, the current multi-objective optimization problem was represented by Eq. 8.

$$\begin{aligned} &\text{Minimize } Q \text{ / Maximize } \Gamma \\ &\text{Subject to:} \\ &0.5 < H/D < 2.0 \\ &0.1 < d/D < 0.3 \\ &0.2 < w/D < 0.5 \\ &0.2 < h/D < 0.6 \\ &0.5 < L/D < 3.0 \\ &90° < \gamma < 180° \end{aligned} \tag{8}$$

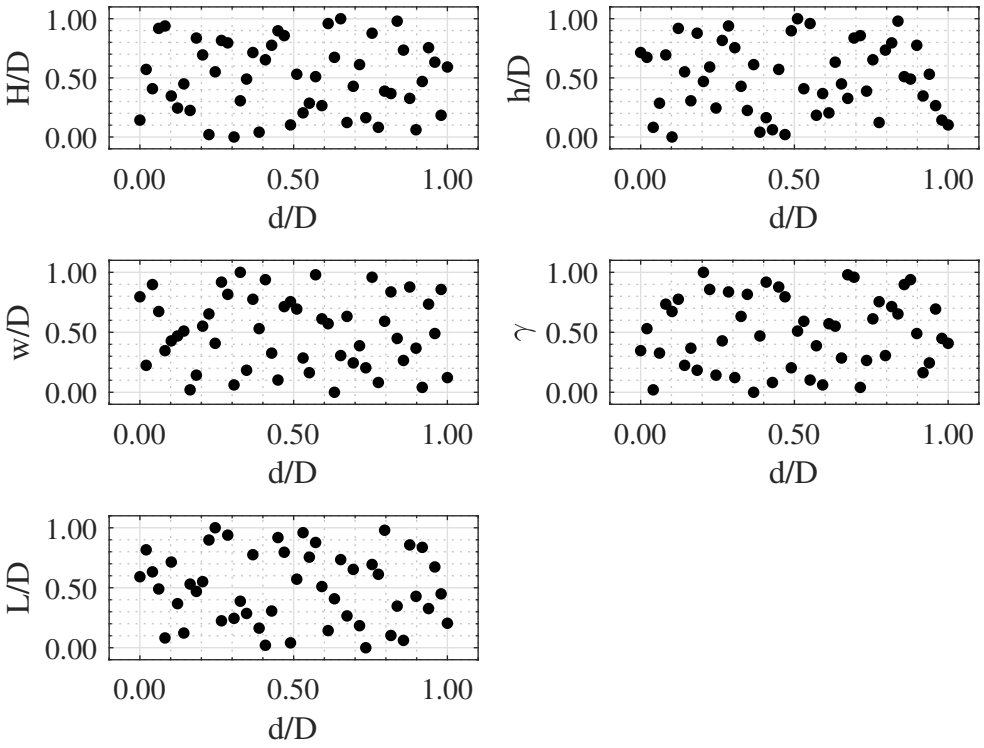

Fig. 3: The Latin hypercube sampling distribution.

Through this multi-objective optimization process, the purpose is to obtain a turbine, where the value of the vortex strength is maximized for a critical condition of minimum volume flow rate. The optimization problem using genetic algorithms was implemented using the *Gamultiobj* (NSGA-II) function in Matlab R2018b software. The *Gamultiobj* function attempts to create a set of Pareto optimal front for a multiobjective problem. The function proceeds as follows: I. Selecting parents for the next generation using the selection function on the current population (initial samples); II. Creating children from the selected parents by mutation and crossover; III. Scoring the children by calculating their objective function values and feasibility; IV. Combining the current population and the children. The combination is called the extended population; V. Trimming the extended population to have a determined population size. The *Gamultiobj* function stopped when the maximum number of generations is exceeded or the time limit is exceeded [81]. For the current study, a maximum generation of 500 [82] and a population size of 300 were established. As reported in the literature, population sizes between 200 and 400 individuals were found in multiple references [83, 84, 85, 65, 86, 87]. In this regard, the specific value of 300 was selected since it was the average value of this range.

All other parameters were set according to the default values. The population size defines the dimension of the population at each generation. When the population size is large, more time the algorithm takes to compute each

Table 2
Initial sample data.

Run	Design variables						Γ [m^2/s]	Q [m^3/s]
	d/D	w/D	h/D	L/D	γ [Deg]	H/D		
1	0.2388	0.2735	0.5347	2.1327	176.3265	1.1429	1.7724	0.0036
2	0.2143	0.4939	0.2735	2.6939	124.8980	1.2653	1.6208	0.0047
3	0.1204	0.3286	0.2000	2.2857	150.6122	1.0204	1.5672	0.0028
4	0.2510	0.4878	0.4612	2.2347	145.1020	1.8163	0.8493	0.0056
5	0.1367	0.2429	0.5510	1.6735	106.5306	1.7551	1.8262	0.0042
6	0.3000	0.2367	0.2408	1.0102	126.7347	1.3878	1.1485	0.0043
7	0.1857	0.2980	0.2245	1.2653	97.3469	1.6633	1.8797	0.0051
8	0.1980	0.4265	0.5592	0.6020	108.3673	0.6531	1.5094	0.0033
9	0.1612	0.2184	0.5020	1.1122	101.0204	0.5000	1.3942	0.0026
10	0.2265	0.2000	0.4531	1.5204	139.5918	1.5102	1.8917	0.0052
11	0.2061	0.2857	0.3633	2.8980	143.2653	0.8061	1.5531	0.0037
12	0.2796	0.3102	0.5102	1.5714	134.0816	0.5918	1.4756	0.0030
13	0.1449	0.3959	0.4367	2.7449	167.1429	0.5306	1.2450	0.0024
14	0.2306	0.2918	0.3796	2.3367	115.7143	2.0000	1.7668	0.0059
15	0.1571	0.4449	0.5755	2.8469	165.3061	1.6939	1.6978	0.0046
16	0.2102	0.2490	0.5837	2.3878	99.1837	0.9286	1.6944	0.0040
17	0.2224	0.3714	0.2816	0.8571	141.4286	1.9388	1.6052	0.0058
18	0.1245	0.3408	0.5673	1.4184	159.7959	0.8673	1.4885	0.0027
19	0.1082	0.4694	0.2327	2.0816	91.8367	1.1122	1.6286	0.0026
20	0.2184	0.3837	0.3469	1.7755	95.5102	0.8980	1.7052	0.0040
21	0.1653	0.5000	0.3714	1.4694	146.9388	0.9592	1.5221	0.0036
22	0.1694	0.2551	0.2898	1.2143	163.4694	1.2347	1.8007	0.0042
23	0.2878	0.4204	0.4122	1.3163	112.0408	1.6327	0.8444	0.0049
24	0.2469	0.2612	0.3551	0.5000	113.8776	0.7449	1.6117	0.0036
25	0.2633	0.4510	0.5184	0.7551	154.2857	1.0510	1.5078	0.0042
26	0.1898	0.2306	0.4286	2.7959	168.9796	1.8469	1.8924	0.0054
27	0.2592	0.3776	0.4939	2.9490	117.5510	1.0816	1.5987	0.0043
28	0.1776	0.3592	0.2163	0.9082	132.2449	0.5612	1.4224	0.0029
29	0.2837	0.2122	0.3388	2.5918	104.6939	1.2041	1.5837	0.0042
30	0.1735	0.4327	0.4449	2.4388	90.0000	1.5714	1.8912	0.0048
31	0.2020	0.4082	0.6000	1.9286	135.9184	1.2959	1.7603	0.0047
32	0.1939	0.4143	0.2082	2.4898	161.6327	1.7857	1.7184	0.0054
33	0.1286	0.3531	0.4204	0.8061	110.2041	1.1735	1.6743	0.0032
34	0.2959	0.4571	0.2571	1.6224	130.4082	0.7755	1.0763	0.0032
35	0.2714	0.2796	0.4041	0.6531	170.8163	1.6020	1.4726	0.0050
36	0.1408	0.3653	0.3878	1.8776	180.0000	1.5408	1.7288	0.0040
37	0.1041	0.2673	0.4694	2.5408	137.7551	1.3571	1.6090	0.0027
38	0.1122	0.4020	0.3143	1.7245	119.3878	1.8776	1.6733	0.0035
39	0.2347	0.3898	0.3306	1.1633	178.1633	0.6837	1.4588	0.0035
40	0.1327	0.2061	0.3224	1.8265	123.0612	0.8367	1.5658	0.0028

generation; however, increasing the population size allows to explore more points and thus achieve a better result [88]. The default population size is 15 times the number of variables. The *Gamultiobj* functions return a table containing both objective function values (vortex circulation and volume flow rate), and the value of the design variables. *Gamultiobj* function is applicable only to minimization problems [56] and, therefore, the maximization function (vortex circulation) in this work was converted into a minimization function by multiplying the objective function with -1. The surrogate model was constructed using Matlab R2018b software, as well. Here, the function $f = pred(x)$ was used to carry out the Kriging prediction. This function is explained with details in Yondo et al. [68]. Once the result of the surrogate model and genetic algorithm was obtained, some of the new data are added to the initial population to produce a new meta-model that provides a more optimal objective function, and the optimization process (or optimization cycle) is

repeated until the quality of the model is reached.

2.3. Numerical simulation

The numerical simulations were implemented in Ansys-FLUENT. Initially, 40 geometries were prepared using computer-aided design (CAD). The geometries were created using a diameter D of 500 mm. The geometries consist of two sections: the inlet channel and the conical basin. Then, the meshes were made in Fluent meshing. Poly-hex core mesh was used to mesh both sections. Poly-hex core mesh is a novel meshing strategy to solve flow around complex geometries with greater accuracy and speed. This mesh employs polyhedral and hexahedral elements, providing an optimal combination of mesh elements [89] and it allows a reduction of approximately 40% in computational time [89].

The Unsteady Reynolds-Averaged Navier-Stokes (URANS) equations were solved by employing the coupled scheme for pressure-velocity, and the second-order upwind discretization. The URANS equations are a formulation based on the ensemble averaging: the instantaneous velocity of the flow (u_i) is represented as the sum of a mean value ($\langle u_i \rangle$) and its corresponding fluctuations over time (U_i), Eq. 9 [90]:

$$u_i = \langle u_i \rangle + U_i \tag{9}$$

The URANS equations, in conservation form, can be written as described in Eqs. 10 and 11 [36]:

$$\frac{\partial \langle u_i \rangle}{\partial x_i} = 0 \tag{10}$$

$$\frac{\partial \langle u_i \rangle}{\partial t} + \frac{\partial \langle u_i u_j \rangle}{\partial x_j} = -\frac{\partial \langle P \rangle}{\partial x_i} + \frac{\partial}{\partial x_j}\left(\nu \frac{\partial \langle u_i \rangle}{\partial x_j} + \tau_{ij}\right) + F_B \tag{11}$$

In Eq. 10 and 11, P denotes the pressure divided by the density of the fluid (ρ), ν is the kinematic viscosity, F_b is body force, and τ_{ij} the Reynolds stress tensor given by Eq. 12 [36]:

$$\tau_{ij} = -\langle U_i U_j \rangle \tag{12}$$

The turbulence was solved using k-ϵ RNG turbulence model with scalable wall function as a near-wall treatment. The k-ϵ model uses two equations to solve the dissipation ϵ and the turbulent kinetic energy k. k and ϵ are obtained from Eqs. 13 and 14 [91]:

$$\frac{d}{dt}(\rho k) + \frac{d}{dx_i}(\rho k u_i) = \frac{d}{dx_j}\left[\left(\mu + \frac{\mu_t}{\sigma_k}\right)\frac{dk}{dx_j}\right] + G_k + G_b - \rho\epsilon - Y_M + S_k \tag{13}$$

$$\frac{d}{dt}(\rho \epsilon) + \frac{d}{dx_i}(\rho \epsilon u_i) = \frac{d}{dx_j}\left[\left(\mu + \frac{\mu_t}{\sigma_\epsilon}\right)\frac{d\epsilon}{dx_j}\right] + C_{1\epsilon}\frac{\epsilon}{k}(G_k + C_{3\epsilon}G_b) - C_{2\epsilon}\rho\frac{\epsilon^2}{k} + S_\epsilon \tag{14}$$

In Eqs. 13 and 14, $C1_\epsilon$, $C2_\epsilon$ and $C3_\epsilon$ are constant values. G_b is the generation of k because of buoyancy. In turn, G_k refers to the generation of k due to the velocity gradients, and Y_M stands for the contribution of the fluctuating dilatation compressible turbulence to the overall dissipation rate. S_k and S_ϵ refer to the user-defined terms. σ_ϵ and σ_k stand for the turbulent Prandtl numbers for ϵ and k, respectively. μ_t is the turbulence viscosity and it is calculated as expressed in Eq. 15 [92], where C_μ is a constant.

$$\mu_t = \rho C_\mu \frac{k^2}{\epsilon} \tag{15}$$

In the k-ϵ model, which is available in ANSYS Fluent, the constants and their values by default are $C1_\epsilon$, $C2_\epsilon$, $C3_\epsilon$, C_μ, σ_k, and σ_ϵ of 1.44, 1.92, 0.09, 1.0 and 1.3, respectively.

Inside the turbine, two fluids cohabit: air and water; therefore, the volume of fluid method (VoF) was chosen to perform the simulations. An inlet velocity was imposed at the inlet channel, as boundary conditions, the inlet velocity changed in each simulation depending on the geometric characteristics of the study models. For the discharge hole and at the upper surfaces, a relative pressure of 0 Pa was imposed. The computational domain and boundary conditions is shown in Figure 4.

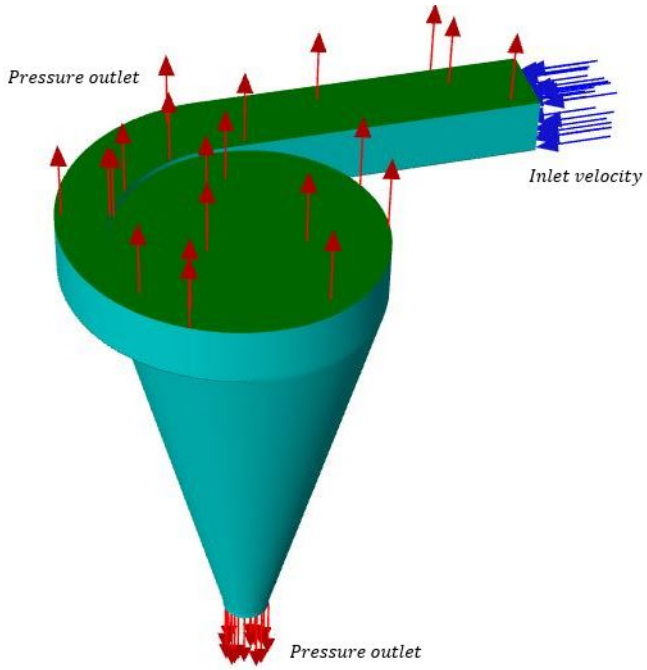

Fig. 4: Three-dimensional view of computational domain and boundary conditions.

The Grid Convergence Index (GCI) was the technique applied to define the optimal values of the time step (Δt) and element number used for the mesh. GCI is based on Richardson extrapolation [93, 94]. If the value of GCI is close to 1.0, the solution is within the asymptotic range of convergence and the numerical solution does not change with further refinement of the mesh and time step [95, 96]. The test allowed the selection of the most appropriate mesh and time-step to guarantee good result accuracy and low computational costs. For calculating the GCI value, the following steps are required: I. Choosing a parameter (f) indicating the convergence of the mesh. The control parameter used in these independence tests was Γ; II. Defining the refinement constant (r). Traditionally, with Richardson extrapolation, a refinement constant of 2 is used. The refinement may be spatial or in time; III. Executing at least 3 simulations (f_1, f_2 and f_3) with the refinement constant (r). Coarse, medium, and fine meshes are expressed as f_3, f_2 and f_1, respectively; IV. Calculating the order of convergence (p) using Eq. 16; V. Estimating the value of f when the separation (h) between the mesh elements tends to zero by using Eq. 17; VI. Utilizing Eq. 18, calculating the GCI for the fine and medium meshes, GCI_{12} and GCI_{23}, respectively. The values of GCI_{23} and GCI_{12} represent the relative change from coarse to medium mesh/time step and from medium to fine mesh/time step; and VII. With the Eq. 19, checking that the meshes are in the asymptotic range. [97, 98, 95].

$$p = \frac{ln\frac{f_3 - f_2}{f_2 - f_1}}{ln(r)} \tag{16}$$

$$f_{h=0} = f_2 + \frac{f_1 - f_3}{r^p - 1} \tag{17}$$

$$GCI_{12} = \frac{F_s|\epsilon|}{r^p - 1} \tag{18}$$

where F_s is a factor of safety. This factor is recommended to be F_s=3.0 for comparisons of two grids and F_s=1.25 for comparisons over three or more grids. $|\epsilon|$ is the relative error and it is defined as $(f_2 - f_1)/(f_1)$. To calculate the value of GCI_{23}, the expression $(f_3 - f_2)/(f_2)$ is used.

$$GCI = \frac{GCI_{23}}{r^p \times GCI_{12}} \approx 1.0 \tag{19}$$

The number of elements used in the mesh independence, and the Δt values used for the time independence tests are shown in Table 3. Table 3 also presents the results for the independence tests when using GCI.

Table 3
Results for the independence tests using GCI.

	Mesh type and GCI	Number of elements	Δt [s]
f_3	Coarse	211.158	0.2
f_2	Medium	330.238	0.1
f_1	Fine	435.116	0.05
	GCI	1.006	0.999
	GCI_{12}	3.50%	0.07%
	GCI_{23}	4.93%	0.10%

According to Table 3, with GCI values of 1.006 and 0.999, for the mesh and Δt, respectively, the solution is within the asymptotic range. Additionally, the GCI values for the finer mesh (GCI_{12}) are small when compared to the coarser one (GCI_{23}), it can be concluded that the aim of a mesh independent solution is reached, and no further mesh modification is necessary. This also applies to time-step independence. In this regard, the medium time-step of Δt =0.1 s and the medium mesh were selected for the analysis to minimize the computational time and the errors. The final mesh is shown in Figure 5.

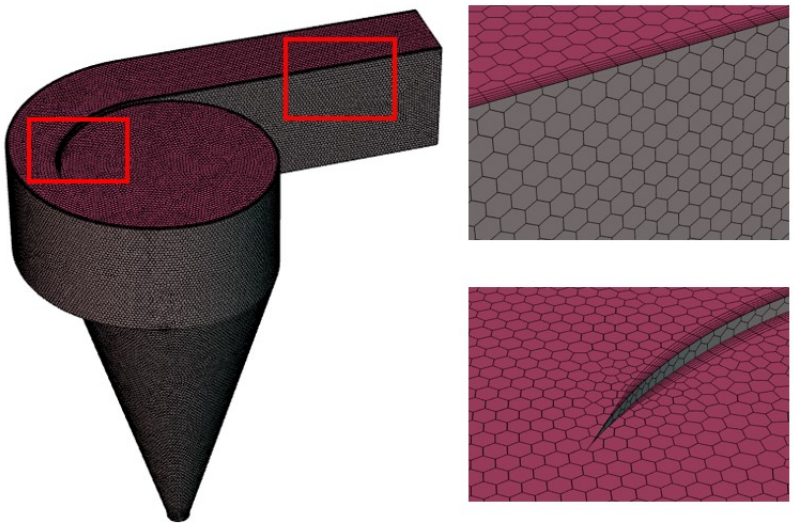

Fig. 5: Hexcore Mesh.

To determine the inlet velocity to each simulation, Eq. 20, proposed by Velasquez et al. [39] for the coefficient of discharge, C_d, was used.

$$C_d = [0.7721e^{-6.4409\frac{d}{D}}] - 0.0464 \tag{20}$$

This coefficient related the ideal and the real Q. The ideal Q was calculated as a function of d, H, and the gravity, g, as described by Eq. 21.

$$C_d = \frac{4Q}{\pi d^2 \sqrt{2gH}} \tag{21}$$

3. Results and discussion

The highest Γ of the initial sampling was reached in run 26, with a Γ of 1.8924 m^2/s. The lowest Γ corresponded to run 23, with a circulation of 0.8444 m^2/s. The maximum and minimum Q values were reached in runs 14 and 13, respectively, with values of 0.0059 and 0.0024 m^3/s. Figure 6 shows the volume fraction of water to run 26, 23, 14 and 13. The blue zone corresponds to the volume of air. In Table 4, the values of the design variables and the objectives for the four models with the lowest and the highest values of Q and Γ are listed.

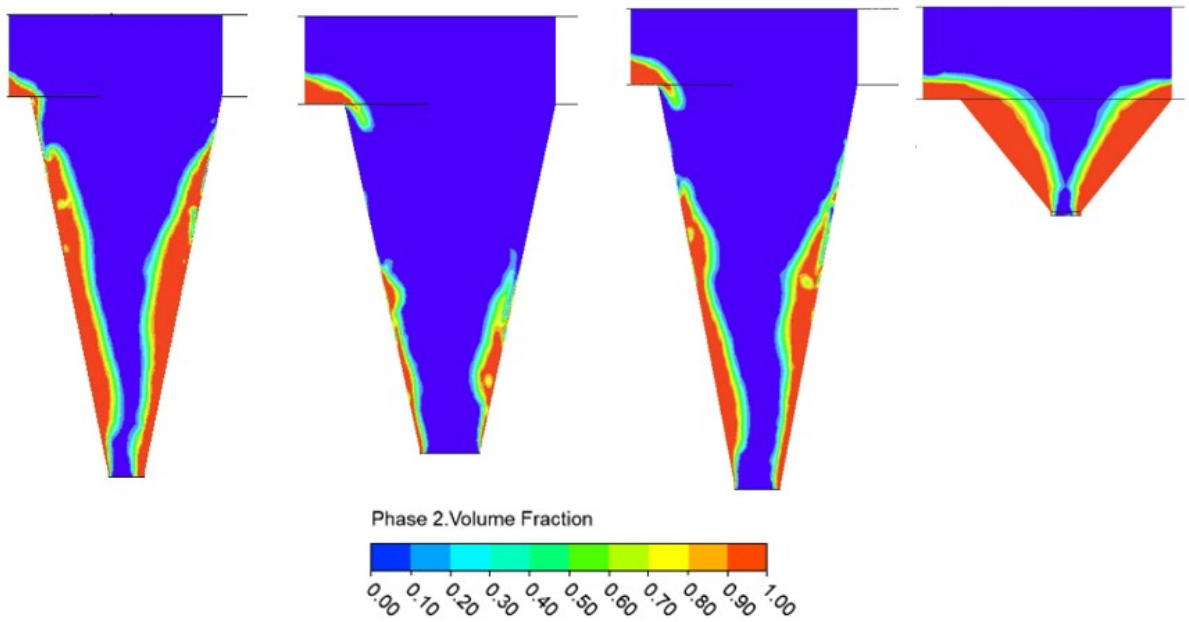

Fig. 6: Volume fraction of water: a) run 26, b) run 23, c) run 14, and d) run 13.

The geometry with the lowest Q is the geometry with the smallest outlet diameter, d, and the shortest conical basin height, H, while the geometry with the highest Q has the longest conical basin. However, the geometry with the lowest Γ has the largest outlet diameter and the shortest channel length, L, while the geometry with the highest Γ has the longest channel. The parameters d/D and H/D seem to be the parameters that most affect the volume flow rate, while d/D and L/D seem to be the parameters that most affect the circulation. Between simulations 23 and 26, there is a difference of 55.4% in the value of Γ. Between these same two simulations, there is a difference of only 9.3% in the values of Q. For a difference of 59.3% in the value of Q for simulations 13 and 14, the difference for the value of gamma is 29.53%.

From the point of view of the physical phenomenon, a high or low value of Γ depends on the angular momentum of the strong vortex formed in the basin. In a vortex, a fluid particle away from the center has an angular momentum, resulting in a small angular velocity with a large radius. The radius gradually reduces while the particle moves to the centre, and thus to conserve the angular momentum, angular velocity is increased [99]. When all simulation models have the same basin top diameter ($D = 500$ mm), then the velocity at which the flow enters the basin from the channel defines the angular momentum of the vortex. The inlet velocity of the flow to the basin depends on the geometry of the inlet channel (w/D, h/D, γ) and the value of Q.

The inlet velocity v of the flow in the channel is given by Eq. 2. Due to the spiral geometry of the inlet channel, this velocity increases as it approaches the basin, as the cross-sectional area decreases. The smaller the value of γ is,

Table 4
Models with the lowest and highest values of Q and Γ.

Run	Design variables						Γ [m^2/s]	Q [m^3/s]
	d/D	w/D	h/D	L/D	γ [Deg]	H/D		
13	0.1449	0.3959	0.4367	2.7449	167.1429	0.5306	1.2450	0.0024
14	0.2306	0.2918	0.3796	2.3367	115.7143	2.0000	1.7668	0.0059
23	0.2878	0.4204	0.4122	1.3163	112.0408	1.6327	0.8444	0.0049
26	0.1898	0.2306	0.4286	2.7959	168.9796	1.8469	1.8924	0.0054

the smaller the flow input area to the basin is found. Therefore, small values of h/D, w/D and γ, and large values for Q increase the velocity of the flow entering the basin. This, in turn, allows a higher value of angular momentum.

From 4, run 26 (the highest Γ) has the smaller w/D, and the highest γ. Run 23 (the lower Γ) has the highest w/D and the smaller γ. Runs 26 and 23 have only one of the desired characteristics to obtain a high circulation. Runs 26 and 23 have only one of the desired characteristics to obtain high circulation; for run 26, the w/D ratio, while for run 23, the γ angle: Therefore, for the inlet channel, the w/D ratio is the geometric characteristic that most influences the value of the circulation.

From the initial sampling, a Pareto front was created using the genetic algorithm. Figure 7 shows the two objectives that were simultaneously minimized. The initial sampling (starting solutions), the designs suggested by the surrogate model (feasible and unfeasible solutions), and the selected design are shown in Figure 7. The horizontal black lines correspond to the minimum and the maximum values for the volume flow rate, while the vertical black lines correspond to the minimum and maximum values for Γ. From Figure 7, only a few of the starting solutions contribute to the Pareto front. This means that if the initial population is used to establish the optimal geometry, the entire design space, i.e., other possible combinations of the design variables, would not has been explored. To improve the Kriging model and the Pareto Front, three additional samplings were selected in each optimization cycle. In total, 20 optimization cycles (60 new samples) were required to validate the surrogate model through the hypervolume indicator. Out of these three points added in each cycle, one point was the maximum circulation point and another, the minimum volume flow rate point. The third point was selected between two extreme points [100]. It allows to explore different regions of the design space and fill the gaps in the Pareto front [75]. Table 5 shows the sample data added to improve the Pareto front.

From Table 5, the highest Γ of the new samples was reached through run 35, resulting in a Γ value of 2.1074 m^2/s. The minimum volume flow rate was reached with 13 different geometries, with a value of 0.0016 m^3/s, as it can be seen in Figure 7, where multiple points are found on the same horizontal-dotted line. With respect to the maximum circulation (1.8924 m^2/s) and the minimum volume flow rate (0.0024 m^3/s) found in the initial sample, with the new samples, there was an increase of 11.1% in the circulation and a decrease of 33.3% in the volume flow rate. In Figure 8a and Figure 8b, the effect of d/D and H/D on the volume flow rate and the circulation is illustrated. For geometries corresponding to Q of 0.0016 m^3/s, d/D varies between 0.1000 and 0.1026, while H/D varies between 0.5 and 0.544, and the value of the circulation is between 1.2 and 1.4 m^2/s. This information allows to confirm the assumption that the parameters d/D and H/D are the parameters affecting the most the value of the flow. The volume flow rate of these 13 geometries is the same due to the similarity that exists between the values of d/D and H/D. The volume flow rate does not depend on the values that the other parameters have taken. There are four geometries in the new sample data with very close circulation values, between 2.0548 and 2.1074 m^2/s. These geometries correspond to d/D values between 0.1887 and 0.2149, and L/D values between 2.9589 and 3.000, for Q between 0.0055 and 0.0059 m^3/s. A larger value of H means a larger distance to be travelled by the flow and a longer time to exit the turbine, while a larger value of d means a larger area for the flow to exit from the turbine. By having a larger outlet area and a greater height, the turbine has the possibility of receiving a greater amount of flow without exceeding its capacity and causing spills. With respect to the value of L, the greater the length of the channel, the greater the possibility that the flow entering the basin will be a more organized flow with lower energy losses, thus having this flow more energy available.

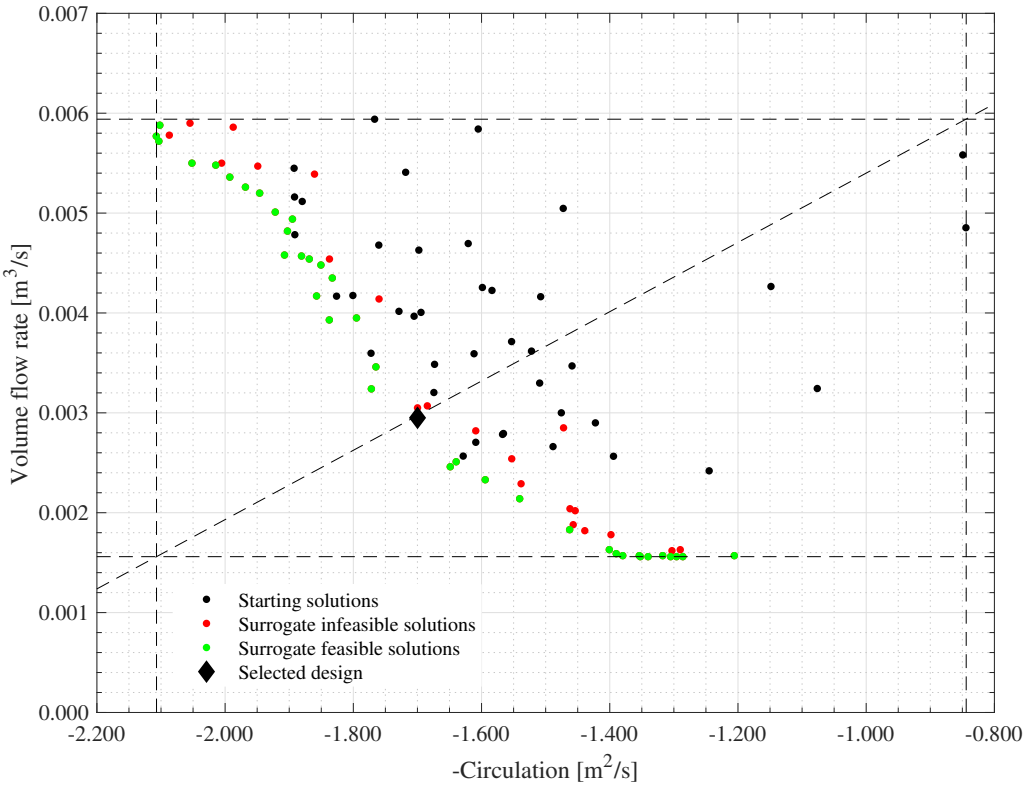

Fig. 7: Final Pareto front.

3.1. Validation of the Pareto front

One of the most common metrics to determine the convergence of the Pareto front is the hypervolume indicator (HV) [101, 102, 103, 104]. Given a Pareto front, this metric estimates the non-overlapping volume of the hypercubes formed by a reference point R and every point in the Pareto front [75]. The reference point was determined by choosing the worst point based on the initial observations. The worst point consists of the point of the least circulation ($\Gamma = 0.8844$ m^2/s) and the highest volume flow rate ($Q = 0.0059$ m^3/s), that is, the opposite point to the objectives of the optimization process. Figure 9 shows the Pareto front for optimization cycles 5, 10 and 20. The objectives were normalized onto the range [0, 1] to generate a unit hypercube (or hyper-rectangle). A value of 1.0 for this metric indicates that the solutions are closer to the true Pareto front because the maximum area in the hyper-rectangle is 1.0 [105, 106]. The HV is the red area, defined by the non-dominated solutions and the reference point R. If more sampling points are added, in each optimization cycle, the value of HV increases, as it can be observed in Figure 9b and Figure 9c, where the red area is greater than the red area in Figure 9a.

Figure 10 shows the HV evolution; i.e., the HV value for each new sample point added to the Pareto front in each optimization cycle. Figure 10 indicates that the HV converges for a value of 0.91. This means that it does not matter if more sample points are added to the Pareto front, the value of HV does not change. Since the algorithm converges, the Pareto front in Figure 7 is considered the true Pareto front. This Pareto front can be used to determine a compromise solution between both objectives of study.

The best solution is subjective and depends on the need of the designer [107]. Selecting the best design, a line was drawn between point R and the best design point P. The best point consists of the point of the highest circulation ($\Gamma = 2.1074$ m^2/s) and the least volume flow rate ($Q = 0.0016$ m^3/s), which are precisely the objectives of the optimization process. The final design is the point of the Pareto front that is cut by the line between R and P. This point corresponds to the run 54 of the new sample points. For this point, the values of the geometric parameters are $\gamma = 92.141°$, $H/D = 1.572$, $L/D = 1.518$, $h/D = 0.565$, $w/D = 0.361$, and $d/D = 0.108$, and Γ and Q are 1.6999 m^2/s and 0.0030 m^3/s, respectively. Figure 11 shows the vortex profiles and the angular velocity of the vortex as a function of the radius of

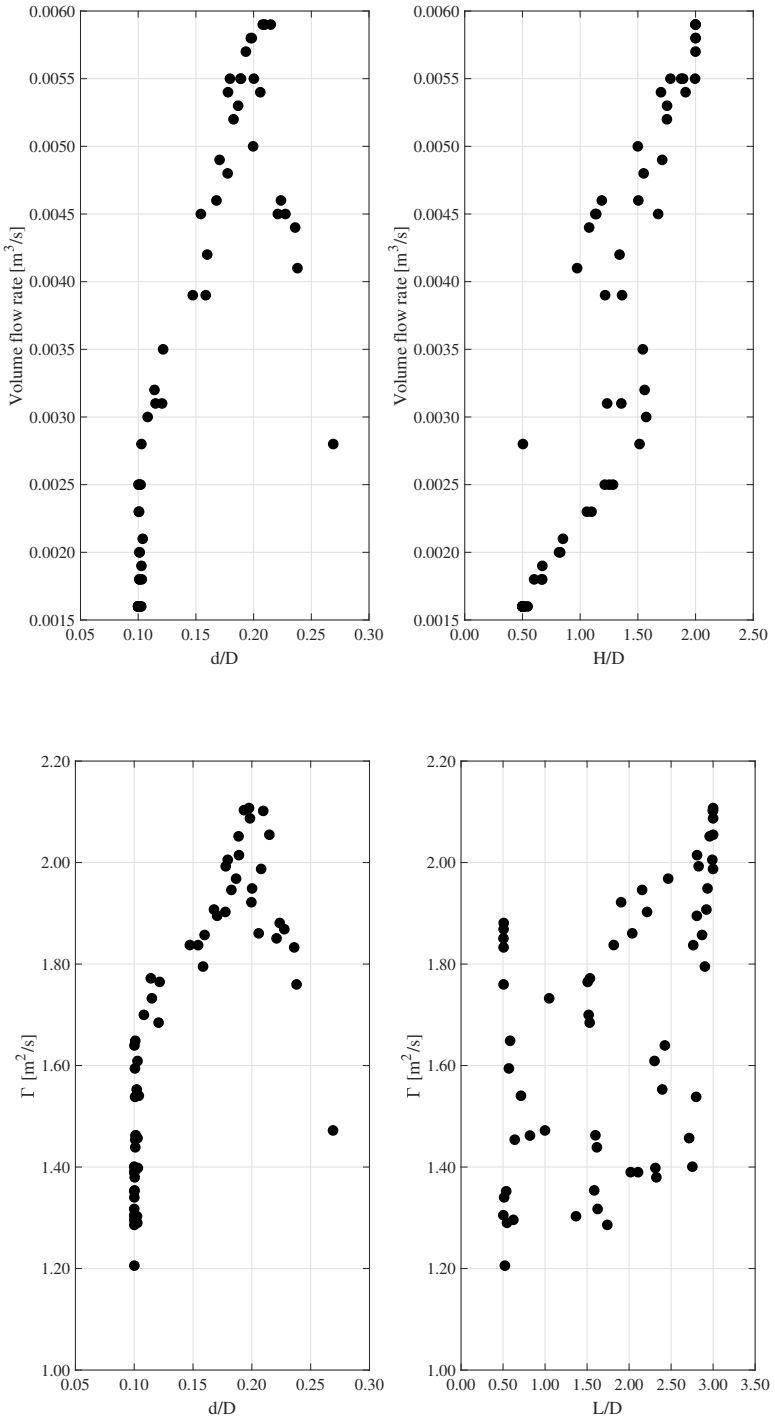

Fig. 8: a) Effect of d/D and H/D on the volume flow rate, and b) Effect of d/D and L/D on the circulation.

the basin for the highest (run 35) and the lowest circulation (run 24), as well as for the selected design (run 54). Fig. 11a shows that run 24 produced a more symmetrical vortex than the other geometries, but it is a low vortex. The vortex for runs 46 and 54 had a similar profile and height. From Figure 11b, it was found that the angular velocity increased to a maximum value when the radius of the vortex approached zero, reaching a velocity of up to 85 rad/s in run 54. For all runs, the angular velocity is zero at the basin walls.

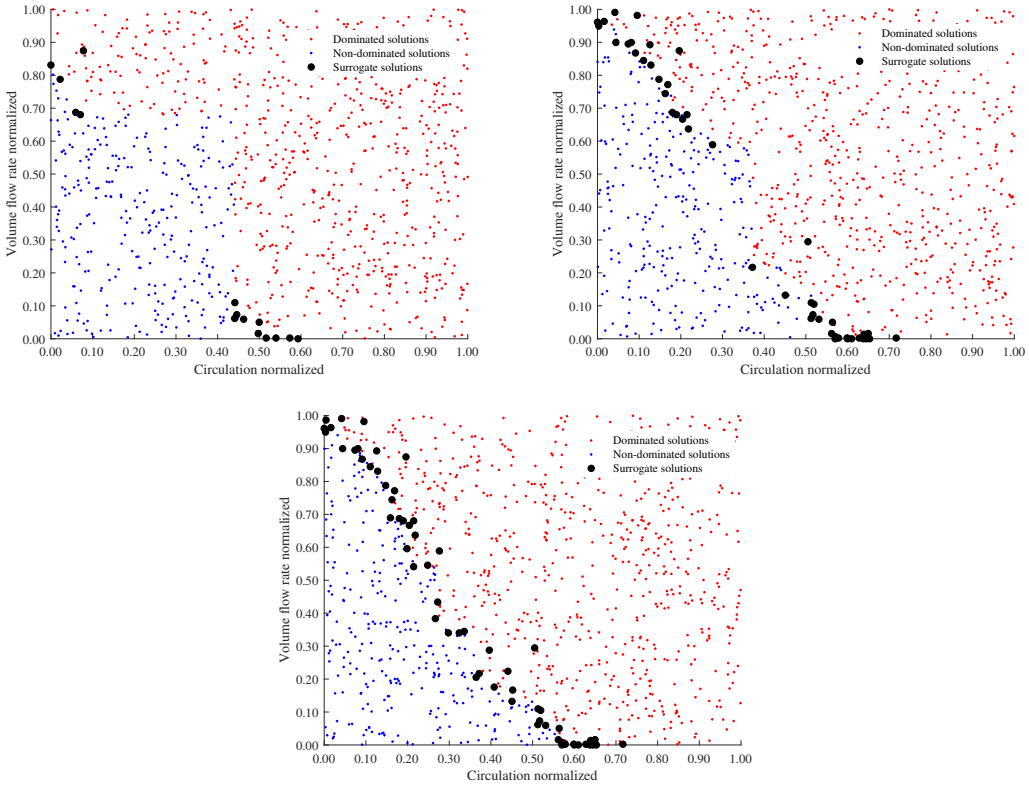

Fig. 9: Hypervolume evolution: a) cycle 5, b) cycle 10, and c) cycle 20.

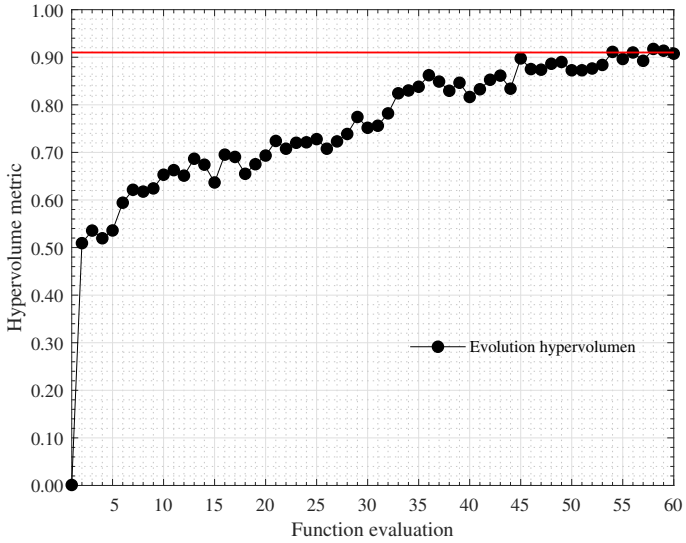

Fig. 10: HV evolution.

Velásquez et al. [39] performed a single-objective optimization using the same six geometric factors of this investigation. The purpose of a single-objective optimization is to establish the best solution for a certain condition. The referred authors, through the response surface methodology, proposed a GWVHT that allows to maximize the circulation. Their results indicated that the highest Γ was 2.089 m^2/s, while the volume flow rate for this geometry, according to Eqs. 20 and 21, was 0.0051 m^3/s (H/D=1.840, γ=179.976°, h/D=0.599, d/D=0.167, w/D=0.2, and L/D=0.500). The geometry of maximum circulation found by Velásquez et al. [39] can be compared with run 35

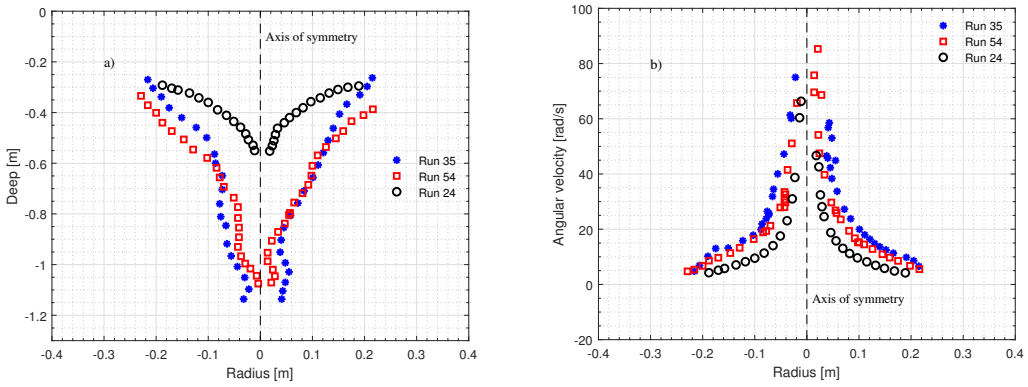

Fig. 11: a) vortex profile and b) Tangential velocity.

(H/D=2.000, h/D=0.2594, w/D=0.3618, L/D=3.000, d/D=0.1976, and γ=108.452°) of the Pareto front because both geometries represent the geometries of maximum circulation (same optimization objective) but obtained using two different methodologies. Figure 12 represents the vortex profiles and the angular velocity of the vortex as a function of the radius of run 35 and the optimized geometry found by Velasquez et al. (2022) [39]. From the Pareto front, the maximum circulation was 2.1074 m^2/s and corresponded to a volume flow rate of 0.0058 m^3/s. With respect to the geometry of Velásquez et al. [39], run 35 increased 0.87% the circulation and 13.79% the volume flow rate. The increase in the circulation may be due to the increase in the volume flow rate, of which as previously stated are directly related. According to Figure 12a, both vortexes have similar profiles, the vortex for geometry 35 was higher because the H/D ratio was greater than for the optimized Velásquez et al. [39] geometry. The angular velocity resulted to be also quite similar in both geometries, Figure 12b.

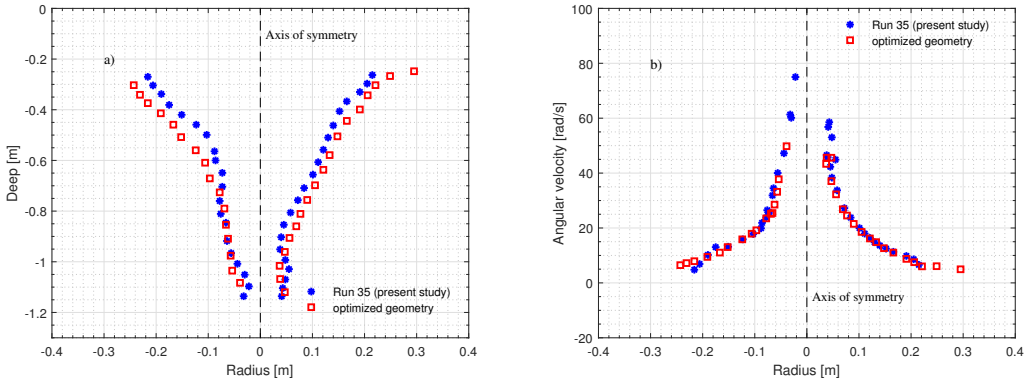

Fig. 12: a) vortex profile and b) Tangential velocity for the optimized geometry (Velasquez et al. [39]) and Run 35 (present study).

Using the polynomial proposed by Velásquez et al. [39] to calculate the circulation, it was found that with the data from run 35, a circulation of 1.9047 m^2/s was predicted, with respect to the simulation result, presenting a difference of 9.61%. This percentage of difference is within the prediction range of the model proposed by Velásquez et al. [39] since the regression model has an adjusted-R_2 of 87.92%. Now, using the data from run 54, the predicted circulation was 1.687 m^2/s, while the simulation result was 1.699 m^2/s, which represents a difference of 0.76%. The difference between both optimization methodologies, the response surface methodology with a single-objective and a multi-objective optimization using two objectives lies in the number of results obtained at the end of each process. While in the response surface methodology, only a single result was obtained for the single objective, for the multi-objective methodology, through the Pareto front, multiple solutions were obtained, which were a compromise between the two objectives set [108, 28]. Therefore, the selection of the final model depends on the needs and requirements of the designer. The multi-objective optimization methodology encompasses the results that can be obtained through optimizations with

response surfaces. That is, with the results of the Pareto Front it is possible to solve problems with a single objective. In that case, a design should be selected at the extreme points of the front, depending on whether it requires maximizing or minimizing the single objective [109].

4. Conclusions

A multi-objective genetic algorithm is an efficient technique for solving optimization problems. In these problems, multiple conflicting objectives must be satisfied. The current problem pursuits to examine the factors that affect the circulation of a vortex for an efficient power generation system. Two conflicting objectives were considered: (1) the minimization of the volume flow rate, and (2) the maximization of the vortex circulation. With these multiple objectives, an optimum design problem can then be expressed. This optimization problem was solved using the function *gamultiobj* in the Matlab R2018b software. The algorithm combines the multi-objective genetic algorithm with Kriging interpolation to find the true Pareto front (optimal solutions). The initial population size was set to 40 and the maximum number of generations was set to 500. The initial population was established by a Latin hypercube sampling. The convergence to the Pareto front was obtained by the algorithm after 20 function evaluations and 60 new samples. The convergence of the solutions obtained by the algorithm was calculated using the metrics called HV. With an HV value of 0.91, the algorithm generates a good distribution of the Pareto front. This Pareto front was used to determine a compromise solution between both objectives. The compromise solution corresponded to the run 54 of the new sample points. For this point, the values of the geometric parameter H/D=1.572, h/D=0.565, w/D=0.361, L/D=1.518, d/D=0.108 and γ=92.141° were obtained. The circulation and the volume flow rate were 1.6999 m^2/s and 0.0030 m^3/s, respectively. Since the geometric parameters selected were dimensionless, with these results, it was possible to generate new geometries. On the other hand, as the final solution depends on the designer criteria, other authors could use the established Pareto front to choose their own solution, since the solution presented in this study was an intermediate solution between the best and the worst design points. It is important to highlight that the results obtained through this optimization are only valid for the initially established study geometry; any change in the shape of the turbine components implies that the results of this optimization may not be valid. For new geometries, the multi-objective genetic algorithm, employed in the present study can be used to improve those new geometries. The new optimization processes can include too geometrical variables to define the runner. For further work, it is necessary to validate the numerical results by means of the execution of experimental tests.

References

[1] S. Chitrakar, B. W. Solemslie, H. P. Neopane, O. G. Dahlhaug, Review on numerical techniques applied in impulse hydro turbines, Renewable Energy 159 (2020) 843–859.

[2] B. R. Cobb, K. V. Sharp, Impulse (turgo and pelton) turbine performance characteristics and their impact on pico-hydro installations, Renewable energy 50 (2013) 959–964.

[3] P. Kumar, R. Saini, Study of cavitation in hydro turbines—a review, Renewable and Sustainable Energy Reviews 14 (2010) 374–383.

[4] D. K. Okot, Review of small hydropower technology, Renewable and Sustainable Energy Reviews 26 (2013) 515–520.

[5] A. Židonis, D. S. Benzon, G. A. Aggidis, Development of hydro impulse turbines and new opportunities, Renewable and Sustainable Energy Reviews 51 (2015) 1624–1635.

[6] O. Yaakob, Y. M. Ahmed, A. Elbatran, H. Shabara, A review on micro hydro gravitational vortex power and turbine systems, Jurnal teknologi 69 (2014).

[7] L. Velásquez, E. Chica, J. Posada, Jestr r, Journal of Engineering Science and Technology Review 14 (2021) 1–14.

[8] M. Kayastha, P. Raut, N. K. Subedi, S. T. Ghising, R. Dhakal, Cfd evaluation of performance of gravitational water vortex turbine at different runner position (2019).

[9] S. Mulligan, Experimental and numerical analysis of three-dimensional free-surface turbulent vortex flows with strong circulation, Ireland: Institute of Technology Sligo (2015).

[10] A. B. Timilsina, S. Mulligan, T. R. Bajracharya, Water vortex hydropower technology: a state-of-the-art review of developmental trends, Clean Technologies and Environmental Policy 20 (2018) 1737–1760.

[11] S. Dhakal, A. B. Timilsina, R. Dhakal, D. Fuyal, T. R. Bajracharya, H. P. Pandit, N. Amatya, A. M. Nakarmi, Comparison of cylindrical and conical basins with optimum position of runner: Gravitational water vortex power plant, Renewable and Sustainable Energy Reviews 48 (2015) 662–669.

[12] A. Gautam, A. Sapkota, S. Neupane, J. Dhakal, A. B. Timilsina, S. Shakya, Study on effect of adding booster runner in conical basin: gravitational water vortex power plant: a numerical and experimental approach, in: Proceedings of IOE Graduate Conference, 2016, pp. 107–113.

[13] R. Dhakal, T. Bajracharya, S. Shakya, B. Kumal, N. Kathmandu, K. Khanal, N. Kavre, S. Williamson, S. Gautam, D. Ghale, Computational and experimental investigation of runner for gravitational water vortex power plant, in: Proceedings of a meeting held, volume 5, 2017, p. 8.

[14] R. Ullah, T. A. Cheema, A. S. Saleem, S. M. Ahmad, J. A. Chattha, C. W. Park, Performance analysis of multi-stage gravitational water vortex turbine, Energy Conversion and Management 198 (2019) 111788.
[15] J. A. Chattha, T. A. Cheema, N. H. Khan, Numerical investigation of basin geometries for vortex generation in a gravitational water vortex power plant, in: 2017 8th International Renewable Energy Congress (IREC), IEEE, 2017, pp. 1–5.
[16] L. Velásquez, A. Rubio-Clemente, E. Chica, Numerical analysis of the inlet channel and basin geometries for vortex generation in a gravitational water vortex power plant, in: 18th Inter Conference on Renew Energies and Power Quality, 2020.
[17] C. Christopher, D. Adanta, et al., The effect of basin geometry on gravitational vortex hydropower, in: IOP Conference Series: Materials Science and Engineering, volume 788, IOP Publishing, 2020, p. 012081.
[18] V. J. A. Guzmán, J. A. Glasscock, Analytical solution for a strong free-surface water vortex describing flow in a full-scale gravitational vortex hydropower system, Water Science and Engineering 14 (2021) 72–79.
[19] M. Rahman, J. Tan, M. Fadzlita, A. W. K. Muzammil, A review on the development of gravitational water vortex power plant as alternative renewable energy resources, in: IOP Conference Series: Materials Science and Engineering, volume 217, IOP Publishing, 2017, p. 012007.
[20] M. A. Abdel-Rahman, S. E. Hassan, M. N. El-Din, M. S. Azab, E. F. El-Belely, H. Alrefaey, T. Elsakhawy, One-factor-at-a-time and response surface statistical designs for improved lactic acid production from beet molasses by enterococcus hirae ds10, SN Applied Sciences 2 (2020) 1–14.
[21] K. I. Karamba, S. A. Ahmad, A. Zulkharnain, M. A. Syed, K. A. Khalil, N. A. Shamaan, F. A. Dahalan, M. Y. Shukor, Optimisation of biodegradation conditions for cyanide removal by serratia marcescens strain aq07 using one-factor-at-a-time technique and response surface methodology, Rendiconti Lincei 27 (2016) 533–545.
[22] N. Rezazadeh, S. Danesh, M. Eftekhari, Tx-100 adsorption from aqueous solution using modified graphene oxide; optimization by response surface methodology and one factor at a time techniques, Journal of Dispersion Science and Technology (2021) 1–12.
[23] C. Segura, C. A. Coello Coello, G. Miranda, C. León, Using multi-objective evolutionary algorithms for single-objective optimization, 4OR 11 (2013) 201–228.
[24] Y. Lu, S. Wang, Y. Zhao, C. Yan, Renewable energy system optimization of low/zero energy buildings using single-objective and multi-objective optimization methods, Energy and Buildings 89 (2015) 61–75.
[25] M. Z. Zakaria, H. Jamaluddin, R. Ahmad, S. M. Loghmanian, Comparison between multi-objective and single-objective optimization for the modeling of dynamic systems, Proceedings of the institution of mechanical engineers, part i: journal of systems and control engineering 226 (2012) 994–1005.
[26] J. Wang, J. Zhang, X. Wei, Evolutionary multi-objective optimization algorithm with preference for mechanical design, in: Advances in Machine Learning and Cybernetics, Springer, 2006, pp. 497–506.
[27] A. Izadi, E. Kashani, A. Mohebbi, Combining 10 meta-heuristic algorithms, cfd, doe, mggp and promethee ii for optimizing stairmand cyclone separator, Powder Technology 382 (2021) 70–84.
[28] G. Chiandussi, M. Codegone, S. Ferrero, F. E. Varesio, Comparison of multi-objective optimization methodologies for engineering applications, Computers & Mathematics with Applications 63 (2012) 912–942.
[29] Y. Gao, L. Shi, P. Yao, Study on multi-objective genetic algorithm, in: Proceedings of the 3rd World Congress on Intelligent Control and Automation (Cat. No. 00EX393), volume 1, IEEE, 2000, pp. 646–650.
[30] M. N. Thombre, H. A. Preisig, M. B. Addis, Developing surrogate models via computer based experiments, in: Computer Aided Chemical Engineering, volume 37, Elsevier, 2015, pp. 641–646.
[31] K. Deb, P. C. Roy, R. Hussein, Surrogate modeling approaches for multiobjective optimization: Methods, taxonomy, and results, Mathematical and Computational Applications 26 (2021) 5.
[32] S. Razavi, B. A. Tolson, D. H. Burn, Review of surrogate modeling in water resources, Water Resources Research 48 (2012).
[33] D. Gorissen, I. Couckuyt, E. Laermans, T. Dhaene, Multiobjective global surrogate modeling, dealing with the 5-percent problem, Engineering with Computers 26 (2010) 81–98.
[34] J. Aguilar, A. Rubio-Clemente, L. Velasquez, E. Chica, Design and optimization of a multi-element hydrofoil for a horizontal-axis hydrokinetic turbine, Energies 12 (2019) 4679.
[35] M. M. Ghorani, M. H. S. Haghighi, A. Riasi, Entropy generation minimization of a pump running in reverse mode based on surrogate models and nsga-ii, International Communications in Heat and Mass Transfer 118 (2020) 104898.
[36] C. A. R. Do Nascimento, V. C. Mariani, L. dos Santos Coelho, Integrative numerical modeling and thermodynamic optimal design of counter-flow plate-fin heat exchanger applying neural networks, International Journal of Heat and Mass Transfer 159 (2020) 120097.
[37] Z. Zhang, C. Liao, H. Chai, X. Ni, K. Pei, M. Sun, H. Wu, S. Jiang, Multi-objective optimization of controllable configurations for bistable laminates using nsga-ii, Composite Structures 266 (2021) 113764.
[38] C. Power, A. McNabola, P. Coughlan, A parametric experimental investigation of the operating conditions of gravitational vortex hydropower (gvhp), Journal of Clean Energy Technologies 4 (2016) 112–119.
[39] L. Velásquez, A. Posada, E. Chica, Optimization of the basin and inlet channel of a gravitational water vortex hydraulic turbine using the response surface methodology, Renewable Energy (2022).
[40] G. Marian, T. Sajin, I. Florescu, D. Nedelcu, C. Ostahie, C. Bîrsan, The concept and theoretical study of micro hydropower plant with gravitational vortex and turbine with rapidity steps, Buletinul AGIR 3 (2012) 219–226.
[41] B. Zhao, H. Shen, Y. Kang, Development of a symmetrical spiral inlet to improve cyclone separator performance, Powder Technology 145 (2004) 47–50.
[42] B. Zhao, Y. Su, J. Zhang, Simulation of gas flow pattern and separation efficiency in cyclone with conventional single and spiral double inlet configuration, Chemical Engineering Research and Design 84 (2006) 1158–1165.
[43] P. Baltrėnas, D. Platova, Experimental analysis of the six-channel cyclone with spiral shell, Environmental technology 37 (2016) 652–661.
[44] F. Zhou, G. Sun, X. Han, Y. Zhang, W. Bi, Experimental and cfd study on effects of spiral guide vanes on cyclone performance, Advanced Powder Technology 29 (2018) 3394–3403.

[45] T. Dziubak, L. Bąkała, Computational and experimental analysis of axial flow cyclone used for intake air filtration in internal combustion engines, Energies 14 (2021) 2285.
[46] Y. A. Cengel, Fluid mechanics, Tata McGraw-Hill Education, 2010.
[47] S. Mulligan, J. Casserly, R. Sherlock, Experimental and numerical modelling of free-surface turbulent flows in full air-core water vortices, in: Advances in Hydroinformatics, Springer, 2016, pp. 549–569.
[48] A. Soler, L. Moctezuma, E. Giraldo, M. Molinas, Automated methodology for optimal selection of the minimum electrode subset for accurate eeg source localization based on genetic algorithm optimization (2021).
[49] B. Yuepeng, S. Wenping, H. Zhonghua, Y. Zhang, L. Zhang, Aerodynamic/aeroacoustic variable-fidelity optimization of helicopter rotor based on hierarchical kriging model, Chinese Journal of Aeronautics 33 (2020) 476–492.
[50] A. Moreno Garrido, Técnicas evolutivas multiobjetivo para la evolución de matrices de proyección en problemas de clasificación, Master's thesis, 2012.
[51] P. D. Justesen, Multi-objective optimization using evolutionary algorithms, University of Aarhus, Department of Computer Science, Denmark 33 (2009).
[52] C. A. C. Coello, G. B. Lamont, D. A. Van Veldhuizen, et al., Evolutionary algorithms for solving multi-objective problems, volume 5, Springer, 2007.
[53] D. Simon, Evolutionary optimization algorithms, John Wiley & Sons, 2013.
[54] S. Sivanandam, S. Deepa, Genetic algorithms, in: Introduction to genetic algorithms, Springer, 2008, pp. 15–37.
[55] D. Veit, Genetic algorithms and evolution strategy in textile engineering, in: Advances in Modeling and Simulation in Textile Engineering, Elsevier, 2021, pp. 99–138.
[56] T. Goel, R. Vaidyanathan, R. T. Haftka, W. Shyy, N. V. Queipo, K. Tucker, Response surface approximation of pareto optimal front in multi-objective optimization, Computer methods in applied mechanics and engineering 196 (2007) 879–893.
[57] K. Deb, A. Pratap, S. Agarwal, T. Meyarivan, A fast and elitist multiobjective genetic algorithm: Nsga-ii, IEEE transactions on evolutionary computation 6 (2002) 182–197.
[58] A. Ganjehkaviri, M. M. Jaafar, S. E. Hosseini, H. Barzegaravval, Genetic algorithm for optimization of energy systems: Solution uniqueness, accuracy, pareto convergence and dimension reduction, Energy 119 (2017) 167–177.
[59] M. E. M. Varela, Diseño e implementación de un modelo subrogado en evolución diferencial para optimización con restricciones (2018).
[60] K. Crombecq, Surrogate modeling of computer experiments with sequential experimental design, Ph.D. thesis, Ghent University, 2011.
[61] M. B. Salem, Model selection and adaptive sampling in surrogate modeling: Kriging and beyond, Ph.D. thesis, Université de Lyon, 2018.
[62] K. Shimoyama, K. Sato, S. Jeong, S. Obayashi, Updating kriging surrogate models based on the hypervolume indicator in multi-objective optimization, Journal of Mechanical Design 135 (2013) 094503.
[63] Y. Chen, X. Zou, W. Xie, Convergence of multi-objective evolutionary algorithms to a uniformly distributed representation of the pareto front, Information Sciences 181 (2011) 3336–3355.
[64] Z. Qian, C. C. Seepersad, V. R. Joseph, J. K. Allen, C. Jeff Wu, Building surrogate models based on detailed and approximate simulations (2006).
[65] K. Behzadian, Z. Kapelan, D. Savic, A. Ardeshir, Stochastic sampling design using a multi-objective genetic algorithm and adaptive neural networks, Environmental Modelling & Software 24 (2009) 530–541.
[66] S. Bagheri, W. Konen, T. Bäck, Comparing kriging and radial basis function surrogates, in: Proc. 27. Workshop Computational Intelligence, 2017, pp. 243–259.
[67] M. Puri, A. Solanki, T. Padawer, S. M. Tipparaju, W. A. Moreno, Y. Pathak, Introduction to artificial neural network (ann) as a predictive tool for drug design, discovery, delivery, and disposition: Basic concepts and modeling, in: Artificial neural network for drug design, delivery and disposition, Elsevier, 2016, pp. 3–13.
[68] R. Yondo, E. Andrés, E. Valero, A review on design of experiments and surrogate models in aircraft real-time and many-query aerodynamic analyses, Progress in Aerospace Sciences 96 (2018) 23–61.
[69] M. A. Bouhlel, J. T. Hwang, N. Bartoli, R. Lafage, J. Morlier, J. R. Martins, A python surrogate modeling framework with derivatives, Advances in Engineering Software 135 (2019) 102662.
[70] M. Ahmed, N. Qin, Surrogate-based aerodynamic design optimization: Use of surrogates in aerodynamic design optimization, in: International Conference on Aerospace Sciences and Aviation Technology, volume 13, The Military Technical College, 2009, pp. 1–26.
[71] H. Liu, J. Cai, Y.-S. Ong, An adaptive sampling approach for kriging metamodeling by maximizing expected prediction error, Computers & Chemical Engineering 106 (2017) 171–182.
[72] H. Wang, X. Zhu, Z. Du, Aerodynamic optimization for low pressure turbine exhaust hood using kriging surrogate model, International communications in heat and mass transfer 37 (2010) 998–1003.
[73] E. Bernardini, S. M. Spence, D. Wei, A. Kareem, Aerodynamic shape optimization of civil structures: A cfd-enabled kriging-based approach, Journal of Wind Engineering and Industrial Aerodynamics 144 (2015) 154–164.
[74] G. Xu, X. Liang, S. Yao, D. Chen, Z. Li, Multi-objective aerodynamic optimization of the streamlined shape of high-speed trains based on the kriging model, PloS one 12 (2017) e0170803.
[75] N. L. Lukić, M. Božin-Dakić, J. A. Grahovac, J. M. Dodić, A. I. Jokić, Multi-objective optimization of microfiltration of baker's yeast using genetic algorithm, Acta Periodica Technologica (2017) 211–220.
[76] A. Arias-Montano, C. A. C. Coello, E. Mezura-Montes, Multi-objective airfoil shape optimization using a multiple-surrogate approach, in: 2012 IEEE Congress on Evolutionary Computation, IEEE, 2012, pp. 1–8.
[77] J. C. Helton, F. J. Davis, Latin hypercube sampling and the propagation of uncertainty in analyses of complex systems, Reliability Engineering & System Safety 81 (2003) 23–69.
[78] A. Olsson, G. Sandberg, O. Dahlblom, On latin hypercube sampling for structural reliability analysis, Structural safety 25 (2003) 47–68.
[79] A. Keane, A. Forrester, A. Sobester, Engineering design via surrogate modelling: a practical guide, American Institute of Aeronautics and

Astronautics, Inc., 2008.
[80] S. Koziel, L. Leifsson, Surrogate-based modeling and optimization, Springer, 2013.
[81] G. O. Toolbox, User's guide (r2011b), The MathWorks Inc (2011).
[82] E. L. Landguth, S. A. Cushman, M. K. Schwartz, K. S. McKelvey, M. Murphy, G. Luikart, Quantifying the lag time to detect barriers in landscape genetics, Molecular ecology 19 (2010) 4179–4191.
[83] D. L. Tong, R. Mintram, Genetic algorithm-neural network (gann): a study of neural network activation functions and depth of genetic algorithm search applied to feature selection, International Journal of Machine Learning and Cybernetics 1 (2010) 75–87.
[84] M. Hassan, D. Liu, Performance evaluation of an evolutionary multiobjective optimization based area partitioning and allocation approach, in: 2018 IEEE/ASME International Conference on Advanced Intelligent Mechatronics (AIM), IEEE, 2018, pp. 527–532.
[85] W.-C. Yeh, M.-C. Chuang, Using multi-objective genetic algorithm for partner selection in green supply chain problems, Expert Systems with applications 38 (2011) 4244–4253.
[86] K. Deb, A. Kumar, Light beam search based multi-objective optimization using evolutionary algorithms, in: 2007 IEEE Congress on Evolutionary Computation, IEEE, 2007, pp. 2125–2132.
[87] A. Gaspar-Cunha, J. A. Covas, Robustness in multi-objective optimization using evolutionary algorithms, Computational Optimization and Applications 39 (2008) 75–96.
[88] Q. Xu, Extended surrogate modeling techniques for large scale structural design optimization, Ph.D. thesis, Technische Universität München, 2014.
[89] K. Zore, B. Sasanapuri, G. Parkhi, A. Varghese, Ansys mosaic poly-hexcore mesh for high-lift aircraft configuration, in: 21st AeSI Annual CFD Symposium, 2019.
[90] S. B. Pope, Turbulent flows, 2001.
[91] I. ANSYS, Ansys fluent 12.0 theory guide, ANSYS FLUENT Release (2009).
[92] Q. Chen, Comparison of different k-ϵ models for indoor air flow computations, Numerical Heat Transfer, Part B Fundamentals 28 (1995) 353–369.
[93] K. Zore, D. Caridi, I. Lockley, Fast and accurate prediction of vehicle aerodynamics using ANSYS mosaic mesh, Technical Report, SAE Technical Paper, 2020.
[94] M. Rakowitz, Grid refinement study with a uhca wing-body configuration using richardson extrapolation and grid convergence index gci, in: New results in numerical and experimental fluid mechanics III, Springer, 2002, pp. 297–303.
[95] N. Baker, G. Kelly, P. D. O'Sullivan, A grid convergence index study of mesh style effect on the accuracy of the numerical results for an indoor airflow profile, International Journal of Ventilation 19 (2020) 300–314.
[96] M. Potgieter, C. Bester, M. Bhamjee, Experimental and cfd investigation of a hybrid solar air heater, Solar Energy 195 (2020) 413–428.
[97] A. Meana-Fernández, J. M. Fernandez Oro, K. M. Argüelles Díaz, M. Galdo-Vega, S. Velarde-Suárez, Application of richardson extrapolation method to the cfd simulation of vertical-axis wind turbines and analysis of the flow field, Engineering Applications of Computational Fluid Mechanics 13 (2019) 359–376.
[98] S.-C. Luo, J. Liu, K. Li, Grid convergence and influence of wall temperature in the calculation of thermochemical non-equilibrium heat flux, Journal of Physics D: Applied Physics 53 (2020) 285502.
[99] K. Hutter, Y. Wang, Conservation of angular momentum—vorticity, in: Fluid and Thermodynamics, Springer, 2016, pp. 159–195.
[100] S. Yi, H. I. Kwon, S. Choi, Efficient global optimization using a multi-point and multi-objective infill sampling criteria, in: 52nd Aerospace Sciences Meeting, 2014, p. 0898.
[101] T. Friedrich, C. Horoba, F. Neumann, Multiplicative approximations and the hypervolume indicator, in: Proceedings of the 11th Annual conference on Genetic and evolutionary computation, 2009, pp. 571–578.
[102] J. Branke, W. Zhang, Y. Tao, Multio-bjective ranking and selection based on hypervolume, in: 2016 Winter Simulation Conference (WSC), IEEE, 2016, pp. 859–870.
[103] E. Zitzler, D. Brockhoff, L. Thiele, The hypervolume indicator revisited: On the design of pareto-compliant indicators via weighted integration, in: International Conference on Evolutionary Multi-Criterion Optimization, Springer, 2007, pp. 862–876.
[104] A. B. Colaço, V. C. Mariani, M. R. Salem, L. dos Santos Coelho, Maximizing the thermal performance index applying evolutionary multi-objective optimization approaches for double pipe heat exchanger, Applied Thermal Engineering 211 (2022) 118504.
[105] L. While, P. Hingston, L. Barone, S. Huband, A faster algorithm for calculating hypervolume, IEEE transactions on evolutionary computation 10 (2006) 29–38.
[106] M. Pal, S. Bandyopadhyay, Reliability of convergence metric and hypervolume indicator for many-objective optimization, in: 2016 2nd International Conference on Control, Instrumentation, Energy & Communication (CIEC), IEEE, 2016, pp. 511–515.
[107] A. Mukhopadhyay, U. Maulik, S. Bandyopadhyay, Multiobjective genetic algorithm-based fuzzy clustering of categorical attributes, IEEE transactions on evolutionary computation 13 (2009) 991–1005.
[108] K. K. Mishra, S. Harit, A fast algorithm for finding the non dominated set in multi objective optimization, International Journal of Computer Applications 1 (2010) 35–39.
[109] K. Deb, Multi-objective optimization, in: Search methodologies, Springer, 2014, pp. 403–449.

Table 5
Sample data added

Run	Design variables						Γ [m^2/s]	Q [m^3/s]
	d/D	w/D	h/D	L/D	γ [Deg]	H/D		
1	0.1826	0.3065	0.3030	2.1551	106.7397	1.7517	1.9461	0.0052
2	0.1004	0.2131	0.2391	2.3249	91.7373	0.5008	1.3797	0.0016
3	0.1031	0.2508	0.2499	2.3129	95.0146	0.6012	1.3981	0.0018
4	0.1000	0.4286	0.2007	0.6227	90.0000	0.5000	1.2959	0.0016
5	0.1996	0.2001	0.5192	1.9050	167.5826	1.4997	1.9218	0.0050
6	0.1013	0.4074	0.3036	0.8202	95.0597	0.8272	1.4621	0.0020
7	0.2058	0.2014	0.4364	2.0378	119.5744	1.7003	1.8605	0.0054
8	0.1000	0.2324	0.4123	2.7532	90.3430	0.5449	1.4007	0.0016
9	0.1028	0.2601	0.4417	2.7147	92.0086	0.6723	1.4570	0.0019
10	0.2276	0.2018	0.5476	0.5064	144.9121	1.1314	1.8687	0.0045
11	0.1003	0.2207	0.2006	1.5851	90.7328	0.5011	1.3540	0.0016
12	0.1012	0.2251	0.2170	1.5993	90.9768	0.6710	1.4626	0.0018
13	0.1000	0.2945	0.4678	1.6253	92.8593	0.5036	1.3174	0.0016
14	0.1009	0.2752	0.4723	1.6169	92.9062	0.6673	1.4389	0.0018
15	0.2237	0.2040	0.5580	0.5080	147.3854	1.1874	1.8809	0.0046
16	0.2380	0.2009	0.5828	0.5064	136.8831	0.9737	1.7599	0.0041
17	0.1024	0.2132	0.5609	1.3682	118.8226	0.5061	1.3030	0.0016
18	0.2690	0.2228	0.5298	0.9989	129.1677	0.5041	1.4721	0.0028
19	0.1026	0.2068	0.5746	0.5463	127.9947	0.5120	1.2900	0.0016
20	0.2360	0.2225	0.5382	0.5063	143.3651	1.0779	1.8328	0.0044
21	0.1039	0.2104	0.4759	0.7133	126.5848	0.8509	1.5405	0.0021
22	0.1009	0.2768	0.5097	0.6391	129.3838	0.8168	1.4539	0.0020
23	0.2210	0.2061	0.5603	0.5048	141.1587	1.1395	1.8506	0.0045
24	0.1001	0.4509	0.5857	0.5218	124.6339	0.5063	1.2057	0.0016
25	0.1001	0.2001	0.5822	0.5131	93.3912	0.5001	1.3402	0.0016
26	0.1543	0.4033	0.4523	2.7637	108.8962	1.6758	1.8372	0.0045
27	0.1705	0.3960	0.5390	2.8063	109.3063	1.7112	1.8950	0.0049
28	0.1887	0.3254	0.2384	2.9589	108.6728	1.8919	2.0517	0.0055
29	0.1002	0.2520	0.2564	2.4256	93.5493	1.2846	1.6396	0.0025
30	0.1000	0.4996	0.2212	0.5033	93.5121	0.5000	1.3051	0.0016
31	0.1001	0.4992	0.5968	1.7410	90.0007	0.5008	1.2860	0.0016
32	0.1778	0.3341	0.3160	2.8276	102.8612	1.9136	1.9926	0.0054
33	0.1933	0.3486	0.2130	2.9994	106.1530	1.9995	2.1033	0.0057
34	0.1001	0.2430	0.2289	2.0192	90.0412	0.5171	1.3899	0.0016
35	0.1976	0.3618	0.2594	3.0000	108.4521	2.0000	2.1074	0.0058
36	0.1890	0.3568	0.2520	2.8091	107.5548	1.8757	2.0146	0.0055
37	0.1000	0.2002	0.3702	0.5377	91.1376	0.5000	1.3523	0.0016
38	0.2002	0.2073	0.3113	2.9333	101.0156	1.7824	1.9490	0.0055
39	0.2149	0.2023	0.3023	2.9999	101.4582	1.9986	2.0548	0.0059
40	0.1000	0.2000	0.2519	2.1066	90.1954	0.5000	1.3898	0.0016
41	0.1795	0.2291	0.3427	2.9908	105.7225	1.9955	2.0054	0.0055
42	0.1984	0.2282	0.3444	3.0000	105.8784	2.0000	2.0871	0.0058
43	0.2079	0.3122	0.4429	2.9992	106.3844	2.0000	1.9874	0.0059
44	0.1775	0.3369	0.4936	2.2141	106.0822	1.5501	1.9027	0.0048
45	0.1866	0.2090	0.2722	2.4653	105.1671	1.7529	1.9683	0.0053
46	0.2097	0.2010	0.2407	2.9965	113.8667	2.0000	2.1018	0.0059
47	0.1207	0.2447	0.4049	1.5311	103.9600	1.2337	1.6846	0.0031
48	0.1473	0.2394	0.5870	1.8172	110.5051	1.3633	1.8375	0.0039
49	0.1009	0.2162	0.5959	0.5842	116.6781	1.2133	1.6488	0.0025
50	0.1006	0.2099	0.5931	0.5696	116.5187	1.0987	1.5943	0.0023
51	0.1028	0.3007	0.5213	2.3028	110.9942	1.5147	1.6090	0.0028
52	0.1007	0.2647	0.2292	2.7983	132.7494	1.0584	1.5383	0.0023
53	0.1021	0.3164	0.5280	2.3945	109.1960	1.2517	1.5529	0.0025
54	0.1082	0.3614	0.5654	1.5189	92.1414	1.5721	1.6999	0.0030
55	0.1216	0.3700	0.5693	1.5075	91.1285	1.5427	1.7648	0.0035
56	0.1141	0.3692	0.5707	1.5338	92.0339	1.5586	1.7719	0.0032
57	0.1598	0.2764	0.2557	2.8685	96.4049	1.3413	1.8573	0.0042
58	0.1585	0.2764	0.2537	2.9024	95.9755	1.2163	1.7951	0.0039
59	0.1678	0.2804	0.2531	2.9204	99.1167	1.5043	1.9074	0.0046
60	0.1150	0.2717	0.4295	1.0490	130.7839	1.3568	1.7325	0.0031

CHAPTER 5

SINGLE-OBJECTIVE OPTIMIZATION USING THE RESPONSE SURFACE METHODOLOGY II

Numerical optimization and experimental validation of the runner of a gravitational water vortex hydraulic turbine with spiral inlet channel and conical basin

Submitted article

Highlights

- The runner for a GWVHT was optimized through a response surface methodology with a central composite design (CCD).
- The effect of the relative position of the runner (p), the number of blades (n), and the mean diameter (D_b/D) of the blades on the efficiency of the turbine was evaluated.
- The highest efficiency of 65.18% was reached when the independent variables are set to D_b/D =0.45, n =6 and p =0.6.

Numerical optimization and experimental validation of the runner of a gravitational water vortex hydraulic turbine with spiral inlet channel and conical basin

Laura Velásquez, Fredys Romero-Menco, Alejandro Posada and Edwin Chica

ABSTRACT

This paper describes the use of response surface methodology for the numerical optimization of the runner of a gravitational water vortex hydraulic turbine with a conical basin and a spiral inlet channel. The effect of the relative position of the runner (p), the number of blades (n), and the relation between the mean diameter of the blades (D_b) and the diameter of basin (D), (D_b/D), on the efficiency of the turbine was evaluated and the optimum runner was determined. A second-order response model for the efficiency of the turbine was developed. From this model it was found that the highest efficiency of 65.18% is reached when all the independent variables are set to their higher values, i.e., D_b/D, n, p equal to 0.45, 6, 0.6, repectively. Experiments were performed using the optimal runner (D_b/D =0.45, n =6) and four values for p (0.4, 0.45, 0.50, and 0.55). It was not possible to test the optimal condition with p =0.6, due to the final quality of the acrylic model, the runner collided with the walls of the cone. The experimental efficiencies for the p values were 30.13, 38.35, 53.19, and 60.77%, respectively. According to the response model, these efficiencies correspond to 28.84, 40.46, 50.80, and 59.99%, respectively.

1. Introduction

Hydropower is one of the renewable energy sources that are used to generate electricity in many countries in the world. In 2021, the hydropower contributed with a 16.2% (3427 terawatt) to the total global electricity generation [1, 2, 3]. In 20 years, hydropower sector will have a significant growth; it is expected that more than 37% of the world's energy consumption will be covered by renewable sources [4, 5]. To generate electricity from hydropower, one of the methods used is creating an artificial lake. This artificial lake is developed when a dam is placed in a river pathway [6]. The ecological effects of this artificial lake and dam are significant [7, 8]. An alternative to produce energy from water is the use of micro-hydro and mini-hydro power plants. These plants can be used to produce electricity at small scale without dams or reservoirs from small water sources, such as rivers or streams [9, 10]. Micro and mini-hydro power plants can generate electricity up to a capacity of 100 kW [11, 12]. In the usual hydropower plants, the hydraulic turbines take advantage of the potential and kinetic energy of the water. In these facilities, Pelton, Kaplan, or Francis's turbines are used extensively [13, 14]. An interesting option for hydropower generation is the gravitational water vortex hydraulic turbine (GWVHT) [15]. A gravitational water vortex hydraulic turbine can work in a low head range of 0.7 to 2 m. GWVHT works in a similar way to Kaplan turbine. A Kaplan turbine uses guide vane to generate a swirl in a closed vessel [16], while a GWVHT, the swirl comes from the naturally organized water vortex on a free surface.

One of the main inconvenient of GWVHT is its efficiency. Its average efficiency is 54% $\pm$ 12% [17]. GWVHTs are less efficient than other commercial hydro turbines [18]. Since its first deployment in 2006, researchers have been employed numerical and experimental methods to improve its performance [17, 19, 20]. Still, there are not generic design approaches that allow to design and establish performance metrics for the GWVHT. To maximize the power output, several authors have highlighted the optimization of runners [21]. Variations in the curvature, height, width, and the number of blades has been explored. The positioning of the blades in the vortex has also been considered. These parameters were individually varied, while all others were maintained constant. Bajracharya et. al [22] suggested that the optimum position of runner is 65% of the total height of basin from the top position, since this is the point where maximum velocities can be achieved [23]. Different researchers affirm that the blades with curved profile are more efficient in comparison to straight profile blades [21, 24]. The studies of Bajracharya et al. [22] and Power et al. [25]

ORCID(s): 0000-0003-1483-0104 (L. Velásquez); 0000-0002-6364-4298 (F. Romero-Menco); 0000-0001-5836-0680 (A. Posada); 00000-0002-5043-6414 (E. Chica)

are in contradiction for maximum power output when the number of blades is increased [21, 24]. Bajracharya et al. affirm that the efficiency decreases with an increase in the number of blades, since they cause a greater distortion in the vortex. They concluded that the efficiency also decreases with increase in radius of the blades, since the water velocities at radius far away from the core are lower [23].

The conclusions about the optimum position of runner (p), the number of blades (n), and the radius of the blades (r_b) can change when these parameters are studied simultaneously, that is, when their combined effect on the efficiency of GWVHT is analyzed. Because of that, the current work is focused on the optimization of the runner of a GWVHT to increase its efficiency. In this regard, computational fluid dynamics (CFD) simulations and central composite design (CCD) show experimental design was employed for modelling a second-order response surface, followed by an experimental verification of the optimal model found (the runner with the highest efficiency). Nine different runners and three different positions have been considering by numerical optimization. During the process of analysis, the dimension of the inlet channel, basin, and discharge were taken constant.

2. Methods and materials

2.1. Gravitational water vortex hydraulic turbine (GWVHT)

GWVHT is an impulse turbine of ultra-low head hydropower technology [26, 27, 28, 18]. It was developed by Franz Zotloterer in 2006 [17, 27]. In a GWVHT, the water passes through a straight inlet channel into a conical basin tangentially, in which a free surface water vortex is formed [15, 28]. A vertical runner is positioned in the center of the basin. The runner rotates with the water vortex, thus generating mechanical energy which can be converted to electrical energy using a generator [29, 25]. The water vortex discharges through an outlet hole at the bottom of the basin [29, 25]. The scheme of the hydropower plant studied is shown by Figure 1. The inlet channel, basin, and discharge studied was optimized previously by Velasquez et. al [30] who employed the multi-objective optimization to maximize the vortex strength (Γ) and minimize the volume flow rate (Q). In Velasquez et. al [30], the main dimensions of inlet channel, basin, and discharge were a function of the diameter of the basin (D) as follows H/D =1.572, L/D =1.518, h/D =0.565, w/D =0.361, d/D =0.108, and γ =92.141°. For the current study, the basin diameter used was 500 mm.

The equations used for calculating the available power of a hydraulic turbines are also used for calculating the available power of GWVHT. The maximum available power (P) of GWVHT is given by Eq. 1:

$$P = \rho g Q(H_n) \tag{1}$$

where ρ is the density of the fluid, g the gravity, Q the volume flow rate, and H_n is difference height between the level of fluid in the inlet channel and the position of the runner in the basin [17]. The power generated (P_{out}) by a turbine is given by equation Eq. 2:

$$P_{out} = T\omega \tag{2}$$

where ω is the angular velocity, and T is the torque. The hydraulic efficiency (η) is defined by equation Eq. 3:

$$\eta = \frac{P_{out}}{P} = \frac{T\omega}{\rho g Q(H_n)} \tag{3}$$

2.1.1. Runner design

In an impulse turbine, water travels from the inlet to the outlet of the blade; the outlet velocity and direction of water changes from that of the inlet [29]. The change in velocity and direction changes the momentum of the water jet, and this change in momentum is absorbed by the runner [31]. Figure 2 shows the inlet and outlet velocity triangles for an impulse turbine. In Figure 2, V_b is the linear velocity of the blade, V is the absolute velocity, V_r is the relative velocity of the jet with respect to the blades, V_f is the velocity of the flow at entrance of the blade (vertical component of V), V_w is the velocity of swirl at entrance of the blade (horizontal component of V), θ is the angle which the relative velocity of the jet makes with the direction of the motion of the blades, and α is the angle with the direction of motion of the blade at which the jet enters the blade. Subscript 1 corresponds to values at exit of the blade.

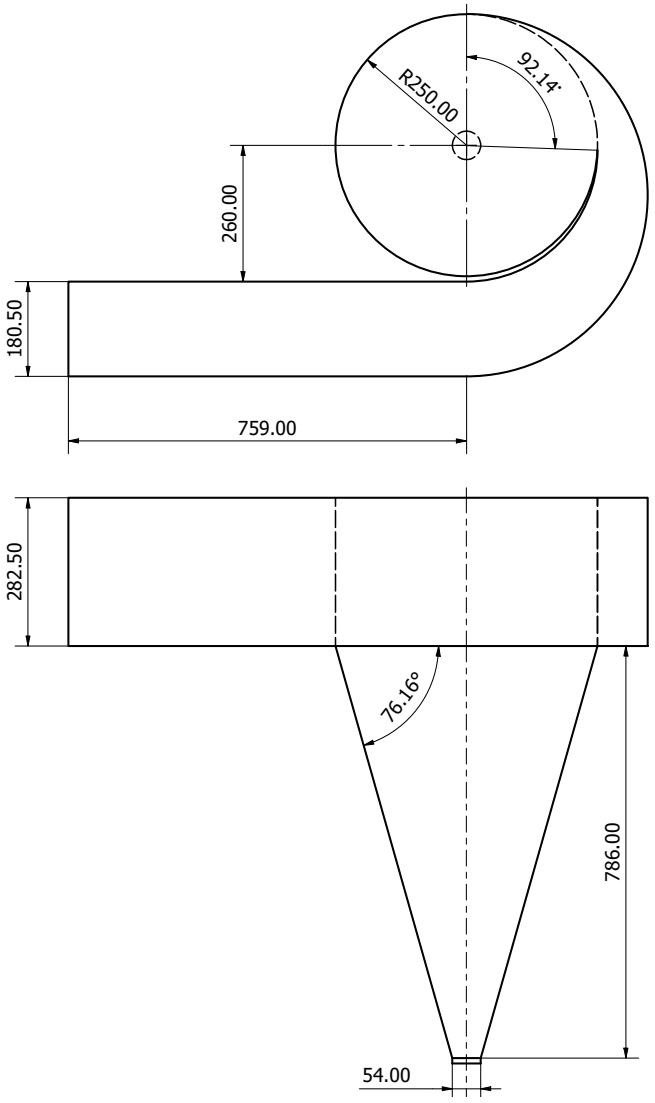

Fig. 1: The scheme of the hydropower plant. Dimensions are expressed in mm.

In a GWVHT, V_b changes across the radius of the vortex [29]. Therefore, the velocity triangles vary across the radius of the runner. Seeking to take advantage of the components of the flow velocity in the vortex, studies have been carried out mainly on 4 types of runners for a GWVHT: runner with straight blades aligned with the axis of the turbine [25, 32, 33, 34, 20, 19, 35, 36], runner with curved blades aligned to the axis of the turbine [29, 36, 37, 27, 38, 39, 40, 41], runner with straight blades inclined with respect to the axis of the turbine [29, 20, 35], and runner with curved blades with twist angle [29, 20, 36, 31, 42, 21]. The twist angle is the angle that the cross section of the blade makes at the top with respect to its counterpart at the bottom. These runners are shown in Figure 3.

Between runner with straight or curved blades aligned to the axis of the turbine, from the past studies, it was concluded that the curved blades runner is the most efficient runner. The authors found better performance with runners that had curved blades with twist angle, managing to take better advantage of the tangential and axial velocity of the fluid. Therefore, the runner with curved blades with twist angle was chosen over straight and curved blade profile.

2.2. Response surface methodology analysis with CCD

Response surface methodology (RSM) is a statistical method that uses data from experiments to establish a regression model and to optimize a response which is influenced by several independent variables [43, 44, 45, 46]. The

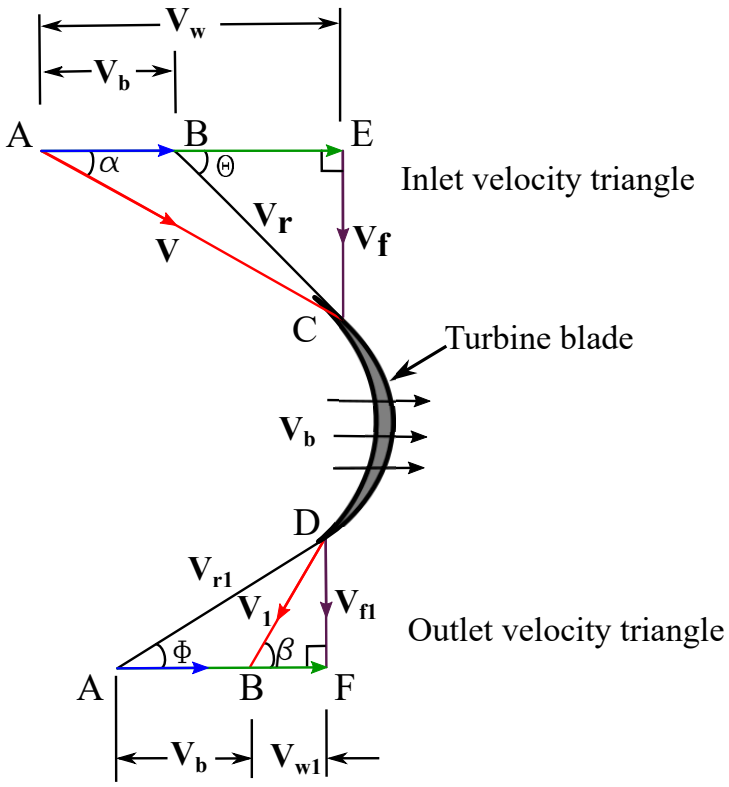

Fig. 2: Velocity Triangle for an impulse turbine. Adapted from: [29].

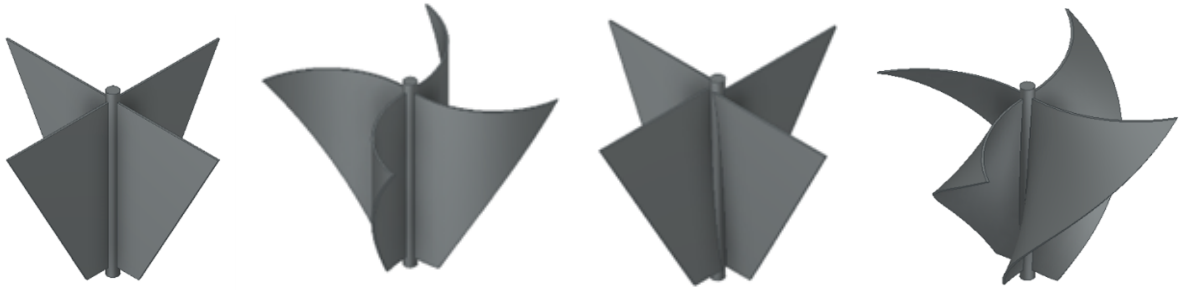

Fig. 3: Types of runners for a GWVHT: a) runner with straight blades aligned with the axis of the turbine, b) runner with curved blades aligned to the axis of the turbine, c) runner with straight blades inclined with respect to the axis of the turbine and d) runner with curved blades with twist angle.

optimization processes using RSM consists of six consecutive steps: I) select the independent factors and desired responses, II) choose the strategy for experimental design, III) run the experiments and obtain the results, IV) estimate the coefficients in a mathematical model that fit the experimental data, V) check the adequacy of the model, and VI) determine of optimal conditions [43].

The independent variables chosen for this optimization process were the relative position of runner (p), the number of blades (n), and the mean diameter of the blades ($D_b = 2 \times r_b$). The response variable was the efficiency (η) of the GWVHT. The mean diameter is measured at the middle height of the runner. The variable p is a function of the position of the runner (h) and the basin height (H), $p = h/H$, h is measured to the middle height of the runner as shown in Figure 4.

The mean diameters of the blades of the present study were determined considering the diameter of the conical basin at three different positions, obtaining diameters of 145.25 m (D_b/D =0.29), 185.25 mm (D_b/D =0.37) and 225.25 mm (D_b/D =0.45). The mean diameter of the blades was divided by the diameter of the basin (D) to obtain a non-dimensional variable. The other dimension of the runners depends on the vortex formed in the basin. The vortex

Table 1
Blades design summary.

Symbol	Variable	Db/D 0.29	Db/D 0.37 value	Db/D 0.45
α	Blade inlet angle [Deg]	16.00	16.00	16.00
α_1	Blade outlet angle [Deg]	90.00	90.00	90.00
β	Water inlet angle [Deg]	40.00	40.00	40.00
β_1	Water outlet angle [Deg]	43.80	43.10	42.7
λ	Twist angle [Deg]	68.80	68.80	68.80
L	Blade height [mm]	200	200	200

Table 2
Independent factors and levels.

Factor	High level	Medium level	Low level
D_b/D (x_1)	0.45	0.37	0.29
n (x_2)	6	4	2
p (x_3)	0.6	0.5	0.4

profile for the selected basin was analyzed from the results presented by Velasquez et. al [30]. Table 1 summarizes the inlet and outlet angles of the blade for three different runners of study as a function of the diameter of the blade.

The other independent factors chosen were varied over three levels: the lower, medium, and high level. The levels of the factors are shown in Table 2. The selection of suitable levels for n and p was obtained from the literature [29, 25, 32, 33, 34, 20, 19, 35, 36, 37, 27, 38, 39, 40, 41, 31, 42, 21].

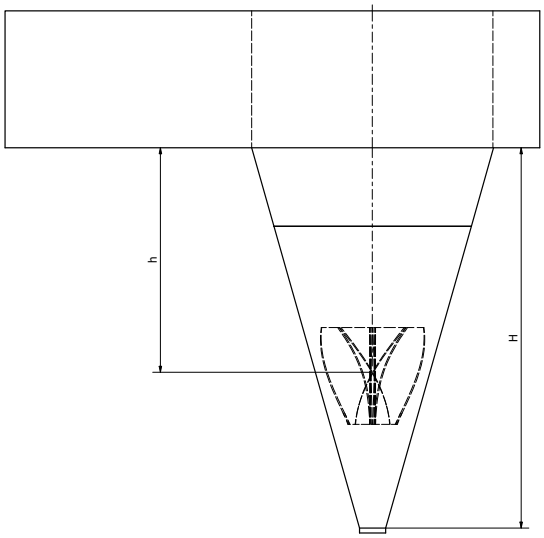

Fig. 4: Position of the runner.

To the experimental design, the central composite design (CCD) was chosen. CCD is the most used fractional factorial design used in RSM [44, 46]. CCD can generate response surfaces with fewer runs required [47].

For a CCD, the total required runs (N) is calculated by Eq. 4:

$$N = 2^k + 2k + n_c \tag{4}$$

Table 3
Required runs and numerical results.

Run	D_b/D	n	p	Outlet power [W]	Efficiency	
					CFD [%]	Model [%]
1	0.37	6	0.5	3.04	34.76	34.03
2	0.45	6	0.6	7.24	65.18	67.79
3	0.29	2	0.6	1.98	17.82	19.41
4	0.29	4	0.5	1.16	13.27	14.59
5	0.29	6	0.4	0.02	0.34	1.04
6	0.45	2	0.6	5.79	52.09	51.08
7	0.37	2	0.5	1.86	21.28	23.99
8	0.45	2	0.4	1.25	19.51	19.51
9	0.37	4	0.6	4.91	44.20	41.70
10	0.45	4	0.5	3.82	43.66	44.32
11	0.45	6	0.4	1.97	30.74	28.83
12	0.37	4	0.4	0.44	6.86	11.35
13	0.29	6	0.6	3.39	30.49	30.17
14	0.29	2	0.4	0.04	0.59	-2.33
15	0.37	4	0.5	2.64	30.18	29.03
16	0.37	4	0.5	2.64	30.18	29.03
17	0.37	4	0.5	2.64	30.18	29.03

where k is the number of factors, and n_c is the number of centers points runs. For three independent factors, and three center runs, the total number of runs is 17. They are listed in Table 3. Tables 3 shows the required runs together with the numerical results. According to Table 3, in the final 17 runs there are combinations of 9 different runner. These runners are shown in Figure 5.

The quadratic model equation for predicting and analyzing the efficiency or the runner was expressed according to Eq. 5:

$$\eta = \beta_0 + \beta_1 x_1 + \beta_2 x_2 + \beta_3 x_3 + \beta_{11} x_1^2 + \beta_{22} x_2^2 + \beta_{33} x_3^2 + \beta_{12} x_1 x_2 + \beta_{13} x_1 x_3 + \beta_{23} x_2 x_3 \quad (5)$$

The coefficients of the equation were denoted by β_0 (constant term), β_1, β_2, and β_3 (linear effects), β_{11}, β_{22}, and β_{33} (quadratic effects), and β_{12}, β_{13}, and β_{23} (interaction effects). The coefficients, which should be determined in the second-order model, are obtained by the least square method [36]. Then, an analysis of variance (ANOVA) was used to calculate the statistical parameters to define the interaction between the independent variables and the response. To determine if the quadratic model equation is fit to data, the coefficient of determination (R_2) and adjusted coefficient of determination (adjusted-R_2) were used.

2.3. Numerical simulation

Numerical simulations were performed using Ansys Fluent. The simulation domain was divided into two domains: a stationary domain, and a rotating domain. The stationary domain included the inlet channel and basin, and the rotating domain contains the runner. The domains were meshed using poly-hex core mesh elements.

Volume of fluid method (VoF), Transition-state, and $k-\omega$ SST turbulence model were selected to execute the simulations. The VoF method allows examining the interaction of two fluids in the domains: air (primary phase) and water (secondary phase). VoF method uses α as a phase indicator. A value of 1 or 0 shows that a control volume is entirely filled or empty, respectively, with the primary phase, and a value between 1 and 0 indicates an interface. In the initialization of the domains, α was set to 1. As boundary conditions, a relative pressure of 0 Pa was used at the discharge; and an inlet velocity of 0.0597 m/s was imposed at the inlet channel. The inlet velocity was calculated according to the equation proposed by Velasquez et al. [48] in their study on optimization of the inlet channel and basin. The upper surfaces of the channel and basin were set with a static pressure of 0 Pa, the air could enter and exit freely. The rotating domain was set to rotate with increments of 27 rpm beginning from 0 up to 200 rpm. Figure 6 (a) and (b) shows the domains and meshes used for the numerical study.

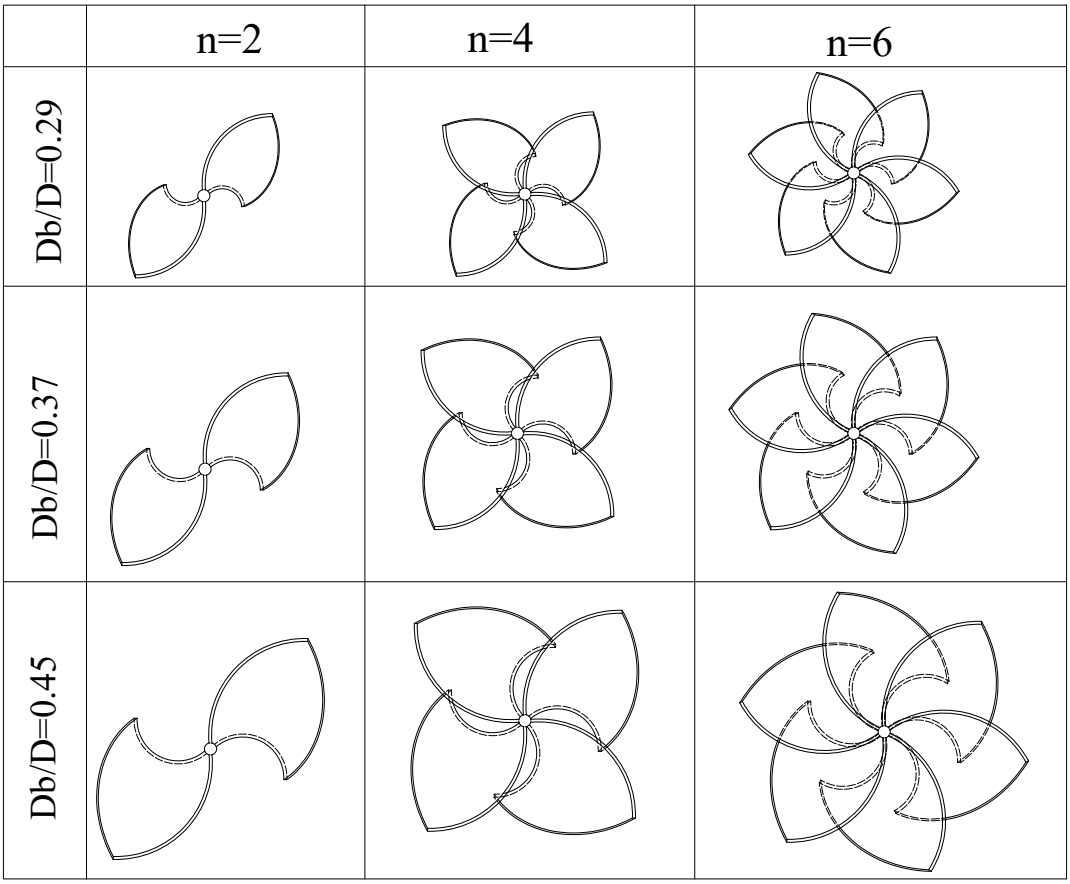

Fig. 5: Studied runners.

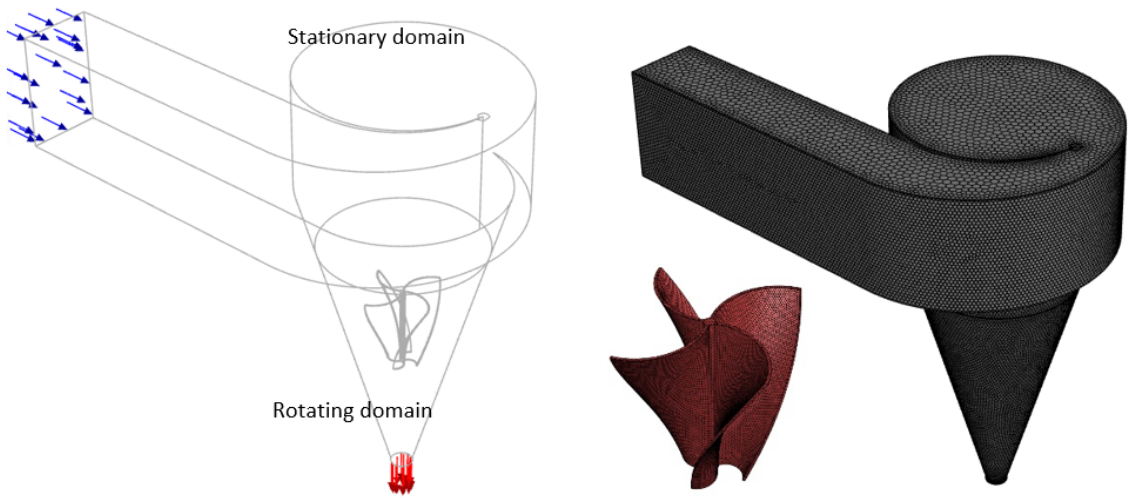

Fig. 6: a) Domains and b) Mesh.

A mesh independency was performed to verify how much the output parameter (efficiency) result deviated. The mesh independence test was performed using the grid convergence index (GCI) method. The GCI indicates how far the

numerical solution is from the asymptotic range and how much the numerical solution changes with further refinement. If the value of GCI is close to 1.0, the solution is within the asymptotic range of convergence [49]. The GCI method was accomplished employing three different numbers of elements, and three different time-step.

The number of cells for the analysis was set to be around 2,036,6661 (fine mesh), 870,064 (medium mesh) and, 524,025 (coarse mesh). Δt used for the test were 0.005, 0.0025, and 0.00125 s. Figure 7 presents the results for independence tests. The values of GCI_{23} and GCI_{12} represent the relative change from coarse to medium mesh/time step and from medium to fine mesh/time step, respectively. According to Figure 7, with a GCI of 0.9976 and 1.0023, for the mesh and Δt, respectively, the solution is in the asymptotic range of convergence. The medium time-step of Δt =0.0025 and the medium mesh is chosen for the analysis to minimize the computational time and the errors.

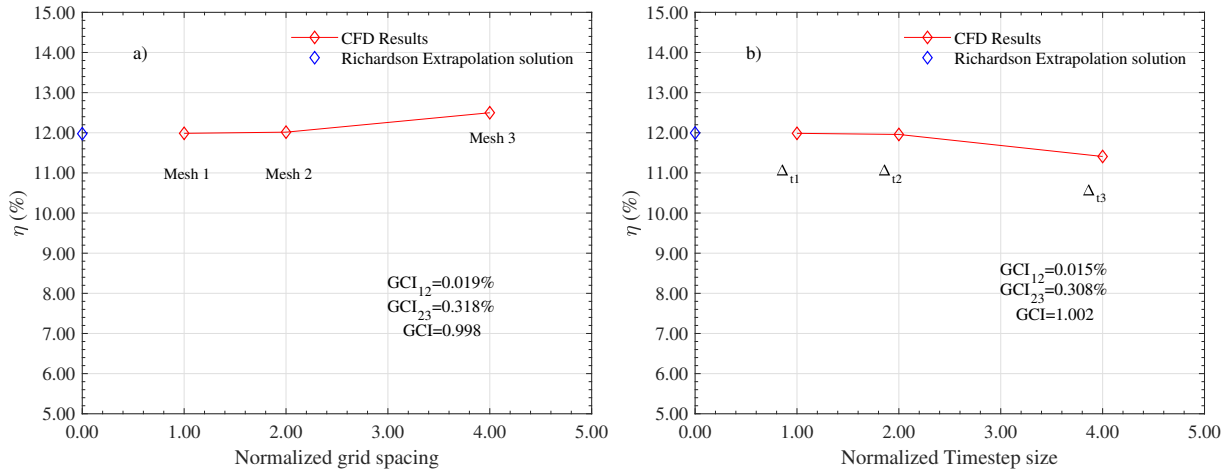

Fig. 7: Mesh independence study.

2.4. Experimental setup

To validate the CFD calculations, a test bench with GWVHT was built. The bench was composed of two water tanks, a centrifugal pump, basin, inlet channel and runner. The experimental setup is shown in Figure 8. The pump was used to move water from the lower tank to the upper tank at a controlled volume flow rate. To observe the flow behavior, the basin and inlet channel were made from transparent acrylic. The runner was printed in a 3D-print using polylactic acid (PLA). The flow rate Q was measured with a flow meter (Siemens SITRANS FM MAG 5100W). The angular velocity ω and torque T over the runner were measured with a rotary torque Sensor (Futek TRS 605-FSH02057). Knowing the flow rate and the location of the runner in the basin, the available power is calculated using Eq. 1. The power generated by the turbine is calculated using Eq. 2 together with the values of angular velocity and torque. With the available power and generated power values, the efficiency of the turbine is determined using Eq. 3. The experiment was performed under the condition of constant flow rate Q =3.05 L/s. A variable load was imposed on the runner. When the tests were started, the reading of torque sensor is set at zero when the angular velocity is constant. The load was increased to reduce the angular velocity until 0 rpm. The load was controlled by a motor and an inverter.

3. Results and discussion

3.1. Numerical results

The results obtained from numerical simulation are represented in Figures 9 and 10. Figure 9 shows the changes in the output mass flow rate as a function of the simulation time for 18 geometries (17 geometries studied and a geometry without runner). The mass flow stabilized (constant flow in the gravitational vortex of 2.9 kg/s) closer to 40 seconds, except for run 5, whose mass flow rate does not stabilize in the period studied, changing between 1.5 and 4.7 kg/s. Run 5 corresponds to the geometry with the smallest D_b/D, smallest p and largest number of blades.

Figure 10 shows the efficiency of GWVHT as a function of the angular velocity of the runner for the 17 geometries studied. Run 2 (D_b/D =0.45, n =6 and p =0.6) has the maximum efficiency, that corresponds of a value of 65.18% achieved at 14 rad/s. The following two efficiencies correspond to geometries 6 (D_b/D =0.45, n =2, p =0.6) and 9

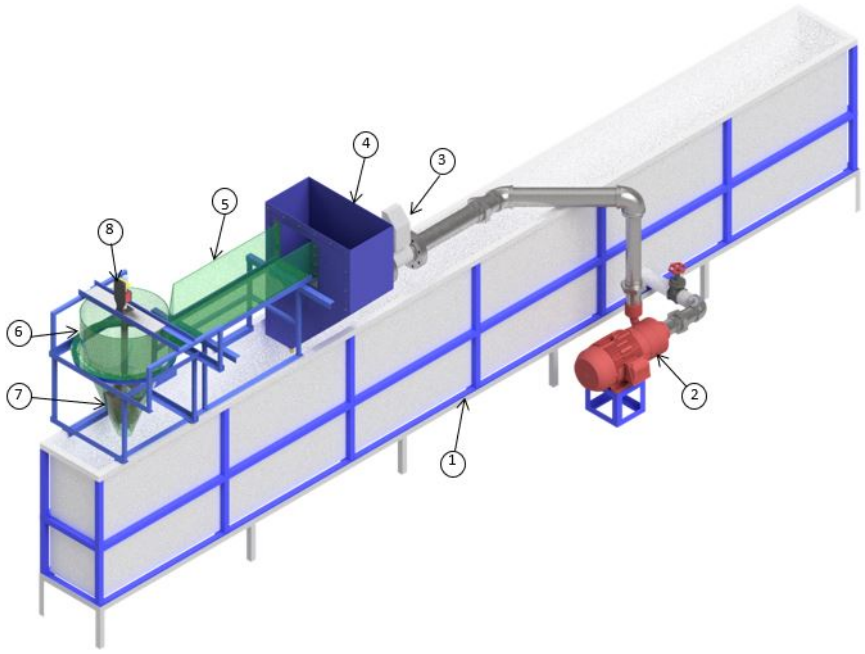

Fig. 8: Experimental setup. 1-Lower tank, 2-Centrifugal pump, 3-Flow meter, 4-Superior tank, 5-Inlet channel, 6-Basin, 7-Runner, and 8-Torque sensor.

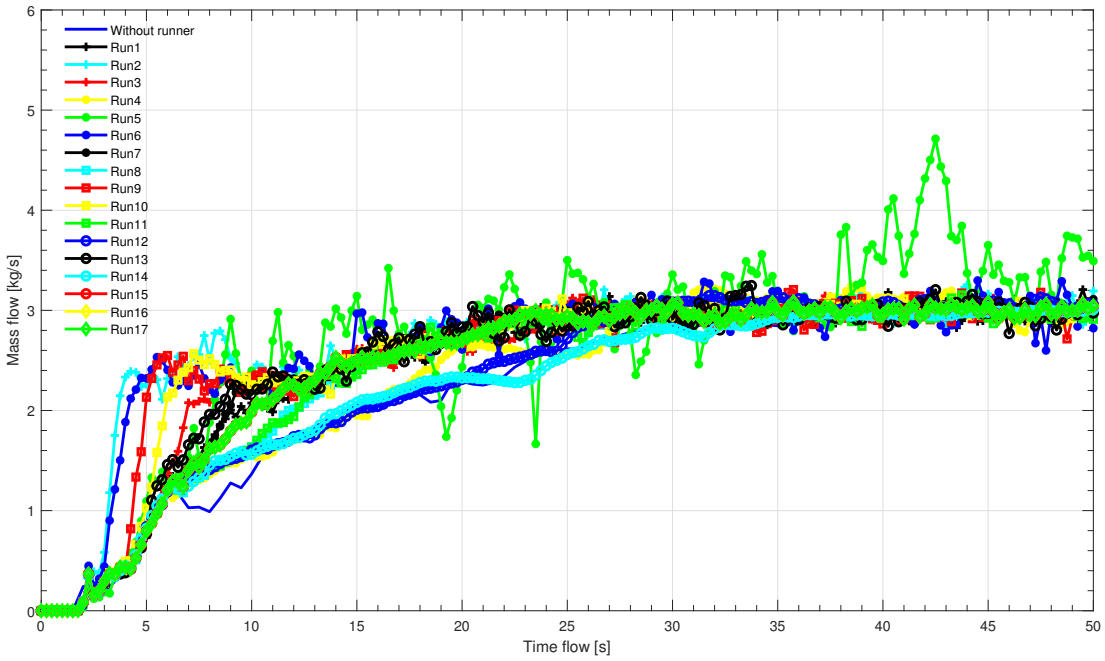

Fig. 9: Mass flow rate vs. time flow.

(D_b/D =0.37, n =4, p =0.6), with efficiencies of 52.09% and 44.20%, respectively. Therefore, the geometries with the highest efficiency are those whose p value is equal to 0.6, that is, the runners located closer to the discharge hole. The geometries with the lowest efficiencies, 0.34% and 0.59%, correspond to Runs 5 (D_b/D =0.29, n =6 and p =0.4) and 14 (D_b/D =0.29, n =2 and p =0.4), respectively, both geometries have the lowest D_b/D ratio, in addition to the

fact that they are runners located further from the discharge hole.

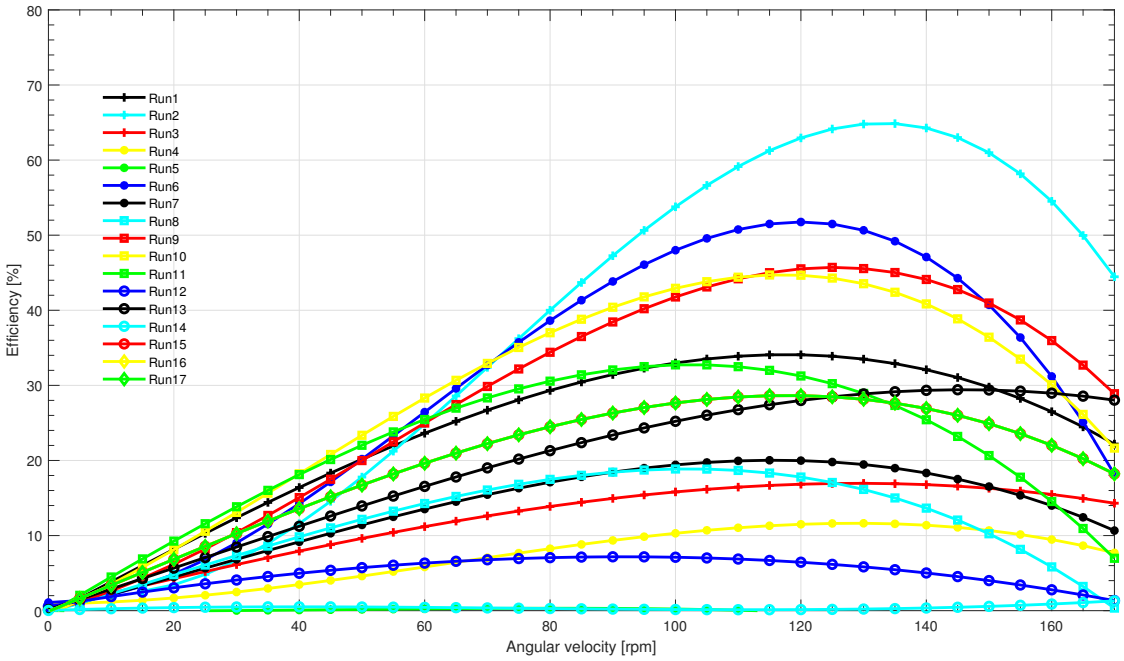

Fig. 10: Turbine performance curves: Efficiency vs. angular velocity. CFD data.

3.2. Statistical analysis

The statistical software package R-Studio was employed for the regression analysis of experimental data. The accuracy of the quadratic model equation was determined by the coefficient of R_2 and adjusted-R_2. The significant model terms were estimated by the probability value (P-value) at 95% (or 0.95) that corresponds to a significance level of 5% (or 0.05) [41]. The smaller P-value the more significant is the term [42]. The P-value for all terms of the quadratic model equation is given in Table 4. In addition, R_2 and adjusted-R_2 were calculated, and they are shown in Table 4. For a well-fitted model, R_2 and adjusted-R_2 should not be less than 80% (or 0.8) [50, 51]. For the model, R_2 and adjusted-R_2 were 98.71% and 97.06% respectively. The value of R_2 estimate how the model describes the data and the adjusted-R_2 measured the amount of variation about mean explained by the model.

From Table 4, the terms D_b/D, n, p, and $(D_b/D)(p)$ have the smallest P-value, which means these factors have the highest influence on the efficiency. Of these 4 terms, 3 terms correspond to the main factors while one of them is an interaction. The final quadratic model equation that describes the efficiency of a GWVHT is expressed by Eq. 6.

$$\begin{aligned}\eta = -0.9000781 - 0.548995 D_b/D - 0.055194 n + 2.514443 p + 0.675054 (D_b/D)^2 - 0.000041 (n)^2 \\ -2.503499 (p)^2 + 0.0930254 (D_b/D)(n) + 3.069728 (D_b/D)(p) \\ +0.092321 (n)(p)\end{aligned} \tag{6}$$

Before progressing with the analysis of the fitted model to find the optimal runner, the model assumptions should be checked. The model assumptions are residual independence, homoscedasticity, and normality [52]. Normal probability and frequency distribution were plotted to check the normality. Normality assumption is satisfied where data adjusted to the red represented lines in Figure 11. In addition, to check the normality assumption, numerical tests were performed. Numerical tests can help to ensure the assumption of normality. The results of the normality tests are shown in Table 5.

From Table 5, the efficiency residuals follow a normal distribution because the set of tests had a P-value higher than 0.05 [53, 54]. To verify residual independence and homoscedasticity, Durbin-Watson test, and studentized Breusch-

Table 4
ANOVA results.

Term	Degrees of freedom	Sum of squares	Mean squares	p-value	F-ratio
$D_b/D\ (x_1)$	1	0.2210	0.22100	1.07e-6	243.505
$n\ (x_2)$	1	0.02523	0.02523	0.00116	27.794
$p\ (x_3)$	1	0.23027	0.2307	9.33e-7	253.716
$(D_b/D)^2$	1	0.00031	0.00031	0.57888	0.3390
$(n)^2$	1	0.0023	0.0023	0.63198	0.251
$(p)^2$	1	0.00168	0.00168	0.21594	1.850
$(D_b/D)\times(n)$	1	0.00177	0.00177	0.20485	1.954
$(D_b/D)\times(p)$	1	0.00482	0.00482	0.05454	5.316
$(n)\times(p)$	1	0.00273	0.00273	0.12660	3.005
Residuals	7	0.00635	0.00091		
R_2		0.9871			
Adjusted-R_2		0.9706			

Table 5
Normality tests.

Test	P-value
Jarque-Bera test	0.622
D'Agostino & Pearson test	0.513
Shapiro-Wilk test	0.645
KS Lilliefors modification	0.200
Shapiro-Francia test	0.590
Cramer- von Mises test	0.524
Anderson-Darling test	0.575

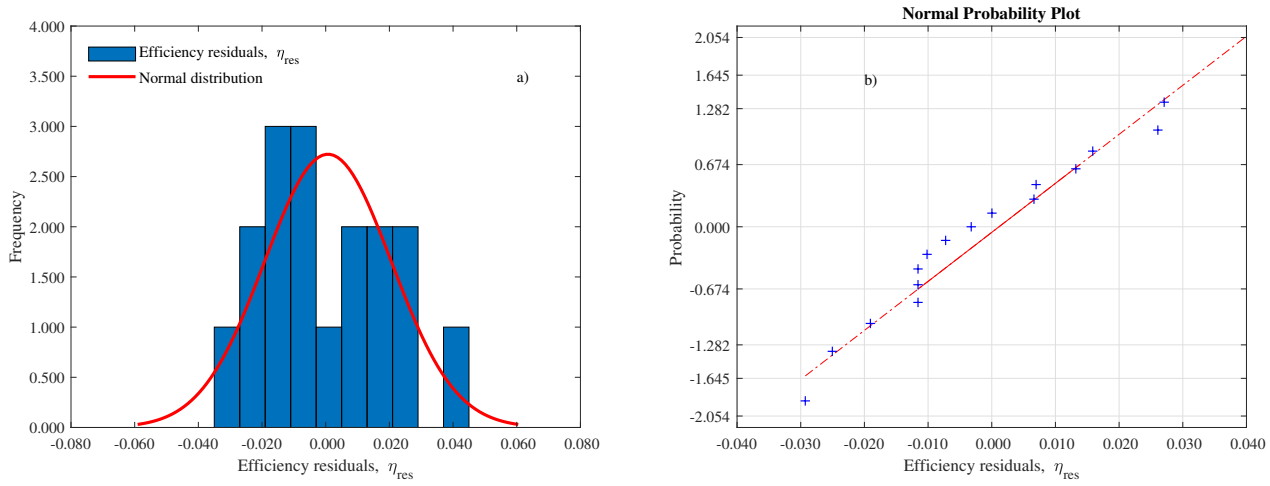

Fig. 11: a) Normal probability plot and b) Frequency distribution for the efficiency residuals.

Pagan step, respectively, were utilized. The tests returned P-values of 0.928 and 0.237, respectively. With a P-value greater than 0.05, the residuals are not autocorrelated and are not a dependency of the error variance. Therefore, the model is adequate for predicting the efficiency of GWVHT within the studied range. The response surfaces of the regression model for different interactions are shown as 2D contour plots in Figure 12. Figure 13 shows the individual effect of D_b/D, n and p on the efficiency.

From Figure 12, the highest efficiency is reached when all the independent variables are set to their highest values,

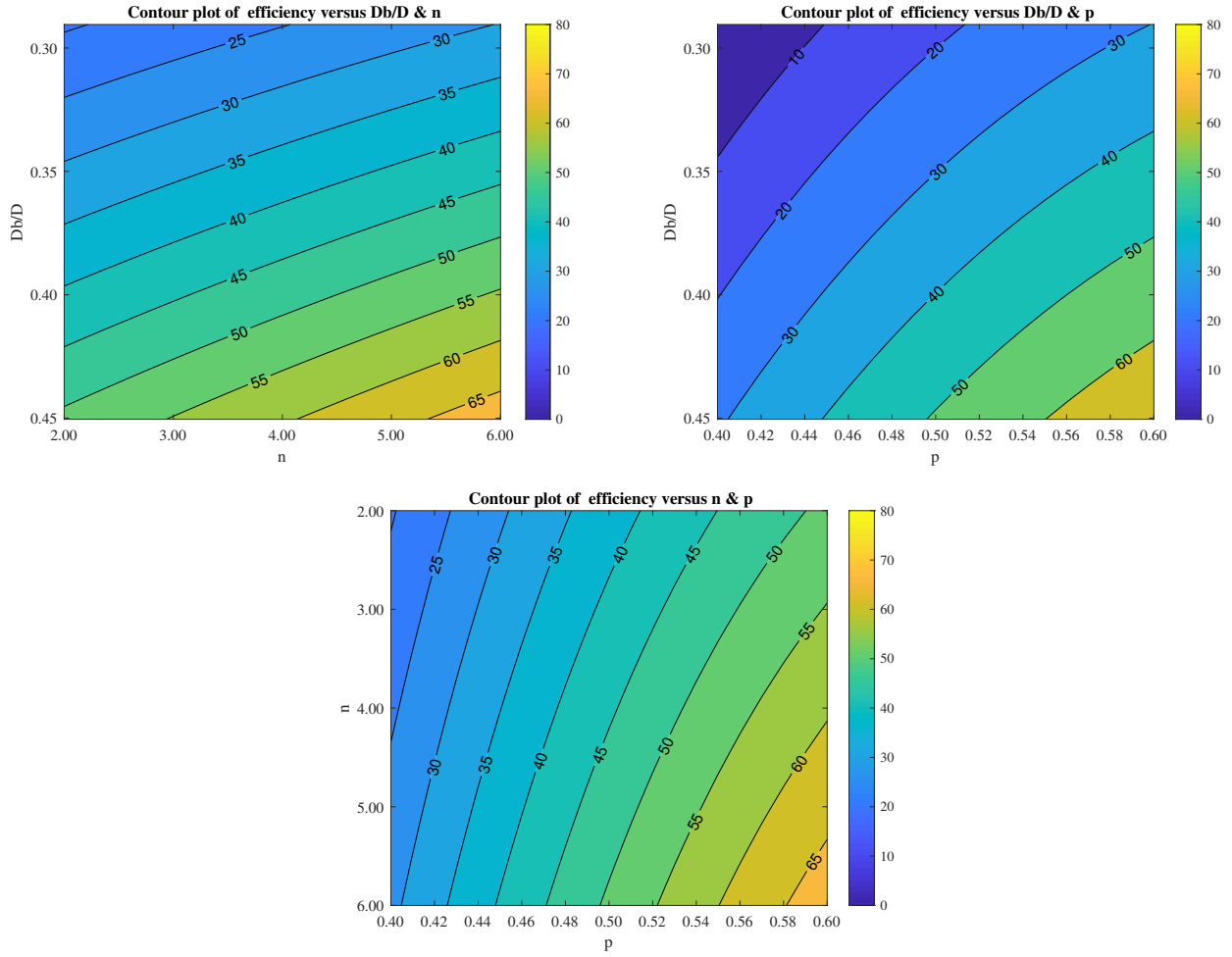

Fig. 12: Response surface contour plots for the efficiency (η). a) Interaction of D_b/D and n, b) Interaction of factors D_b/D and n, and c) Interaction of factors p and n.

i.e., $D_b/D = 0.45$, $n = 6$ and p =0.6. The efficiency was 65.18% which is in good concordance with the predicted response for the model (67.79%). According to Figure 14, the efficiency decreases with the decrease of p, while it increases with the increase of D_b/D. The increase in D_b/D means an increase in the area in contact of the blades with the vortex, which would allow a greater extraction of energy. The impact of blade number on efficiency is less clear; the increase in blade number, increase the blade area, however, the effect is not like the increase of D_b/D. There is a run with only two blades with a high efficiency (52.09%) and a run with six blades with the lower efficiency (0.34%). As an individual parameter, the optimum number of blades is not clear. The conclusion about n could vary depending on the type of runner installed in the basin.

The optimal runner found with the regression model is shown in Figure 14. To validate the mathematical model, a set of experiments was executed. For the experiments, the optimal runner was used (D_b/D =0.45, n =6), the position p of the runner within the cone was varied between 0.55 and 0.40. It was not possible to test the optimal condition with p =0.6, due to the final quality of the acrylic model, the runner collided with the walls of the cone.

3.3. Experimental results

Figures 15 and 16 show the vortex formation with and without runner. With runner, the formation of the vortex is shown for two angular velocities. When the runner is not present, the vortex height is easy to maintain. When the runner is inserted, the vortex height abruptly decreases, the vortex is distorted by the runner gaining power and decreasing the tangential velocity while increasing the axial velocity. The height of the vortex is also a function of the angular velocity, if the velocity decreases, the height of the vortex also decreases. When the applied load is zero, the turbine rotates at maximum angular velocity, Figure 16a; but, with an increase in the load, the angular velocity

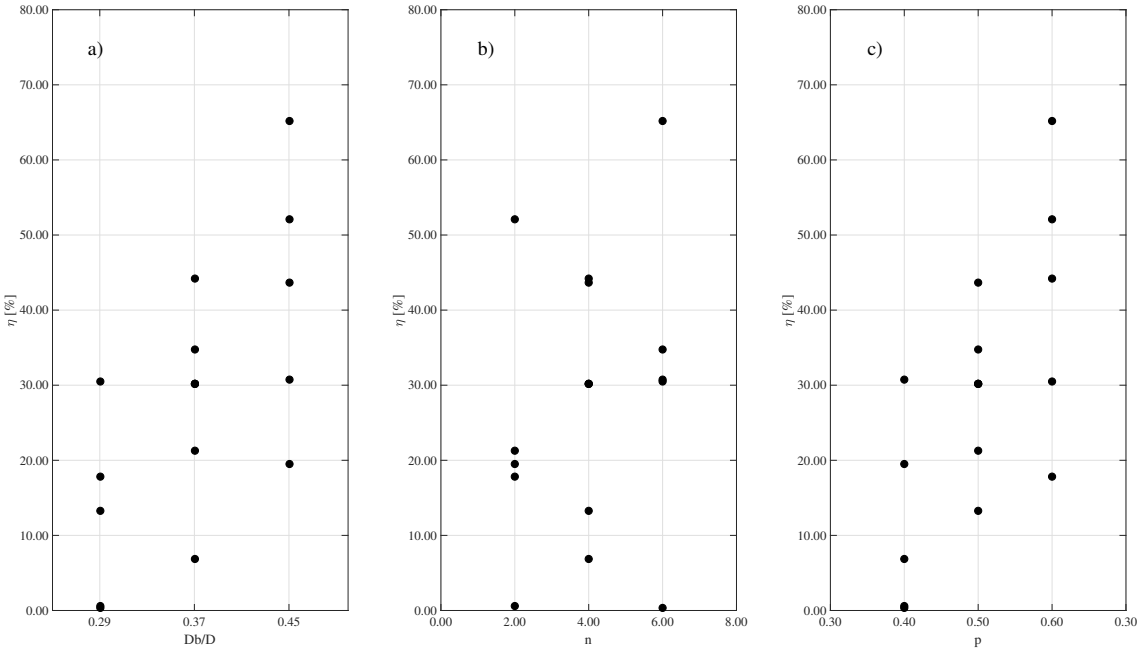

Fig. 13: Effect of a) D_b/D, b) n and c) p on the efficiency

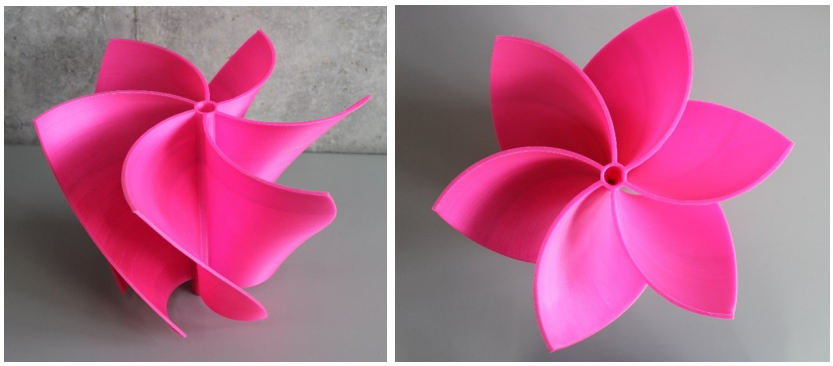

Fig. 14: Optimized runner.

decreases, it becomes zero at a certain value of load [20]

Figure 17 shows the measured efficiency of GWVHT across a range of angular velocity between 0 and 15 rad/s, for four conditions: I) D_b/D =0.45, n =6 and p =0.55, II) D_b/D =0.45, n =6 and p =0.50, III) D_b/D =0.45, n =6 and p =0.45, and IV) D_b/D =0.45, n =6 and p =0.40. These experimental efficiencies are I) 60.77%, II) 53.19%, III) 38.35%, and VI) 30.13%. Using the mathematical model, Eq. 6, the numerical efficiencies are: I) 59.99%, II) 50.80%, III) 40.46%, and VI) 28.84%. Comparing the numerical and experimental results, the numerical efficiencies have a difference of less than 3% with respect to the experimental results. The percentage of difference between the results is equal to the percentage of variation that the regression model has with adjusted-R_2 = 97%.06.

Along with the experimental results, Figure 17 also presents the curve of efficiency vs angular velocity for run 11 (D_b/D =, n =6, p =0.40). Of the 4 experimental tests carried out, only 1 of them, specifically test IV, coincide with one of the numerical models analyzed in Ansys Fluent (Table 3), therefore the only complete curve that can be compared is run 11 and test experimental IV.

As can be seen in Figure 17, despite reaching similar efficiencies, the angular velocity in the experimental tests is lower than the angular velocity achieved in the numerical study. The difference in the behaviour of the curves can

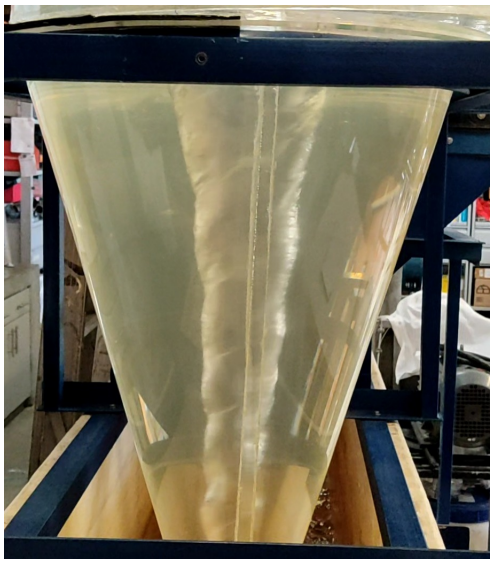

Fig. 15: Vortex formation without runner.

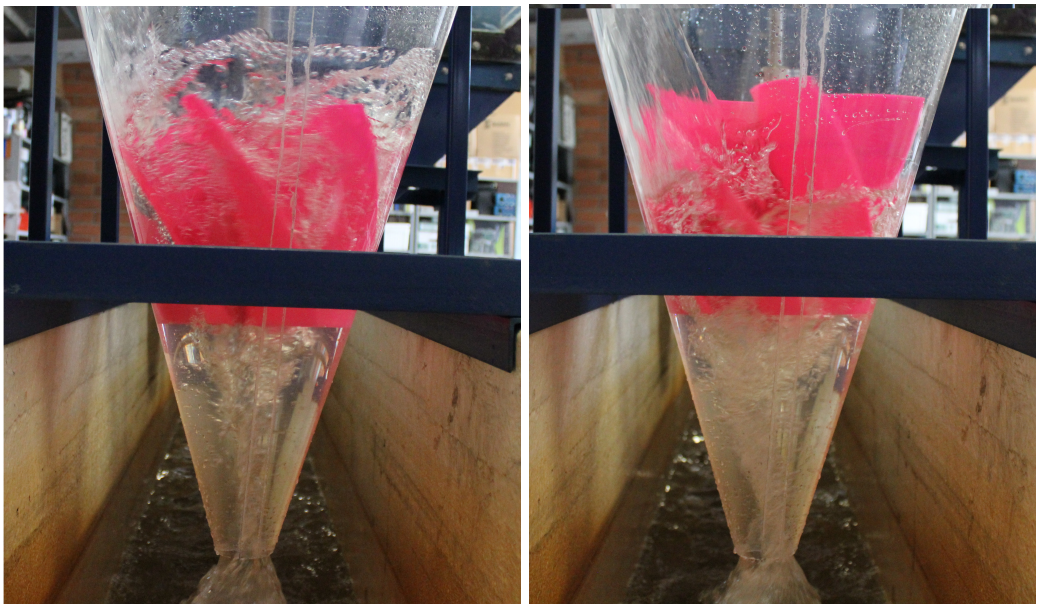

Fig. 16: Vortex formation with runner: a) 14.6 rad/s and b) 8.37 rad/s.

be attributed to the losses in the experimental bench, surface friction in the runner, and mechanical losses that are not accounted for the numerical models. Additionally, due to the way in which the acrylic components of the experimental bench (thermoforming) were constructed, it was not possible to guarantee that the measurements are exact to those reported in Figure 1. In the thermoforming process, an acrylic sheet is heated to a flexible forming temperature, then the sheet is given a specific shape in a mold, and finally, the sheet is cooled to obtain the desired final shape [55, 56, 57].

The experimental results therefore allow validating the numerical model for predicting the efficiency of a gravitational vortex turbine, Eq. 6. The efficiency is a function of the number of blades (n), the position of the rotor in the basin (p) and the ratio of the mean diameter of the runner and the diameter of the basin (D_b/D). The results obtained from this study could be used as a reference for the design of GWVHT.

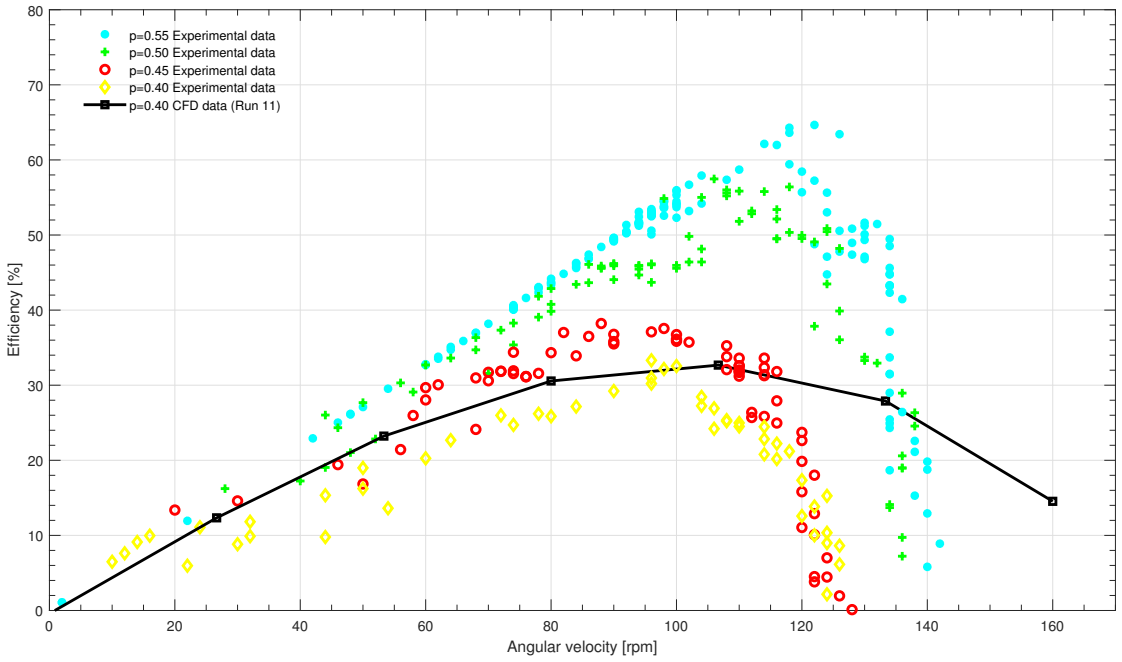

Fig. 17: Turbine performance curves: Efficiency vs. angular velocity. Experimental data.

4. Conclusions

Gravitational water vortex hydraulic turbine (GWVHT) is one of the interesting new hydro power plants because the requirements for their implementation are lower than those of conventional turbines. The electricity produced by this technology can be considered renewable and have slight negative environmental impacts associated. This study described the optimization and experimental validation of a runner for a GWVHT. A detailed performance evaluation of the turbine was executed, and the turbine performance curves were determined. The effect of the relative position of the runner (p), the number of blades (n), and the mean diameter of the blades (D_b) on the efficiency of the turbine has been investigated, and a second-order response model for the efficiency of the turbine was developed. This model allows predicting the efficiency of the turbine as a function of p, n, and D_b/D. Numerical analysis of 17 geometries shows that the maximum numerical efficiency was 65.18%. This was found with the largest value of all the independent variables (D_b/D =0.45, n =6 and p =0.6). An experimental bench was built to validate the numerical results and the second-order response model. The difference between numerical and experimental efficiency was acceptable and was mainly attributed to the losses in the experimental bench, surface friction in the runner, and mechanical losses that are not accounted for in the numerical models. The results found also indicate that it is not appropriate to optimize the rotor for this type of turbines considering a single parameter of its geometry, such as the number of blades or the diameter, because the conclusions are not general, and may change depending on the geometry studied. As the parameters used in the optimization process are dimensionless, the results can be scaled to build larger or smaller turbines.

References

[1] M. Bilgili, H. Bilirgen, A. Ozbek, F. Ekinci, T. Demirdelen, The role of hydropower installations for sustainable energy development in turkey and the world, Renewable Energy 126 (2018) 755–764.

[2] T. R. Jadoon, M. K. Ali, S. Hussain, A. Wasim, M. Jahanzaib, Sustaining power production in hydropower stations of developing countries, Sustainable Energy Technologies and Assessments 37 (2020) 100637.

[3] R. Siri, S. R. Mondal, S. Das, Hydropower: A renewable energy resource for sustainability in terms of climate change and environmental protection, Alternative Energy Resources (2020) 93–113.

[4] T. Ahmad, D. Zhang, A critical review of comparative global historical energy consumption and future demand: The story told so far, Energy Reports 6 (2020) 1973–1991.

[5] L. J. Sonter, M. C. Dade, J. E. Watson, R. K. Valenta, Renewable energy production will exacerbate mining threats to biodiversity, Nature communications 11 (2020) 1–6.
[6] R. Premkumar, R. Karthikeyan, S. Kumar, S. Jagadesh, et al., Regen electricity, Elementary Education Online 20 (2022) 4781–4781.
[7] A. Kuriqi, A. N. Pinheiro, A. Sordo-Ward, M. D. Bejarano, L. Garrote, Ecological impacts of run-of-river hydropower plants—current status and future prospects on the brink of energy transition, Renewable and Sustainable Energy Reviews 142 (2021) 110833.
[8] M. Kumar, Social, economic, and environmental impacts of renewable energy resources, Wind solar hybrid renewable energy system 1 (2020).
[9] T. B. Couto, J. D. Olden, Global proliferation of small hydropower plants–science and policy, Frontiers in Ecology and the Environment 16 (2018) 91–100.
[10] W. Uddin, K. Zeb, A. Haider, B. Khan, S. ul Islam, M. Ishfaq, I. Khan, M. Adil, H. J. Kim, et al., Current and future prospects of small hydro power in pakistan: A survey, Energy Strategy Reviews 24 (2019) 166–177.
[11] M. N. Ali, A. J. Nahian, A. H. Siddique, M. Hasan, N. Chowdhury, C. A. Hossain, Prospect of mini-hydel power generation in drainage systems of bangladesh, in: 2021 2nd International Conference on Robotics, Electrical and Signal Processing Techniques (ICREST), IEEE, 2021, pp. 278–281.
[12] S. Hoseinzadeh, M. H. Ghasemi, S. Heyns, Application of hybrid systems in solution of low power generation at hot seasons for micro hydro systems, Renewable Energy 160 (2020) 323–332.
[13] Y. Itani, M. R. Soliman, M. Kahil, Recovering energy by hydro-turbines application in water transmission pipelines: A case study west of saudi arabia, Energy 211 (2020) 118613.
[14] R. K. Karre, K. Srinivas, K. Mannan, B. Prashanth, C. R. Prasad, A review on hydro power plants and turbines, in: AIP Conference Proceedings, volume 2418, AIP Publishing LLC, 2022, p. 030048.
[15] M. Rahman, J. Tan, M. Fadzlita, A. W. K. Muzammil, A review on the development of gravitational water vortex power plant as alternative renewable energy resources, in: IOP Conference Series: Materials Science and Engineering, volume 217, IOP Publishing, 2017, p. 012007.
[16] T. C. Kueh, S. L. Beh, D. Rilling, Y. Ooi, Numerical analysis of water vortex formation for the water vortex power plant, International Journal of Innovation, Management and Technology 5 (2014) 111.
[17] A. B. Timilsina, S. Mulligan, T. R. Bajracharya, Water vortex hydropower technology: a state-of-the-art review of developmental trends, Clean Technologies and Environmental Policy 20 (2018) 1737–1760.
[18] D. S. Edirisinghe, H.-S. Yang, S. Gunawardane, Y.-H. Lee, Enhancing the performance of gravitational water vortex turbine by flow simulation analysis, Renewable Energy (2022).
[19] T. C. Kueh, S. Beh, Y. Ooi, D. Rilling, Experimental study to the influences of rotational speed and blade shape on water vortex turbine performance, in: Journal of Physics: Conference Series, volume 822, IOP Publishing, 2017, p. 012066.
[20] A. S. Saleem, T. A. Cheema, R. Ullah, S. M. Ahmad, J. A. Chattha, B. Akbar, C. W. Park, Parametric study of single-stage gravitational water vortex turbine with cylindrical basin, Energy 200 (2020) 117464.
[21] R. Ullah, T. A. Cheema, A. S. Saleem, S. M. Ahmad, J. A. Chattha, C. W. Park, Performance analysis of multi-stage gravitational water vortex turbine, Energy Conversion and Management 198 (2019) 111788.
[22] T. R. Bajracharya, S. R. Shakya, A. B. Timilsina, J. Dhakal, S. Neupane, A. Gautam, A. Sapkota, Effects of geometrical parameters in gravitational water vortex turbines with conical basin, Journal of Renewable Energy 2020 (2020).
[23] S. Acharya, S. K. Ghimire, H. B. Dura, Design study of runner for gravitational water vortex power plant with conical basin, in: Proceedings of IOE Graduate Conference, 2019.
[24] O. Yaakob, Y. M. Ahmed, A. Elbatran, H. Shabara, A review on micro hydro gravitational vortex power and turbine systems, Jurnal teknologi 69 (2014).
[25] C. Power, A. McNabola, P. Coughlan, A parametric experimental investigation of the operating conditions of gravitational vortex hydropower (gvhp), Journal of Clean Energy Technologies 4 (2016) 112–119.
[26] S. Dhakal, A. B. Timilsina, R. Dhakal, D. Fuyal, T. R. Bajracharya, H. P. Pandit, N. Amatya, Mathematical modeling, design optimization and experimental verification of conical basin: Gravitational water vortex power plant, in: dalam World Largest Hydro Conference, 2015.
[27] S. Dhakal, A. B. Timilsina, R. Dhakal, D. Fuyal, T. R. Bajracharya, H. P. Pandit, N. Amatya, A. M. Nakarmi, Comparison of cylindrical and conical basins with optimum position of runner: Gravitational water vortex power plant, Renewable and Sustainable Energy Reviews 48 (2015) 662–669.
[28] R. Ullah, T. A. Cheema, A. S. Saleem, S. M. Ahmad, J. A. Chattha, C. W. Park, Preliminary experimental study on multi-stage gravitational water vortex turbine in a conical basin, Renewable Energy 145 (2020) 2516–2529.
[29] R. Dhakal, T. Bajracharya, S. Shakya, B. Kumal, N. Kathmandu, K. Khanal, N. Kavre, S. Williamson, S. Gautam, D. Ghale, Computational and experimental investigation of runner for gravitational water vortex power plant, in: Proceedings of a meeting held, volume 5, 2017, p. 8.
[30] L. Velásquez, A. Posada, E. Chica, Multi-objective optimization of a gravitational water vortex hydraulic turbine, Applied Energy – (2022) –.
[31] A. Gautam, A. Sapkota, S. Neupane, J. Dhakal, A. B. Timilsina, S. Shakya, Study on effect of adding booster runner in conical basin: gravitational water vortex power plant: a numerical and experimental approach, in: Proceedings of IOE graduate conference, 2016, pp. 107–113.
[32] S. Wanchat, R. Suntivarakorn, S. Wanchat, K. Tonmit, P. Kayanyiem, A parametric study of a gravitation vortex power plant, in: Advanced Materials Research, volume 805, Trans Tech Publ, 2013, pp. 811–817.
[33] M. Rahman, T. J. Hong, R. Tang, L. L. Sung, F. B. M. Tamiri, Experimental study the effects of water pressure and turbine blade lengths & numbers on the model free vortex power generation system, International Journal of Current Trends in Engineering & Research (IJCTER) 2 (2016) 13–17.
[34] A. Venukumar, M. Nandakumar, M. Venkateswara Rao, M. Shekhar Kumar, Run-of-the-river micro hydroelectric power generation from artificially induced vortices, Power Research 11 (2015) 741–750.
[35] I.-H. Choi, J.-W. Kim, G.-S. Chung, Experimental study of micro hydropower with vortex generation at lower head water, Journal of Wetlands

Research 22 (2020) 121–129.
[36] N. H. Khan, T. A. Cheema, J. A. Chattha, C. W. Park, Effective basin–blade configurations of a gravitational water vortex turbine for micro-hydropower generation, Journal of Energy Engineering 144 (2018) 04018042.
[37] Y. Nishi, T. Inagaki, Performance and flow field of a gravitation vortex type water turbine, International Journal of Rotating Machinery 2017 (2017).
[38] P. Sritram, R. Suntivarakorn, Comparative study of small hydropower turbine efficiency at low head water, Energy Procedia 138 (2017) 646–650.
[39] P. Wichian, R. Suntivarakorn, The effects of turbine baffle plates on the efficiency of water free vortex turbines, Energy Procedia 100 (2016) 198–202.
[40] H. Shabara, O. Yaakob, Y. M. Ahmed, A. Elbatran, M. S. Faddir, Cfd validation for efficient gravitational vortex pool system, Jurnal Teknologi 74 (2015).
[41] P. Sritram, W. Treedet, R. Suntivarakorn, Effect of turbine materials on power generation efficiency from free water vortex hydro power plant, in: IOP Conference Series: Materials Science and Engineering, volume 103, IOP Publishing, 2015, p. 012018.
[42] E. M. Wardhana, A. Santoso, A. R. Ramdani, Analysis of gottingen 428 airfoil turbine propeller design with computational fluid dynamics method on gravitational water vortex power plant, International Journal of Marine Engineering Innovation and Research 3 (2019).
[43] S. K. Behera, H. Meena, S. Chakraborty, B. Meikap, Application of response surface methodology (rsm) for optimization of leaching parameters for ash reduction from low-grade coal, International Journal of Mining Science and Technology 28 (2018) 621–629.
[44] S. Karimifard, M. R. A. Moghaddam, Application of response surface methodology in physicochemical removal of dyes from wastewater: a critical review, Science of the Total Environment 640 (2018) 772–797.
[45] A. Azizi, A. Dargahi, A. Almasi, Biological removal of diazinon in a moving bed biofilm reactor–process optimization with central composite design, Toxin Reviews 40 (2021) 1242–1252.
[46] B. S. Mohammed, V. C. Khed, M. F. Nuruddin, Rubbercrete mixture optimization using response surface methodology, Journal of Cleaner Production 171 (2018) 1605–1621.
[47] T. M. Laid, K. Abdelhamid, L. S. Eddine, B. Abderrhmane, Optimizing the biosynthesis parameters of iron oxide nanoparticles using central composite design, Journal of Molecular Structure 1229 (2021) 129497.
[48] L. Velásquez, A. Posada, E. Chica, Optimization of the basin and inlet channel of a gravitational water vortex hydraulic turbine using the response surface methodology, Renewable Energy 187 (2022) 508–521.
[49] N. Baker, G. Kelly, P. D. O'Sullivan, A grid convergence index study of mesh style effect on the accuracy of the numerical results for an indoor airflow profile, International Journal of Ventilation (????).
[50] A. Ash, M. Shwartz, R2: a useful measure of model performance when predicting a dichotomous outcome, Statistics in medicine 18 (1999) 375–384.
[51] D. C. Montgomery, G. C. Runger, N. F. Hubele, Engineering statistics, John Wiley & Sons, 2009.
[52] M. Bouvant, J. Betancour, L. Velásquez, A. Rubio-Clemente, E. Chica, Design optimization of an archimedes screw turbine for hydrokinetic applications using the response surface methodology, Renewable Energy 172 (2021) 941–954.
[53] M. J. Schuemie, P. B. Ryan, W. DuMouchel, M. A. Suchard, D. Madigan, Interpreting observational studies: why empirical calibration is needed to correct p-values, Statistics in medicine 33 (2014) 209–218.
[54] E. C. Alexopoulos, Introduction to multivariate regression analysis, Hippokratia 14 (2010) 23.
[55] J. L. Throne, Understanding thermoforming, Hanser Gardner Publications Cincinnati, 2008.
[56] P. Klein, Fundamentals of plastics thermoforming, Synthesis Lectures on Materials and Optics 10 (2009) 1–97.
[57] J. Throne, Thermoforming, in: Applied Plastics Engineering Handbook, Elsevier, 2011, pp. 333–358.

CHAPTER 6

TURBULENCE MODELS

CFD analysis of a gravitational water vortex hydraulic turbine by using k-ϵ and k-ω turbulence models

Submitted article

Highlights

- A hydraulic turbine is the most critical element of any hydro power project.
- CFD analysis is the most promising approach for hydraulic design of the turbine.
- standard k-ϵ, Renormalization Group (RNG) k-ϵ, shear stress transport (SST) k-ω, and standard k-ω turbulence models were used to simulate a gravitational water vortex hydraulic turbine.
- An analysis of variance (ANOVA) and a least significant difference (LSD) test were made to compare the results between turbulence models.

CFD analysis of a gravitational water vortex hydraulic turbine by using k-ϵ and k-ω turbulence models

Laura Velásquez, Alejandro Posada, Ainhoa Rubio-Clemente and Edwin Chica

ABSTRACT

This work compares the suitability of standard k-ϵ, Renormalization Group (RNG) k-ϵ, shear stress transport (SST) k-ω, and standard k-ω turbulence models when simulating a gravitational water vortex hydraulic turbine. These models are incorporated in ANSYS Fluent. The performance of the models was compared for the first time by using the same turbine geometry and boundary conditions. The results indicated that the four turbulence models are able to predict a similar behaviour for the mass flow rate but not for the vortex circulation. To identify which models were different, or which caused the difference, an analysis of variance (ANOVA) and a least significant difference (LSD) test were made. ANOVA and LSD test indicated the turbulence model influenced the vortex circulation, being the behaviour for the vortex circulation significantly different in the four models used. The final selection of the turbulence model depends on the computational resources, the time available and the required level of accuracy.

1. Introduction

Humankind requires energy services to satisfy basic needs (lighting, cooking, education quality, mobility, communication and comfort) and attend the production processes. The demand for this energy is increasing due to exponential population growth and economic development, especially in emerging market economies. By the year 2040, world energy needs are projected to be increased by 30%, while the population expands from 7,400 to 9,000 million [1]. This is the reason why the world must be prepared to meet this future energy demand in a sustainable way. It must be highlighted that global energy consumption grew with an average of 2%/year over 2000-2018 and slowdown 0.8% in 2019 [2].

Among the sources of energy with the highest current use, fossil fuels, including coal, oil and natural gas, stand out with 62.8% [3]. A fundamental characteristic of these non-renewable fuels (resources available in amounts that can be considered relatively abundant but finite) is the energy produced, which is due to the combustion of the carbon (C) contained, so their use consumes C, oxygen (O_2) from the atmosphere, and releases carbon dioxide (CO_2) and energy (exothermic reaction). Since the C contained in these fuels is sequestered in the reservoirs, the CO_2 released increases its concentration in the atmosphere. It is important to note that CO_2 is a greenhouse gas that allows the passage of short-wave radiation from the sun and retains the infrared radiation emitted by the Earth [4]. That is, it retains the heat that would otherwise escape into space, causing an increase in the temperature of the planet. The increase in the temperature produces direct effects on ecosystems, constituting a considerable risk to biodiversity, natural resources and human, animal and plant health [5].

On the other hand, the remaining 37.2% comes from renewable sources [3]. The potential of renewable energy (RE) sources is infinite. RE sources come from the energy that reaches the planet continuously as a consequence of the gravitational attraction of other planets and satellites of the solar system, as well as the solar radiation. The main sources are solar, wind, hydraulic, tidal, geothermal and biomass energy. These types of sources have a particular characteristic related to the variability of their generation. This variability is a reflection of the behavior of its primary source, such as the solar radiation and wind, which depend on the climatic, meteorological, and hydrological phenomena of each moment [6].

Given the availability of at least one of the RE sources in any geographical position on the Earth, RE sources represent immense energy potentials to be used. Among the alternatives to produce energy from renewable sources, the use of energy from water is named. However, the novelty of taking profit from water energy is the design characteristics of new turbines that allow them to be installed in places where conventional turbines (e.g., Pelton, Kaplan and Francis

ORCID(s): 0000-0003-1483-0104 (L. Velásquez); 0000-0001-5836-0680 (A. Posada); 0000-0003-1527-260X (A. Rubio-Clemente); 0000-0002-5043-6414 (E. Chica)

turbines) cannot be operated. The gravitational water vortex hydraulic turbine (GWVHT) is one of those new designs. GWVHT is an appropriate turbine to be implemented in a hydraulic resource from small to medium water flow rates and low head. GWVHT uses a co-axial runner with a vertical axis to extract energy from an induced vortex. The vortex is generated in the basin. GWVHT is a micro hydropower plant, whose maximum reported power is less than 0.1 MW [7]. To date, the world has installed 15 vortex turbines with a maximum capacity of 20 kW. These plants report efficiency between 17 and 85% [7].

The investigation and development of GWVHTs are limited. The literature review shows that researchers have been focused on increasing the efficiency of the turbine through numerical [8, 9, 10] and experimental studies [11, 12, 13] . In numerical studies, computational fluid dynamics (CFD) models become convenient to predict the behavior of the flow inside the turbine. CFD simulations use different turbulence models to solve the turbulent part of the flow.

Under this scenario, the current work is focused on the selection of the turbulence model to predict the behavior of the free-surface vortex in a gravitational water vortex hydraulic turbine. In this regard, k-ω and k-ϵ turbulence models were used. From the authors' knowledge, the performance of these models has not been compared by utilizing the same boundary conditions in the same turbine geometry. The turbulence models were compared by using the numerical results of the vortex circulation and the mass flow rate.

2. Methods and materials

2.1. Gravitational water vortex hydraulic turbine (GWVHT)

A power generation system with a GWVHT is a run-of-river plant, so that water energy must be used as soon as it is available to drive the turbine. The run-of-river plants do not have a water reservoir. The flow supplied varies according to the seasons of the year. In the season of abundant rainfall, they develop their maximum power and allow an excess water to pass through. In contrast, during the dry season, the power decreases depending on the flow, becoming almost zero in some rivers in the summertime.

The GWVHT is considered a new technology that was created by the Austrian engineer Frank Zotlöterer around 2006 [7]. GWVHT consists of a channeled water inlet into a cylindrical or conical basin. The transfer of energy from water to the turbine runner is due to the vortex created on the basin. The flow is regulated by the discharge hole at the bottom of the basin. The vortex causes the flow rotation to speed up and, in turn, causes the pressure in the center of the vortex to decrease [14]. The pressure reduces below the atmospheric pressure. As a consequence of the low pressure, the air is sucked into the basin forming an air core. The rotational movement or circulation in vortices may be studied by employing CFD. An adequate selection of simulation parameters, such as turbulence models, is necessary to reliably predict the behavior of the vortex inside the turbine. The selected geometry for the comparison of the turbulence models is shown in in Fig. 1. In this work, the geometry employed was a turbine with a conical basin and a wrap-around inlet channel. Six variables were used to define the turbine geometry. The variables were dimensionless since they were expressed in terms of the diameter (D) of the basin, being D equal to 500 mm. The runner was excluded from the analysis.

2.2. Vortex circulation and mas flow rate

The turbulence models were compared through the behavior of the mass flow rate ($\dot{m}$) and the vortex circulation (Γ) from the beginning to the stabilization of the vortex. The circulation is a measure of the rotation of the fluid. Γ is defined as the line integral, which was evaluated along a curve C, of the component of the velocity that is tangent to C [15]. Thus, for a curve in the horizontal plane, the circulation is given by Eq. 1:

$$\Gamma = \oint_C \vec{v} \cdot d\vec{l} \tag{1}$$

where $\vec{v}$ corresponds to the velocity around C and $d\vec{l}$ is a vector representing the differential length of C. By using Stokes' theorem, circulation can be written like a surface integral curve [16], as expressed in Eq. 2:

$$\Gamma = \oint_S \vec{\omega} \cdot dS \tag{2}$$

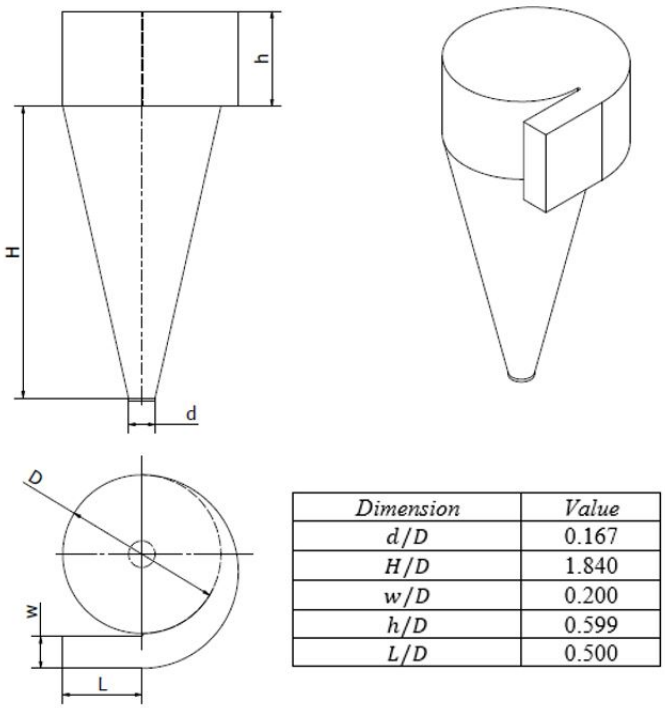

Dimension	Value
d/D	0.167
H/D	1.840
w/D	0.200
h/D	0.599
L/D	0.500

Fig. 1: Dimensions of the gravitational vortex turbine with a conical basin and a wrap-around inlet channel.

where the vorticity ($\vec{\omega}$) of the fluid is defined as expressed in Eq. 3: (Cengel, 2010):

$$\vec{\omega} = \nabla \times \vec{v} \tag{3}$$

The term $\dot{m}$ is the mass of fluid passing per unit of time through the discharge hole. It is defined by Eq. 4. This parameter can also be calculated by 5 [17]:

$$\dot{m} = \frac{dm}{dt} \tag{4}$$

$$\dot{m} = \rho Q = \rho A V \tag{5}$$

where A is the area of the discharge hole, V refers to the velocity of the fluid, and ρ stands for the density of the fluid.

$\dot{m}$ was selected as one of the analysis variables since its final value was known before performing the simulations. The vortex circulation was selected because it is directly related to the hydrodynamic forces [18]. The hydrodynamic forces generate a moment ($v\vec{M}$) about a specific point or axis. This moment will move the turbine runner.

2.3. Numerical simulation

2.3.1. Computational domain and meshing

By using ANSYS Fluent, a numerical simulation of the GWVHT was executed. The mesh was created in Fluent meshing solver. The domain was composed of two parts: the inlet channel and the conical basin. Both parts were meshed by using poly-hex core mesh elements. This type of element allows a reduction from 20 to 50% in the total number of elements compared to the conventional hexcore mesh [19]. The mesh used in the simulations is presented in Fig. 2.

Transition-state and volume of fluid (VoF) were chosen to perform the simulations. The VoF method allows capturing the interface between air and water. These fluids cohabit inside the turbine. Transition-state enables to observe

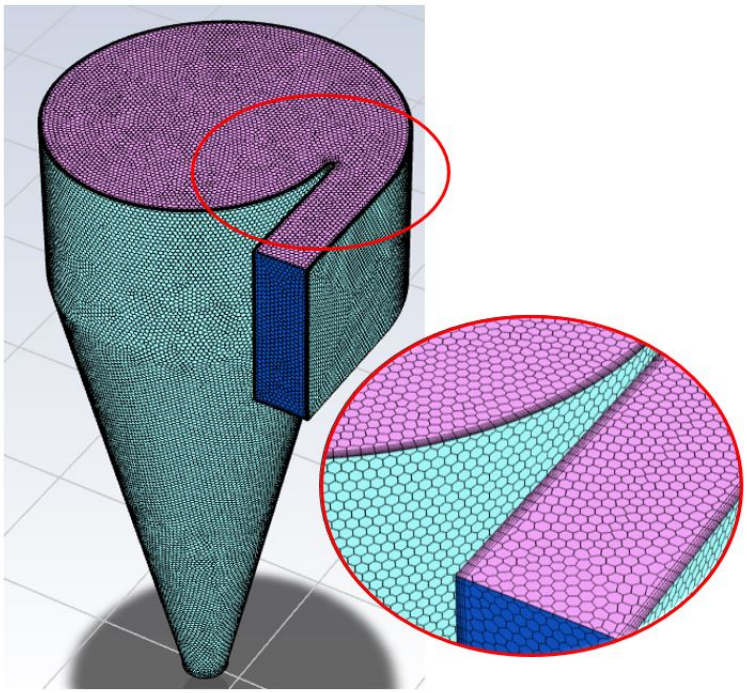

Fig. 2: Hexcore Mesh.

the changes in the vortex, from the beginning of the formation to its stability. It was imposed as an initial condition that the turbine was composed only of air. Gravity was considered in the analysis.

The Unsteady Reynolds-averaged Navier-Stokes (URANS) equations were solved by employing the coupled scheme for pressure-velocity and the second-order upwind discretization. As boundary conditions, an inlet velocity of 0.169 m/s was established at the inlet channel, and a relative pressure of 0 Pa was imposed at the discharge hole. The air could exit and enter freely through the upper surfaces of the channel and the basin. The turbulence models used are discussed in Section 2.3.2.

An independence test for the mesh and the time-step (Δt) were performed. The test allowed the selection of the most appropriate mesh and time-step to guarantee good result accuracy and low computational costs. The grid convergence index (GCI) was the method used to define the optimal values for these parameters. GCI is founded on the Richardson extrapolation, in which an estimation of the exact solution can be provided [20, 21]. The GCI indicates how far the numerical solution is from the asymptotic range and how much the numerical solution changes with further refinement. If the value of GCI is close to 1.0, the solution is within the asymptotic range of convergence [22]. Element numbers used for the mesh independence were 435,116 (fine mesh, expressed by number 3), 330,238 (medium mesh, expressed by number 2) and 211,158 (coarse mesh, expressed by number 1). The Δt values used for the test were 0.05, 0.1 and 0.2 s. The control variable used in these independence tests was the circulation. Table 1 presents the results for independence tests. The values of GCI_{23} and GCI_{12} represent the relative change from the coarse to medium mesh/time step and from the medium to fine mesh/time step, respectively.

According to Table 1, with a GCI of 1.006 and 0.999, for the mesh and Δt, respectively, the solution is within the asymptotic range of convergence. In this regard, the medium time-step of Δt=0.1 s and the medium mesh were selected for the analysis in order to minimize the computational time and the errors.

2.3.2. Turbulence model

CFD simulations employ turbulence models to predict the statistical evolution of turbulent flows [23]. The turbulence models commonly used in modern engineering applications, specifically for vortex turbines, are the k-ϵ and k-γ turbulence models [24, 25, 26, 10, 27, 28, 29]. The selection of the turbulence model depends on the physics involved in the flow, the computational resources available, the level of precision required and the amount of time available for the simulation.

Table 1
Grid convergence index (GCI). Coarse, medium and fine meshes are expressed as 1, 2 and 3, respectively.

	Mesh type and GCI	Number of elements	Δt [s]
1	Coarse	211,158	0.2
2	Medium	330,238	0.1
3	Fine	435,116	0.05
	GCI_{12} [%]	1.59	0.008
	GCI_{23} [%]	0.84	0.006
	GCI	1.006	0.999

The k-ϵ model uses two equations to solve the dissipation ϵ and the turbulent kinetic energy k. k and ϵ are obtained from Eqs. 6 and 7 [30]:

$$\frac{d}{dt}(\rho k) + \frac{d}{dx_i}(\rho k u_i) = \frac{d}{dx_j}\left[\left(\mu + \frac{\mu_t}{\sigma_k}\right)\frac{dk}{dx_j}\right] + G_k + G_b - \rho\epsilon - Y_M + S_k \tag{6}$$

$$\frac{d}{dt}(\rho \epsilon) + \frac{d}{dx_i}(\rho \epsilon u_i) = \frac{d}{dx_j}\left[\left(\mu + \frac{\mu_t}{\sigma_\epsilon}\right)\frac{d\epsilon}{dx_j}\right] + C_{1\epsilon}\frac{\epsilon}{k}(G_k + C_{3\epsilon}G_b) - C_{2\epsilon}\rho\frac{\epsilon^2}{k} + S_\epsilon \tag{7}$$

In Eqs. 6 and 7, $C1_\epsilon$, $C2_\epsilon$ and $C3_\epsilon$ are constant values. G_b is the generation of k because of buoyancy. In turn, G_k refers to the generation of k due to the velocity gradients, and Y_M stands for the contribution of the fluctuating dilatation compressible turbulence to the overall dissipation rate. S_k and S_ϵ refer to the user-defined terms. σ_ϵ and σ_k stand for the turbulent Prandtl numbers for ϵ and k, respectively. μ_t is the turbulence viscosity and it is calculated as expressed in Eq. 8 [31], where C_μ is a constant.

$$\mu_t = \rho C_\mu \frac{k^2}{\epsilon} \tag{8}$$

In the k-ϵ model, which is available in ANSYS Fluent, the constants and their values by default are $C1_\epsilon$, $C2_\epsilon$, $C3_\epsilon$, C_μ, σ_k, and σ_ϵ of 1.44, 1.92, 0.09, 1.0 and 1.3, respectively.

The k-ϵ model has been widely selected in the study of vortex turbines since it is a general-purpose model that allows a first approach to the vortex phenomenon [32]. Additionally, the k-ϵ model is easy to be implemented, has low memory requirements and a fast convergence. It is suitable for incompressible, compressible and external flow interactions with complex geometries. However, it is not an accurate model for jets and adverse pressure gradients [33]. The k-ω model is also a two-equation model. This model solves for the specific dissipation rate ω and the turbulence kinetic energy k. The values related to ω and k are obtained from Eqs. 9 and 10 [30].

$$\frac{d}{dt}(\rho k) + \frac{d}{dx_i}(\rho k u_i) = \frac{d}{dx_j}\left[\Gamma_k \frac{d_k}{dx_j}\right] + G_k - Y_k + S_k \tag{9}$$

$$\frac{d}{dt}(\rho \omega) + \frac{d}{dx_i}(\rho \omega u_i) = \frac{d}{dx_j}\left[\Gamma_\omega \frac{d_\omega}{dx_j}\right] + G_\omega - Y_\omega + S_\omega \tag{10}$$

In Eqs. 9 and 10, S_k and S_ω are user-defined source terms. G_ω is the generation of ω and G_k is the generation of turbulence kinetic energy associated with velocity gradients. Γ_k and Γ_ω are the effective diffusivity of k and ω, respectively. In turn, Y_ω and Y_k are the dissipation of ω and k due to turbulence, respectively.

In the k-ω model, also available in ANSYS Fluent, the constants and their values by default are α^*_∞, α_∞, α_0, β^*_{inf}, β_i, R_β, R_k, R_ω, ζ^*, M_{t0}, σ_k and σ_ω of 1.00, 0.52, 0.11, 0.09, 0.072, 8.00, 6.00, 2.95, 1.5, 0.25, 2.00 and 2.00, respectively.

The k-ω model is quite sensitive to initial conditions and, therefore, it is often used in combination with the k-ϵ model to perform initial iterations [34]. It is a suitable model for adverse pressure gradients, jets and the boundary layer [35]. Nevertheless, the convergence time is longer and requires more memory. Selecting the most suitable turbulence model is not enough to guarantee that the results of the simulations are reliable. As previously shown, within these turbulence models, there are constants whose values can be changed by the user. There are different types of k-ϵ and k-ω turbulence models, among which Renormalization Group (RNG) k-ϵ, standard k-ω, standard k-ϵ, realizable k-ϵ and shear stress transport (SST) k-ω models can be named. These models differ from each other in the value of their constants. Some of the turbulence models also add more terms to the transport equations. The value of the constants and the new terms gives each model special characteristics to solve certain types of flow. The additional equations of these models can be checked in ANSYS Fluent theory guide [30] and are not listed in this work. To analyze the behavior of the vortex inside the turbine, four of the methods mentioned above were selected; i.e., the SST k-ω, standard k-ω and the standard k-ϵ and RNG k-ϵ methods.

The standard k-ϵ method is the simplest complete turbulence model. This model contains sub-models for combustion, buoyancy and compressibility. It is not a good model for large pressure gradient, large streamline curvature and flows with strong separation RNG k-ϵ and standard k-ϵ models are similar. RNG k-ϵ contains the effect of swirl on turbulence, improving the accuracy for swirling flows [30].

SST k-ω and standard k-ω methods have similar forms. The standard k-ω model contains adjustments for shear flow spreading and low-Reynolds-number effects [30]. In the SST k-ω, the turbulence viscosity is adapted to include the turbulence shear stress. SST k-ω is the model most widely adopted in turbo-machinery and aerospace applications [36], because of the special characteristics of this model, since it includes a term that allows improving the estimates of the flow separation on smooth surfaces with adverse pressure gradients, such as flows over airfoils.

3. Results and discussion

The turbulence models use here were compared through the behavior of the vortex circulation and the mass flow rate from the beginning to the stabilization of the vortex ($0 < t < 100$ s). The results are shown in Figs. 3 and 4. Figs. 3 and 4 indicate that the vortex circulation and the mass flow rate have a similar behavior. Therefore, they appear to be independent on the turbulence model used.

Fig. 5 shows the vortex profiles for the four turbulence models during a time of 100 s. The black lines were added to make the identification of the basin. The differences in vortex profile prediction among the models are not significant. As it is not possible to conclude whether or not there are differences between the turbulence models using Figs. 3, 4, and 5, data collected for circulation and mass flow rate were analyzed through statistical analysis. These analyses made it possible to conclude whether significant differences were evidenced in the studied variables according to the turbulence model used. The statistical analysis was carried out in R statistical software [37]. The period used in the analysis was between 50 and 100 s. During this period and as observed in Figs. 3 and 4, the flow inside the turbine was stable.

3.1. Statistical analysis

A box-plot is a graphical way of displaying a dataset based on the median, the maximum, the minimum and the first and third quartiles of a set of data. Box-plots allow visualizing differences among treatments or groups [38]; in this case, the differences among the turbulence models used. Fig. 6 shows the box-plots for the circulation and mass flow rate for each turbulence model, known as treatments. From Fig. 6a, it can be observed that all the treatments have a similar median (horizontal black line in the middle of the boxes); the median is close to 5.060 kg/s. The expected mass flow rate value was 5.059 kg/s. The box-plots for T1 and T4 are short; i.e., the data are concentred around their median. For treatments T2 and T3, the data above and below the median are more dispersed since the box-plots are tall. The upper whiskers in treatment T2 and T3 are shorter than the whiskers located at the bottom, which means that the data are more concentrated in quartile 3 (75%) than in quartile 1 (25%). The treatment T2 has the tallest box. This box overlaps the boxes of the other treatments. The size of the box-plots suggests a difference between models. From Fig. 6b, all treatments have different median values, being all the data concentred around them. There is not a whisker; in fact, there are no boxes. These differences indicated that the turbulence models are statistically different.

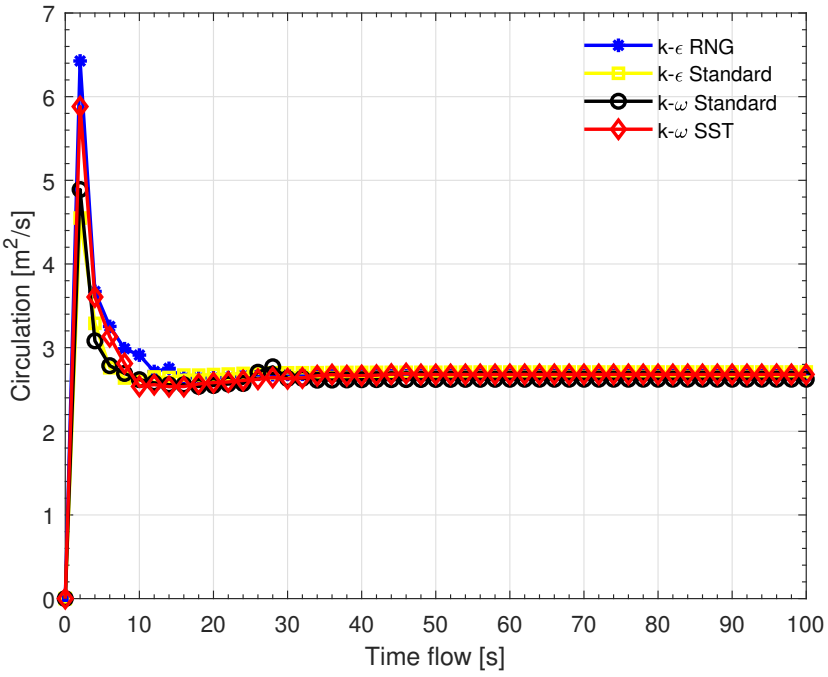

Fig. 3: Vortex circulation.

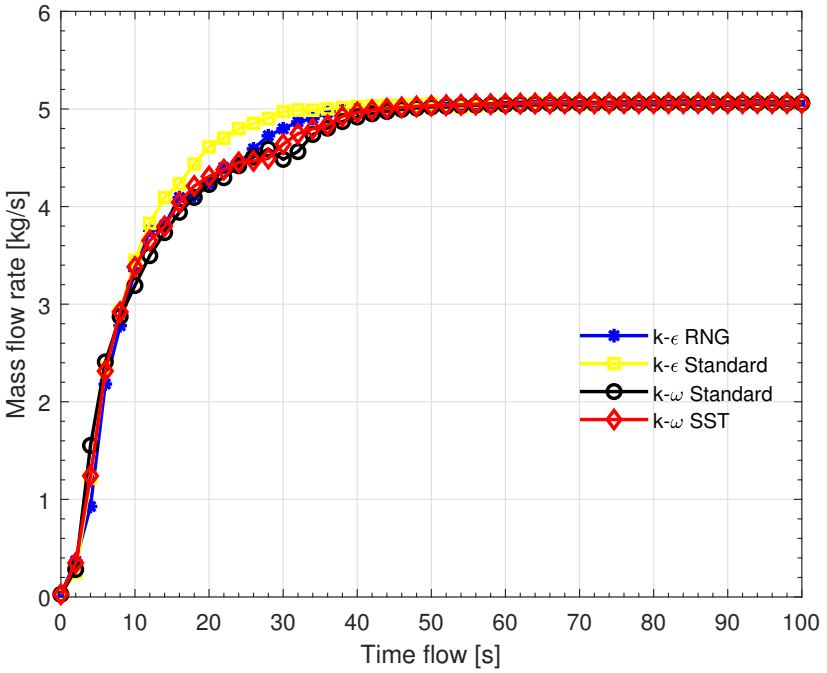

Fig. 4: Mass flow rate.h.

Table 2 shows the median for the mass flow rate and the circulation for each treatment. Additionally, for the mass flow, Table 2 shows the error among the expected mass flow rate value and the median obtained. The difference among models must be confirmed by an ANOVA, since it allows checking if at least one of the treatment means is different concerning to the other treatments. When the p-value obtained from the ANOVA is less than a significance level (α) of 0.05, the treatment mean is determined to be different from each other as at least one of the means is significantly different [39]. For the mass flow rate, a p-value of 0.2397 was obtained, while the p-value for the circulation was 2.2×10^{-16}. The p-values indicated that the turbulence model does not have significant effects on the mass flow rate but is

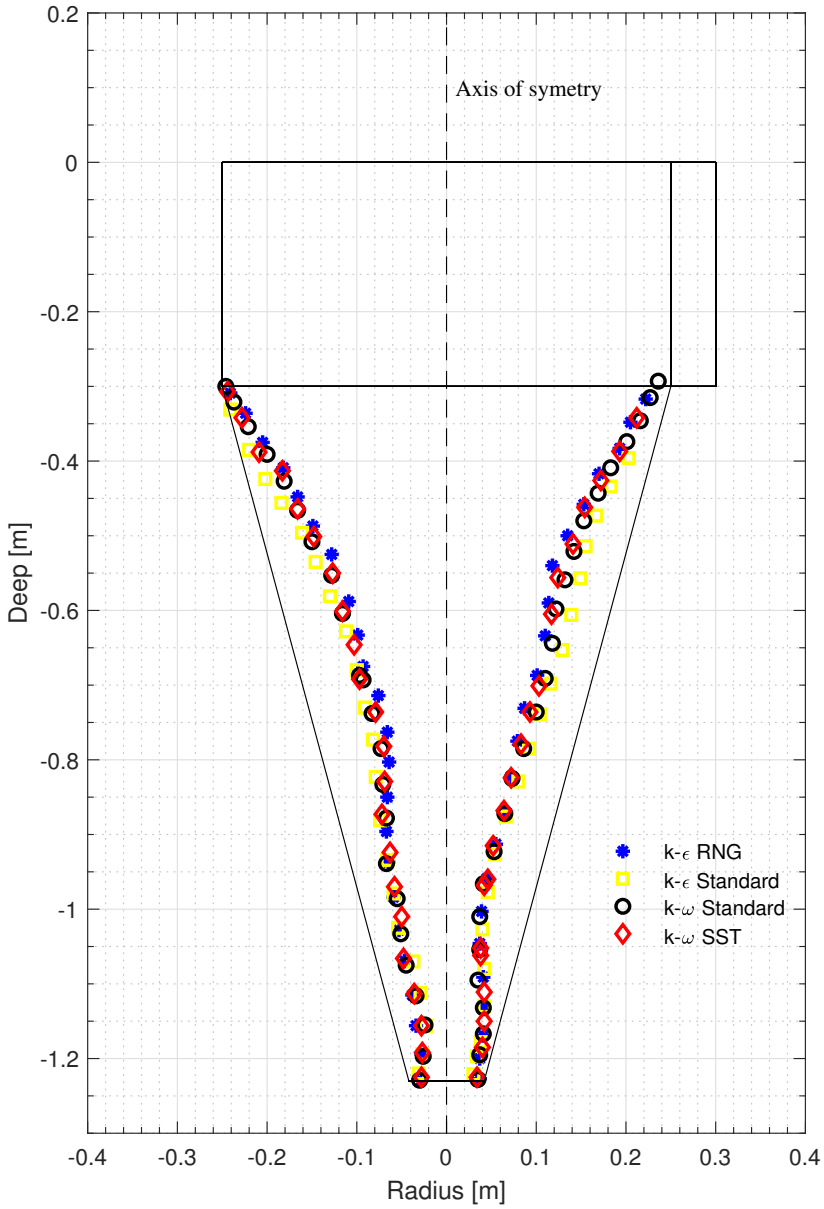

Fig. 5: Vortex profile for a time of 100 s.

significant on the circulation.

Once it has been determined that there are differences among the means for the circulation, it is necessary to investigate which treatments were different and what caused the difference. These questions were answered by testing the equality of all possible pairs of means through multiple comparison methods (MCMs) [40]. There are several methods for performing MCMs, such as Scheffé's test, Bonferroni method, Newman-Keuls, Tukey method and Fisher's least significant difference (LSD) test. In this paper, the LSD test was used. LSD test was the first pairwise comparison test that was developed by Ronald Fisher in 1935. This test helps identify the treatments whose means are statistically different. It can be used only when the ANOVA indicates significant differences (p-value $<\alpha$). The results of the LSD test are shown in Table 3. LSD test assigned a letter to each treatment; the treatments with the same letters are not

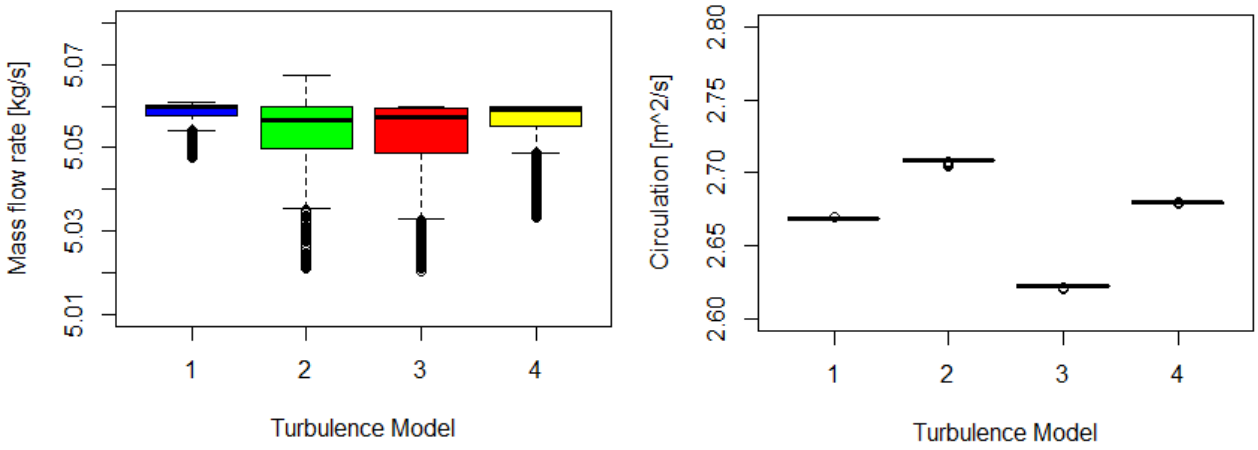

Fig. 6: Box-plots for the a) mass flow rate and the b) vortex circulation. 1, 2, 3 and 4 correspond to the RNG k-ϵ model (T1), standard k-ϵ model (T2), standard k-ω model (T3) and SST k-ω model (T4).

Table 2
Means for the turbulence models. RNG k-ϵ model (T1), standard k-ϵ model (T2), standard k-ω model (T3) and SST k-ω model (T4)

Turbulence model		Mass flow rate [kg/s]	Error [%]	Circulation [$m^2/2$]
T1	RNG k-ϵ	5.0585	0.0098	2.6690
T2	Standard k-ϵ	5.0532	0.1146	2.7084
T3	Standard k-ω	5.0524	0.1304	2.6223
T4	SST k-ω	5.0557	0.0652	2.6794

significantly different.

Table 3
Least significant difference (LSD) test results. ULC and LCL stand for upper and lower control limits.

Turbulence model	Standard deviation	Letter	UCL	LCL
T1	3.84×10^{-5}	C	2.66893	2.66890
T2	$2.90\times10\times10^{-5}$	A	2.70900	2.70898
T3	0	D	2.62281	2.62278
T4	$2.71\times10\times10^{-4}$	B	2.67967	2.67964

From Table 3, as a letter is assigned to each turbulence model, the LSD test indicated that there is an influence of the turbulence model on the vortex circulation mass because the mean of each treatment is significantly different. UCL and LCL, are the upper and the lower control limits, respectively. UCL and LCL are the limits of the confidence intervals defined by the LSD test in order to make comparisons between treatments. According to the values of LCL and UCL in Table 3, it is possible to know that these confidence intervals do not overlap, as indicated by the box-plots in Fig 6b. This means that there are no values in common between the results obtained for each treatment [41].

The results indicated that all the turbulence models of the analysis can properly predict the behavior of the flow inside the turbine. However, there are some differences in the vortex circulation, which is a vital variable in the analysis of a GWVHT. The turbulence model with the lowest error for the estimation of the mass flow rate was the RNG k-ϵ model. The difference between the expected and the predicted mass flow rate was only 0.0098%. The small error associated to the mass flow rate does not guarantee that the four turbulence models used can predict the vortex circulation or another variable. Taking the RNG k-ϵ model as a reference, the difference in circulation obtained by

using this in comparison with the other models studied is shown in Table 4.

Table 4
Differences in the vortex circulation

Turbulence models	Error [%]
T1-T2	1.4762
T1-T3	1.7497
T1-T4	0.3896

In the literature, several researches have been focused on comparisons between the turbulence models available in ANSYS Fluent. As a matter of fact, Wang et al. [42] compared six turbulence models, including the models of this study, for an axial flow blood pump. They validated their results through experiments comparing the velocity field and streamline. The authors concluded that the SST k–ω model had the smallest error associated. The streamlines are consistent with the streamlines of experimental results. On the other hand, the SST k–ω model has been recommended for numerical analysis of the axial flow blood pump. In an axial flow pump, the flow entering the pump rotates with the impeller [43] and creates a vortex, which is the same phenomenon of study than that in a GWVHT.

In turn, Muiruri et al. [44] compared four turbulence models, including SST k-ω and RNG k-ϵ , for an upscale wind turbine blade. The aerodynamic torque of the rotor blade was the control variable. The results were checked by comparing with works of other numerical studies. The authors concluded, in agreement with the literature sources [45], that the SST k–ω model is the most appropriate turbulence model for numerical simulations of wind turbines.

4. Conclusions

An analysis of four turbulence models, including standard k-ϵ, RNG k-ϵ, SST k-ω and standard k-ω models, for simulations of a gravitational water vortex hydraulic turbine (GWVHT) with a wrap-around inlet channel and a conical basin is presented. The runner was not included. The mass flow rate and the vortex circulation were the analyzed parameters.

According to the statistical analysis, any of the studied turbulence models can be used when the numerical analysis is based on the mass flow. Statistical results showed that there are no significant differences between the turbulence models for this response variable. The difference between the expected and the predicted mass flow rate values was below 0.14%, which was a good sign that the mass flow rate was resolved properly. The means of the vortex circulation for all the treatments are significantly different from each other; i.e., the turbulence models do generate differences in the calculation of the circulation inside the turbine.

The RNG k-ϵ model was the best model to predict the mass flow rate, which was followed by the SST k–ω model. In terms of circulation, which was the variable where differences were identified, comparing numerical and experimental results is required. From the numerical results obtained in RNG k-ϵ and SST k-ω models, which were the models with the lowest error to predict the mass flow rate, the differences between the predicted vortex circulation was only 0.3896%. Therefore and without considering the runner, the RNG k-ϵ and SST k-ω models could be considered as good predictors of the flow behavior within the turbine. The special characteristic of the SST k-ω model allows it to be considered for analyzing the GWVHT with runner. In this regard, this report is expected to be useful for fluid researches using simulation methodology, especially for the study of GWVHT.

References

[1] L. Doman, Eia projects 28% increase in world energy use by 2040, US Energy Information Administration (2017).
[2] G. E. S. Yearbook, Global energy statistical yearbook, 2018.
[3] B. Looney, Statistical review of world energy, 2020|, Bp 69 (2020) 66.
[4] J. Monteith, M. Unsworth, Principles of environmental physics: plants, animals, and the atmosphere, Academic Press, 2013.
[5] R. L. Singh, P. K. Singh, Global environmental problems, in: Principles and applications of environmental biotechnology for a sustainable future, Springer, 2017, pp. 13–41.
[6] K. Engeland, M. Borga, J.-D. Creutin, B. François, M.-H. Ramos, J.-P. Vidal, Space-time variability of climate variables and intermittent renewable electricity production–a review, Renewable and Sustainable Energy Reviews 79 (2017) 600–617.
[7] A. B. Timilsina, S. Mulligan, T. R. Bajracharya, Water vortex hydropower technology: a state-of-the-art review of developmental trends, Clean Technologies and Environmental Policy 20 (2018) 1737–1760.

[8] G. Marian, T. Sajin, I. Florescu, D. Nedelcu, C. Ostahie, C. Bîrsan, The concept and theoretical study of micro hydropower plant with gravitational vortex and turbine with rapidity steps, Buletinul AGIR 3 (2012) 219–226.
[9] H. Shabara, O. Yaakob, Y. M. Ahmed, A. Elbatran, M. S. Faddir, Cfd validation for efficient gravitational vortex pool system, Jurnal Teknologi 74 (2015).
[10] S. Sreerag, C. Raveendran, B. Jinshah, Effect of outlet diameter on the performance of gravitational vortex turbine with conical basin, International Journal of Scientific & Engineering Research 7 (2016) 457–463.
[11] P. Sritram, W. Treedet, R. Suntivarakorn, Effect of turbine materials on power generation efficiency from free water vortex hydro power plant, in: IOP Conference Series: Materials Science and Engineering, volume 103, IOP Publishing, 2015, p. 012018.
[12] C. Power, A. McNabola, P. Coughlan, A parametric experimental investigation of the operating conditions of gravitational vortex hydropower (gvhp), Journal of Clean Energy Technologies 4 (2016) 112–119.
[13] P. Wichian, R. Suntivarakorn, The effects of turbine baffle plates on the efficiency of water free vortex turbines, Energy Procedia 100 (2016) 198–202.
[14] S. Mulligan, Experimental and numerical analysis of three-dimensional free-surface turbulent vortex flows with strong circulation, Ireland: Institute of Technology Sligo (2015).
[15] J. R. Holton, An introduction to dynamic meteorology, American Journal of Physics 41 (1973) 752–754.
[16] M. Antuono, A. Colagrossi, D. Le Touzé, J. J. Monaghan, Conservation of circulation in sph for 2d free-surface flows, International Journal for Numerical Methods in Fluids 72 (2013) 583–606.
[17] Y. A. Cengel, Fluid mechanics, Tata McGraw-Hill Education, 2010.
[18] J. D. Anderson Jr, Fundamentals of aerodynamics, Tata McGraw-Hill Education, 2010.
[19] K. Zore, G. Parkhi, B. Sasanapuri, A. Varghese, Ansys mosaic poly-hexcore mesh for high-lift aircraft configuration, in: 21th Annual CFD Symposium, 2019, pp. 1–11.
[20] M. Rakowitz, Grid refinement study with a uhca wing-body configuration using richardson extrapolation and grid convergence index gci, in: New results in numerical and experimental fluid mechanics III, Springer, 2002, pp. 297–303.
[21] T. S. Phillips, C. J. Roy, Richardson extrapolation-based discretization uncertainty estimation for computational fluid dynamics, Journal of Fluids Engineering 136 (2014).
[22] N. Baker, G. Kelly, P. D. O'Sullivan, A grid convergence index study of mesh style effect on the accuracy of the numerical results for an indoor airflow profile, International Journal of Ventilation 19 (2020) 300–314.
[23] S. B. Pope, S. B. Pope, Turbulent flows, Cambridge university press, 2000.
[24] P. Maruzewski, H. Hayashi, C. Munch, K. Yamaishi, T. Hashii, H. Mombelli, Y. Sugow, F. Avellan, Turbulence modeling for francis turbine water passages simulation, in: IOP Conference Series: Earth and Environmental Science, volume 12, IOP Publishing, 2010, p. 012070.
[25] S. Dhakal, A. B. Timilsina, R. Dhakal, D. Fuyal, T. R. Bajracharya, H. P. Pandit, Effect of dominant parameters for conical basin: Gravitational water vortex power plant, in: Proceedings of IOE graduate conference, 2014, p. 381.
[26] S. Dhakal, A. B. Timilsina, R. Dhakal, D. Fuyal, T. R. Bajracharya, H. P. Pandit, N. Amatya, A. M. Nakarmi, Comparison of cylindrical and conical basins with optimum position of runner: Gravitational water vortex power plant, Renewable and Sustainable Energy Reviews 48 (2015) 662–669.
[27] J. A. Chattha, T. A. Cheema, N. H. Khan, Numerical investigation of basin geometries for vortex generation in a gravitational water vortex power plant, in: 2017 8th International Renewable Energy Congress (IREC), IEEE, 2017, pp. 1–5.
[28] Y. Nishi, T. Inagaki, Performance and flow field of a gravitation vortex type water turbine, International Journal of Rotating Machinery 2017 (2017).
[29] S. Havaldar, P. Gadekar, S. Baviskar, N. Jadhav, S. Inamdar, Analyzing geometries for inlet flow channels to gravitational water vortex chamber, no. August (2020).
[30] I. ANSYS, Ansys fluent 12.0 theory guide, ANSYS FLUENT Release (2009).
[31] Q. Chen, Comparison of different k-ϵ models for indoor air flow computations, Numerical Heat Transfer, Part B Fundamentals 28 (1995) 353–369.
[32] L. Velásquez, E. Chica, J. Posada, Advances in the development of gravitational water vortex hydraulic turbines., Journal of Engineering Science & Technology Review 14 (2021).
[33] L. F. Toapanta-Ramos, J. A. Zapata-Cautillo, A. I. Cholango-Gavilanes, W. Quitiaquez, C. Nieto-Londoño, Z. Zapata-Benabithe, Estudio numérico y comparativo del efecto de turbulencia en codos y dobleces para distribución de agua sanitaria, Revista Facultad de Ingeniería 28 (2019) 101–118.
[34] D. Monk, E. A. Chadwick, Comparison of turbulence models effectiveness for a delta wing at low reynolds numbers, in: 7th European conference for aeronautics and space sciences (EUCASS), volume 1303, 2017.
[35] C. D. Argyropoulos, N. Markatos, Recent advances on the numerical modelling of turbulent flows, Applied Mathematical Modelling 39 (2015) 693–732.
[36] I. F. Notes, Introduction to cfd analysis. introductory fluent training, ansys, 2006.
[37] R. C. Team, et al., R: A language and environment for statistical computing (2013).
[38] K. Potter, H. Hagen, A. Kerren, P. Dannenmann, Methods for presenting statistical information: The box plot, Visualization of large and unstructured data sets 4 (2006) 97–106.
[39] D. C. Montgomery, Design and analysis of experiments, John wiley & sons, 2017.
[40] J. A. Rafter, M. L. Abell, J. P. Braselton, Multiple comparison methods for means, Siam Review 44 (2002) 259–278.
[41] D. C. Montgomery, G. C. Runger, Applied statistics and probability for engineers, Wiley Hoboken, NJ, 2018.
[42] S. Wang, J. Tan, Z. Yu, Comparison and experimental validation of turbulence models for an axial flow blood pump, Journal of Mechanics in Medicine and Biology 19 (2019) 1940063.
[43] D. Kafagy, H. Gitano-Briggs, Axial flow artificial heart blood pumps: A brief review., Trends in Biomaterials & Artificial Organs 27 (2013).

[44] P. I. Muiruri, O. S. Motsamai, R. Ndeda, A comparative study of rans-based turbulence models for an upscale wind turbine blade, SN Applied Sciences 1 (2019) 1–15.

[45] A. Meana-Fernández, J. M. Fernández Oro, K. M. Argüelles Díaz, S. Velarde-Suárez, Turbulence-model comparison for aerodynamic-performance prediction of a typical vertical-axis wind-turbine airfoil, Energies 12 (2019) 488.

CHAPTER 7

TECHNICAL, ECONOMICAL AND ENVIRONMENTAL IMPACTS

Gravitational water vortex hydraulic turbine implementation in Colombia: hydropower potential and prospects

Submitted article

Highlights

- The first types of energy used by humanity were renewable energies: biomass, wind, and water. But, for the last two centuries, fossil fuels have been the protagonists of world energy consumption.
- From renewable energies, hydroelectricity is currently the most important source in the Latin American electricity matrix.
- New turbine designs, such as gravitational vortex hydraulic turbines, have drawn the attention of many researchers due to their easy installation and maintenance, and their low environmental impact.
- Law 1715 of 2014 marked a milestone in the country's energy history, encouraging the use of non-conventional sources of energy.

Gravitational water vortex hydraulic turbine implementation in Colombia: hydropower potential and prospects

Laura Velásquez, Ainhoa Rubio-Clemente, Alejandro Posada and Edwin Chica

ABSTRACT

The availability of the energy has changed the humanity over the last centuries. The first types of energy used by humanity were renewable energies: biomass, wind, and water. But, for the last two centuries, fossil fuels have been the protagonists of world energy consumption. However, recently there has been an awareness of the great energy dependence on a finite resource, geographically concentrated in a few countries, which in addition to degrading the environment, is subject to large fluctuations in price. From renewable energies, hydroelectricity is currently the most important source in the Latin American electricity matrix. Current projections suggest that the installed hydroelectric capacity will continue to grow to meet future electricity demand. This growth must consider the rehabilitation of the existing hydroelectric power plants, and the development of new projects. New turbine designs, such as gravitational water vortex hydraulic turbines, have drawn the attention of many researchers due to their easy installation and maintenance, and their low environmental impact. This work presents the hydropower potential and prospects for the implementation of this type of turbine in the Colombian context, and as well as a general description of the current panorama of the Colombian energy system.

1. Introduction

Throughout the human prehistory and history, several sources of energy have been used worldwide, from the human own-self strength to the energy generated in a water wheel for smashing grains and fruits [1]. However, for last two centuries, fossil fuels continued to be the protagonist of the world energy consumption although it is a finite resource that is geographically concentrated in a few countries, damage the environment, and is subjected of speculation in international markets [2, 3]. For all this, most of the measures taken in relation to energy are aimed at curbing consumption, increasing efficiency and diversification by committing to renewable energies. An interesting option for the generation and employing renewable energy, specifically hydropower energy, is the gravitational water vortex hydraulic turbine (GWVHT). These turbines operate at flow rates of 0.05–5 m^3/s and hydraulic heads between 0.5 and 2.0 m [4]. The hydraulic head is considered too low for conventional hydroelectric turbines. Francis, Pelton, and cross-flow turbines are incompatible when the hydraulic head is less than 3.0 m [5]. It was found that GWVHT, due to its ability to sustain relatively high efficiencies at low heads and small to medium flow rates, addresses a gap in the current turbine application chart [6]. Compared to traditional large-scale hydroelectric systems, GWVHT has a much lower impact on the ecosystem as construction of a large dam is not necessary. Only a fraction of the river flow is diverted and passes through the system, and all water is returned downstream to the river [7]. The system also demonstrates potential to be able to function as a fish passage [6]. The current work focuses on the implementation of a GWVHT in developing countries, such as Colombia. The implementation of this type of turbine was analyzed through technical, economic, and environmental perspectives. The work is organized as follows: a count of the evolution of energy sources along the prehistory and history, followed by an analysis of energy consumption in the world, especially in Colombia. Next, a description of the operation of a gravitational water vortex hydraulic turbine and its advantages and its advantages; and finally, an analysis of the barriers and opportunities hydropower development in Colombia.

2. Evolution of energy sources along the prehistory and history

For a primitive man, well-being was linked to satisfying his need to feed himself daily through hunting and gathering. For this purpose, the only energy source was that derived from his own muscular strength [8]. 500,000 years ago,

ORCID(s): 0000-0003-1483-0104 (L. Velásquez); 0000-0003-1527-260X (A. Rubio-Clemente); 0000-0001-5836-0680 (A. Posada); 00000-0002-5043-6414 (E. Chica)

with the discovery of fire [9] derived from wood as the first fuel, a fundamental step was made in the use of energy, which represents a turning point in the evolution of the humanity. As the human population increased, the use of fire intensified, leading to the agriculture rise and domestication of animals. This resulted in the inclusion of animal strength as another energy source. Over the centuries, means of transportation on lakes, rivers and seas were developed, and the wind acting on fabric sails was widely used to propel boats [10]. Nevertheless, due to wind direction and power, the wind energy was combined with human muscular energy. Later, the energy of water began to be used, thanks to the invention of the water wheel, as a source of energy. This energy was used to turn stones or millstones [11]. Around 1180, wind energy found an important application in Europe when it began to be used to move the grinding wheels of grain mills [12], when other sources of energy, such as hydraulics, were difficult to be exploited. With the use of hydraulic power, animal power and energy from burning wood, mining, metallurgy and other industrial activities were developed [13]. Due to the disproportionate increase in wood burning during the Middle Ages and the Renaissance, from the 17th century, there was a shortage of wood in Western Europe [14]. England began burning mineral coal as the main source of energy, but it was considered dirty and harmful to health [15, 16]. Coal was the most used fuel par excellence in developed countries until it gave way to oil in the 20th century. The invention of the steam engine, in the 18th century, was the first great modern energy invention [17]. Thanks to this, a means of mechanical energy production was available that made it possible to obtain high powers and was less geographically limited than the resources previously used. This invention was a banner of the First Industrial Revolution [18]. In 1729, the first studies on electricity began. The first electric battery dates to 1800, when Volta invented the first electrochemical generator capable of producing an electric current maintained over time [19]. In 1821, Faraday's first electric motor appeared [20], and in 1881, Thomas Alva Edison's invented the incandescent lamp [21]. These kinds of energy sources, along with the water wheels, resulted in the increase in the current hydraulic turbines, and with them, the production of electricity. However, electrical energy, as a widely used energy, did not reach most of the population of developed countries until the first third of the 20th century [22]. In 1863 and 1885, with the invention of the internal combustion engine [23] and the automobile [24], respectively, the accelerated use of oil and its derived fuels began. Afterwards, the use of this type of energy spreads in the navy, in steam generators, in industrial ovens and in-home heating; today, oil represents the main source of energy in the world [25] despite its non-renewable character. Later, the first types of energy used by humanity were then renewable energies, including biomass, wind, sun, and water [26]. Nowadays, the use of renewable energy sources is in the target of both developed and developing countries around the world, especially in the former ones due to the negative environmental and health impacts associated with the use of fossil fuels.

3. Energy in the world and in the particular case of Colombia

The annual global energy consumption is estimated as 13,865 million tons of oil equivalents (Mtoe), or about 580 million TJ [27]. By 2040, global energy consumption will reach 740 million TJ - equivalent to additional 30% growth. The United States and China, with 2040 and 3381 Mtoe, respectively, are the countries with the highest energy consumption [28]. Figure 1 shows the percentage of electricity generation by fuel and region in 2020.

According to Figure 1, natural gas is the dominant fuel used for power generation in Africa, North America, the Middle East and CIS (Commonwealth of Independent States). In turn, in Asia, coal comprises 57% of the generation mix, while 58% of the power in South and Central America is hydroelectricity and renewables. Of 58%, 77% of the electricity produced corresponds to the derived from hydroelectric plants, followed by wind and solar generation that together add up to 13%, 9% biomass, and 1% geothermal. Currently, the region has about 200,000 MW of installed hydropower capacity, of which 25,000 MW have been added in the last 5 years.

3.1. Electricity generation and provision in Colombia

Colombia is the fourth country in South America with the largest installed capacity in hydroelectricity, closely followed by Argentina and Venezuela, but very far from the first producer, Brazil, with an installed capacity of 110,000 MW [30, 31]. Colombia has an installed capacity of approximately 19,000 MW, of which 68.4% is generated from hydroelectric plants, 30.7% corresponding to thermal plants, and 1% to other renewable energy sources [32, 33, 34]. Brazil produces 62.9% of its electricity through hydropower [35]. Figure 2 shows the evolution of electricity production by source in Colombia between 2000 and 2020.

As observed in the Figure, hydropower is the main source in Colombia producing energy. It is important to note that hydroelectric power plants are essential for the sustainable development of the region's electrical matrix, not

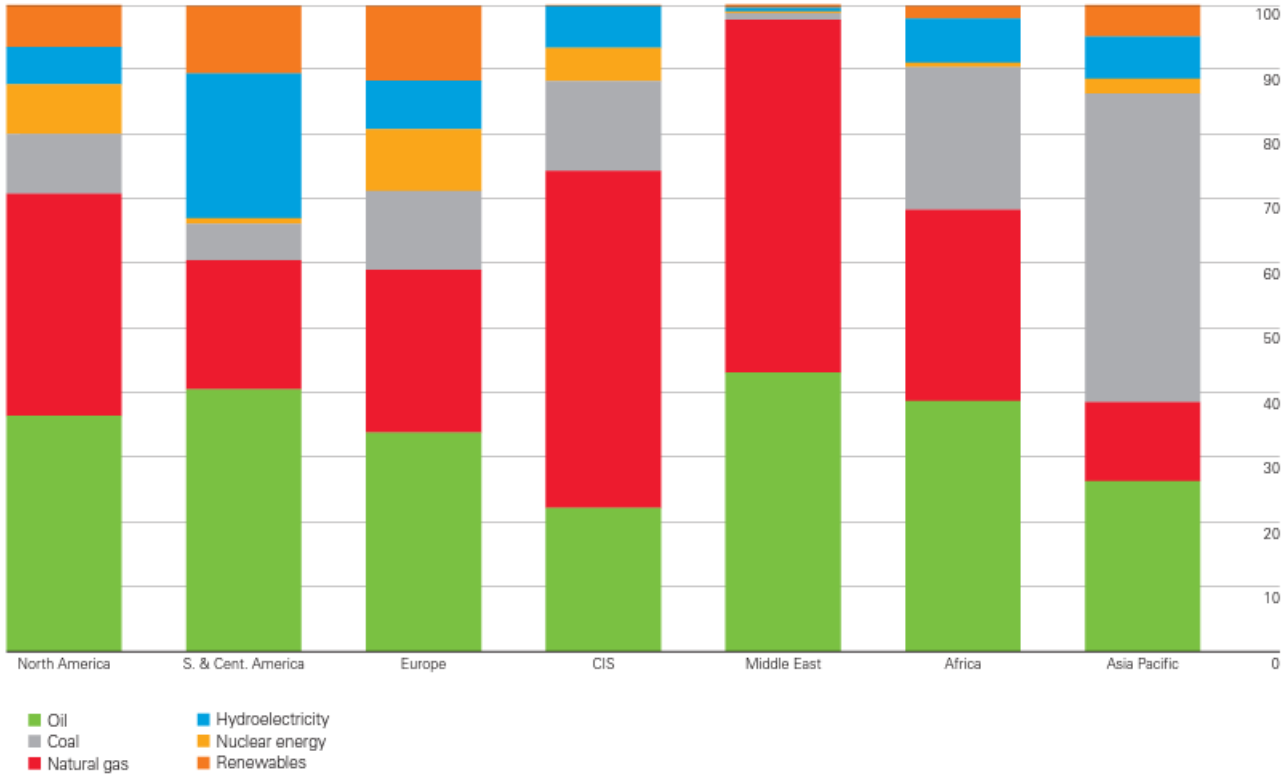

Fig. 1: The percentage of electricity generation by fuel and region in 2020. Adapted from: [29].

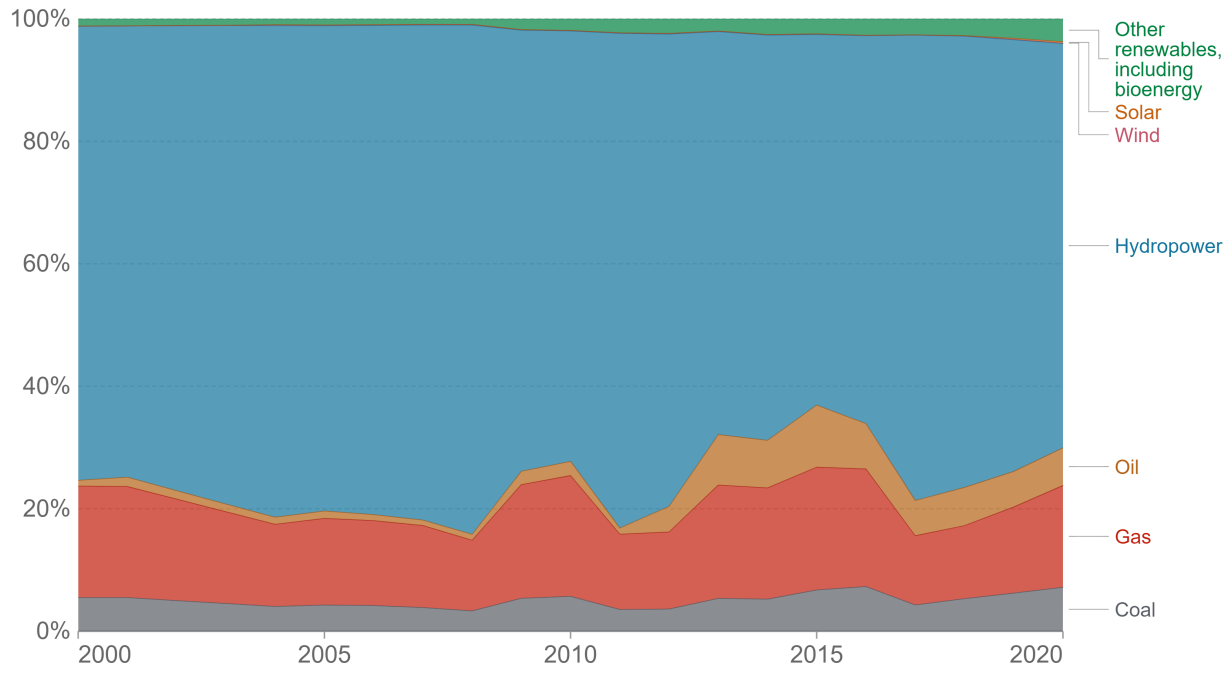

Fig. 2: Electricity production by source, Colombia [36].

only because of the renewable energy supply they provide, but also because of the technological capacity to provide other services, such as flexibility and peak generation, frequency regulation, energy storage, among others, which

currently allow the massive incorporation of intermittent generation sources (as solar and wind). For this reason, the advances that can be achieved in the regulatory frameworks so that they adequately recognize the value of all services that hydroelectric plants provide to the system, beyond energy, will be essential to encourage investments not only the development of new hydroelectric projects, but also to accelerate the modernization of the existing hydroelectric power plants, essential to accompany the transformation toward low-carbon generation and its sustainability. For years, hydroelectric plants have been considered synonymous of development. Colombia, owing to its topography, rainfall and water resources, has an exceptionally high potential to develop this type of engineering projects. In fact, Colombia has been classified as the second country in Latin America with the largest hydraulic capacity. The country has a flow among its main rivers of $52,075$ m^3/s, and the water supply is 6 times higher than the world average. In hydroelectric power plants, their construction is less expensive than nuclear plants. Additionally, the operation is cheaper than thermoelectric plants, energy can be provided on a large or small scale, and low emissions of greenhouse gases (GG) are generated. Large or small scales refers to the generated power. A large hydropower plant produces 10 MW or more, whereas a small hydropower plant (SHP) produces less of 10 MW [37]. A small hydropower plant is divided into further categories depending on its size, such as mini- (less than 1,000 kW), micro-hydro (less than 100 kW) and pico-hydro (less than 5kW). The definitions may vary according to manufacturers and countries [38]. The above reasons are sufficient that decision-makers at the state level have considered the construction of hydroelectric plants on important tributaries of the country, such as Alto Chicamocha, Betania, Calima, Chivor, Guavio, El Quimbo, Hidromiel, Hidrosogamoso, Ituango, Peñol-Guatapé, San Carlos, among others [31]. However, the construction and maintenance of large hydroelectric power plants mean an undeniable environmental, social and economic costs. Small-hydraulic power plants bring a great deal of research consideration. SHP is characterized by varying flows, low-head and highly valued river functions, including sediment transport, fish preservation and recreational usage, etc. [39, 40, 41]. According to the National Energy Plan, in SHP , Colombia has a potential of $25,000$ MW. Despite this great power, 0.67% in SHP has been exploited. Several sites of small hydro-energy potential remain untapped due to the limitations of the hydraulic head besides the requirement of large flow rates for the power generation. This potential energy resource can be used if new-innovative turbines that balance efficiency, economics and environmental sustainability are developed [42]. The supply of electrical energy, with a commercial approach, began in Colombia by private initiative at the end of the 19th century, when the Bogotá Electric Light Company was created in 1888. In the following years, also driven by private initiative, generation-distribution systems were developed in isolation in the main cities of the country [43]. Nowadays, the provision of electricity service and its expansion are carried out through the physical connection of users to the National Interconnected System (or SIN, by its acronym in Spanish). The geographical areas that are not electrically coupled to the SIN, are called Non-interconnected Zones (NIZ, ZNI in Spanish). NIZ do not have access to the electricity service through an interconnected system; however, several local solutions can be adopted, such as the use of diesel [44]. NIZ are shown in Figure 3. These locations have 130,000 population and contributes to 52% of Colombia's land, averagely 868 km^2 [44]. The department with the highest number of localities with ZNI is Nariño, followed by Chocó and Caquetá. Generally, the population density of the NIZ is extremely low (44 habitants/km2), due to the dispersion of both the municipalities and dwellings, a factor that makes the logistics of service assistance difficult, with high unit investment and operating costs [45]. This is due to the deficient, and in some places non-existent, mobility and transport infrastructure, aggravated by the political and socioeconomic conditions of the regions. Despite all, the NIZ are characterized by their great wealth of natural resources. Thanks to the abundance of resources, energy solutions should be based on renewable power sources as the hydraulic energy.

3.2. Electricity consumption in Colombia

The electricity consumption of a home is the sum of the electricity cost of all electrical appliances in the house in a given period (daily, weekly, monthly, annual, etc.). This is established using electrical energy measurement equipment, from which the electricity distributors extract the data for billing. Figure 4 shows the evolution of energy consumption per person. Energy consumption includes electricity, cooking, transport, and heating. In Colombia, the average consumption per person is $10,000$ kWh per year [28]. Between 1965 and 2021, the energy consumption had an increment of 120%; the average electricity consumption of a home depends directly on its dimensions, the number of people who live in it, appliances, and uses of electricity. Normally, the electrical appliances (oven, washing machine, television, refrigerator, computer, and air conditioning) are the same, and mostly, the electricity is consumed at night or on weekends. The average consumption of electricity in Colombia is still low compared to that is registered in the other economies of the region, as shown in Figure 4. This is the consequence of not having a "highly developed"

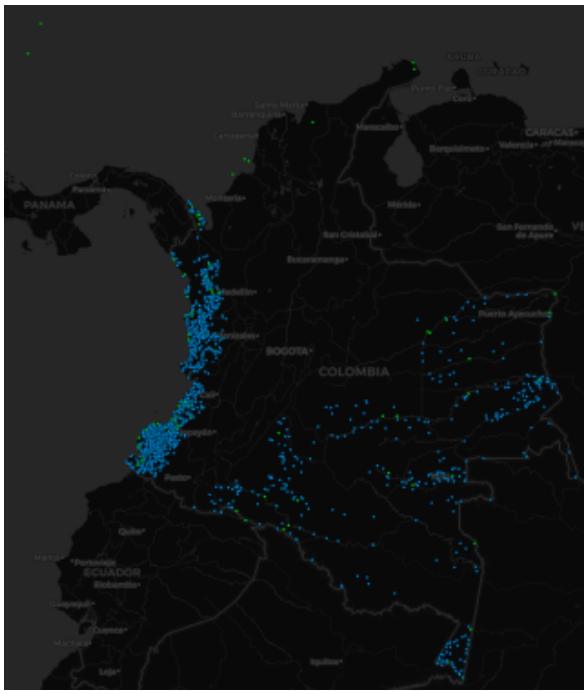

Fig. 3: Non-interconnected zones. Adapted from: [46].

electricity market and because gas, wood, and coal are still used as a source of energy, instead of electricity, in homes.

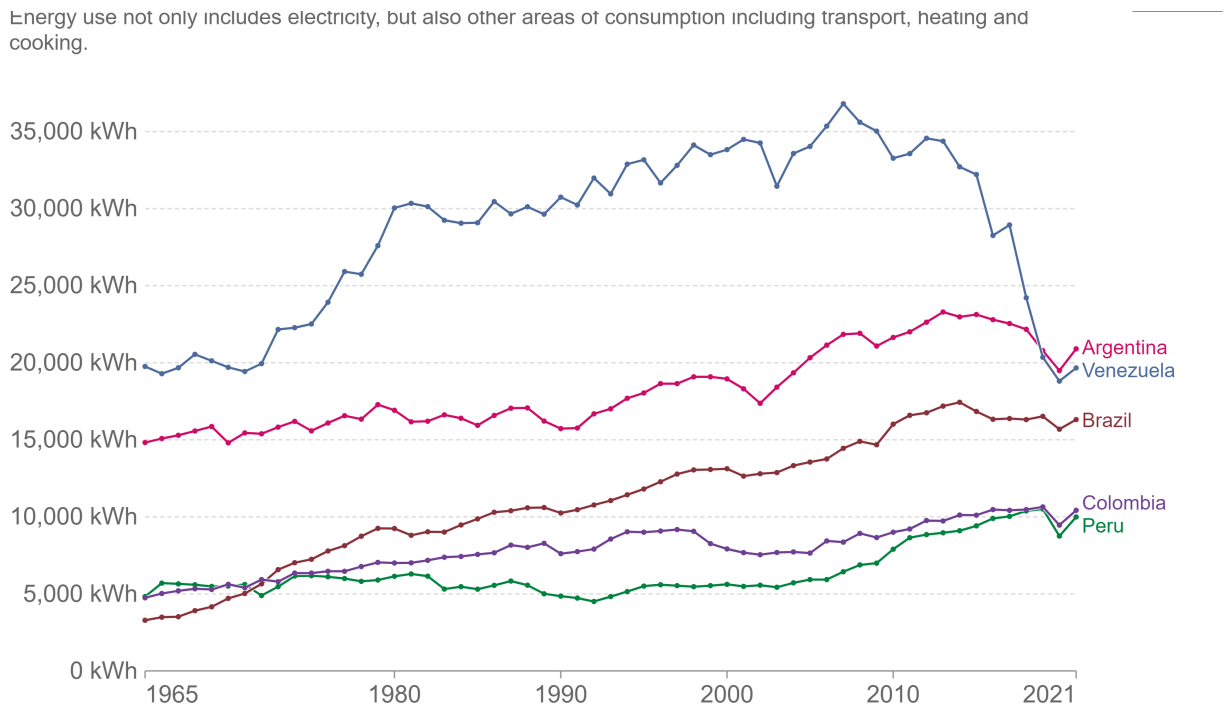

Fig. 4: Energy use per person in Latin America [36].

In the world, the countries with the highest energy consumption per person are Qatar (183,000 kWh per year), Netherlands Antilles (179,000 kWh per year) and Iceland (170,000 kWh per year). The consumption of United States of America ranks 18th with an average of 78,000 kWh per year. The world energy consumption per person is shown

in Figure 5.

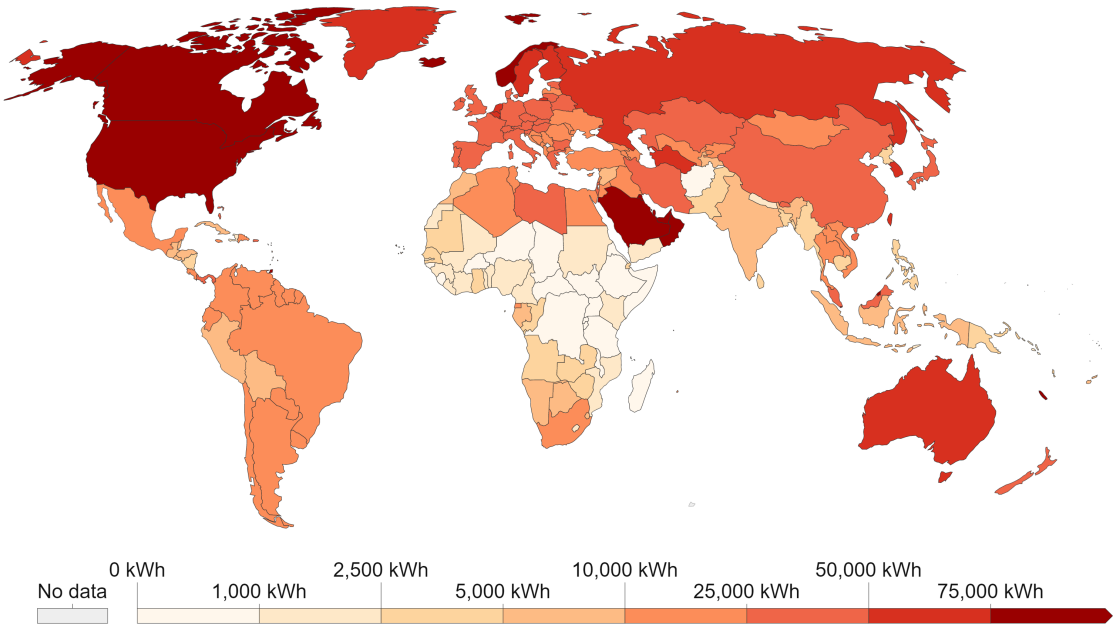

Fig. 5: Energy use per person in the world [36].

4. Gravitational water vortex hydraulic turbine (GWVHT)

One of the new innovative turbines that take advantage of the potential energy resource for SHP is the GWVHT. GWVHT is an impulse turbine of low-head hydropower technology [47]. Low-head hydropower can generate electricity from rivers that were traditionally unsuitable for developing hydraulic power plants [42, 48]. In a GWVHT, the water passes through an inlet channel into a conical or cylindrical circulation chamber, in which a free surface water vortex is formed [49]. A vertical-axis runner is positioned in the center of the chamber. The runner rotates with the swirling flow, thus generating mechanical energy which can be converted to electrical energy using a generator [5]. The water discharges through an outlet hole at the bottom of the circulation chamber. A small hydroelectric plant with GWVHT is shown in Figure 6. The main components of this turbine are the inlet channel, circulation chamber or vortex chamber, and a runner or impeller.

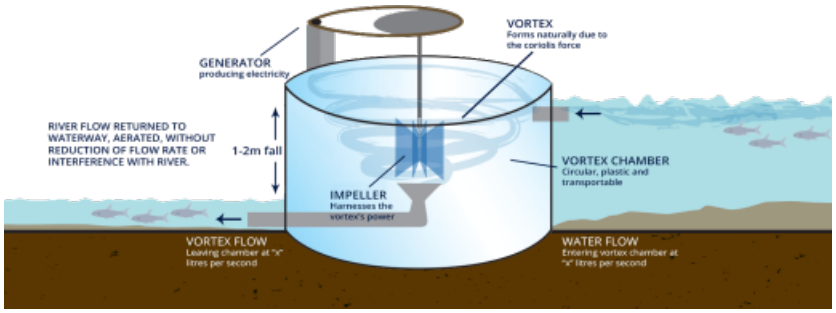

Fig. 6: Small hydroelectric plant with GWVHT [50].

The basic principle of any hydropower generation plant is impulse momentum [38]. Water potential is transformed into the mechanical energy by rotating a runner; next, mechanical energy is transformed into the electrical energy by using a generator. The diagram of converting the energy of water is shown in Figure 7.

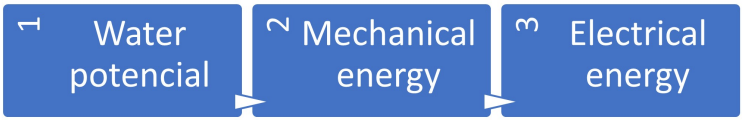

Fig. 7: Block diagram of hydropower generation. Adapted from: [38].

The available power in an impulse turbine is given by Eq. 1:

$$P = \rho g Q(H_n) \tag{1}$$

where ρ is the density of the fluid, Q the volume flow rate, g the gravity, and H is the difference in height between the level of fluid in the inlet channel and the position of the runner in the basin [51]. The power generated by any turbine is given by equation Eq. 2:

$$P_{out} = T\omega \tag{2}$$

where T is the torque, and ω is the angular velocity. The efficiency η of the turbine is defined by equation Eq. 3:

$$\eta = \frac{P_{out}}{P} = \frac{T\omega}{\rho g Q(H_n)} \tag{3}$$

Twenty of these turbines have been installed. The turbines installed have output powers ranging from 0.01 to 20 kW with an average efficiency of 54%± 12% [6]. This efficiency is low compared with the efficiencies reported by conventional turbine, with values that exceed 95% [52].

4.1. Prospects for the implementation of a GWVHT in Colombia

If Colombia has a potential of 25,000 MW for generation with SHP, for a power of 20 kW, about 1 million turbines could be installed. The potential for generation is higher than this installed capacity (19,000 MW). With a capacity of 20 kW, operating 18 h a day on average, and 350 days per year, each hydropower plant would supply the electricity for 13 million people. The NIZ only have 130,000 population. Producing electricity taking advantage of the potential available in the country not only makes it possible to supply the energy needs of the NIZ, but it would also allow generating electricity for the rest of the country, including neighboring countries. An interesting proposal to produce electricity for non-interconnected zones, or to deal with the growing demand for electricity, is to use the water discharges available in large-hydroelectric plants. Water discharges are the amount of water expressed in energy [GWh] that is evacuated from the reservoirs (damns) through their discharge structures. This occurs in the rainy seasons when the reservoir level exceeds its maximum physical level. The spillway is a hydraulic structure built to allow free passage or control the water stored in a reservoir. There are different types of discharge structures. In Colombia, the most used types of landfills are those with the free edge, landfills with gates and landfills with fuse dams [53]. In a free - edge weir, the water passes freely over them once the reservoir exceeds the level of said structure. Weirs with gates are those that can control the discharge by partially or totally opening their gates. These spillways do not have to wait for the reservoir to reach its maximum operating level to start opening their gates; the operation begins in advance seeking to regulate the discharge of the flow and maintain the level of the reservoir. A fusible dam spillway is made up of independent units that collapse when the water level in the reservoir reaches a certain level, causing the flow to discharge downstream through the space released by this unit. Figure 8 shows the water discharge that is evacuated from the reservoirs for all hydropower plants in Colombia in the last two years. In total, in the last 2 years, 12,612 GWh of energy has been wasted through discharge structures.

Figure 9 shows the evolution of the average daily price of electricity from 2016 to 2020. In Colombia, the highest percentage of generation is covered by generators with hydroelectric plants. When the weather affects the level of the reservoir downwards, it puts pressure on the price, and this effect is noticeable. According to Figure 9, in the first months of 2016 with the formation of the El Niño phenomenon that affected the country between 2015 and 2016, when

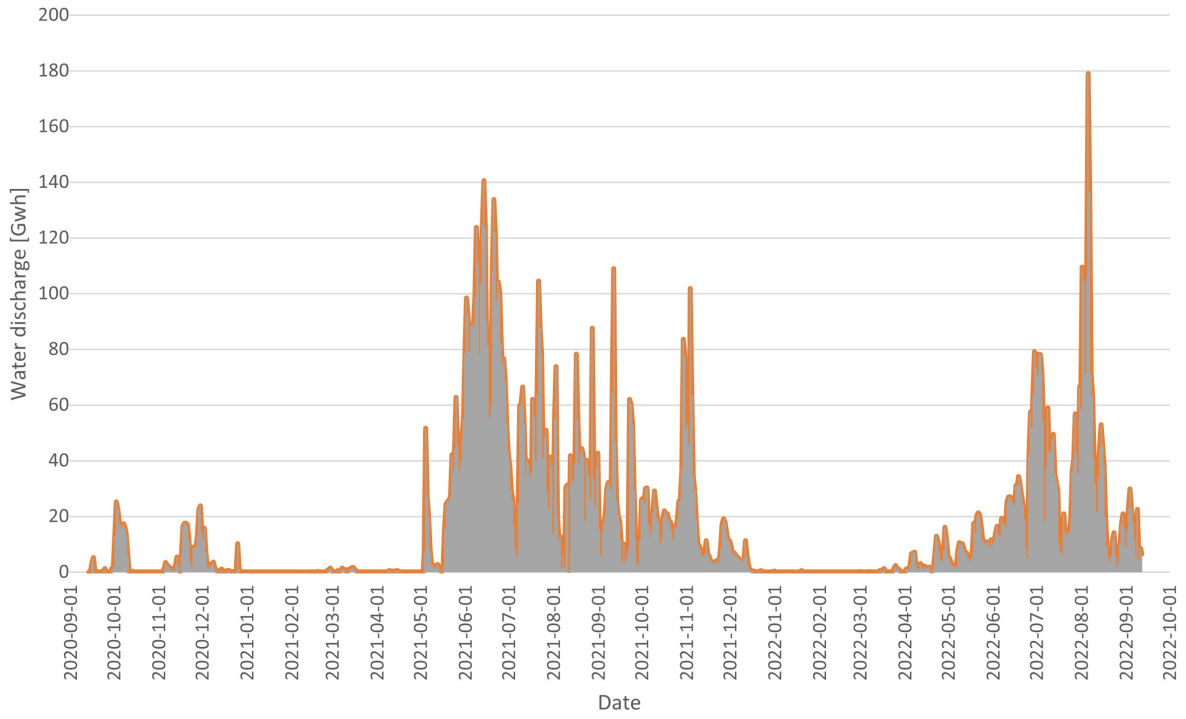

Fig. 8: Water discharge. Adapted from: [53].

the price reached 871 COP. Throughout 2019 and 2020, the effects of climate change and the influence of the El Niño phenomenon are observed too. With an average cost of 200 COP per kWh, the water discharged in the last two years (12, 612 GWh) was equivalent to 2, 522, 400, 000 COP. In the NIZ, the cost of electricity (generated with fossil fuels) is on average 1, 250 COP per kWh [54], so the value of water discharges would be equivalent to 15, 765, 000, 000 COP. In the ZNI, the cost of electricity increases due to the transport of fossil fuel added to the difficulty of access.

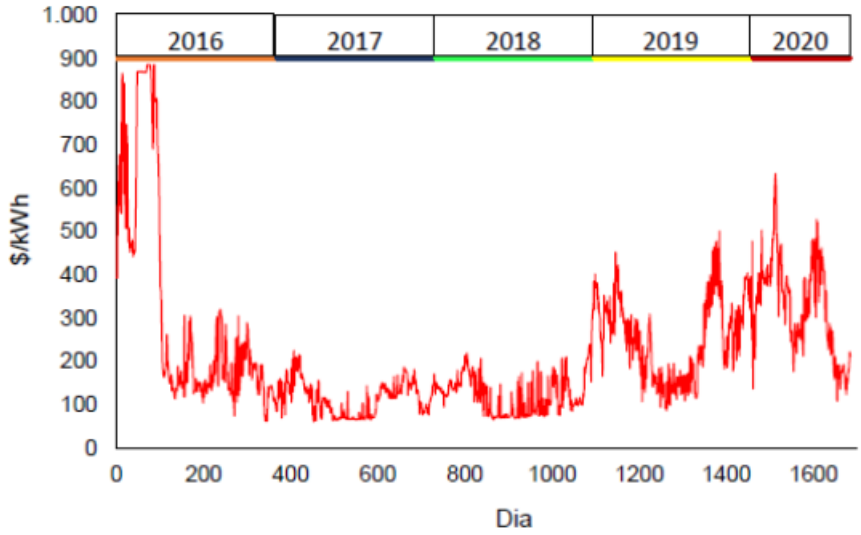

Fig. 9: The evolution of the average daily price of electricity [55].

A barrel of oil is equal to 6.1178632×10^9 or 1,700 kWh [56]. water discharge is equivalent to 7,400 barrels of oil. Figure 10 shows the evolution of the price of OPEC oil. OPEC oil has been quoted during 2022 at an average

of 94 U.S. dollars per barrel [53]. OPEC is the Organization of Petroleum Exporting Countries, coordinates the oil policies of its member countries to influence the international oil market. OPEC member countries are the United Arab Emirates, Saudi Arabia, Algeria, Venezuela, Nigeria, Angola, Qatar, Ecuador, Libya, Gabon, Iran, Iraq, and Kuwait [57]. The 7,400 barrels will cost 695,600 U.S. dollars (or approximately 3, 082, 168, 820 COP).

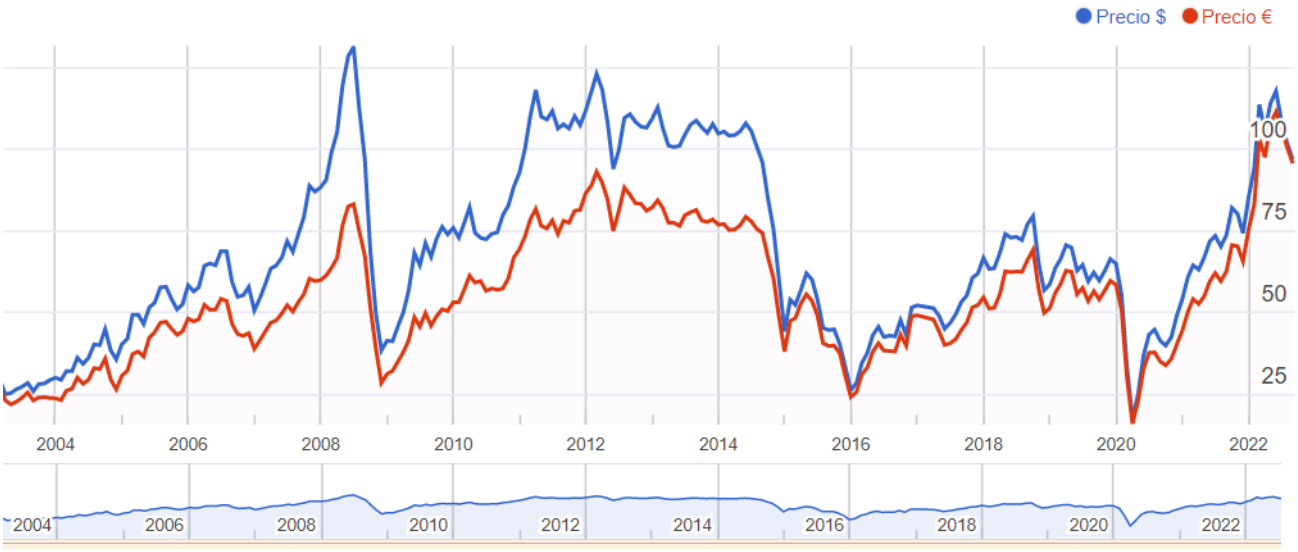

Fig. 10: Evolution of the price of OPEC oil [58].

5. Barriers and opportunities in Colombian hydropower development

The future of humanity depends on the way energy is produced (XX). Currently, most countries worldwide aim to supply their internal energy demand from renewable energy sources [59]. Colombia is not a stranger to this approach, as in the National Energy Plan, a strategy to reduce the vulnerability of the energy sector is the search to diversify the matrix of electricity generation in the medium and long term in all supply chains energy supply, increasing its complementarity, availability, and reliability with renewable energy sources [60]. In this regard, developing countries are facing the following challenges: i) development and technological adaptation of devices for the use from renewable energy sources; ii) the formation of human capital in aspects related to energy generation and energy efficiency; and iii) the search for sources of investment for developing the energy infrastructure necessary to continue guaranteeing equity and social development, while simultaneously addressing the effects of climate change and sustainable development. From renewable energy sources, hydropower is considered as one of the most convenient and popular renewable energy technologies [61, 59, 62].

- Environmental sustainability and land use

  During the construction period of a hydropower plant, land is busy to make temporal activities like construction of roads, stores, and worksites [59, 63]. The temporal land occupied for constructing may include urban, forests and farmlands. After the conclusion of the construction period, large areas of land are permanently flooded. Large storage of water in big artificial lake causes biomass decomposition of flooded land and produces methane (CH_4) and carbon dioxide (CO_2) emissions. Additionally, flooded land destroys arable land, wildlife, and can included residential areas. Reservoirs in hilly regions can store more water in smaller areas, whereas in flat regions the area covered by the reservoir is large [59]. For instance, the hydroelectric power plant located in "El Peñol" dam (Guatapé, Antioquia) floods 74 km^2 of land to generate 560 MW [64]. The Three Gorges Dam, the world's largest hydropower plant, floods 1,084 km^2 of land to generate 22,500 MW [65, 66].

  Small-hydropower plants, especially run of river type schemes, do not have the same environmental problems associated with large-hydroelectric projects since these types of plants do not require large reservoirs [67], even some of them, such as gravitational water vortex hydraulic turbine, do not require any type of reservoir. As in

any turbine, GWVHT can produce downstream flow alterations; nevertheless, in the case of GWVHT, these alterations can be advantageous because they allow aerating the water, disseminating internal pollutants in the water, and reducing the temperature by increasing the rate of evaporation [68, 6, 4].

- Government policies

  In the New Policies Scenario, the world meets its growing energy needs in a radically different way than in the last 25 years, now led by natural gas, the rapid rise of renewable energies, and energy efficiency [42]. The decisions agreed at United Nations Climate Change Conference 2015 (COP21) light up the future of renewable energies. The international community has understood its debt to strengthen the transition to a low-carbon economy for the sustainable future. The unanimity in favor of the decarbonization of the economy constitutes a very favorable framework for the promotion of clean energy technologies. As large hydropower projects are not accepted as a clean renewable energy source by environmentalists and ecologists, many countries accelerated the growth of SHP [69, 70]. To promote the expansion of SHP, the governments have financed investigations and developments of technologies to make such power plant a competitive one, establishing regulatory frameworks and policies to the renewable energy sector [71]. In the case of Colombia, Law 1715 of 2014 marked a milestone in the country's energy history, encouraging the use of non-conventional sources of energy, turning them into a matter of public utility and social, public, and national interest, which triggered a high interest in the promotion and implementation of energy projects through non-conventional sources of energy in the country [72, 73].

6. Conclusions

In Colombia, the electricity sector is one of the most competitive in the region and thanks to its good management, it is one of the sectors with the highest profits and projection. More than 52% of the territory does not have a constant electricity service at reasonable prices, which prevents the development of these areas, increasing the inequality that already affects Colombian society, especially at the regional level. Access in rural areas and particularly in NIZ is very poor and, although coverage has been expanded in recent years, quality has not been increased to the same extent. Therefore, it is important that electrification projects not only provide electricity to inhabitants, but also temporary and permanent jobs allowing community development and the inclusion of the various local actors that lead local development, and the project to be carried out. For this purpose, a fundamental and integral role of the state that allows reducing the technological, social and economic gap is required, in which people without electricity can live, respecting and rescuing their worldviews, cultures and social constructions. Due to the present restrictions to lead to the interconnection of the NIZ to the SIN, it is important to pay special attention and allocation to research and development in alternative energies that enable access to electricity at reasonable costs and without having permanent impacts on the environment. In this regard, public and private interventions are necessary in the electricity service providers in the NIZ to make attractive and safe investments in the sector. Likewise, understanding the role played by the glider when seeking reasonable and applicable solutions in each of the NIZ is a complex task, due not only to the growing supply of new alternatives, but also to the complexity of the Colombian territory that sometimes makes the application of such technologies difficult. GWVHT are a promising technology because they allow to take advantage of locations that until now were impossible with conventional generation systems (Pelton, Kaplan, and Francis turbine) since this technology requires a low hydraulic head.

References

[1] E. F. Moran, People and nature: An introduction to human ecological relations, John Wiley & Sons, 2016.
[2] T. Van de Graaf, B. K. Sovacool, Global energy politics, John Wiley & Sons, 2020.
[3] I. Stoddard, K. Anderson, S. Capstick, W. Carton, J. Depledge, K. Facer, C. Gough, F. Hache, C. Hoolohan, M. Hultman, et al., Three decades of climate mitigation: why haven't we bent the global emissions curve?, Annual Review of Environment and Resources 46 (2021) 653–689.
[4] L. Velásquez, E. Chica, J. Posada, Advances in the development of gravitational water vortex hydraulic turbines., Journal of Engineering Science & Technology Review 14 (2021).
[5] A. T. Kora, V. R. Ancha, G. S. Tibba, Numerical analysis of the effect of runner-to-basin diameter ratio on the performance of gravitational water vortex turbine in a scroll basin, International Journal of Energy and Environmental Engineering (2022) 1–17.
[6] A. B. Timilsina, S. Mulligan, T. R. Bajracharya, Water vortex hydropower technology: a state-of-the-art review of developmental trends, Clean Technologies and Environmental Policy 20 (2018) 1737–1760.
[7] V. J. A. Guzmán, J. A. Glasscock, Analytical solution for a strong free-surface water vortex describing flow in a full-scale gravitational vortex hydropower system, Water Science and Engineering 14 (2021) 72–79.

[8] J. A. Aguilera Folgueiras, et al., Fuentes de energía y protocolo de kioto en la evolución del sistema eléctrico español (2012).
[9] J. A. Gowlett, The discovery of fire by humans: a long and convoluted process, Philosophical Transactions of the Royal Society B: Biological Sciences 371 (2016) 20150164.
[10] G. A. Tokaty, A history and philosophy of fluid mechanics, Courier Corporation, 1994.
[11] R. L. Hills, Power from wind: a history of windmill technology, Cambridge University Press, 1996.
[12] J. Langdon, Water-mills and windmills in the west midlands, 1086-1500 1, The Economic History Review 44 (1991) 424–444.
[13] A. V. Perez, M. R. Gámez, C. G. V. Viteri, A. M. V. Quiroz, Community power as a driving force for sustainable local development, Journal of College and University. This is an open access article under the 2454 (2017) 2261.
[14] G. Parker, Global Crisis: War, Climate Change, & Catastrophe in the Seventeenth Century, Yale University Press, 2013.
[15] S. Liu, T. Rehren, D. Qin, J. Chen, W. Zhou, M. Martinón-Torres, X. Huang, W. Qian, Coal-fuelled crucible lead-silver smelting in 12th-13th century china: A technological innovation in the age of deforestation, Journal of Archaeological Science 104 (2019) 75–84.
[16] J. Dodson, X. Li, N. Sun, P. Atahan, X. Zhou, H. Liu, K. Zhao, S. Hu, Z. Yang, Use of coal in the bronze age in china, The Holocene 24 (2014) 525–530.
[17] H. W. Dickinson, A short history of the steam engine, Cambridge University Press, 2011.
[18] J. A. Montagna, The industrial revolution, Yale-New Haven Teachers Institute (1981).
[19] M. Piccolino, The bicentennial of the voltaic battery (1800–2000): the artificial electric organ, Trends in neurosciences 23 (2000) 147–151.
[20] E. Laithwaite, The influence of michael faraday on power engineering, Power Engineering Journal 5 (1991) 209–219.
[21] G. Adair, Thomas Alva Edison: Inventing the Electric Age, Oxford University Press, 1996.
[22] G. Constable, B. Somerville, A century of innovation: Twenty engineering achievements that transformed our lives, Joseph Henry Press, 2003.
[23] S. RAŢIU, The history of the internal combustion engine, Annals of the faculty of engineering Hunedoara (2003) 145–148.
[24] J. J. Flink, The automobile age, mit Press, 1990.
[25] V. Balzani, N. Armaroli, Energy for a sustainable world: from the oil age to a sun-powered future, John Wiley & Sons, 2010.
[26] J. Mohtasham, Renewable energies, Energy Procedia 74 (2015) 1289–1297.
[27] M. Taylor, et al., Energy subsidies: Evolution in the global energy transformation to 2050, International Renewable Energy Agency, Abu Dhabi (2020).
[28] T. Ahmad, D. Zhang, A critical review of comparative global historical energy consumption and future demand: The story told so far, Energy Reports 6 (2020) 1973–1991.
[29] B. Petroleum, Bp full report–statistical review of world energy 2021, 2021.
[30] S. Arango-Aramburo, J. Ríos-Ocampo, E. Larsen, Examining the decreasing share of renewable energy amid growing thermal capacity: The case of south america, Renewable and Sustainable Energy Reviews 119 (2020) 109648.
[31] S. Carrizo, S. Velut, Energy transitions and regional integration in south america, Territorial planning and La Plata Basin borders. Porto Alegre: Editora Letra 1 (2018) 167–187.
[32] S. Zapata, M. Castaneda, A. J. Aristizabal, I. Dyner, Renewables for supporting supply adequacy in colombia, Energy 239 (2022) 122157.
[33] A. L. Caceres, P. Jaramillo, H. S. Matthews, C. Samaras, B. Nijssen, Hydropower under climate uncertainty: Characterizing the usable capacity of brazilian, colombian and peruvian power plants under climate scenarios, Energy for Sustainable Development 61 (2021) 217–229.
[34] T. Santos, Regional energy security goes south: Examining energy integration in south america, Energy Research & Social Science 76 (2021) 102050.
[35] S. N. Abdul Latif, M. S. Chiong, S. Rajoo, A. Takada, Y.-Y. Chun, K. Tahara, Y. Ikegami, The trend and status of energy resources and greenhouse gas emissions in the malaysia power generation mix, Energies 14 (2021) 2200.
[36] H. Ritchie, Energy: Key charts (2021).
[37] O. A. Hoes, L. J. Meijer, R. J. Van Der Ent, N. C. Van De Giesen, Systematic high-resolution assessment of global hydropower potential, PloS one 12 (2017) e0171844.
[38] V. K. Singh, S. K. Singal, Operation of hydro power plants-a review, Renewable and Sustainable Energy Reviews 69 (2017) 610–619.
[39] T. S. Kishore, E. R. Patro, V. Harish, A. T. Haghighi, A comprehensive study on the recent progress and trends in development of small hydropower projects, Energies 14 (2021) 2882.
[40] J. Górecki, E. Płoszaj, Cost risk of construction of small hydroelectric power plants, in: MATEC Web of Conferences, volume 262, EDP Sciences, 2019, p. 07004.
[41] H. Jangavar, Y. Noorollahi, A. Emami Meybodi, Economic and environmental analysis of the small hydropower plants development, Iranian journal of Ecohydrology 4 (2018) 1255–1268.
[42] J. Chen, A. Engeda, Standard module hydraulic technology: A novel geometrical design methodology and analysis for a low-head hydraulic turbine system, part i: General design methodology and basic geometry considerations, Energy 196 (2020) 117151.
[43] A. Quicaza, S. Mora, et al., Formulación de estrategias para la implementación y fomento de fuentes no convencionales de energías renovables en zonas no interconectadas de colombia (????).
[44] S. d. S. P. Domiciliarios, Zonas no interconectadas zni, diagnóstico de la prestación del servicio de energía eléctrica 2017, Superintendencia de Servicios Públicos Domiciliarios-SSPD 68 (2019).
[45] S. D. P. E. Y. GAS, Zonas no interconectadas–zni informe sectorial de la prestación del servicio de energía eléctrica 2021 (2020).
[46] J. Vivas, El mapa de 1.710 poblados que aún se alumbran con velas en colombia, El tiempo (2019).
[47] V. J. A. Guzmán, J. A. Glasscock, F. Whitehouse, Design and construction of an off-grid gravitational vortex hydropower plant: A case study in rural peru, Sustainable Energy Technologies and Assessments 35 (2019) 131–138.
[48] D. S. Edirisinghe, H.-S. Yang, S. Gunawardane, Y.-H. Lee, Enhancing the performance of gravitational water vortex turbine by flow simulation analysis, Renewable Energy (2022).
[49] L. Velásquez, A. Posada, E. Chica, Optimization of the basin and inlet channel of a gravitational water vortex hydraulic turbine using the

response surface methodology, Renewable Energy 187 (2022) 508–521.
[50] Kourispower, Waterway embodiment of kct (2021).
[51] I. Adejumobi, D. Shobayo, Optimal selection of hydraulic turbines for small hydro electric power generation–a case study of opeki river, south western nigeria, Nigerian Journal of Technology 34 (2015) 530–537.
[52] D. Y. Goswami, F. Kreith, Energy conversion, CRC press, 2007.
[53] XM, Vertimientos (2022).
[54] N. I. E. L. LAS ZONAS, Estado de la cobertura electrica y las zonas no interconectadas en la región central (2020).
[55] F. Moreno Gamboa, E. G. Flórez Serrano, G. Guerrero Gómez, Mercados de energía en colombia, una introducción (2021).
[56] E. L. Gonzales Titi, P. A. Loayza Quiñones, A. M. More Dávila, V. A. R. Simeon Vega, Propuesta de utilización del gas natural licuefactado en los camiones mineros: evaluación de beneficios (2019).
[57] B. C. Olopade, H. Okodua, M. Oladosun, A. J. Asaleye, Human capital and poverty reduction in opec member-countries, Heliyon 5 (2019) e02279.
[58] Datosmacro.com, Precio del petróleo opep por barril (2022).
[59] H. Nautiyal, V. Goel, Sustainability assessment of hydropower projects, Journal of Cleaner Production 265 (2020) 121661.
[60] M. Antonio, C. Camargo, plan energético nacional colombia: ideario energético 2050, Bogotá DC (2015).
[61] M. Kumar, Social, economic, and environmental impacts of renewable energy resources, Wind solar hybrid renewable energy system 1 (2020).
[62] M. Abdel-Basset, A. Gamal, R. K. Chakrabortty, M. J. Ryan, Evaluation approach for sustainable renewable energy systems under uncertain environment: A case study, Renewable energy 168 (2021) 1073–1095.
[63] C. Li, J. Zhang, S. P. Philbin, X. Yang, Z. Dong, J. Hong, P. Ballesteros-Pérez, Evaluating the impact of highway construction projects on landscape ecological risks in high altitude plateaus, Scientific Reports 12 (2022) 1–16.
[64] J. A. Vélez Henao, L. D. Vélez Gómez, Evaluación de las transferencias del sector eléctrico. el caso de san carlos y el oriente antioqueño, Revista Ingenierías Universidad de Medellín 14 (2015) 147–161.
[65] Y.-m. Lu, C.-l. Shang, The environmental impact of the three gorges project and the countermeasures, Frontiers of Engineering Management 1 (2014) 120–128.
[66] Z. Huang, B. Wu, An overview of project and its environmental issues, Three Gorges Dam (2018) 1–14.
[67] A. Kumar, Z.-G. Yu, J. J. Klemeš, A. Bokhari, A state-of-the-art review of greenhouse gas emissions from indian hydropower reservoirs, Journal of Cleaner Production 320 (2021) 128806.
[68] M. Rahman, J. Tan, M. Fadzlita, A. W. K. Muzammil, A review on the development of gravitational water vortex power plant as alternative renewable energy resources, in: IOP Conference Series: Materials Science and Engineering, volume 217, IOP Publishing, 2017, p. 012007.
[69] T. B. Couto, J. D. Olden, Global proliferation of small hydropower plants–science and policy, Frontiers in Ecology and the Environment 16 (2018) 91–100.
[70] T. Abbasi, S. Abbasi, Small hydro and the environmental implications of its extensive utilization, Renewable and sustainable energy reviews 15 (2011) 2134–2143.
[71] E. RENOVABLES, D. IRENA, 10 argumentos a favor de las energias renovables (2015).
[72] A. L. Gómez, C. Arredondo, M. Luna, S. Villegas, J. Hernández, Regulating the integration of renewable energy in colombia: Implications of law 1715 of 2014, in: 2016 IEEE 43rd Photovoltaic Specialists Conference (PVSC), IEEE, 2016, pp. 3317–3321.
[73] J. A. Hernández, C. A. Arredondo, D. J. Rodríguez, Analysis of the law for the integration of non-conventional renewable energy sources (law 1715 of 2014) and its complementary decrees in colombia, in: 2019 IEEE 46th Photovoltaic Specialists Conference (PVSC), IEEE, 2019, pp. 1695–1700.

CHAPTER 8

CONCLUDING REMARKS

In modern societies, electricity is a basic need, and renewable resources, especially hydraulic resources, have a key role to play in supporting electricity increased demand. Hydropower is the primary source of renewable energy; it contribute almost 60% of the global renewable supply and nearly 20% of all electricity production. Small hydropower plants constitute a feasible and attractive solution to cover the increasing demand and to produce electricity in isolated regions, this facilities can produce electricity operating in small rivers. Among the different type of turbine, gravitational water hydraulic turbine (GWVHT) allows to take advantage of locations that until now were impossible with conventional generation systems because is a low hydraulic head hydropower turbines. The GWVHT is very promising for application in developing countries where the large hydroelectric power plants can be run into financial, environmental, and social nature obstacles.

The main findings of the compendium of short scientific presented are:

- From the literature review, Chapter 2, the previous studies allowed asserting that the conical basins are better than the cylindrical basins because in the conical basins the velocities reached in the vortex are higher. Additionally, there are no recirculation regions in the conical basin as compared to cylindrical basins. These conclusion allowed to identify the best geometry for the turbine but not the dimensions of this geometry. In GWVHT, two of the main components: inlet channel and basin can be constructed on-site using concrete or other construction materials. These designs allow the requirements for the implementation of a GWVHT to be less than the requirements for conventional systems, facilitating the construction of many of these plants along the path of a river.

  Materials such as plastic, aluminium or composite materials can be used for fabrication of the runners because they are lightweight materials; changing the material will increase the power/weight ratio, its useful life and the modularity of the system. With a modular and lightweight turbine, the system can be transported and installed in remote areas with significant hydraulic potentials. It is important to develop simple design geometries with reduced civil works that employs basic workshop facilities and local manufacturing to produce these systems possible at a lower cost.

- In Chapters 3, a equation to determine the optimal inlet velocity of the water flow entering to the turbine was established. The inlet velocity is a function of the coefficient of discharge (C_d), the volume flow rate Q, the acceleration gravity (g), the basin height (H), and the relationship between diameter of the basin (D) and the outlet diameter (d), (d/D). With this equation is possible to increase the vortex circulation, which in turn increases the efficiency of the turbine.

- The vortex circulation (Γ) is defined mathematically as the line integral of a vector field around a closed curve C. In fluid dynamics, that field is the fluid velocity field $\vec{u}$. Γ was chosen as the response variable because it allows to quantify the real force of a vortex, therefore, an increase in circulation produces an increase in the force of the flow.

- Using a multi-objective genetic algorithm with two conflicting objectives: (1) the minimization of the volume flow rate Q, and (2) the maximization of the vortex circulation Γ, a Pareto front (set of optimal solutions) was found. The multi-objective optimization problem was resolved by applying the *gamultiobj* function in Matlab R2018b software. The optimization combines the genetic algorithm with Kriging interpolation to obtain the Pareto front. The geometrical parameters considered in the optimization of a turbine with spiral inlet channel and conical basin were the basin height (H), the basin diameter (D), the inlet channel length (L), the inlet channel height (h), the inlet channel width (w), the outlet diameter (d) and the wrap-around angle (γ). It was found from the Pareto front that the values of the six variables providing the compromise solution (solution in the middle of Pareto front), between Γ and Q, were H/D =1.572, L/D =1.518, h/D =0.565, w/D =0.361, d/D =0.108, and γ=92.141°. This solution reaches a Q of 0.00305 m^3/s and a Γ of 1.699 m^2/s.

  It is important to highlight that the results obtained through this optimization are only valid for the turbine with conical basin and spiral inlet channel; any change in the shape of the turbine components implies that the results of this optimization may not be valid.

- The effect of the relative position of the runner (p), the number of blades (n), and the mean diameter of the blades (D_b) on the efficiency of the turbine has been investigated, and a second-order response model for the efficiency of the turbine was developed. This model allows predicting the efficiency of the turbine as a function of p, n, and D_b/D. In this optmization, only characteristic of the runner were considered, the geometries and dimensions of the inlet channel and conical basin were the geometries and dimensions found in Chapters 2 and 4. Numerical analysis of 17 geometries shows that the maximum numerical efficiency was 65.18%. This was found with the largest value of all the independent variables (D_b/D =0.45, n =6 and p =0.6).

  An experimental bench was built to validate the numerical results and the second-order response model. The difference between numerical and experimental efficiency was acceptable and was mainly attributed to the losses in the experimental bench, surface friction in the runner, and mechanical losses that are not accounted for in the numerical models. The results found also indicate that it is not appropriate to optimize the rotor for this type of turbines considering a single parameter of its geometry, such as the number of blades or the diameter, because the conclusions are not general, and may change depending on the geometry studied. As the parameters used in the optimization process are dimensionless, the results can be scaled to build larger or smaller turbines.

- For a fluid to move a solid body, such as the runner of GWVHT, there must be surface forces, also called aerodynamic or hydrodynamic forces, generated by the fluid in which the body is submerged. Aerodynamic forces arise from two causes: the normal force due to pressure on the body surface, and the shear force on the body surface due to fluid viscosity. The net aerodynamic force $\vec{F}$ on the solid body is the sum of the normal and shear forces on the surface. The resultant force $\vec{F}$ can be divided into two components: lift force and drag force. Knowing the distributions of velocity and pressures in the flow allows to understand and calculate the behavior and magnitude of the aerodynamic forces. Then, with the aerodynamic forces, the power that the turbine generates can be calculated. If the generated power increases, and the available power entering the system remains constant, the hydraulic efficiency of the turbine increases.

- Computer simulations were the great source of information to train the optimization models developed. The most important characteristic of the computational simulations is the correct selection of the

equations that govern the flow of fluids. These equations can only be solved directly for simple cases of flow. For most real-life turbulent flows, CFD simulations use turbulent models to predict the evolution of turbulence. These turbulence models are simplified constitutive equations that predict the statistical evolution of turbulent flows. The models commonly used in modern engineering applications, specifically for vortex turbines, are the k-ϵ and k-ω models.

- The future of humanity and the planet depends on the way energy is produced: a reliable, affordable, and decarbonized energy system is essential. Currently, most countries worldwide aim to supply their internal energy demand from renewable energy sources. Colombia is no stranger to this approach, which is why, in its National Energy Plan, a strategy to reduce the vulnerability of the energy sector is the search to diversify the matrix of electricity generation in the medium and long term in all supply chains energy supply, increasing its complementarity, availability and reliability with renewable energy sources. The 1715 of 2014 reforces the idea of use of non-conventional sources of energy, turning them into a matter of public utility and social, public, and national interest, which triggered a high interest in the promotion and implementation of energy projects through non-conventional sources of energy in the country. With this panoram, the implementation of the gravitational water vortex hydraulic turbine in Colombia is an attractive alternative to produce electricity to supply the demand in conditions of environmental sustainability.

APPENDIX A

Methodology for the design of GWVHT

The optimization of GWVHT was performed in two stages due to the large number of independent variables that could be taken into account in this process. In the first stage, a multi-objective genetic algorithm was implemented where only geometric factors of the inlet channel, circulation chamber and discharge were included. In this first stage the runner was not included, and the objectives or response variables of the optimization were the maximization of the circulation of the vortex (Γ) and the minimization of the voluem flow rate (Q). The selected baseline geometry for the first optimization task is shown in Fig. 8.1. The geometry employed was a turbine with a conical basin and wrap-around inlet channel. Six parameters were considered for the optimization: the relations between the basin diameter (D) and the basin height (H), H/D; the wrap-around angle (γ), the outlet diameter (d) and D, d/D; the inlet channel width (w) and D, w/D; the inlet channel height (h) and D, h/D; and the inlet channel length (L) and D, L/D. These variables are dimensionless since each of them was divided by D.

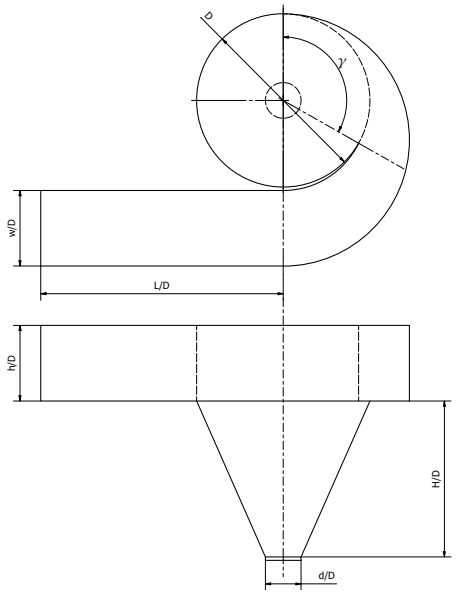

Figure 8.1: The selected baseline geometry and geometric factors.

From the Pareto front, the values of the six variables providing the compromise solution, between Γ and Q, were:

$$
\begin{aligned}
H/D &= 1.572 \\
L/D &= 1.518 \\
h/D &= 0.565 \\
w/D &= 0.361 \\
d/D &= 0.108 \\
\gamma &= 92.141^{\circ}
\end{aligned}
\tag{8.1}
$$

In the second stage, the response surface methodology with a single-objective was implemented. The optimized geometry of the first stage was used as a basis and three geometric parameters of the runner were taken: the relative position of the runner (p), the number of blades (n), and the relation between the mean diameter of the blades (D_b) and the diameter of basin (D), (D_b/D). The mean diameter of the blades was divided by the diameter of the basin (D) to obtain a non-dimensional variable as the first stage variables. The response variable was the maximization of hydraulic efficiency (η). The mean diameter is measured at the middle height of the runner. The variable p is a function of the position of the runner (h_r) and the basin height (H), $p = h_r/H$, h_r is measured to the middle height of the runner as shown in Figure 8.2.

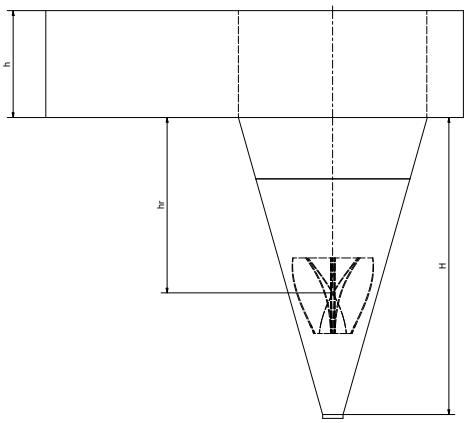

Figure 8.2: Position of the runner.

To take advantage of the components of the flow velocity in the vortex, a runner with curved blades with twist angle was chosen. The twist angle is the angle that the cross section of the blade makes at the top with respect to its counterpart at the bottom. Table 8.1 shows the inlet and outlet angles of the blade for the selected runner. These angles were taken from previous studies. The runners with curved blades with twist angle and different number of blades are shown in Figure 8.3.

Table 8.1: Blades design summary.

Symbol	Variable	Value
α	Blade inlet angle [Deg]	16.00
α_1	Blade outlet angle [Deg]	90.00
β	Water inlet angle [Deg]	40.00
β_1	Water outlet angle [Deg]	42.7
λ	Twist angle [Deg]	68.80
L	Blade height [mm]	200

From the second-order response model, the value of the three variables providing the maximum efficiency of the turbine were:

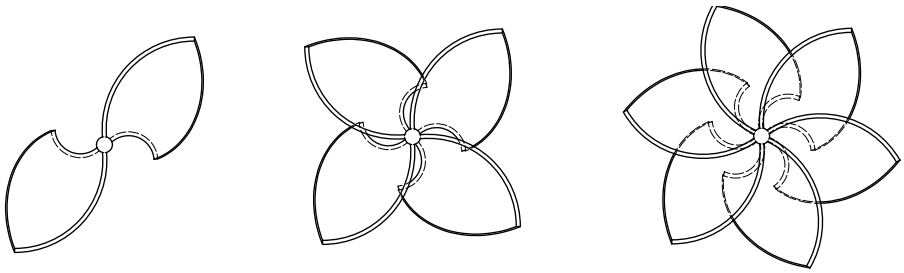

Figure 8.3: Runner: number of blades.

$$\begin{aligned} D_b/D &= 0.45 \\ n &= 6 \\ p = h_r/H &= 0.6 \end{aligned} \tag{8.2}$$

In addition to the value of the nine geometric factors to define the dimensions of the turbine, the coefficient of discharge (C_d) equation for conical basin gravitational vortex turbines was determined. This equation allows estimate the volume flow rate (Q) to develope the maximum circulation of the vortex (Γ). The developed equation for C_d is related with the parameter d/D, as described by Eq. 8.3.

$$C_d = [0.7721e^{-6.4409\frac{d}{D}}] - 0.0464 \tag{8.3}$$

The coefficient of discharge also relates the variables Q and H, as described by Eq. 8.4.

$$C_d = \frac{4Q}{\pi d^2\sqrt{2gH}} \tag{8.4}$$

Example To determine the value of Q, it is neccesary to establish the value of H or D. The basin height or diameter can be known in advance because they depend on the space constraints of the turbine installation site. For example, if $D = 1$ m, the value of H, L, h, w, d, and γ, from Equations 8.1 and 8.2, are:

$$\begin{aligned} H &= 1.572m \\ L &= 1.518m \\ h &= 0.565m \\ w &= 0.361m \\ d &= 0.108m \\ \gamma &= 92.141° \\ D_b &= 0.45m \\ n &= 6 \\ p &= 0.9432m \end{aligned} \tag{8.5}$$

Then, using Equation 8.3 and the optimized relation $d/D = 0.108$, the value of C_d is 0.3386. Finally, using Equation 8.4, the volume flow rate is 0.0172 m^3/s (17.22 L/s).

ADDITIONAL REFERENCES

J. A. Aguilera Folgueiras. Fuentes de energía y protocolo de kioto en la evolución del sistema eléctrico español. 2012.

M. C. Arango. Panorama energetico de colombia. *Actualidad economica y sectorial*, 2019.

Y. A. Cengel. *Fluid mechanics*. Tata McGraw-Hill Education, 2010.

I. Dincer and M. F. Ezzat. 3.4 renewable energy production. In I. Dincer, editor, *Comprehensive Energy Systems*, pages 126–207. Elsevier, Oxford, 2018. ISBN 978-0-12-814925-6. doi: https://doi.org/10.1016/B978-0-12-809597-3.00310-2. URL https://www.sciencedirect.com/science/article/pii/B9780128095973003102.

L. Doman. Eia projects 28% increase in world energy use by 2040. *EIA Report Today in Energy*, 2017.

B. Dudley et al. Bp statistical review of world energy 2018. *London, UK*, 2018.

FAO. Oferta y demanda de energÃa: tendencias y perspectivas, 2018.

J. D. Gallego Triana et al. *Políticas para el aprovechamiento del potencial hidroenergético en Colombia mediante pequeñas centrales*. PhD thesis, Universidad Nacional de Colombia-Sede Medellín, 2015.

R. Goodland. The concept of environmental sustainability. *Annual review of ecology and systematics*, 26(1): 1–24, 1995.

D. Y. Goswami and F. Kreith. *Energy conversion*. CRC press, 2007.

J. Gummer. Hydraulic turbines. In *Thermopedia*. Begel House Inc., 2011.

IRENA. Renewable capacity statistics 2019, 2019.

C. Lins, L. E. Williamson, S. Leitner, and S. Teske. The first decade: 2004-2014: 10 years of renewable energy progress. *Renewable Energy Policy Network for the 21st Century.*, 2014.

UPME. Informe de gestión, 2018.

L. Velásquez, A. Rubio-Clemente, and E. Chica. Numerical analysis of the inlet channel and basin geometries for vortex generation in a gravitational water vortex power plant. In *18th Inter Conference on Renew Energies and Power Quality*, 2020.

L. Velásquez, E. Chica, and J. Posada. Advances in the development of gravitational water vortex hydraulic turbines. *Journal of Engineering Science & Technology Review*, 14(3), 2021.

L. Velásquez, A. Posada, and E. Chica. Optimization of the basin and inlet channel of a gravitational water vortex hydraulic turbine using the response surface methodology. *Renewable Energy*, 187:508–521, 2022.

L. Velásquez, A. Posada, and E. Chica. Surrogate modeling method for multi-objective optimization of the inlet channel and the basin of a gravitational water vortex hydraulic turbine. *Applied Energy*, 330:120357, 2023.